Thèse présentée pour obtenir le grade de

Docteur de l'Université Paris-Est

Discipline: Géotechnique

par

Ni AN

Etude numérique de l'interaction sol-atmosphère : application aux remblais en sols traités

Jury

Prof. Farimah Masrouri	Université de Lorraine (France)	Président
Prof. Cristina Jommi	Delft University of Technology (Netherlands)	Rapporteur
Prof. Said Taibi	Université du Havre (France)	Rapporteur
M^{me} Yasmina Boussafir	IFSTTAR (France)	Examinatrice
M^{me} Isabelle Charles	CEREMA (France)	Examinatrice
M. Daniel Puiatti	DPST Consulting (France)	Examinateur
M^{me} Cindy Maisonnave	Direction Départementale des Territoires et de la Mer de la Seine-Maritime (France)	Invitée
Dr. Sahar Hemmati	IFSTTAR (France)	Co-encadrante
Prof. Yu-Jun Cui	Ecole des Ponts ParisTech (France)	Directeur de thèse

Dissertation presented for the degree of

Doctor of l'Université Paris-Est

Discipline: Geotechnical engineering

by

Ni AN

Numerical investigation of soil-atmosphere interaction: application to embankments of treated soils

Jury

Prof. Farimah Masrouri	Université de Lorraine (France)	Président
Prof. Cristina Jommi	Delft University of Technology (Netherlands)	Rapporteur
Prof. Said Taibi	Université du Havre (France)	Rapporteur
M^{me} Yasmina Boussafir	IFSTTAR (France)	Examinatrice
M^{me} Isabelle Charles	CEREMA (France)	Examinatrice
M. Daniel Puiatti	DPST Consulting (France)	Examinateur
M^{me} Cindy Maisonnave	Direction Départementale des Territoires et de la Mer de la Seine-Maritime (France)	Invitée
Dr. Sahar Hemmati	IFSTTAR (France)	Co-encadrante
Prof. Yu-Jun Cui	Ecole des Ponts ParisTech (France)	Directeur de thèse

Résumé

Face au changement climatique global, il est de plus en plus important de prêter attention à la performance thermique-hydro-mécanique des constructions géotechniques sous l'effet des conditions atmosphériques. L'objectif principal de cette étude est d'étudier le comportement hydro-thermique des sols soumis aux effets du changement climatique par la modélisation numérique.

Un modèle hydro-thermique couplé est tout d'abord développé pour décrire le comportement du sol hydro-thermique. La théorie utilisée pour décrire l'interaction sol-atmosphère est présentée sous forme des bilans de masse et d'énergie. Ensuite, une approche numérique pour analyser le comportement hydro-thermique du sol est proposée en combinant le modèle hydro-thermique couplé avec un modèle d'interaction sol-atmosphère. La validation de cette approche est réalisée par la comparaison entre les résultats numériques obtenus en utilisant le code FreeFem++ et les données des essais de la colonne de séchage qui sont trouvées dans la littérature. Cette approche est d'abord utilisée pour la modélisation numérique des essais à la chambre environnementale, réalisés par Song en 2014. Des résultats de simulation satisfaisants sont obtenus en termes de variations de la température et de la teneur en eau volumétrique du sol. Ensuite, cette approche est appliquée à deux remblais, à Héricourt et à Rouen. Pour le remblai d'Héricourt, une étude numérique a été menée pour une durée de 20 jours. La bonne concordance obtenue entre les résultats de simulation et les mesures montre que l'approche proposée est pertinente pour l'analyse du comportement hydro-thermique du sol dans le cas de remblais bidimensionnels. Elle prouve également que les conditions aux limites et les paramètres du sol adoptés sont appropriés. Dans le cas du remblai de Rouen, deux périodes différentes, 187 jours et 387 jours, sont prises en considération. On vérifie également la bonne performance de l'approche proposée pour estimer le comportement hydro-thermique du remblai sous l'effet du climat. La comparaison entre les calculs et les mesures révèle également l'importance d'adopter correctement les conditions aux limites thermiques et hydrauliques ainsi que les paramètres du sol. De plus, à partir des simulations numériques, plusieurs suggestions

sont faites pour collecter des données d'entrée dans l'application de cette approche pour prédire les variations de la température et de la teneur en eau du sol à plus long terme.

Mots clés: interaction entre sol-atmosphère; couplé modèle de hydro-thermique; bilans de masse et d'énergie; code FreeFem++; étude numérique; essais de chambre environnementale; remblais en bidimensionnels; variations de la température du sol; variations de la teneur en eau volumétrique du sol.

Abstract

Facing the global climate change, it is more and more important to pay attention to the thermal-hydro-mechanical performance of geotechnical constructions under the effect of atmospheric conditions. The main objective of this study is to investigate the hydro-thermal behavior of soil subjected to climate change through numerical modelling.

A coupled hydro-thermal model is developed for describing the coupled hydro-thermal soil behavior. The soil-atmosphere interaction is studied through the mass and energy balances. Afterwards, a numerical approach to estimate soil hydro-thermal behavior by integrating the coupled hydro-thermal model with a soil-atmosphere interaction model is proposed. The validation of this approach is performed through the comparison between the numerical results using FreeFem++ code and the experimental data available from column drying tests reported in literature. This approach is firstly used for the numerical modelling of the environmental chamber tests carried out by Song in 2014. Satisfactory simulation results are obtained in terms of variations of soil temperature and soil volumetric water content. Afterwards, this approach is further applied to two cases of embankments, in Héricourt and in Rouen respectively. For Héricourt embankment, a numerical investigation was conducted for 20 days, and a good agreement between simulation results and filed measurements is obtained, showing that the proposed approach is suitable for analyzing the soil hydro-thermal behavior in the case of two-dimensional embankments. It proves also that the boundary conditions and the soil parameters adopted are appropriate. In the case of Rouen embankment, two different periods, 187 days and 387 days, are considered. The good performance of the proposed approach in estimating the embankment hydro-thermal behavior under the climate effect is also verified. The comparison between calculations and measurements also reveals the importance of appropriately adopting the thermal and hydraulic boundary conditions as well as the soil parameters. Based on the numerical simulations, several suggestions are made in terms of collection of input data for the application of this approach to predict soil temperature and volumetric water content variations in long term.

Key words: soil-atmosphere interaction; coupled hydro-thermal model; mass and energy balances; FreeFem++ code; numerical investigation; environmental chamber tests; two-dimensional embankments; variations of soil temperature; variations of soil volumetric water content.

Acknowledgements

First and foremost, my deepest gratitude goes to Prof. Yu-Jun Cui, my supervisor for his continuous encouragement and professional guidance during the whole period of my PhD study. He always provides his profound scientific visions, relevant advices, and systematic guidance in my research work, assisting me to move forward smoothly and inspiring me to explore more scientific knowledge. Moreover, he builds a charming academic model by his words and deeds, which unconsciously influenced me to behave with self-motivation, self-restraint and positive attitude when facing any challenges. I deeply appreciate the training full of his good intentions and all his selfless help in my study and life. “One day as a teacher, a life as a father”. In my future, I will follow the light this father sheds on me and make it shining continuously to inspire more people.

I would like to express my deep and sincere gratitude to Dr. Sahar Hemmati, my co-supervisor for her consistent guidance with patience in the past three years. Her constant encouragement and valuable suggestions are invaluable asset for completing this dissertation. She shared her profound understanding and abundant experiences in the numerical calculations, helping me overcome different problems I met.

My sincere thanks also go to Madame Cindy Maisonnave, Madame Isabelle Charles, and Monsieur Dimitri Mercadier in CEREMA. Their supports enable me to undertake abundant information of field embankments and accomplish the study with strong engineering background. Additionally, the high quality meteorological data from METEO FRANCE is gratefully acknowledged.

I would like to specially thank the two rapporteurs of my dissertation, Prof. Cristina Jommi and Prof. Said Taibi, for giving me their insightful comments. My gratitude also goes to the examiners, Prof. Farimah Masrouri, Monsieur Daniel Puiatti, and Madame Yasmina Boussafir, for accepting to be part of the jury and for the suggestions they proposed to this work.

I would like to thank sincerely Dr. Anh-Minh Tang for his kind assistances in my research work. He gave me his constructive opinions to improve my experimental work and papers. I would

like to specially thank Dr. Siavash Ghabezloo for his significant help to solve the numerical problems I met. My sincere thanks also go to Prof. Chao-Sheng Tang in Nanjing University. Extended discussion with him helps me develop my understanding on the soil water evaporation process.

My sincere thanks also go to Prof. François Schlosser, Prof. Roger Frank and Prof. Pierre Delage for their encouragement and support to my research work. My gratitude also goes to Mr. Emmanuel De Laure, Mr. Baptiste Chabot, and Miss Marine Lemaire for their help in my experimental work.

My thanks also go to my friends and colleges in CERMES for their encouragement, support and all the happy time we spend together. My special gratitude goes to my dear friends, Lina Guayacan-Carrillo, Philipp Braun, Han-Lin Wang, Ling-Ling Zeng, Feng Zhang, Wen-Jing Sun, Yong He, Ye-Jiao Wang, Sheng-Shi Dong, Qiong Wang, Wei-Kang Song, Peng-Yun Hong and Zhan Zhao for their moral supports. I would like to record my special appreciation to Prof. Hong-Yue Sun in Zhejiang University for her constant encouragement in my life.

I am also grateful to Ecole des Ponts Paris-Tech, and China Scholarship Council (CSC) for their financial supports.

Finally, my loving thanks go to my dear parents and sister, for their everlasting patience and encouragement, for always being there to support and hold me. Thanks for allowing and reminding me to be free and brave but with responsibility to pursue my life and future.

Publications

1. **An, N.,** Hemmati, S., and Cui, Y.J. 2017. Numerical analysis of soil volumetric water content and temperature variations in an embankment due to soil-atmosphere interaction. Computers and Geotechnics, **83**: 40-51.

2. **An, N.,** Hemmati, S., Cui, Y.J., Tang, A.M., and Mercadier, D. 2017. Assessment of rainfall runoff based on the field measurements on an embankment. Geotechnical Testing Journal, **40** (1): 29-36.

3. **An, N.,** Hemmati, S., Cui, Y.J., and Tang, A.M. 2017. Assessment of the methods for determining net radiation on different time-scales of meteorological variables. Journal of Rock Mechanics and Geotechnical Engineering (Available online).

4. **An, N.,** Hemmati, S., Cui, Y.J., Maisonnave, C., Charles, I., and Tang, C.S. 2016. Numerical analysis of hydro-thermal behavior of Rouen embankment under climate effect. Canadian Geotechnical Journal (Revision submitted).

5. **An, N.,** Hemmati, S., Cui, Y.J., and Tang, A.M. 2016. The determination of model dimension for an embankment to study soil atmosphere interaction with Finite Element Method. UNSAT 2016, Paris, France.

6. Tang, C.S., Cui, Y.J., Shi, B., Tang, A.M., **An, N.** 2016. Effect of wetting-drying cycles on soil desiccation cracking behavior. UNSAT 2016, Paris, France.

7. **An, N.,** Hemmati, S., Cui, Y.J., and Tang, A.M. 2015. Development of a Hydro-thermal coupled model for unsaturated soil. AP-UNSAT 2015, Guilin, China.

Contents

General introduction 1
Chapter 1: Literature review 5
1.1 Influence of climate change on geotechnical constructions 5
1.2 Coupled modelling of soil behavior 10
1.2.1 Heat flow, water flow, air flow and mechanical modelling 11
1.2.2 Coupled models 17
1.2.3 Evaluation of coupled models 24
1.3 Interaction between soil and atmosphere 24
1.3.1 Experimental investigation 24
1.3.2 Numerical investigation 30
1.3.3 Discussion 35
1.4 Conclusions 37
Chapter 2: Development of a coupled hydro-thermal numerical model for unsaturated soils 39
2.1 Introduction of FreeFem++ code (Hecht 2012) 39
2.2 Heat flow 41
2.3 Water flow 45
2.4 Simple coupled hydro-thermal model 51
2.4.1 Introduction 51
2.4.2 Validation and analysis 55
2.4.3 Discussion 62
2.5 Fully coupled hydro-thermal model 63
2.5.1 Liquid flow and vapor flow 63
2.5.2 Heat flow 67
2.6 Weak forms of fully coupled hydro-thermal model 70
2.6.1 Weak form of water flow 70
2.6.2 Weak form of heat flow 72
2.7 Conclusions 73
Chapter 3: Development and validation of the numerical approach adopted 75
3.1 Soil-atmosphere interaction 75
3.1.1 Balance equations used for the description of soil-atmosphere interaction 75

3.1.2 Initial and boundary conditions 94
3.2 Validation of the proposed numerical approach based on a column drying test 95
3.2.1 Introduction of column drying test (Wilson, 1990) 95
3.2.2 Model dimension, initial and boundary conditions 97
3.2.3 Soil parameters 98
3.2.4 Results and analysis 101
3.3 Conclusions 103
Chapter 4: Modelling of evaporation tests in environmental chamber 105
4.1 Environmental chamber 105
4.2 Definition of numerical model 109
4.2.1 Model dimension, initial and boundary conditions 109
4.2.2 Soil parameters 112
4.3 Results and analysis 116
4.3.1 Test 1 116
4.3.2 Test 2 119
4.3.3 Test 3 122
4.3.4 Test 4 124
4.4 Discussion 127
4.4.1 Definition of typical evaporation stages 127
4.4.2 Dry soil layer 129
4.4.3 The application of Gardner model 131
4.5 Conclusions 137
Chapter 5: Modelling of Héricourt embankment 139
5.1 Héricourt embankment 139
5.2 Definition of numerical model 144
5.2.1 Soil parameters 144
5.2.2 Model dimension 147
5.2.3 Initial and boundary conditions 154
5.3 Results and analysis 158
5.3.1 Soil hydro-thermal behavior 158
5.3.2 Influence depths of soil temperature and volumetric water content by climate change 162
5.4 Sensitivity analysis about initial condition effect 165

5.4.1 Initial condition of soil temperature 165
5.4.2 Initial condition of soil volumetric water content 180
5.4.3 Suggestions for determining soil initial conditions 183
5.5 Conclusions 184
Chapter 6: Modelling of Rouen embankment 186
6.1 Rouen embankment 186
6.2 Definition of numerical model 189
6.2.1 Soil parameters 189
6.2.2 Model dimension, initial and boundary conditions 192
6.3 Modelling of Rouen embankment for 187 days 196
6.3.1 Presentation of meteorological data 196
6.3.2 Results and discussions 198
6.4 Modelling of Rouen embankment for 387 days 203
6.4.1 Presentation of meteorological data 203
6.4.2 Results and discussions 205
6.5 Discussions 211
6.5.1 Soil temperature variations 211
6.5.2 Soil volumetric water content variations 211
6.6 Conclusions 218
General conclusions 221
Perspectives 224
Nomenclature 226
References 229

General introduction

Changing climate alters the performance of geotechnical constructions, giving rise to disruption, financial lost and casualties, along with significant damages. It is reported by EEA (2012) that the hydro-meteorological events (storms, floods, and landslides) account for 64 % of the known damage costs due to natural disasters in Europe since 1980, the climatological events (extreme temperatures, droughts, and forest fires) accounting for another 20 %. The financial lost due to extreme weather events has increased from EUR 9 billion in the 1980s to more than EUR 13 billion in the 2000s. The increase in damages is primarily due to the increase in population, economic wealth and human activities in hazard-prone areas and also to better reporting. Furthermore, the contribution of climate change to the damage costs from natural disasters is expected to increase due to the projected changes in the intensity and frequency of extreme weather events. The stability of geotechnical infrastructures in long term is of increasing concern among geotechnical engineers. Thereby, the effect of climate change on the geotechnical infrastructure, especially the extreme weather events such as more intense winter rainfall events and drier summer weather, needs to be paid more attention.

A large-scale environmental chamber was designed and used for investigating soil water evaporation in the laboratory (Cui et al. 2013; Song 2014; Song et al. 2014; Ta 2009). It is equipped with various sensors, enabling the monitoring of different parameters: wind speed, air temperature and relative humidity, soil volumetric water content, soil temperature, etc. Four evaporation tests on Fontainebleau sand were carried out by Song in 2014 at different air temperatures and wind speeds, providing rich data for further numerical analysis.

In the project “ANR-07-PCGU-006-10-TerDOUEST”, a field embankment at Héricourt was conducted in 2010. It was planned for several objectives: understanding the coupling between the chemical and geotechnical behavior of treated soils; understanding of the long term behavior of treated soils; building a reference embankment to study the construction and monitoring processes; studying the effect of environment and various operations during the earthwork.

Abundant equipments were set up during the construction, including a field weather station for recording climate variations and various sensors for monitoring soil state parameters' variations. This embankment allows the experimental investigation of soil-atmosphere interaction and further numerical investigation as well.

Another field embankment in Rouen was built in 2011 for the project "Digues et Ouvrages Fluviaux, Érosion Affouillements et Séismes (DOFEAS)". The objective of this study is to better understand the mechanical, hydraulic and erosion behavior of silt treated by lime in the field situations. The embankment was constructed by Centre d'Expérimentation et de Recherche (CER) with treated and untreated silt, and instrumented with various sensors and a nearby weather station. Various soil parameters were recorded continuously: soil volumetric water content, soil temperature, slope surface erosion photography, etc. The field measurements also enable the numerical investigation of soil-atmosphere interaction.

The main objective of our study is to numerically investigate the soil hydro-thermal behavior in embankments under the climate effect. Several specific aspects need to be particularly studied:

1) To establish a state-of-the-art in the numerical investigations of soil-atmosphere interaction through literature review;

2) To propose a numerical approach to estimate soil hydro-thermal behavior by integrating a coupled hydro-thermal model with a soil-atmosphere interaction model;

3) To verify the chosen numerical tool and to conduct the validation of the proposed numerical approach;

4) To investigate the numerical modelling of soil hydro-thermal behavior in the tests using environmental chamber by Song in 2014;

5) To incorporate meteorological information properly (depending on the time scale and site position) to estimate the boundary conditions of the coupled hydro-thermal model;

6) To study the soil hydro-thermal behavior in two-dimensional embankments by numerical

investigation.

Consequently, the whole thesis consists of six chapters.

Chapter 1 is devoted to the presentation of a general literature review of the current knowledge concerning soil-atmosphere interaction. The first part summarizes the four aspects of the main hydraulic and thermal factors that characterize the climate changes, indicating the significance of climate effect on soil behavior. The second part introduces the general knowledge of heat, water liquid, water vapor, air and mechanical modelling as well as their couplings. The third part shows the study of soil-atmosphere interaction conducted through experimental and numerical investigations, respectively. This chapter is finished by a conclusion and the presentation of the aspects that are dealt with in this study.

Chapter 2 focuses on the numerical aspects of the study. Firstly, the accuracy of the numerical solution using FreeFem++ code is verified through heat and water flows by comparing the calculation results with the known theoretical solutions. Afterwards, the numerical modelling of a simple coupled hydro-thermal model is conducted. The simulation results show a high consistency with the known results in terms of soil volumetric water content and temperature variations. Furthermore, a fully coupled hydro-thermal model is developed and the weak forms of equations for water and heat flows are established for the following study.

Chapter 3 proposes a numerical approach by combing the coupled hydro-thermal model and the soil-atmosphere interaction model. The first part of this chapter introduces the theory about soil-atmosphere interaction by presenting mass and energy balances. The second part indicates the method used to define the initial and boundary conditions for the proposed model. The third part validates this numerical approach through a column drying test carried out by Wilson (1990).

Chapter 4 introduces four different evaporation tests on Fontainebleau sand in an environmental chamber, carried out by Song (2014) firstly. After the definitions of model dimension, soil parameters, initial and boundary conditions, the corresponding numerical modellings of the four tests are conducted accordingly. An overall satisfactory agreement is obtained between the

simulations and measurements, proving the good performance of the proposed approach in simulating the environmental chamber tests.

Chapter 5 applies the proposed numerical approach to Héricourt embankment. The first part of this chapter introduces the field situation. In the second part, the model dimension, soil parameters, initial and boundary conditions are defined, respectively. The third part compares the calculated results of soil temperature and volumetric water content with the corresponding measured data. The fourth part is devoted to the sensitivity analyses of initial condition effects.

Chapter 6 investigates the soil hydro-thermal behavior of Rouen embankment under the climate effect. The field situation of Rouen embankment is introduced firstly, followed by the presentation of soil parameters, initial and boundary conditions. Afterwards, two periods of 187 and 387 days are studied, respectively. A satisfactory agreement is obtained between the calculated and measured results of soil temperature and volumetric water content variations. Furthermore, several suggestions are proposed for the collection of input data in case of some missing information.

Chapter 1: Literature review

1.1 Influence of climate change on geotechnical constructions

The climate change is occurring globally, posing problems for the society, human health and ecosystems. The related studies have revealed the changes in frequency and intensity of climate in different regions, leading to floods, droughts, heat waves, windstorms, etc. The climate change can have also potential impacts on water resources, agriculture, food security, human safety, geotechnical and geo-environmental constructions (Várallyay 2002, 2007, 2010; Barnett et al. 2005; Harley et al. 2006; Várallyay and Farkas 2008; Harnos and Csete 2008; Tubiello et al. 2008; Yusuf and Francisco 2009; Harris et al. 2009; Koetse and Rietveld 2009; Nikulin et al. 2011; EEA 2012). In the field conditions, geotechnical constructions are unavoidably subjected to the climate change. In some cases, disruption, financial lost and casualties can occur, along with significant damages. It is thus a great challenge for geotechnical engineers to propose appropriate solutions based on the knowledge of the thermo-hydro-mechanical behavior of soils under the effect of climate change. Basically, the effect of climate change on constructions is dealt with through consideration of the interaction between soil and atmosphere. That is why this topic attracts more and more attention of researchers (McKeen and Johnson 1990; Wilson et al. 1994, 1995, 1997; Hignett et al. 1995; Blight 1997, 2002, 2003, 2009; Potts et al. 1997; Toll et al. 1999, 2011, 2012; Dehn et al. 2000; McCarthy et al. 2001; Toll 2001; Nelson et al. 2002; Rahardjo et al. 2002, 2005, 2013; Várallyay 2002, 2010; Alonso et al. 2003; Cui et al. 2005, 2010, 2013b; Dixon et al. 2006; Gitirana et al. 2006; Chowdhury and Flentje 2007; Bittelli et al. 2008; Gens 2010; Tang et al. 2010, 2011; Smits et al. 2011; Al Qadad et al. 2012; Lee and Khairoutdinov 2012; Smethurst et al. 2012; Daniel et al. 2014; Rianna et al. 2014; Vardon 2015; Bárta et al. 2016)

Blight (1997) indicated that the interaction between the atmosphere and the earth can be rapid and catastrophic, leading to the failure of structures such as dams and bridges, loss of life and widespread environmental devastation. On the other hand, it can also be slow and insidious,

being destructive and costly in long term, for instance, the problems caused by the swelling or shrinking of clay in shallow foundations of buildings. The major hydraulic and thermal factors characterizing the climate changes can be classified in four categories: increasing intense rainfalls that cause flooding, soil erosion and hydro-mechanical failure constructions; increasing drought events that lead to soil desiccation; temperature rise that leads to soil drying and temperature drop that causes soil freezing.

Many geotechnical problems are observed during heavy rainfalls, e.g. slope failures frequently occurred all over the world (Brand 1984, 1992; Lim et al. 1996; Toll et al. 1999, 2011, 2012; Toll 2001; Rahardjo et al. 2002, 2005, 2013; Collins and Znidarcic 2004; Jan et al. 2016; Suradi et al. 2016). In the studies of the effect of rainfall on the deformation and stability of slope, several aspects are involved: field monitoring of pore-water pressure (Chipp et al. 1982; Sweeney 1982; Krahn et al. 1989; Fredlund and Rahardjo 1993; Lim et al. 1996; Rahardjo et al. 2002, 2005, 2013; Ng et al. 2003; Li et al. 2005; Toll et al. 2011, 2012), numerical investigation of soil pore-water pressure distribution (Potts et al. 1997; Alonso 2003; Ferrari et al. 2009; Rouainia et al. 2009) and further evaluation of slope displacement and sustainability (Dehn et al. 2000; Alonso et al. 2003; Dixon et al. 2006; Dijkstra and Dixon 2010; Laloui et al. 2016). Besides, it is specified that soil hydro-mechanical properties also play an essential role in the geotechnical problems induced by rainfalls (Alonso et al. 2003; Hughes et al. 2007; Ferrari et al. 2013).

On the other hand, the evaporation effect on soil performance has been paid particular attention in some geotechnical problems (Wilson 1990; Wilson et al. 1993, 1994, 1995; Blight 1997; Yanful and Choo 1997; Yanful et al. 1999, 2003; Rykaart et al. 2001; Yang and Yanful 2002; Swanson et al. 2003; Cui et al. 2005, 2010, 2013b; Gitirana 2005; Weeks and Wilson 2006; Gitirana et al. 2006; Rayhani et al. 2007; Gerard et al. 2008, 2010; Ta 2009; Tang et al. 2010, 2011, 2012; Leung and Ng 2013; Song 2014; Song et al. 2014). For instance, the performance of soil cover system in a waste disposal site (Wilson et al. 1993; Yanful and Choo 1997; Yanful et al. 1999, 2003; Yang et Yanful 2002; Swanson et al. 2003; Gerard et al. 2008), the pore-water

pressure distribution within tailings impoundment (Rykaart et al. 2001) and the seepage problems within soil layers (Gitirana 2005; Gitirana et al. 2006; Gerard et al. 2008; Leung and Ng 2013) are strongly affected by the presence of evaporation. In particular, soil desiccation cracks and settlement induced by the decreasing of water content can also occur during the evaporation in clayey soils (Rayhani et al. 2007; Ta 2009; Tang et al. 2010, 2011, 2012; Song 2014; Song et al. 2014). The study by Rahardjo et al. (2013) indicates that various problems related to evaporation are mainly attributed to the increase of negative pore-water pressure and soil shear strength within the soil layer along with the decrease of soil water content. Thereby, it is further suggested to consider evaporation in the analysis of the slope stability problems, the design of dams, the construction of mining waste cover systems, etc.

Even though the variation of air temperature does not cause adverse effects on soil performance directly, it governs several coupled processes such as evapotranspiration, soil shrinkage and desiccation, vegetation growth or loss (Vardon 2015). During a drought period, elevated soil temperatures and low soil moisture levels can lead to the reduction of soil effective stress and soil strength (Uchaipichat and Khalili 2009; Alsherif and McCARTNEY 2015). In the study of the performance of earthen levees under extreme drought conditions by Robinson and Vahedifard (2016), it was identified that the weakening process of earthen levees during the drought period is related to soil strength reduction, soil desiccation cracking, land subsidence, surface erosion and microbial oxidation of soil organic carbon. Moreover, this weakening process can be similar in other drought-stricken geotechnical infrastructures including embankments, roads, bridges, building foundations and pipelines (Gitirana 2005; Hughes et al. 2009; Toll et al. 2012; Daniel et al. 2014; Glendinning et al. 2014; Bárta et al. 2016; Robinson and Vahedifard 2016). Therefore, the investigation of the effect of drought-induced weakening process is essential in the short and long term behavior of earth constructions.

In terms of temperature drop, related studies mainly focus on frozen ground and freezing–thawing phenomena (Nelson et al. 2002; Gruber et al. 2004; Gruber and Haeberli 2007; Yue 2008; Harris et al. 2009; Thomas et al. 2009a; Gens 2010; Schoeneich et al. 2011; Wang et al.

2014). Gens et al. (2010) pointed out that the process of soil freezing exhibits a certain degree of complexity. As the soil temperature drops to 0 °C, liquid water becomes frozen with the appearance of liquid water/ice interfaces in soil (Figure 1. 1). The ongoing frozen process will result in the increase of soil suction, leading to some potential problems. On the other hand, much attention has been paid to the frost heave accompanied with soil freezing-thawing, which leads to the instability problems of infrastructures in permafrost regions (Nelson et al. 2002; Gruber 2005; Gruber et al. 2004; Gruber and Haeberli 2007; Harris et al. 2009; Wang et al., 2014). As stated by Schoeneich at al. (2011), the common problem in permafrost areas is the local ground movements. It is a complex process, including horizontal downslope movements related to the creep of permafrost bodies and vertical settling movements induced by the melting of ice bodies and/or interstitial ice, etc. Furthermore, these movements may cause problematical variations of soil parameters and arise corresponding damages, hence threatening the stability of buildings and infrastructures.

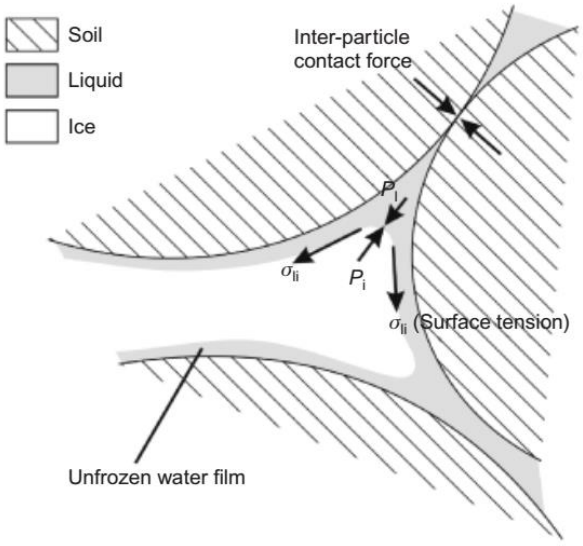


Figure 1. 1. Schematic arrangement of solid phase, unfrozen water, ice and interfaces in a frozen soil (Gens et al. 2010)

In the case study about the impact of climate change on pavement performance by Daniel et al. (2014), the increasing precipitation and flooding events can cause the increase of moisture content of the granular layers under the pavement surface, weakening the pavement base and

subgrade and hastening the failure of the whole pavements structure. Besides, the appearance of drought may lead strength reduction and desiccation cracking of pavement/soil. On the other hand, higher temperature can decrease the stiffness of asphalt concrete, increasing rutting susceptibility. Moreover, the freeze/thaw cycles may potentially increase the thermal fatigue cracking of pavement/soil, further leading its damage. This representative case shows that the variations of climate conditions (rainfall and drought, temperature rise and drop) are complex and their effects on pavement/soil are difficult to be determined: these climate terms interact and appear synchronically, and the behavior of pavement/soil is normally affected by more than one climate factor.

The common factors involved in the interaction between soil and atmosphere are presented in Figure 1. 2, including direct interaction factors (evaporation, solar radiation, etc.) and the possible consequences (soil erosion, desiccation, etc.).

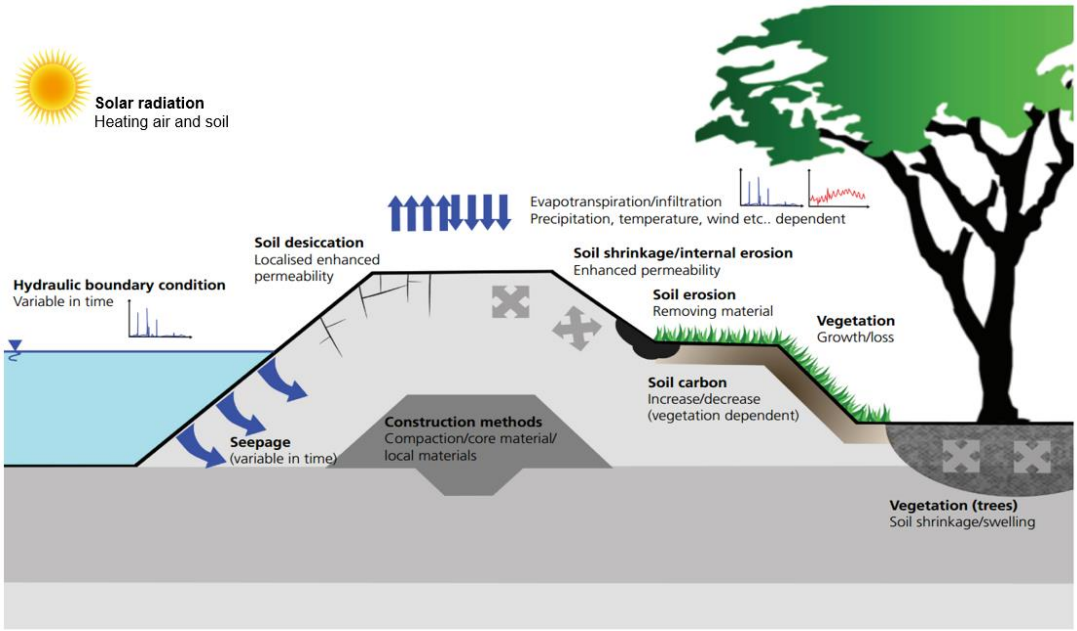


Figure 1. 2. The interactions between geotechnical infrastructure and climate (after Vardon 2015)

Additionally, the general climatic influences on existing and new geotechnical infrastructures were also assessed and summarized by Vardon (2015) (Table 1. 1), indicating the potential

failure mechanisms of geotechnical infrastructure: soil desiccation, shrinkage and displacement etc. It can be concluded that climate change involves several aspects of soil state: the variations of volumetric water content, suction, temperature, stress and strain relationship, as well as the couplings between them.

Table 1. 1. Overview of the potential impacts of climate change on geotechnical infrastructure (Vardon 2015)

Existing infrastructure		
Climate change feature	Potential impact on geotechnical infrastructure	Potential failure mode
Increased temperature	Drying	Uplift
Decreased precipitation (drought)	Soil desiccation	Piping, internal erosion, slope stability
	Soil shrinkage	Piping
	Reduction of vegetation/soil erosion	Piping, slope stability
Increased mean precipitation	Some soil erosion/loss of soil quality	Erosion, piping
	Change in water table leading to instability	Slope stability
Intense precipitation	Significant soil erosion	Piping, slope stability
	Rapid soil wetting, highly dynamic pore pressure changes potentially	Slope stability
	Flooding	Piping, internal erosion, slope stability
Freeze/thaw cycles	Loss of soil structure	Slope stability
New infrastructure		
Climate change feature	Potential impact on geotechnical infrastructure	Potential failure mode
Drought	Reduction of moisture content of fill (compaction more difficult) and mixing of fill with water is expensive	Cost, serviceability failure
Increased precipitation/ Intense precipitation	Collapsing of some fill material due to wetting	Slope stability, serviceability failure

1.2 Coupled modelling of soil behavior

The study of climate effect on soil behavior requires the information of meteorological data, as well as the understanding of coupled phenomena in soil. In this chapter, the heat flow, water flow, air flow and mechanical modelling of soil are presented respectively. As the heat flow, water flow, air flow and mechanical modelling are always coupled in unsaturated soils, the representative coupled models of unsaturated soil are presented, followed by the assessment of these coupled models.

1.2.1 Heat flow, water flow, air flow and mechanical modelling

1.2.1.1 Heat flow

In the studies of heat transfer in soils, the soil is generally assumed to be homogeneous and all process of heat transfer takes place uniformly through the soil (De Vries 1958). The heat flows in soils involve several transportation processes as follows (Farouki 1981):

1) Heat conduction

Heat conduction is the transfer by microscopic collisions of particles and movement of electrons, involving the transfer of kinetic energy at the molecular level. The molecules in warmer regions vibrate rapidly resulting in collisions with, or excitation of their colder "neighbors". In soil, heat conduction occurs in all the soil constituents (solid, water liquid/vapor and pore air), and works as the predominating heat mechanism.

2) Heat radiation

Heat radiation is the emission of energy in the form of electromagnetic waves. According to the Stefan-Boltzmann law, all bodies with temperatures above 0 °C are capable to emit energy. The temperature of the radiating body is the predominating factor in the estimation of heat radiation value: radiation flow is proportional to the fourth power of the absolute temperature. Soils can also provide radiation, emitting most of its radiation as long-wave radiation in a wavelength band between 0.5 and 30.0 μm at soil surface. Generally, it makes a negligible contribution to heat transfer in soil. For instance, the heat radiation in sand is less than 1% of the overall heat transfer under the condition with normal atmospheric temperatures (Farouki, 1981). Especially, its effect is noticeable in nearly dry gravel-size material, amounting to 10% of total heat transfer at normal temperature (Wakao and Kato 1969). Hence, radiation plays a significant role of heat transfer in dry coarse crushed-stone materials.

3) Heat convection

Heat convection refers to the transfer or movement of thermal energy in “heat-carrying” mass (e.g., water or vapor). As the dominant form of heat transfer in liquids and gases, two types of

convection exist in soil: free and forced convection. Free convection is a mass transport caused in fluids by changes in density with temperature gradients. The density of the fluid is lower at higher temperature, giving rise to the upward displacement. On the other hand, the movement of liquids and gases forced to pass through the soil pores by pressure differences is defined as forced convection. In soils under natural condition, convection through air or water is usually negligible (Farouki 1981). Nevertheless, the convection through air and water in soils facilitates the process of heat conduction (De Vries 1952; Johansen 1975).

The contribution of these three heat mechanisms in soil is affected by soil texture and degree of saturation, temperature levels, and soil structure, etc. A rough relation between different heat transfer mechanisms and soil texture and degree of saturation is presented in Figure 1. 3.

4) Evaporation-condensation process

In unsaturated soils, temperature rise may cause water evaporation, consuming latent heat through liquid-vapor transfer. Consequently, the local vapor pressure increases and the water vapor diffuses through the interconnected pores to the regions with lower vapor pressure. By contrast, latent heat is released in cooler locations through condensation.

In addition, there is a geothermal heat flux resulting from the upward heat flow from the hot interior of the Earth, containing soil temperature in a relative constant range. Meanwhile, the air temperature in daily fluctuations is normally superimposed on its seasonal cycles. Due to the diurnal and seasonal cycles, the continuous varying air temperature gradients can affect the variations of soil temperature in the near surface zone, further altering the soil composition, particularly the amount, phase and condition of water in soil (Farouki 1981).

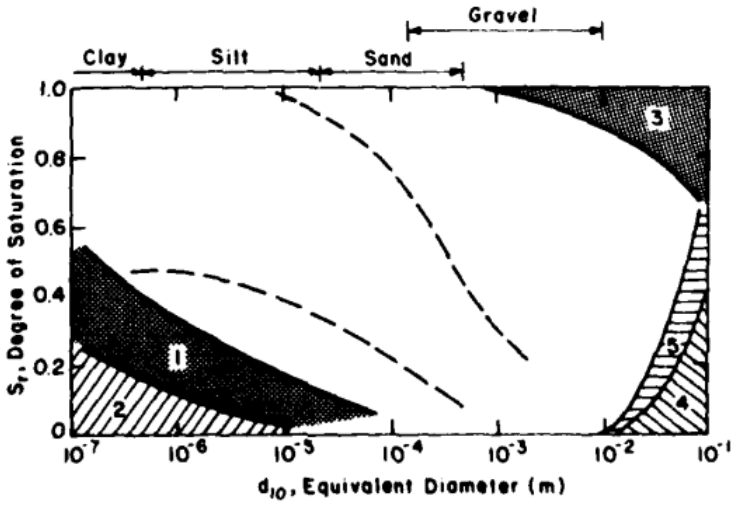


Figure 1. 3. Regions of predominant influence of various heat transfer mechanisms against soil grain size and degree of saturation. Expected variations in degree of saturation under field condition lie in the region bounded by dashed lines (after Johansen 1975 and Farouki 1981): 1-thermal redistribution of moisture; 2-vapor diffusion due to moisture gradient; 3-free convection in water; 4-free convection in air; 5-heat radiation (Farouki 1981)

1.2.1.2 Water flow

Water flow in unsaturated soils consists of two parts: liquid flow and vapor flow. Normally, the analysis of liquid flow requires a law to relate the flow rate to a driving potential. In unsaturated soils, the gradients in water content and hydraulic head have been used to describe the flow of liquid water. Water flow is mainly depending on the positive gradient of soil water content. However, water liquid can also flow from a region of low water content to a region of high water content when the variations of soil type, hysteretic effect or stress history are involved (Fredlund and Rahardjo 1993). Therefore, it is more appropriate to define the water liquid flow in terms of hydraulic head gradient, which is composed of pressure and elevation gradients. This case is also applicable for saturated soils (Darcy 1856; Buckingham 1907; Richards 1931; Childs and George 1950).

Additionally, vapor transfer in unsaturated soil is significant in the near surface zone, involving the heat and water transfer between soil and atmosphere. It is mainly attributed to the large diurnal air temperature fluctuations above the soil surface. In the field cases studied by Cahill and Parlange (1998), water vapor flux in the layer 7~10 cm below soil surface transported a significant amount of the total energy flux (up to 50%) and an appreciable amount of the total moisture flux (up to 25%). Besides, the magnitudes of the heat and water change caused by water vapor flux rise are presented in Table 1. 2 involving the results from some other field experiments. Indeed, the most important factor influencing the vapor flux is the availability of air-filled pore space for vapor diffusion. During the process of evaporation, there is less liquid water in pore space for the surface layer, increasing the air-filled porosity and hence facilitating vapor flux in the near surface zone (Bittelli et al. 2008). Moreover, Bittelli et al. (2008) presented that the vapor flux decreases as depth increases in the zone 2~7 cm below the surface in the case study, indicating that vapor flux is higher in the layer closer to the soil surface. Besides, thermal gradients also exist between the lower and the upper soil layers. However, the vapor migration through soil is merely critical in the study with apparent temperature gradient in the whole soil profile.

Table 1. 2. The magnitude of heat and water change caused by water vapor flux and the corresponding observed zones (Cahill and Parlange 1998)

Author	*Maximum magnitude of heat change caused by vapor flow (W/m^2)*	*Maximum magnitude of moisture change caused by vapor flow (cm/s)*	*Depth of observation (cm)*
Cary (1965)	…	2×10^{-6}	column
Rose (1968)	…	$2\sim6\times10^{-6}$	1~3
		$2\sim4\times10^{-6}$	3~12
Jackson et al. (1974)	…	$2\sim7\times10^{-6}$	0.5, 1
Westcot and Wierenga (1974)	80	…	0.95
	70	…	1.5
	20	…	5
	10	…	11
Cahill and Parlange (1998)	40~60	7×10^{-6}	7~10

The traditional rule of vapor flow proposed by Philip and De Vries (1957) are used widely. However, this rule was established based on the results from tests on sand, and it may over-estimate the vapor flow in highly-compacted clay (Thomas et al. 2009b). Moreover, vapor flux can also be determined as the residuals in the energy and mass balance (Cahill and Parlange 1998). In this case, the values of vapor fluxes estimated contain all the errors associated with the measurements and uncertainties of other factors in the energy and mass balances. Thereby, the selection of the approach to estimate vapor flux requires the consideration of soil type and the case conditions.

1.2.1.3 Air flow

Air flow in soils involves pore dry air and air dissolved in pore water. The former is continuous, occurring when the degree of saturation of soil is reduced to around 85% or lower (Corey 1957). When the degree of saturation is above 90%, air becomes occluded and air flow takes place in soil through diffusion in pore-water (Matyas 1967).

Therefore, different methods should be adopted to estimate the air flows in two different mechanisms: as part of bulk flow of pore air under the air pressure gradient and within the pore liquid water under the influence of pore water pressure gradient. The pore air flow due to air pressure gradient can be described by Fick's law. Besides, a modified form of Darcy's law was suggested to evaluate the air diffusion in occluded air bubbles through the unsaturated soils by Fredlund and Rahardjo (1993), with introduction of a volumetric coefficient of solubility to describe the volumetric mass of dissolved air by Henry's law.

1.2.1.4 Mechanical modelling

The mechanical behavior of soil refers to the volume change behavior and shear strength. In literature, many studies have been reported, attempting to develop the stress state of unsaturated soil for different stress paths and different soil types (Bishop 1959; Jennings and Burland 1962; Bishop and Blight 1963; Blight 1965).

Bishop (1959) proposed a tentative expression of effective stress for unsaturated soils using the notions of net normal stress ($\sigma - u_a$) and matric suction ($u_a - u_w$). Afterwards, different constitutive models have been developed. A nonlinear elastic models was proposed by Fredlund and Morgenstern (1976), describing the deformation of the soil structure and the change of water volume. An elasto-plastic model known as "Barcelona basic model (BBM)" was built by Alonso et al. (1990), being applied widely as one of the fundamental models for unsaturated soils. It is able to estimate the elastoplastic volume decrease caused by wetting mechanical compression, the change of stiffness and shear strength with suction, the volume increase upon wetting. Based on the BBM model, many developments have been done, aiming at describing the mechanical behavior of unsaturated soils. For instance, Cui et al. (1995) and Cui and Delage (1996) described the behavior of compacted silt by taking the net stress and suction as two independent stress variables. In a further attempt to study the observed irreversible swelling upon wetting for swelling soils, a conceptual model was developed by Gens and Alonso (1992). Two additional yield surfaces, one for plastic yielding caused by suction increase (SI) and the other by suction decease (SD) were defined, allowing the prediction of the irreversible shrinkage/expansion under the effect of wetting/drying cycles. Vaunat et al. (2000) developed a constitutive model to address the irreversible behavior of unsaturated soils during cyclic wetting and drying, particularly the irreversible change of degree of saturation. Wheeler et al. (2003a) introduced an elastoplastic constitutive model that fully couples the hydraulic hysteresis with the mechanical behavior of unsaturated soils and applied it for anisotropic soft clays (Wheeler et al. 2003b). In the elastoplastic model proposed by Gallipoli et al. (2003), the effect of suction and degree of saturation on soil mechanical behavior was incorporated. The elastoplastic constitutive model developed by Sheng et al. (2004) considers the hydraulic hysteresis and the irreversible deformation during cyclic drying and wetting.

Basically, soil is composed of solid, liquid water, water vapor, pore-air and dissolved air, making the description of practical flows and mechanical behavior quite complex. In many situations, the variations of these terms occur simultaneously. It is observed that heat flow and water flow are interacted continuously because of vapor flow (Philip and De Vries 1957; Luikov

1965, 1966; Dakshanamurthy and Fredlund 1981; Thomas 1985; Wilson 1990; Wilson et al. 1994; Cahill and Parlange 1998). Moreover, the hydraulic behavior of soil is intimately related to its mechanical behavior (Tang and Cui 2010a; Deng et al. 2011a, 2011b; Wang 2012; Cui et al. 2013a). Recent studies have illustrated the importance of studying the coupling of heat flow, water flow (liquid and vapor), air flow and mechanical modellings in unsaturated soil (Dixon et al. 1985, 1987, 1992, 1996, 1999; Yong et al. 1986; Thomas and He 1995; Thomas and Sansom 1995; Thomas et al. 1998; Romero et al. 1999, 2005, 2011; Lee et al. 1999; Wu et al. 2004; Lloret and Villar 2007; Uchaipichat and Khalili 2009, François et al. 2009; Tang and Cui 2010b; Cui and Tang 2013).

1.2.2 Coupled models

In literature, many coupled models have been reported, attempting to estimate soil behavior properly for different study objectives. According to the forms of these coupled models, they can be classified into four categories: simple coupled hydro-thermal models (Philip and De Vries 1957; Luikov 1965, 1966; Dakshanamurthy and Fredlund 1981; Thomas 1985; Wilson 1990; Wilson et al. 1994; Cui et al. 2005, 2010), fully coupled hydro-thermal models (Milly 1982; Thomas and King 1991, 1992, 1994; Hussain 1997; Jahangir and Sadrnejad 2012), coupled thermal-hydro-mechanical models (Thomas and He 1995, 1997, 1998; Wu et al. 2004; François et al. 2009; Thomas et al. 2009b; Wang et al. 2009; Hemmati et al. 2012), and coupled thermal-hydro-chemical-mechanical models (Olivella et al. 1996; Seetharam et al. 2007).

1.2.2.1 Simple coupled hydro-thermal models

Aiming to study soil moisture content changes under temperature gradients, Philip and De Vries (1957) proposed a method to estimate vapor transfer with consideration of the interaction between vapor, liquid and solid phases in a thermodynamic equilibrium. In this study, vapor flow was found to be a series-parallel flow through liquid “islands” located in a vapor continuum. Moreover, due to the contribution of vapor flow in the soil mass and energy transfer,

a simple hydro-thermal coupled model was further proposed. Its governing equations are constituted through the formulation based on two key variables: soil volumetric water content and temperature. However, its application to geotechnical constructions is limited because of several reasons: the effect of temperature on relative humidity was not included in the expression of vapor density gradient; the variation of temperature caused by latent heat was not considered well in this model (Nakano and Miyazaki 1979); this coupled model was proposed merely for incompressible soil.

Dakshanamurthy and Fredlund (1981) proposed a model by converting the temperature change to the change of pore air pressure. It allows the estimation of the variations of soil temperature, pore water pressure and pore air pressure using finite difference method. In this study, the vapor movement as a result of a vapor pressure gradient was not included, because the phase change between liquid and vapor in water transfer and the corresponding latent heat in heat transfer was ignored. In addition, the thermodynamics of irreversible processes were also considered as a powerful phenomenological method by Luikov (1965, 1966) for the investigation of heat and mass transfer in porous media.

Some coupled hydro-thermal models were reported with different methods of considering vapor flow. In the simple hydro-thermal coupled model proposed by Thomas (1985), the heat flux consists of heat conduction and latent heat of vapor movement, and the liquid moisture is governed by liquid water and vapor transfers. The phase conversion factor introduced initially by Luikov (1964) was adopted to express the vapor flow. When the phase conversion factor equals “1”, it means moisture transfer occurs in the form of vapor. When the phase conversion factor equals “0”, moisture transfer occurs only as a result of liquid transfer. Specifically, the mass of vapor was assumed to be negligible in comparison with the mass of liquid.

In the coupled hydro-thermal model proposed by Wilson (1990) and Wilson et al., (1994), the vapor flow was determined by combing the change of vapor mass due to both diffusion and advection expressed using Fick's Law (Philip and De Vries 1957; De Vries 1975; Fredlund and Dakshanamurthy 1982). Meantime, the vapor pressure was estimated using the widely accepted

thermodynamic relationship given by Edlefsen and Anderson (1943). In this study, the vapor pressure at the soil surface was estimated, allowing the further estimation of actual evaporation. Furthermore, the estimated evaporation was validated successfully by the measurements in column drying tests (Wilson 1990). This coupled hydro-thermal model was applied by Cui et al. (2005, 2008) with consideration of the atmosphere conditions, analyzing the soil hydro-thermal behavior under climate effect.

Overall, the different simple coupled hydro-thermal models allow the evaluation of soil hydro-thermal behavior with different assumptions. Based on the proposed models (Philip and De Vries 1957; Thomas 1985; Wilson 1990; Wilson et al. 1994), the generalized forms of water and heat governing equations can be written, as follows:

$$C_\theta \frac{\partial \theta}{\partial t} = \nabla \cdot \left(D_\theta \nabla \theta \right) + \nabla \cdot \left(D_{\theta T} \nabla T \right) + L_\theta \frac{\partial K}{\partial y} \tag{1.1}$$

$$C_T \frac{\partial T}{\partial t} = \nabla \cdot \left(D_T \nabla T \right) + \nabla \cdot \left(D_{T\theta} \nabla \theta \right) + L_T \frac{\partial K}{\partial y} \tag{1.2}$$

where the volumetric water content θ can be replaced by the hydraulic head φ; the parameters C_θ, C_T, D_θ, $D_{\theta T}$, D_T, $D_{\theta T}$, L_θ, L_T have different expressions in the simple coupled hydro-thermal models introduced above.

In the coupled hydro-thermal model proposed by Philip and De Vries (1957) and Thomas (1985), the dependent variables are soil moisture content and temperature. However, the soil hydraulic head and temperature were adopted by Wilson (1990) for building another coupled hydro-thermal model. Compared with the former model (moisture content based formulations), the latter (hydraulic head based approach) has several distinguished advantages (Thomas and Sansom 1995):

1) Compatibility with the current approaches when the stress/strain behavior of unsaturated soil has been involved;
2) The ability to analyze both saturated and unsaturated conditions;

3) The good simulation using the finite element method, the problem of moisture discontinuity at soil boundaries in heterogeneous soil conditions being avoided (Hussain 1997).

Thereby, it can be inferred that the model depending on hydraulic head and temperature has the theoretical superiority of numerical results than the models depending on moisture content and temperature.

Moreover, merely the moisture content $\theta(\varphi)$ is set on the left of the governing equation for moisture flow, and the temperature T on the left of the governing equation of heat flow. Thereby, the variations of soil moisture content and temperature are not interacted synchronously in the simple coupled hydro-thermal models. A fully coupled hydro-thermal model needs to be developed for better describing the soil hydro-thermal behavior.

1.2.2.2 Fully coupled hydro-thermal models

The hydraulic head and temperature were selected as the dependent variables in the fully coupled hydro-thermal model developed by Milly (1982). Due to the accommodation of the concepts of hysteresis and inhomogeneity of soil properties, this new model has served as a general mathematical derivation of coupled heat and moisture flow in porous media.

Afterwards, a fully coupled hydro-thermal model was proposed by Thomas and King (1991) for non-deforming materials without considering air flow. In the study by Thomas and King (1991, 1992), the performance of this coupled model with and without considering the gravitational effect were presented, indicating the significance of gravitational effect on soil hydro-thermal behavior. However, no further comparison with experimental work was conducted. In the numerical calculation, finite element method was applied to describe the spatial variations and finite difference time-stepping scheme for the transient behaviors. Moreover, a further verification work of this model in two-dimensional cases was presented by Thomas and King (1994). Even though a good agreement between the simulated and experimental temperature variations was obtained, no further information about the comparison of volumetric water content results was provided.

For the fully coupled hydro-thermal models, they were applicable for the non-deformable cases (Milly 1982; Thomas and King 1991). The generalized forms of moisture and heat governing equations in these models can be written as:

$$C_{\varphi}\frac{\partial \varphi}{\partial t}+C_{\varphi T}\frac{\partial T}{\partial t}=\nabla\cdot\left(D_{\varphi}\nabla\theta\right)+\nabla\cdot\left(D_{\varphi T}\nabla T\right)+L_{\varphi}\frac{\partial K}{\partial y} \tag{1.3}$$

$$C_{T\varphi}\frac{\partial \varphi}{\partial t}+C_{T}\frac{\partial T}{\partial t}=\nabla\cdot\left(D_{T}\nabla T\right)+\nabla\cdot\left(D_{T\varphi}\nabla\theta\right)+L_{T}\frac{\partial K}{\partial y} \tag{1.4}$$

where, C_{φ}, $C_{\varphi T}$, $C_{T\varphi}$, C_{T}, D_{φ}, $D_{\varphi T}$, D_{T}, $D_{\varphi T}$, L_{φ}, L_{T} have different values in the fully coupled hydro-thermal models introduced above. Unlike in the simple coupled hydro-thermal model, both hydraulic head φ and temperature T can be observed on the left of the governing equations of moisture and heat flow in the fully coupled hydro-thermal models. It means that these two variables are influenced by each other.

1.2.2.3 Coupled thermal-hydro-mechanical models (Coupled T-H-M models)

As far as deformable soils are concerned, air flow and mechanical modelling need be considered in the coupled models. In literature, various coupled T-H-M models were developed to account for the soil thermal-hydro-mechanical behaviors, further estimating the soil deformation.

Air flow was considered by Thomas and Sansom (1995) to build a new theoretical formulation for unsaturated soils in three-phases (air, liquid, solid). In this study, a mechanistic approach was adopted and constant air pressure was considered, extending the previous coupled hydro-thermal models (Milly 1982; Thomas and King 1991). In addition, Jahangir et al. (2012) improved a hydro-thermal coupled model with consideration of air low. The control equations of this coupled model were expressed in terms of volumetric water content, temperature and pore dry air pressure. Specifically, convection was considered in the heat transfer equation, forming a more general theoretical part than that in the model proposed by Thomas and Sansom (1995). Nevertheless, several parts were not well explained in this model: firstly, the latent heat

of vapor transfer was not considered in the heat transfer conservation equation; secondly, latent heat should represent the product of the vapor flux (evaporation) and latent heat of vaporization of water, rather than the sum of liquid flux and vapor flux and latent heat of vaporization of water as presented in paper. Moreover, the studied case with an internal heat source flow presented merely the variation of soil temperature, and no indication of soil hydraulic performance was provided. Overall, these two coupled models (Thomas and Sansom 1995; Jahangir et al. 2012) are suitable for the studied applications, being limited in the cases of non-deformable soils.

A new theoretical formulation employing a non-linear elastic state surface approach and elastoplastic constitutive model was developed by Thomas and He (1995), taking the volume change behavior of unsaturated soils into account. It needs to be implemented using finite element method for spatial discretization and finite difference method for transient behavior. Specifically, the elasticity theory coupled with the so-called state surface approach relating the volumetric strain to stress, suction and temperature was adopted to express the stress-strain relationship, giving satisfactory results of soil hydro-thermal-mechanical behavior. Nevertheless, due to the data-fitting techniques applied to obtain the analytical expression of the state surface, it is difficult to apply this model to other soil types. A non-linear elastic approach and an elasto-plastic constitutive model were accommodated by Thomas and He (1997) and Thomas and He (1998), constituting coupled T-H-M models that provide better performance in describing the soil T-H-M behavior.

Correspondingly, a geo-environmental software (COMPASS) was proposed (Thomas and He, 1997) and developed by GRC (Thomas et al. 2009b) incorporating these coupled T-H-M models. This tool has the ability to analyze coupled heat, moisture (vapor and liquid), air pressure, and mechanical response of unsaturated soils. Further extensions of the coupled T-H-M models were conducted for different engineering cases, including extreme temperature behavior such as freezing and thawing of ground, impact of temperature beyond 100°C and vapor flow in compacted clays (Thomas and Rees 2009; Thomas et al. 2009a, 2009b). Nevertheless, most of

these applications were related intimately to the estimation of soil thermal performance, being lack of further study of soil hydraulic behavior.

A thermo-hydro-mechanical coupled model for unsaturated soil was proposed by Gatmiri and Delage (1997) and Gatmiri and Arson (2008). It was expressed with dependent variables: soil temperature, air and water pressure, and displacement. Hemmati (2009) extended this model with consideration of soil-vegetation-atmosphere interactions. In their studies, the effect of soil-vegetation-atmosphere interactions were accounted for through the boundary conditions (Blight 1997).

François et al. (2009) investigated a thermo-hydro-mechanical finite element approach with a thermo-plastic constitutive model. Their results present the good performance of the model in describing the thermo-hydro-mechanical behavior of clay submitted to thermal loading. Furthermore, it appears that it is necessary to perform adjustment of soil parameters governing the thermal and hydraulic diffusions in Boom Clay to obtain the agreement between numerical simulation and experiment data.

1.2.2.4 Coupled thermal-hydro-chemical-mechanical models (Coupled T-H-C-M models)

Olivella et al. (1996) took salt condensation of water into consideration in a coupled T-H-C-M model. The numerical solution of this coupled T-H-C-M model was conducted by finite element in space and finite differences in time. Satisfactory simulation results were obtained in terms of soil displacements, liquid pressure, gas pressure, temperature and salt content. Seetharam et al. (2007) studied the geochemical interactions in unsaturated soil and developed another coupled T-H-C-M model based on the coupled T-H-M model proposed by Thomas and He (1998). Satisfactory estimations of soil T-H-C-M behavior were obtained by these two models in the studied cases.

1.2.3 Evaluation of coupled models

The conditions/limitations of each coupled model introduced above are listed in Table 1. 3. The assessment of the limitations of these coupled models illustrate that each coupled model can be applicable for specific situations. Therefore, according to the study goal, suitable coupled model can be selected among the existing ones with consideration of the applicable conditions or be further developed with specific assumptions.

It is noticed that the effect of climate changes has been seldom taken into account in the coupled models. Moreover, none of the above-mentioned studies addressed soil hydro-thermal behavior in details for the real two-dimensional cases even though it is essential for some earth constructions as embankments. Thereby, considerable work is still required to develop fully coupled models and to validate such models against long term laboratory/field measurements.

1.3 Interaction between soil and atmosphere

In section 1.1, the importance of studying the climate effect on soil performance has been stated. On the other hand, various coupled models showing soil hydro/thermal/mechanical behaviors are presented and their applicable conditions are reported in section 1.2. Concerning the implemented approach, the estimation of soil coupled behavior under climate effect is then discussed in terms of experimental and numerical investigations.

1.3.1 Experimental investigations

Through field monitoring of soil responses by various sensors, direct observation of soil hydro/thermal/mechanical behavior can be done under the climate effect. In literature, the related studies have been conducted in two different conditions: laboratory and field conditions.

Table 1. 3. Conditions/limitations of different coupled models

Model	*Author*	*Conditions & limitations*
Simple coupled hydro-thermal model	Philip and De Vries (1957)	1. The effect of temperature on relative humidity is not included; 2. The effect of latent heat on the variations of temperature is not well considered.
	Luikov (1965, 1966)	1. The equation of irreversible thermodynamics related to the fluxes and thermodynamic forces is adopted, making the coupled model complicated to use.
	Dakshanamurthy and Fredlund (1981)	1. Vapor movement as a result of vapor pressure gradient is not presented. The study assumes that the vapor pressure above the boundary of considered layer is the same as the vapor pressure within the soil; 2. Latent heat is not considered in both heat flow and conservation equations.
	Thomas (1985)	1. The vapor-liquid phase change is defined by a conversion factor.
	Wilson et al. (1994)	1. Correction factor for vapor diffusion is used to define vapor-liquid phase change.
Fully coupled hydro-thermal model	Milly (1982)	1. The model is based on variables of hydraulic head (suction) and temperature; 2. The model is able to simulate highly coupled, hysteresis-affected and nonlinear problems.
	Thomas and King (1991)	1. The model is based on variables of hydraulic head (suction) and temperature; 2. The ratio of microscopic to macroscopic temperature gradient was introduced.
Coupled T-H-M model	Thomas and Sansom (1995)	1. Air flow and vapor flow as part of the bulk flow of air are both considered.
	Jahangir et al. (2012)	1. Air flow is considered; 2. The lant heat is not considered in heat conservation equation and is not expressed properly in heat flow equation;
	Thomas and He (1995)	1. The mechanical theory is considered by elasticity model combing with the state surface approach.
	Thomas and He (1998)	1. The mechanical theory is considered by elastoplastic constitutive model.
	Hemmati (2009)	1. The vegetation influence in soil-atmosphere interaction is considered.
Coupled T-H-C-M model	Olivella et al. (1996)	1. Specific saline media is considered as the studied chemical material in soil.
	Seetharam et al. (2007)	1. Chemical effect is expressed in a general form and incorporated into the T-H-M soil model of Thomas and He (1998).

1.3.1.1 Laboratory tests

Aiming to study soil behavior under evaporation, simple column drying tests were designed (Wilson 1990; Wilson et al. 1994; Yang and Yanful 2002; Lee et al. 2003; Smits et al. 2011; among others). The related studies indicate that evaporation results in continuous decreasing of soil volumetric water content and temperature of soil. The values of soil volumetric water content and temperature in the region near the soil surface decrease more quickly than those in deeper regions. Meantime, it is widely recognized that the movement of water vapor is closely coupled to the thermal process in the shallow subsurface below the soil-atmosphere interface. However, merely one-dimensional soil hydro-thermal behavior under the evaporation effect was specified in these studies.

Besides, different rainfall systems were designed and applied in the laboratory to study the soil behavior: the variations of soil moisture and suction, runoff and erosion, breakdown of soil aggregates, sediment transfer, chemical movement and slope stability induced by rainfall (Hignett et al. 1995; Regmi and Thompson 2000; Tohari et al. 2007; Pérez Latorre et al. 2010; Voulgari 2015; among others). The results reveal a strong connection between the variations of soil moisture content and soil behavior. Voulgari (2015) implemented a slope model in the laboratory to study the successive failures of soil. The experimental results illustrate that along with a short-term of rainfall, moisture content increases and soil strength decreases, leading to the appearance of vertical cracks in slope and the development of significant vertical deformations. In the test conducted by Tohari et al. (2007), the occurrence of landslide was initiated by the development of an unstable area near the slope toe, along with the formation of a seepage area. It is pointed out that the volumetric moisture content in the slope region where localized failures initiated approaches a nearly saturated value. Meantime, the major portion of soil slopes involved in the overall instability stay in unsaturated state. Moreover, a prediction model of slope failures was proposed by Tohari et al. (2007) based on the observed moisture content response of the slope models.

The wind tunnel system was developed with the controlled climate conditions (wind speed,

radiation, air temperature and relative humidity) in several studies (Yamanaka et al. 1997, 2004; Komatsu 2003; Yuge et al. 2005; among others). The representative laboratory experimental set-up of wind tunnel system is presented in Figure 1. 4. It was developed to verify the accuracy of different evaporation models. The soil surface evaporation was recorded normally by the weighing micro-lysimeter. However, little attention has been paid to the corresponding soil behavior.

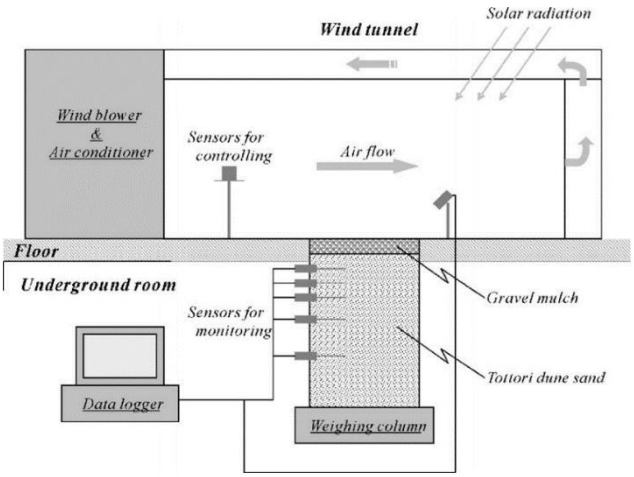


Figure 1. 4. Experimental set-up of wind tunneling for evaporation investigation (Yamanaka et al. 2004)

In addition, environmental chamber tests were conducted to study the soil performance under complex atmosphere conditions (radiation, wind speed, water table, air temperature and relative humidity) (Watanabe and Tsutsui 1994; Yanful and Choo 1997; Mohamed et al. 2000; Aluwihare and Watanabe 2003; Ta 2009; Cui et al. 2013b; Song et al. 2013, 2014; Song 2014). Specifically, a device ‘‘open chamber’’ was developed by Aluwihare and Watanabe (2003) for determining evaporation from bare soil in the climate conditions similar to the filed situations (Figure 1. 5). Comparison between the results obtained in the laboratory and in the field indicates that this equipment is suitable for estimating evaporation under different field conditions, except for the periods of drastic change in atmospheric conditions. The soil behavior under evaporation was poorly instrumented and discussed even though the estimation of actual evaporation was well analyzed (Song 2014). Recently, a new large-scale environmental

chamber was developed by Ta (2009) and Cui et al. (2013b) for studying soil behavior under evaporation. The evaporation process was activated by the heated air flow passing through the soil surface in the environmental chamber. In the tests conducted by Song (2014) to study the sand and clay performance, the variations of soil temperature, volumetric water content and suction were monitored instantaneously, accompanied by synchronous recordings of atmosphere conditions. Moreover, comparative tests with different speeds and temperatures of air flow were conducted, enabling the further analyses of different soil performance.

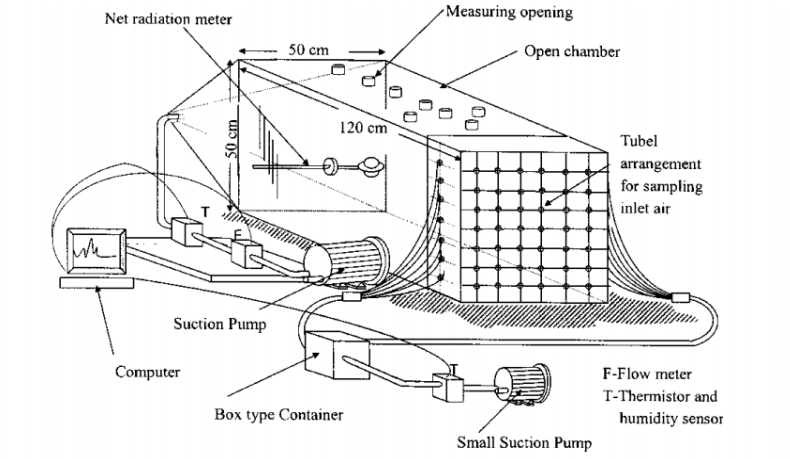


Figure 1. 5. Schematic illustration of the device for measuring evaporation by Aluwihare and Watanabe (2003)

Among these experimental investigations, the environmental chamber has distinguished advantages as compared with others:

1) Unlike the simple column drying test, all atmosphere conditions: radiation, wind speed, water table, air temperature and relative humidity can be considered;
2) Unlike the wind tunneling system, larger soil sample in environmental chamber can be considered, diminishing the lateral border effect on soil behavior and allowing more space for the settlement of monitoring sensors.

1.3.1.2 Field tests

Field tests to investigate climate effect on soil behavior have been presented widely in literature (Rose 1968; Jackson 1973; Kustas and Daughtry 1990; Cahill and Parlange 1998; Schelde et al. 1998; Rahardjo et al. 2002, 2005, 2008; Heusinkveld et al. 2004; Cui et al. 2005, 2010; Cui and Zornberg 2008; Suradi et al. 2016). The field meteorological condition includes rainfall, solar radiation, air temperature, wind speed and relative humidity, etc. The responses of soil behavior under field atmosphere condition normally cover: the variations of soil temperature, volumetric water content/suction, surface movement, heat fluxes, etc.

In the field, the soil performance for a period of six days was studied by Rose (1968), with monitoring of the variations of soil water content and temperature in the top 15 cm zone. Similarly, diurnal changes of soil water content at the top 10 cm zone during drying were investigated by Jackson (1973). This study elucidates the effects of meteorological parameters on the evaporation from bare soil. The water transfer process in a bare soil was examined by Cahill and Parlange (1998) using subsurface monitoring of soil temperature and water content, illustrating the importance of vapor flux during soil-atmosphere interaction. Additionally, the coupled transport of heat and water flux was taken into consideration to evaluate the interactions between liquid and vapor flows in a bare soil by Schelde et al. (1998). Through the comparison between the results by field test and numerical analyses, the importance of vapor flow was confirmed. Rahardjo et al. (2002, 2005, and 2008) investigated the response of a residual soil slope to rainfall. By considering rainfall in natural and simulated conditions, his study investigates the slope runoff in response to rainfall, presenting the changes of pore-water pressure (soil water content) and the corresponding redistribution.

In terms of heat transfer during soil-atmosphere interaction, different approaches to measure soil surface heat flux were examined by Kustas and Daughtry (1990), Heusinkveld et al. (2004) at different sites. As the field techniques were proposed allowing the measurements of sensible heat flux (Wang and Bras 1998; Voogt and Grimmond 2000) and latent heat flux (Bowen 1926), it is also possible to calculate the soil heat flux based on the energy balance at the soil-

atmosphere interface. These studies focus on the measurements or calculations of heat fluxes during soil-atmosphere interactions and the variations of soil temperature. Less attention has been paid to the variations of soil water content.

Based on the studies introduced above, it is concluded that the soil temperature and volumetric water content can be measured by buried sensors at the targeted positions during the studied period, but impossible for the positions without measurements and for longer period. Besides, unpredictable problems during sensors' operation in the long term period may happen, calling for uneconomic expense. Specifically, for the near soil surface region which is sensitive to soil-atmosphere interaction, direct monitoring of volumetric water content and especially suction meet some challenges (Cui and Zonberg 2008). Furthermore, the study about the coupled hydro-thermal behavior of soil is difficult to be analyzed merely with experimental investigation, presenting a challenge to evaluate the heat and water transfer during soil-atmosphere interactions.

1.3.2 Numerical investigation

In literature, various numerical investigations have been reported involving soil-atmosphere interactions. Several representative codes are shown as follows.

FLUX code (Wilson 1990)

As introduced in section 1.2.1, a simple coupled hydro-thermal model was built by Wilson (1990). In order to investigate the soil hydro-thermal behavior in the column drying test, a simple computer program "FLUX" written in Fortran code was proposed with explicit finite difference formulation. The validation of this numerical approach was conducted for heat flux, water flux and vapor flux, respectively: it was verified by the analytical solution for one-dimensional conductive heat transfer in a homogeneous solid for the heat flow; it was confirmed by a commercial program "PC-SEEP" for the moisture flow; it was validated by the measurements in the column drying test for the vapor flow. After validation, the boundary conditions and soil parameters need to be assumed correctly. In the calculation, the soil water

potential and temperature at the top and bottom nodes will be gotten firstly, followed by the estimation of their values at the connected interior nodes. After updating all nodes at each time step during the numerical calculation, the vapor pressure at soil surface can be used to calculate evaporation.

Furthermore, soil-atmosphere interaction was also studied by Cui et al. (2005, 2010) using the coupled model proposed by Wilson (1990) and the soil-atmosphere interaction theory (Blight, 1997). The numerical investigation was conducted by finite difference scheme method in one dimension. For the studied experimental embankments, a satisfactory agreement was obtained between the estimation and measurement results of soil water content and temperature at different depths.

θ-STOCK code (Hemmati 2009; Hemmati et al. 2012)

A two-dimensional model to study soil-vegetation-atmosphere interaction was developed through θ-STOCK finite element program. Standard meteorological data, soil characteristics and canopy parameters were used in the numerical calculation. Based on the mass and energy balances, soil heat and water (evaporation/infiltration) fluxes at soil surface can be determined. Afterwards, the variations of soil temperature, water content or suction during the studied period can be calculated. Furthermore, this coupled model makes it possible to predict the settlement using only the soil physical properties, e.g. soil water retention and state surface.

The flow chart of θ-STOCK code is presented in Figure 1. 6, presenting the estimation of boundary conditions depending on both atmosphere condition and soil surface properties. Hemmati (2009) implemented the study of soil-vegetation-atmosphere interaction though θ-STOCK code, giving the satisfactory estimation of daily variations of soil temperature, water content and displacement.

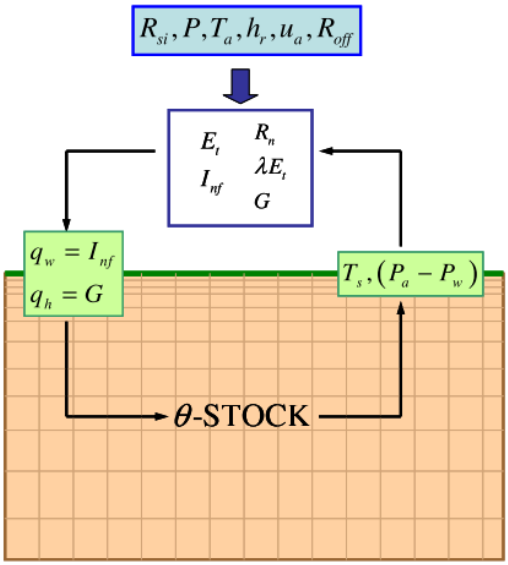


Figure 1. 6. The flow chart of θ-STOCK code (Hemmati et al. 2012)

TRUCHAMP code (Hussain 1997)

Serving for preliminary design of nuclear waste repository, a numerical solution namely "TRUCHAMP" was developed by Hussain (1997). The governing equations proposed by Thomas and King (1991) were formulated by the integrated finite difference method, and applied in the code "TRUCHAMP" to estimate the coupled heat and moisture flow of unsaturated soils. This code was used to simulate the one-dimensional heat and moisture flows in the soil surrounding nuclear waste (Hussain 1997).

HYDRUS code (Šimůnek et al. 1999)

As one of the mostly used models for soil cover design in the United States, the code "HYDRUS" is able to simulate the transport of water, solute and heat in an unsaturated porous media in one/two/three-dimensional conditions (Šimůnek et al. 1999, 2005, 2006, 2008). Saito et al. (2006) presented a numerical calculation of coupled water, vapor and heat transfer in soil using HYDRUS-1D code, allowing a flexible way of using various types of meteorological data to evaluate the water and heat transfers at the soil-atmosphere interface. It is able to estimate all relevant variables such as soil volumetric water content, temperature and liquid water, water vapor, and heat fluxes by considering the mass and energy balances during the soil-atmosphere

interaction. However, only one-dimensional experimental work was carried out for the verification purpose, allowing the soil water content and temperature monitoring in the near soil surface region (<= 25 cm).

Additionally, the HYDRUS-2D program solves the Richards's equation for saturated-unsaturated water flow and the convection-dispersion equation for heat and solute transports. The boundary conditions in the water transport portion can adopt heat and water flux boundaries controlled by atmospheric conditions, free drainage boundary conditions, etc. It was applied by Hansson et al. (2005) to simulate water flow patterns in flexible pavements, with consideration of the subsurface flow and the surface runoff. Furthermore, the extended version HYDRUS (2D/3D) was presented by Sansoulet et al. (2008) to simulate transient spatial distributions of water fluxes in a three-dimensional domain under a banana plant.

UNSAT-H code (Fayer 2000)

"UNSAT-H" code in Fortran was initially developed at Pacific Northwest Laboratory (PNNL) in order to assess the water dynamics of agricultural land and to estimate the recharge fluxes for scenarios of waste disposal facilities (Fayer 2000). In this model, water liquid was described by Richards's equation, water vapor diffusion was described by Fick's law and sensible heat flow was written in Fourier's equation. However, the flow considered in UNSAT-H was assumed to be strictly vertical, limiting its application to one dimension.

This model has been applied to four different cases: 1-year simulation of the water dynamics in layered soil (Fayer and Jones 1990); 3-day period of the water dynamics in layered soil with consideration of heat flow (Fayer and Jones 1990); 1-year simulation of the water dynamics in sandy soil with plants (Fayer and Jones 1990); 35-year simulation of the water dynamics in sandy loam soil without plants (Fayer and Walters 1995). The results obtained illustrate that "UNSAT-H" has the ability to simulate the water balance of various protective barrier designs, to estimate the concurrent flows of water and heat, to model transpiration and to conduct multiyear simulations.

Other codes/models

The soil hydro-thermal behavior in the region near the soil surface was studied by Grifoll et al. (2005) through a general numerical model with consideration of climate effect. This model was validated by two field tests of Rose (1968) and Jackson (1973), being able to estimate soil moisture content and temperature under the effect of non-isothermal diurnal cycles. This study elucidates the significance of the various water transport mechanisms in the upper layer of soil through four kinds of water fluxes involving: diffusion and dispersion of water vapor, and convection in liquid and gas phase. Furthermore, it is specified that the dispersion transport of water vapor could be relevant (up to 35% of the total water flux) in this upper soil layer even in the case where the contribution of gas-phase convection to the overall water transport is relatively small.

A numerical model of coupled heat, water vapor and liquid water fluxes in soil was developed by Bittelli et al. (2008) to compute evaporation from bare soils. Meantime, a field trial was conducted to validate the one-dimensional numerical results. The satisfactory agreement between numerical and experimental results proves the ability of this model to estimate the variations of soil temperature and water content, and the surface evaporation during soil-atmosphere interaction. Nevertheless, the model developed is a simple coupled hydro-thermal model because merely the hydraulic head (φ) is set on the left of the governing equation for moisture flow, and the temperature (T) on the left of the governing equation of heat flow. Moreover, the specified soil hydraulic head (air entry value) is set as upper boundary condition during an irrigation period, and a variable water potential after the end of the irrigation. This limits the general application of this numerical approach.

In the study of soil-atmosphere interaction by Al Qadad et al. (2012), the developed coupled hydro-thermal model was validated using the column-drying test of Wilson (1990) and the numerical results of Gitirana et al. (2006) in terms of suction and evaporation changes. This approach can be used for the determination of drought-induced soil movement and for the assessment of possible structure damage. The results show that the presence of structures may

lead to important change in moisture distribution, particularly in the vicinity of the structure. However, no further information of soil temperature was provided in the validation.

Additionally, there are some other numerical codes giving the possibilities to do the analyses of the coupled thermos-hydro-mechanical behavior of soil with consideration of soil-atmosphere interaction, such as Vadose/W developed by Geo-Slope International Ltd., LAGAMINE by Université de Liège, CODE_BRGITH by Universitat Politécnica de Catalunya, and GEFDYN by Ecole Centrale Paris (Boldini et al. 2014). However, Boldini et al. (2014) stated that the results of these simulations are very sensitive to many parameters that are often unknown. Furthermore, the applications of these possible approaches targeting the soil-atmosphere interaction have not been reported.

1.3.3 Discussion

1.3.3.1 Comparison between experimental and numerical investigations

As presented above, experimental and numerical approaches have been developed widely to investigate the soil behavior under climate effect. Indeed, they are complementary with each other in the study of soil-atmosphere interaction:

1) The accuracy of numerical investigation needs to be verified by the results of experimental investigation;
2) The experimental investigation provides the initial conditions for the numerical investigation;
3) The variation tendency of simulation results can help detect the anomalous values in measured results.

The specific merits and drawbacks of the two methods are further concluded in Table 1. 4.

Table 1. 4. Comparison between experimental and numerical investigations

Numerical investigation	Merits	1. It can be used for long term prediction. No period limitation when initial and boundary conditions are provided; 2. It is able to provide soil performance at all points of soil; 3. It is time saving as compared with the field measurements; 4. It is cheap as compared with the payment for buying and containing sensors in the field; 5. It helps to investigate the complicated coupled soil behviour under climate effect.
	Drawbacks	1. It requires in time meteorological information to determine its boundary condtions; 2. It needs the measurements at the intial moments to set its initial condtions; 3. It needs to be conducted with some assumptions of the field conditions (for the inhomogeneity of soil, the positions of buried sensors, etc.).
Experimental investigation	Merits	1. It is capable to provide direct results of soil behavior; 2. It provides reliable data set.
	Drawbacks	1. It is normally conducted for a targeted period; 2. It may meet some unpredicted problems of sensors during the measurements; 3. It is costy for the construction and maintenance; 4. It can only provide the soil responses at the points where sensors are buried.

1.3.3.2 Further study needed in numerical investigation

Based on the numerical investigations of soil-atmosphere interaction presented above, it is concluded that several aspects require further study:

1) It is observed that some codes are designed for one-dimensional analyses: FLUX, TRUCHAMP, and UNSAT-H. In practice, the effect of lateral border conditions on soil is also significant, such as the behavior of surface cover with side slopes in the case of embankment, requiring application of numerical approach in two-dimensional conditions;
2) In terms of meteorological data, some studies adopted the daily measurements directly to study soil coupled behavior under climate effect (Cui et al. 2005, 2010; Saito et al. 2006;

Al Qadad et al. 2012; Hemmati et al. 2012). The daily information can be applied in hourly through the transformation in empirical formulas (Grifoll et al. 2005). However, little attention has been paid to the significance of hourly meteorological data in the study of soil-atmosphere interaction (Bittelli et al. 2008). Indeed, average daily meteorological information diminishes the maximum and minimum values during the whole day, limiting precise estimation of soil behavior. Hence, short time scale (hourly/half hourly) of meteorological information is suggested to be applied in the study of soil-atmosphere interaction;

3) Furthermore, concerning the applications involving soil-atmosphere interactions, the related works cover the soil behavior in long term landfill management (Hussain 1997; Khire et al. 1997), the detection of buried land mines (Šimůnek et al. 2001), the transpiration of vegetation (Fayer and Jones 1990; Blight 2003; Sansoulet et al. 2008), etc. The coupled hydro-thermal soil behavior under climate effect in two-dimensional field embankments has been rarely examined.

1.4 Conclusions

In this chapter, the effect of climate change on geotechnical constructions is presented firstly, suggesting the importance of studying the soil-atmosphere interaction. Afterwards, the coupled modelling of soil behavior and the interaction between soil and atmosphere are reviewed. The following conclusions can be drawn:

1) According to the four aspects of the main hydraulic and thermal factors that characterize the climate changes (rainfall and drought, temperature rise and drop), the general climatic influences on geotechnical constructions are assessed respectively. It appears that the variations of climate condition are complex due to the synchronal appearance of some climate terms. Besides, the climate effects on soil are difficult to be identified separately because the soil behavior can be affected by more than one climate factor. Moreover, it is observed that the soil-atmosphere interaction requires further study involving two aspects

at the same time: soil coupled behavior and soil-atmosphere interaction;

2) In terms of soil behavior, the general knowledge of heat, water liquid water, water vapor, air transfers and the mechanical modelling is reviewed. Emphasis is put on the couplings between them. Furthermore, various coupled models (simple and fully coupled hydro-thermal, coupled T-H-M, coupled T-H-C-M models) in literature are presented, classified and evaluated depending on their application conditions;
3) The soil-atmosphere interaction is investigated through experimental and numerical investigations. Through the comparison of these two approaches, their merits and drawbacks are summarized. Due to their complementarity, it is suggested to conduct both experimental and numerical investigations in the further studies of soil-atmosphere interaction;
4) None of the present studies addressed soil coupled behavior under climate effect in two-dimensional field conditions even though it is essential for earth constructions in the cases of embankments, slopes, etc. New development of numerical approach applicable for two-dimensional cases is thus needed;
5) In the studies of soil-atmosphere interaction, it is noticed that little attention has been paid to the selection of different time scales of meteorological information. Daily meteorological information was widely adopted in different studies. In fact, the meteorological information in hourly or half hourly is able to provide more precise estimations by catching the maximum and minimum values compared to daily data. Thereby, it is recommended to adopt meteorological information in short time scale (hourly/half hourly) in the further study of soil behavior under climate effect.

Chapter 2: Development of a coupled hydro-thermal numerical model for unsaturated soils

2.1 Introduction of FreeFem++ code *(Hecht 2010, 2012)*

FreeFem++ is an open source platform to solve partial differential equations based on finite element methods. It was developed at the Laboratoire Jacques-Louis Lions, Université Pierre et Marie Curie, Paris by Frédric Hecht in collaboration with other researchers (Sadaka 2012). It is written in C++ and its language is a C++ idiom. It runs on most UNIX, Window XP, and MacOS computers. The adopted version in our study is the third edition, version 3.26.

FreeFem++ code is a high level integrated development environment (IDE) for numerically solving partial differential equations (PDE) in 2-D and 3-D. It has an advanced automatic mesh generator, capable of a posteriori mesh adaptation. It has several triangular finite elements, including discontinuous elements. Also, FreeFem++ provides color display online with zooming and other features and postscript printouts.

Moreover, FreeFem++ is highly adaptive. In geotechnical and geo-environmental engineering, many phenomena involve several coupled systems, for example: fluid-structure interactions, Lorentz forces for aluminum casting and ocean-atmosphere interactions are three such coupled systems. To deal with these systems, different finite element approximations and polynomial degrees are required, possibly on different meshes. Some algorithms like Schwarz' domain decomposition method also require data interpolation on multiple meshes within one program. FreeFem++ can handle these difficulties, i.e. arbitrary finite element spaces on arbitrary unstructured and adapted bi-dimensional meshes.

The main characteristics of FreeFem++ code are cited in the full documentation of FreeFem++, and they are listed below:

1) Problem description (real or complex value) by their variational formulations, with access

to the internal vectors and matrices if needed;

2) Multi-variables, multi-equations, bi-dimensional and three-dimensional static or time dependent, linear or nonlinear coupled systems. However, the user is required to describe the iterative procedures which reduce the problem to a set of linear problems;
3) Easy geometric input by analytic description of boundaries by pieces. However, as it doesn't work as a CAD system, the user needs to specify the intersection points when two boundaries intersect;
4) Automatic mesh generator based on the Delaunay-Voronoi algorithm. The inner point density is proportional to the density of points on the boundaries (Thompson et al. 1999);
5) Metric-based anisotropic mesh adaptation. The metric can be computed automatically from the Hessian of any FreeFem++ function (Hecht 1998);
6) High level user friendly typed input language with an algebra of analytic and finite element functions;
7) Multiple finite element meshes within one application with automatic interpolation of data on different meshes and possible storage of the interpolation matrices;
8) A large variety of triangular finite elements: linear, quadratic Lagrangian elements and more, discontinuous P1 and Raviart-Thomas elements, elements of a non-scalar type, the mini-element, etc., but no quadrangles;
9) Tools to define discontinuous Galerkin finite element formulations P0, P1dc, P2dc and keywords: jump, mean, intalledges;
10) A large variety of linear direct and iterative solvers (LU, Cholesky, Crout, CG, GMRES, etc.) and eigenvalue and eigenvector solvers (ARPARK);
11) Near optimal execution speed (compared with compiled C++ implementations programmed directly);
12) Online graphics, generation of .txt, .eps, .gnu, mesh files for further manipulations of input and output data;
13) Many examples and tutorials: elliptic, parabolic and hyperbolic problems, Navier-Stokes flows, elasticity, fluid structure interactions, Schwarz's domain decomposition method,

eigenvalue problem, residual error indicator, etc;

14) A parallel version using mpi.

It is worth noting that this code has not been widely used in geotechnical engineering. Based on the characteristics of this code presented above, it appears feasible to adopt it for investigating the interaction between soil and atmosphere.

In order to validate the application of FreeFem++ code in our study, the heat flow and water flow in unsaturated soil are firstly studied, respectively. Afterwards, a simple coupled hydro-thermal soil model in literature is adopted in numerical investigation, allowing further verification of this numerical tool in the coupled cases. Finally, a fully coupled hydro-thermal soil model is developed. Furthermore, the formations of their weak forms are presented with details, providing the theoretical basis for the numerical studies presented in the following chapters.

2.2 Heat flow

As presented in Chapter 1, heat conduction, radiation and convection are three major heat transport processes in soils. Even though the contribution of these three mechanisms can be affected by temperature levels, degree of saturation, soil composition and structure, conduction is still the predominating mode of heat transfer in soils.

By considering conduction merely, one-dimensional heat flow in soil is given by Fourier's law:

$$\mathbf{q}_h = -\lambda \nabla T \tag{2.1}$$

where $\mathbf{q}_h$ (W/m^2) is the heat flux; λ (W/(mK)) is the thermal conductivity; ∇T (K/m) is the temperature gradient.

The conservation of heat energy is expressed as:

$$C\frac{\partial T}{\partial t} = -\nabla \cdot \mathbf{q} \tag{2.2}$$

where C is the soil specific heat capacity.

Therefore, by combing equation (2.1) and (2.2), the governing equation of heat flow can be written as:

$$\frac{\partial T}{\partial t} = D_H \frac{\partial^2 T}{\partial z^2} \tag{2.3}$$

where D_H (m^2/s) is soil thermal diffusivity. With equation (2.3), soil temperature variation in time and space can be analyzed.

A simple one-dimensional case is designed to verify the performance of FreeFem++ code in heat flow. The model dimension, initial and boundary conditions are shown in Figure 2. 1. The initial soil temperature of the whole column is assumed to be 14 °C. The top and bottom boundary conditions are set as 20 °C and 14 °C, respectively. In this case, soil thermal diffusivity is assumed to be constant: 0.004 m^2/s. By rewriting the governing equation (2.3) of heat flow to the weak form in FreeFem++ code, the numerical analysis of soil temperature variation can be conducted.

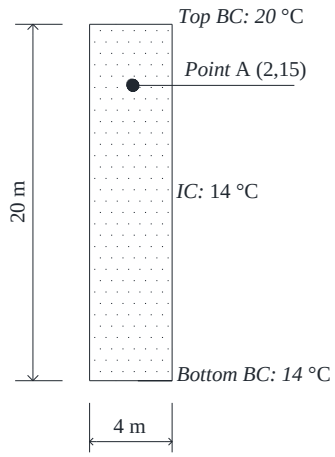


Figure 2. 1. Model details for heat flow in soil

Meanwhile, an analytical solution of the simplified heat flux equation is given by Carslaw and Jaeger (1959):

$$\frac{T-T_0}{T_s-T_0} = efrc\left[\frac{x}{\sqrt{4D_H t}}\right] \tag{2.4}$$

where,

$efrc(u) = 2\pi^{-1/2}\int \exp(-u^2)du$ is the complementary error function;

$T_0 = T(x,0)$ is the initial condition;

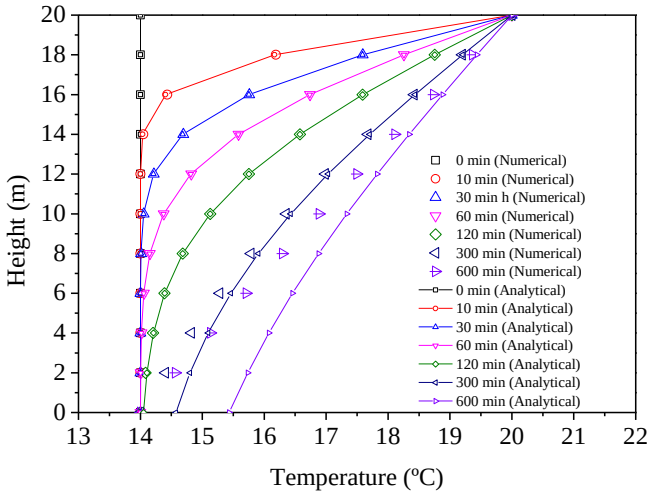
$T_s = T(0,t)$ is the top boundary condition;

$T_0 = T(\infty,t)$ is the bottom boundary condition.

Note that this analytical solution is applicable only if the one-dimensional soil column is sufficiently long so that the temperature at the other face of the column remains unchanged (at the initial temperature value T_0).

The comparison of soil temperature variations between analytical solution and simulation is presented in Figure 2. 2. Figure 2. 2a shows the soil temperature profile by two methods in different moments: t = 0, 10 min, 30 min, 60 min, 120 min, 300 min and 600 min. The soil temperature increases gradually when approaching the top boundary. A satisfactory agreement is obtained for soil temperature profile between analytical and numerical calculations at t = 0, 10 min, 30 min, 60 min, 120 min. The differences of soil temperature are obvious at the bottom of model column as time continues. For instance, the differences are about 1 °C and 2 °C at 300 min and 600 min, respectively. This is attributed to the limitation of the analytical solution, which is based on the assumption of an infinite length of column. Figure 2. 2b presents the soil temperature variation over time. The temperature variation tendencies by analytical and numerical methods are highly consistent. However, their differences appear and increase gradually as time continues.

(a)



(b)

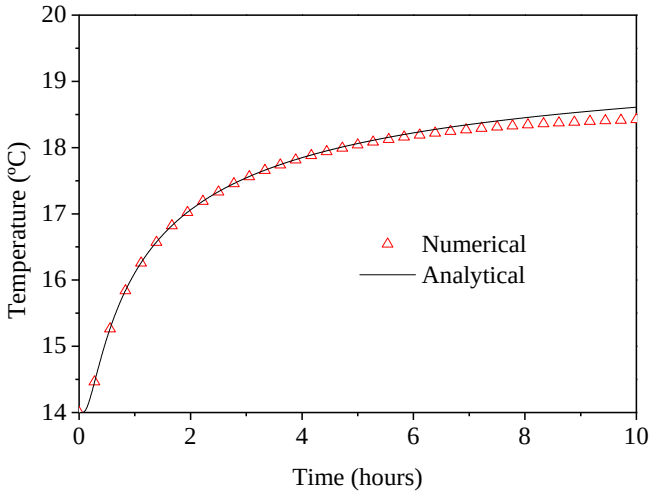


Figure 2. 2. Comparison of soil temperature between numerical simulation and analytical solution: (a) soil temperature profiles at different moments: *t* = 0, 10 min, 30 min, 60 min, 120 min, 300 min, 600 min; (b) soil temperature variation over time at Point A (2, 15)

From the comparisons made above, the following conclusions can be drawn:

1) The tendencies of soil temperature by both numerical simulation and analytical calculation are consistent during the studied period (Figure 2. 2). As time increases, the discrepancy of the bottom temperature goes up between the two methods. Moreover, the difference region is extending to the top. These differences are mainly due to the limitation of the analytical solution for the posed problem. However, the values obtained by the two methods are the

same during the initial short periods. For Point A, a similar variation mode can be observed in the results of soil temperature variations by two methods;

2) At the end of this test, a linear relationship between soil temperature and depth can be observed. It shows that the soil temperature is reaching the thermal equilibrium distribution in the soil column. Nevertheless, the analytical solution is limited to provide accurate values at the bottom of column. It is thus concluded that the numerical investigation using FreeFem++ code provides reliable results of heat flow in soil.

2.3 Water flow

As discussed in Chapter 1, fluid flow in soil requires a law to relate the flow rate to a driving potential. It is appropriate to describe water flow with hydraulic head gradient which includes the pressure and elevation effects. This is true for both saturated and unsaturated soils.

Darcy (1856) postulated that the rate of water flow through soil is proportional to the hydraulic head gradient. The one-dimensional water flow in saturated and unsaturated soil can be expressed by:

$$\mathbf{q}_w = -k_s \frac{\partial H}{\partial y} \tag{2.5}$$

where,

$$H = \frac{\varphi}{\rho_l g} + y \tag{2.6}$$

where $\mathbf{q}_w$ (m/s) is water liquid flux; ρ_l (kg/m^3) is water liquid density; φ (m) is matric suction; k_s (m/s) is the coefficient of permeability; g (m/s^2) is the gravitational acceleration constant. For saturated soils, k_s is constant for a specific soil type. Rather, it is variable depending on water content or suction in case of unsaturated soils. By assuming air pressure to be zero and by neglecting the osmotic suction, the suction term reduces to the pore water pressure in negative

values.

The conservation of water fluid mass yields:

$$\frac{\partial \theta}{\partial t} = -\nabla \cdot \mathbf{q}_w \tag{2.7}$$

where θ is the volumetric water content. Combining equation (2.5) and (2.7), the one-dimensional governing equation of water flow for coupled seepage and deformation can be written as:

$$A\frac{d\varphi}{dt} = \nabla \cdot \left(\rho_w k_s \nabla H\right) \tag{2.8}$$

where,

$$A = \rho_w n\left(\frac{\partial S_r}{\partial \varphi} + S_r \beta_r\right) \tag{2.9}$$

$$S_r = \frac{\theta}{\theta_s} \tag{2.10}$$

where S_r is the degree of saturation; n is the soil porosity; β_r is the coefficient of compressibility (Pa^{-1}).

Aiming to simulate water flow in unsaturated soil, a one-dimensional case is assumed with width of 1 m and height of 10 m. The model dimension, initial and boundary conditions are presented in Figure 2. 3. The studied case has the saturated bottom boundary condition. A constant infiltration rate of 1×10^{-6} m/s is assumed for the top boundary. The initial matric suction distribution is linear over height. The middle section A is used to record the soil matric suction profile variations at the studied moments, and Point E (0.5, 8) is selected to show the soil suction variation over the whole studied period. Moreover, the contour plot of soil initial condition is presented in Figure 2. 4.

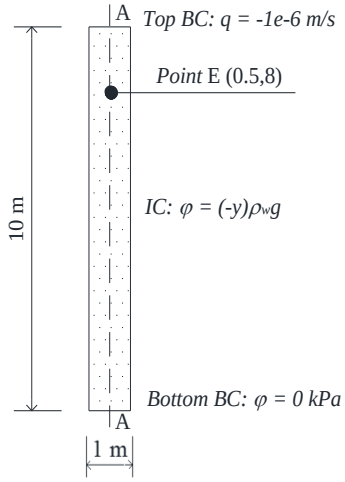


Figure 2. 3. Model details for the verification of water flow in soil

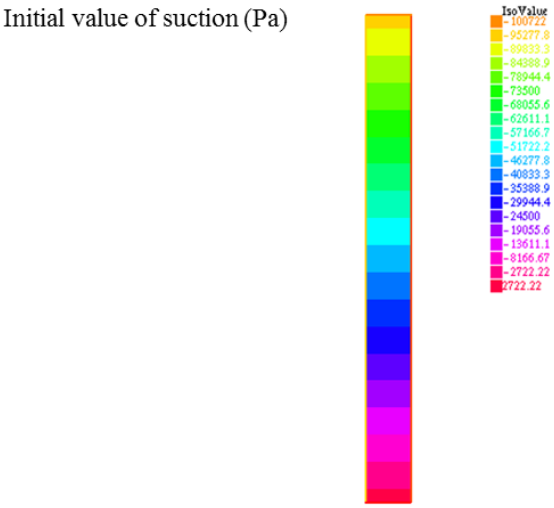


Figure 2. 4. The contour plot of soil initial condition of suction

In addition, soil parameters need to be defined specifically in the numerical investigation. For this purpose, Boltzman model (McKee and Bumb 1984) is adopted for the soil water retention curve as:

$$\theta = \begin{cases} \theta_s & when \quad -\varphi_{ae} \le \varphi \le 0 \\ \theta_s e^{\alpha_u \varphi_{ae}} e^{\alpha_u \varphi} & when \quad \varphi \le -\varphi_{ae} \end{cases} \tag{2.11}$$

The following relationship is also used:

$$S_r(\varphi)=\begin{cases}1 & when \quad -\varphi_{ae}\le\varphi\le 0\\ e^{\alpha_u\varphi_{ae}}e^{\alpha_u\varphi} & when \quad \varphi\le-\varphi_{ae}\end{cases} \tag{2.12}$$

$$\frac{\partial S_r(\varphi)}{\partial\varphi}=\begin{cases}0 & when \quad -\varphi_{ae}\le\varphi\le 0\\ \alpha_u e^{\alpha_u\varphi_{ae}}e^{\alpha_u\varphi} & when \quad \varphi\le-\varphi_{ae}\end{cases} \tag{2.13}$$

The hydraulic conductivity of soil is described by Gardner model (1958):

$$k(\varphi)=\begin{cases}k_s & when \quad -\varphi_{ae}\le\varphi\le 0\\ k_s e^{\alpha_u\varphi_{ae}}e^{\alpha_u\varphi} & when \quad \varphi\le-\varphi_{ae}\end{cases} \tag{2.14}$$

The values and physical meaning of all related soil parameters are presented in Table 2. 1.

Table 2. 1. Soil parameters for water flow analysis

Parameter	*value*	*Physical meaning (unit)*
ρ_w	1000	Water liquid density (kg/m^3)
α_u	0.043×10^{-3}	Desaturation coefficient (Pa^{-1})
k_s	1×10^{-6}	Hydraulic conductivity (m/s)
φ_{ae}	-7000	Air entry value (Pa)
n	0.3	Porosity
β_r	0	Coefficient of compressibility (Pa^{-1})

Note that no soil compression caused by water flowing is considered in this study. Thus, the value of coefficient of compressibility is taken equal to zero.

In addition to the numerical analysis, based on the method provided by Wu and Zhang (2009), a general analytical solution for soil suction distribution is considered:

$$\begin{aligned}\varphi(X,T')=\frac{1}{\alpha}\ln\Bigg\{e^{-X/2}\Bigg[&\sum_{n=0}^{\infty}A'\sin(\beta_n X)e^{-\left(\beta_n^2+0.25\right)T'}+\\ &\sum_{n=0}^{\infty}A''\sin(\beta_n X)\left(1-e^{-\left(\beta_n^2+0.25\right)T'}\right)+\sum_{n=0}^{\infty}A'''\sin(\beta_n X)\left(1-e^{-\left(\beta_n^2+0.25\right)T'}\right)\Bigg]\Bigg\}\end{aligned} \tag{2.15}$$

where,

$$X = \alpha_u \gamma_w x \tag{2.16}$$

$$T' = \alpha_u \gamma_w k_s t / \theta_s \tag{2.17}$$

$$\begin{aligned} A' = \frac{2}{L\left(\beta_n{}^2 + 0.25\right) + 0.5} \Big[& \omega_i \left(\beta_n - \beta_n \cos\left(\beta_n L\right) e^{L/2} + 0.5 \sin\left(\beta_n L\right) e^{L/2}\right) \\ & - \left(\omega_i - e^{-\alpha_u \varphi_0}\right)\left(\beta_n - \beta_n \cos\left(\beta_n L\right) e^{-L/2} - 0.5 \sin\left(\beta_n L\right) e^{-L/2}\right) \Big] \end{aligned} \tag{2.18}$$

$$w_i = \frac{\left(e^{L+\alpha_u \varphi_1} - e^{\alpha_u \varphi_0}\right)}{\left(e^L - 1\right)} \tag{2.19}$$

$$\beta_n \cot\left(\beta_n L\right) = -0.5 \tag{2. 20}$$

$$L = \alpha_u \gamma_w l \tag{2. 21}$$

where φ_0 is the pore water pressure at the bottom; φ_1 is the pore water pressure at the top surface; l represents the thickness of the homogeneous soil layer adopted in the one-dimensional infiltration case; γ_w is the unit weight of water.

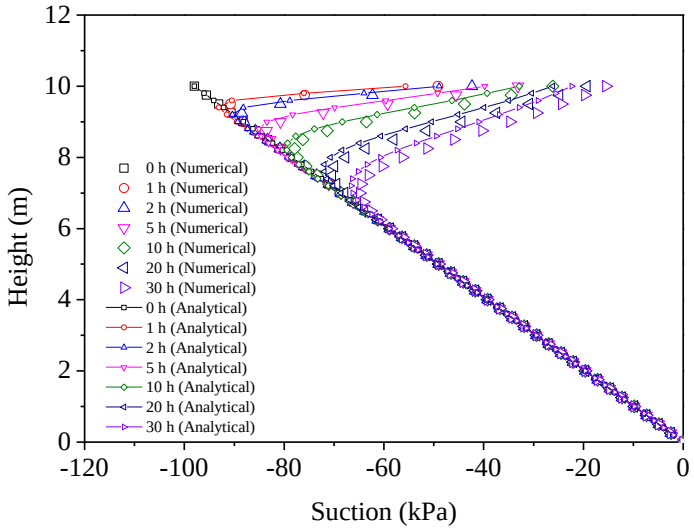
In the case of top boundary condition defined by water flux, Wu and Zhang (2009) proposed that:

$$A'' = \frac{2\beta_n e^{\alpha_u \varphi_0}}{L\left(\beta_n{}^2 + 0.25\right) + 0.5} \tag{2.22}$$

$$A''' = \frac{2e^{L/2} \sin\left(\beta_n L\right)}{k_s e^{\alpha_u \varphi_0}\left[L\left(\beta_n{}^2 + 0.25\right) + 0.5\right]} q_0 \tag{2. 23}$$

Due to its complexity of computation, the analytical solution of soil suction variations is obtained using a Matlab code. Figure 2. 5 compares the results by the numerical and analytical calculation at different moments: t = 1 h, 2 h, 5 h, 10 h, 20 h, 30 h.

(a)



(b)

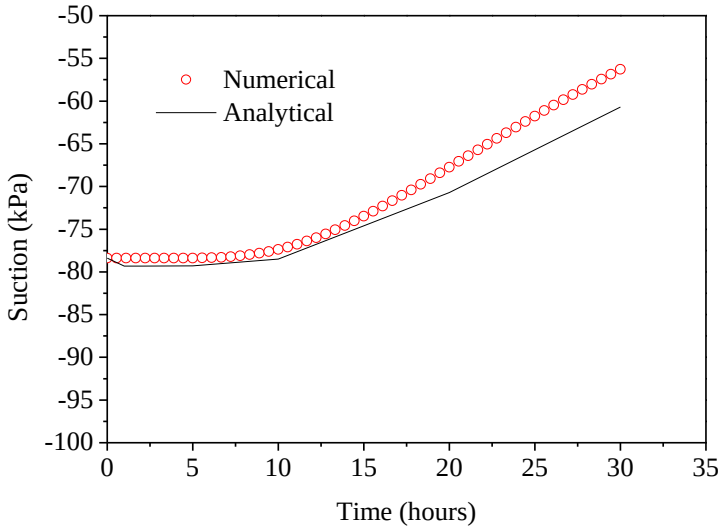


Figure 2. 5. Comparison between numerical and analytical methods: (a) soil suction profile at section A at different moments: *t* = 1 h, 2 h, 5 h, 10 h, 20 h, 30 h; (b) soil suction variation at point E (0.5, 8)

A high consistency between numerical and analytical calculation is obtained for soil suction distribution at section A at different moments: t = 1 h, 2 h, 5 h, 10 h, 20 h, 30 h (Figure 2. 5a). As infiltration goes on, the soil suction at the top surface increases gradually, from -100 kPa at initial moment to about -15 kPa at t = 30 h. Meanwhile, the depth of soil region influenced by infiltration extends over time, from about 1 m *at* t = 1 h to 4 m at t = 30 h. This process is intimately related to the soil coefficient of permeability. In terms of suction variations at point

E, a continuous increase is observed. The two methods give the similar variation curves.

As the results of soil suction variations by the two methods show a good agreement, it can be concluded that the numerical investigation using FreeFem++ code is feasible and reliable.

2.4 Simple coupled hydro-thermal model

2.4.1 Introduction

Soil settlement/swell is intimately related to the variations of soil temperature and volumetric water content/suction. A rigorous analysis would use a fully coupled hydro-thermal-mechanical soil model for assessing the soil behavior. However, in some cases it is possible to assume that the mechanical part is of secondary importance, when dealing with non-deformable soil masses for example. Also, an analysis of simultaneous heat and water flow will constitute a basis for further assessment of soil hydro-thermal-mechanical behavior.

Thomas (1985) developed a simple coupled hydro-thermal model for unsaturated soil based on De Vries' model (De Vries 1958). In his model, the moisture flux density with consideration of coupling effect is expressed as:

$$\mathbf{q}_m/\rho_l = -D_\theta \nabla\theta - D_T \nabla T - k\nabla y \tag{2.24}$$

where $\mathbf{q}_m$ is the flux density of moisture; θ is the total volumetric liquid content; T is the temperature; D_T is the thermal moisture diffusivity; D_θ is the isothermal moisture diffusivity ; k is the permeability of unsaturated soil and ρ_l is the density of liquid water.

Assuming that the mass of vapor is negligible compared with the mass of liquid, the conservation of moisture flux reads:

$$\frac{\partial\theta}{\partial t} = -\nabla\cdot\left(\mathbf{q}_m/\rho_l\right) \tag{2.25}$$

where t is time (s).

Further, the governing equation of soil moisture transfer is given by:

$$\frac{\partial \theta}{\partial t} = -\nabla \cdot \left(\mathbf{q}_m / \rho_l \right) = \nabla \cdot \left(D_\theta \nabla \theta \right) + \nabla \cdot \left(D_T \nabla T \right) + \frac{\partial k}{\partial y} \tag{2.26}$$

The liquid and vapor fluxes are considered respectively as:

$$\frac{\partial \theta_l}{\partial t} = -\nabla \cdot \left(\mathbf{q}_l / \rho_l \right) - E \tag{2.27}$$

$$\frac{\partial \theta_v}{\partial t} = -\nabla \cdot \left(\mathbf{q}_v / \rho_l \right) + E \tag{2.28}$$

where $\mathbf{q}_l$ is the flux density of liquid; $\mathbf{q}_v$ is the flux density of vapor; θ_l is the volumetric water content; θ_v is the volumetric vapor content; E is an evaporation term introduced to represent the source or sink of water along with the liquid water and vapor transfer.

As the incremental change in liquid moisture content $d(\rho_l \theta_l)$ may be considered as being composed of liquid water transfer $d_e(\rho_l \theta_l)$ and phase change $d_i(\rho_l \theta_l)$, ε is introduced as the phase change factor by Luikov (1966):

$$\frac{d_i \left(\rho_l \theta_l \right)}{d_e \left(\rho_l \theta_l \right)} = \frac{\varepsilon}{1 - \varepsilon} \tag{2.29}$$

It can be further arranged as:

$$\frac{\partial \left(\rho_l \theta_l \right)}{\partial t} = \frac{\partial_e \left(\rho_l \theta_l \right)}{\partial t} + \frac{\partial_i \left(\rho_l \theta_l \right)}{\partial t} \tag{2.30}$$

$$\frac{\partial \left(\rho_l \theta_l \right)}{\partial t} = -\nabla \cdot \left(\mathbf{q}_l \right) + \varepsilon \frac{\partial \left(\rho_l \theta_l \right)}{\partial t} \tag{2. 31}$$

It can be also written as:

$$\frac{\partial(\rho_l \theta_l)}{\partial t} = -\nabla \cdot (\mathbf{q}_l) - \nabla \cdot (\mathbf{q}_v) \tag{2.32}$$

On the other hand, neglecting the transfer of sensible heat due to moisture movement and convection effects, the heat flux is considered as the sum of heat conduction and the transfer of latent heat by vapor movement. It is expressed as:

$$\mathbf{q}_h = -\lambda \nabla T + L_v \mathbf{q}_v \tag{2.33}$$

where $\mathbf{q}_h$ is the heat flux ; λ is the thermal conductivity of soil; L_v is the latent heat of vaporization of water.

The conservation of heat flux follows the expression below:

$$C\frac{\partial T}{\partial t} = -\nabla \cdot (\mathbf{q}_h) = \nabla \cdot (\lambda \nabla T) + \nabla \cdot (L_v \nabla \mathbf{q}_v) \tag{2.34}$$

With the assumption of negligible vapor mass in moisture flow, it is obtained:

$$\frac{\partial(\rho_l \theta_l)}{\partial t} \approx \frac{\partial(\rho \theta)}{\partial t} \tag{2.35}$$

Based on equation (2.31), (2.32) and (2.35), it can be inferred further that:

$$\nabla \cdot (\mathbf{q}_v) = -\varepsilon \frac{\partial(\rho_l \theta)}{\partial t} \tag{2.36}$$

Therefore, substituting equation (2.26) and (2.36) into equation (2.34), the governing differential equation can be obtained:

$$C\frac{\partial T}{\partial t} = \nabla \cdot (\lambda + L_v \varepsilon \rho_l D_T) \nabla T + \nabla \cdot (L_v \varepsilon \rho_l D_\theta) \nabla \theta + L_v \varepsilon \rho_l \frac{\partial k}{\partial y} \tag{2.37}$$

Equations (2.26) and (2.37) are the governing equations of the coupled hydro-thermal model,

giving the variations of both θ and T in time and in space. Note that on the left of the governing equations, merely moisture content θ and soil temperature T are presented as the variables in time for the moisture and heat flows, respectively.

The two governing equations can be transformed to:

$$K_q \nabla^2 T + K_\varepsilon \nabla^2 \theta - C_q \frac{\partial T}{\partial t} + L_q \frac{\partial k}{\partial y} = 0 \tag{2.38}$$

$$K_\delta \nabla^2 T + K_\theta \nabla^2 \theta - C_\theta \frac{\partial \theta}{\partial t} + L_\theta \frac{\partial k}{\partial y} = 0 \tag{2.39}$$

where,

$$K_q = D_T \left(\lambda + L_v \varepsilon \rho_l D_T \right) \tag{2.40}$$

$$K_\varepsilon = L_v \varepsilon \rho_l D_\theta D_T \tag{2.41}$$

$$C_q = C D_T \tag{2.42}$$

$$L_q = L_v \varepsilon \rho_l D_T \tag{2.43}$$

$$K_\delta = L_v \varepsilon \rho_l D_\theta D_T \tag{2.44}$$

$$K_\theta = L_v \varepsilon \rho_l D_\theta^{\,2} \tag{2.45}$$

$$C_\theta = L_v \varepsilon \rho_l D_\theta \tag{2.46}$$

$$L_\theta = L_v \varepsilon \rho_l D_\theta \tag{2.47}$$

Further, aiming to conduct numerical investigation by finite element method, the weak forms of heat and moisture flow were rebuilt by Thomas (1985) as:

$$\int_{\Omega} K_q \left(\nabla N_r \cdot \nabla N_s\right) T d\Omega + \int_{\Omega} K_{\varepsilon} \left(\nabla N_r \cdot \nabla N_s\right) \theta_l d\Omega + \int_{\Omega} N_r N_s C_q \frac{\partial T}{\partial t} d\Omega + \int_{\Omega} L_q k \frac{\partial N_r}{\partial y} d\Omega - \int_{\tau} N_r \mathbf{J}_q d\tau - \int_{\tau} N_r L_q \mathbf{J}_{\theta} d\tau = 0 \tag{2.48}$$

$$\int_{\Omega} K_{\delta} \left(\nabla N_r \cdot \nabla N_s\right) T d\Omega + \int_{\Omega} K_{\theta} \left(\nabla N_r \cdot \nabla N_s\right) \theta_l d\Omega + \int_{\Omega} N_r N_s C_{\theta} \frac{\partial \theta_l}{\partial t} d\Omega + \int_{\Omega} L_{\theta} k \frac{\partial N_r}{\partial y} d\Omega - \int_{\tau} N_r \frac{K_{\delta}}{K_q} \mathbf{J}_q d\tau - \int_{\tau} N_r L_{\theta} \mathbf{J}_{\theta} d\tau = 0 \tag{2.49}$$

where N_s is the usual shape function defined element by element; N_r is the shape function used as weighting function. The heat and water flux boundary conditions $\mathbf{J}_q$ and $\mathbf{J}_\theta$ are written in a generalized form as:

$$K_q \frac{\partial T}{\partial n} = \mathbf{J}_q \tag{2.50}$$

$$k \frac{\partial \varphi}{\partial n} = \mathbf{J}_{\theta} \tag{2.51}$$

where, φ is the total potential for moisture flow. The other details of the finite element formulation can be found in the paper by Thomas (1985).

2.4.2 Validation and analysis

Three different applications of this simply soil hydro-thermal model were conducted by Thomas (1985). For the purpose of validation of our numerical model, these three applications are also implemented in FreeFem++ with the governing equations proposed by Thomas (1985).

The basic two-dimensional model is shown in Figure 2. 6. Different regions are considered in three cases: rectangle ABEF is used in Case 1 and Case 2; trapezoid ACDF is used in Case 3. However, the initial soil temperature 10 °C through the soil is assumed for all cases. The initial moisture content and boundary conditions are different and will be introduced in the following parts. In each case, three points at different heights of section S: h = 0 cm, 100 cm, 180 cm are

selected to analyze the soil behavior.

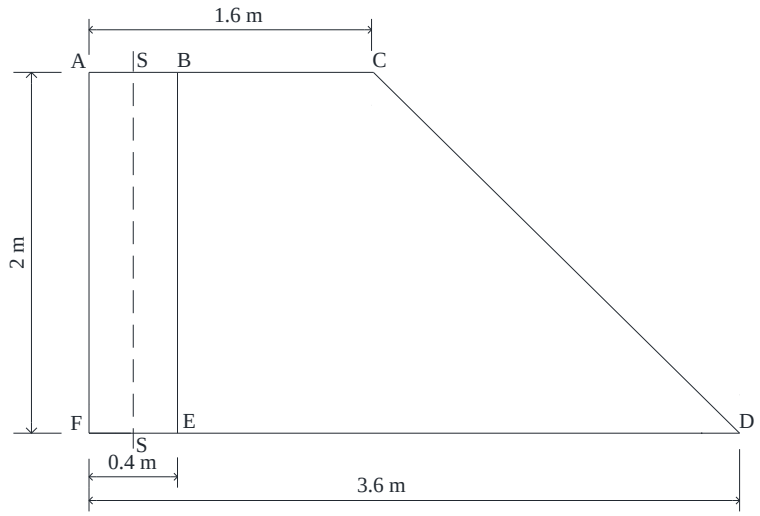


Figure 2. 6. Two-dimensional model used by Thomas (1985)

Moreover, the same soil parameters are adopted to represent a fine sandy soil in the three cases. The details of soil parameters are listed in Table 2. 2. Note that the new value of soil thermal conductivity (0.02 cal/(cms°C)) is used to replace the original value (4×10^{-3} cal/(cms°C)) for better simulation results.

2.4.2.1 Case 1 - vertical soil column ABEF

In this vertical soil column ABEF, the soil initial volumetric water content is assumed to be a constant value of 0.4 throughout the whole model. At the top boundary AB, a temperature of 25 °C and a volumetric moisture content of 0.2 are adopted. Other surfaces are defined as impermeable boundaries to both heat and moisture transfers.

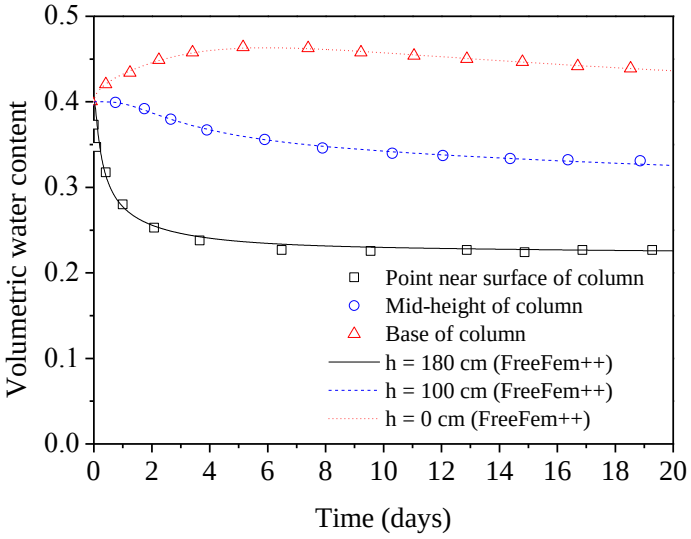
Table 2. 2. Parameters adopted for a fine sandy soil (Thomas 1985)

Parameter	*Value*	*Meaning (unit)*
C	0.48	Volumetric heat capacity (cal/(cm^{3}s°C))
λ	0.02	Thermal conductivity (cal/(cms°C))
L_v	540	Latent heat of vaporization of water (cal/g)
D_T	1×10^{-5}	Isothermal moisture diffusivity (cm^2/(s°C))
ε	0.3	Phase change factor
D_θ	0.01	Thermal moisture diffusivity (cm^2/s)
k	1×10^{-5}	Permeability of unsaturated soil (cm/s)
$\frac{\partial\theta}{\partial\varphi}$	0.1	Specific moisture capacity (m^{-1})

The comparisons of results in Case 1 between the two methods (Thomas's method and FreeFem++) are presented in Figure 2. 7. Satisfactory agreements are obtained for the variations of volumetric water content and temperature. Figure 2. 7a shows that as drying takes place on the surface AB, the volumetric moisture content at the point near the soil surface presents a rapid loss, down to 0.2. The middle point has a decreasing tendency at a lower rate, approaching the value of 0.3. In terms of volumetric moisture content variation at the point near the base, an increase from 0.4 to 0.46 is observed in the first five days. Afterwards, the value decreases gradually to approach 0.4. The first short increasing phase is due to the more prominent effect of gravity than the effect of drying. The analyzed case represents the redistribution process of soil volumetric moisture content from a constant volumetric moisture content profile to an equilibrium state under an assumed temperature gradient.

Figure 2. 7b compares the soil temperature variations at three different positions obtained by the two methods. All the three positions have the same increasing tendency, toward a value of 25 °C. The point near the surface of the column has the rapidest rate. The soil temperature at the base of the column shows an increase in temperature initially at a faster rate than at the middle point in the first four days. It is inferred as the result of the heat carried by the increasing volumetric moisture content. Therefore, it reflects the strong coupling between heat and water flows.

(a)



(b)

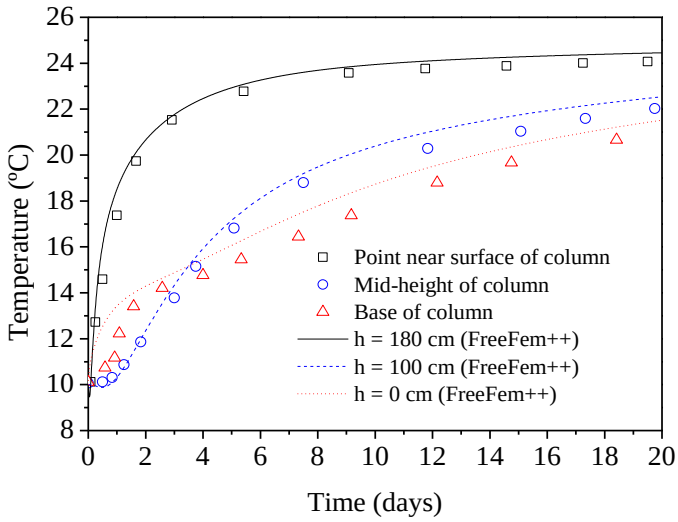


Figure 2. 7. Comparisons of the computation results by two methods in Case 1: (a) volumetric moisture content variations at different positions; (b) temperature variations at different positions

2.4.2.2 Case 2 - vertical soil column ABEF

Case 1 is extended to Case 2 to have the initial moisture varying with depth. This case is defined with an initial equilibrium condition of soil moisture distribution as: $\theta_0 = 0.5\text{-}y/1000$. The value chosen is 0.5 at the base, decreasing to 0.3 at the top surface. At the top boundary AB, a

temperature of 25 °C is set. Other surfaces are defined as impermeable boundaries to both heat and moisture transfers.

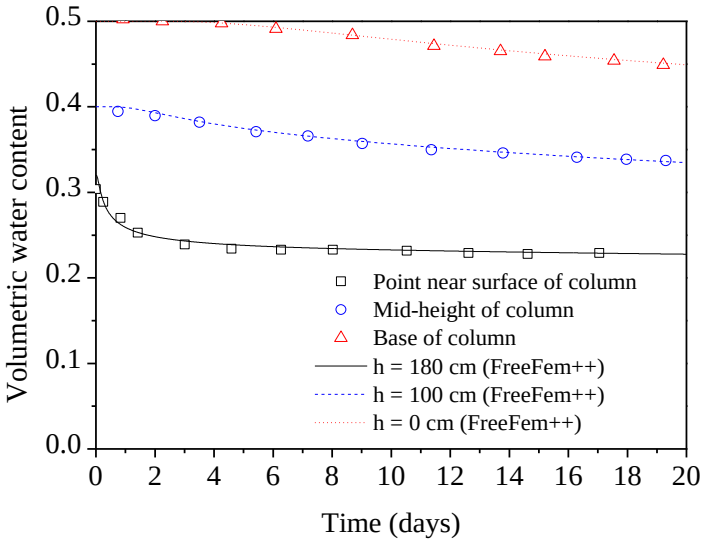
The comparisons of results by two methods (Thomas's method and FreeFem++) are presented in Figure 2. 8. Figure 2. 8a compares the soil volumetric moisture content variations at three positions. Unlike the initial increase at the base point in Case 1, the volumetric moisture contents at the three points show a steady decrease toward the equilibrium values under the gravity effect as drying takes place on the surface AB. Figure 2. 8b presents that comparisons of soil temperature variations at different positions. All the three positions have the similar increasing tendency, approaching a value of 25 °C at different rates according to their distances to the top surface.

2.4.2.3 Case 3 - two-dimensional soil model ACDF

Case 3 is built with the two-dimensional soil model ACDF. The soil initial moisture is assumed to be the same as in Case 2. The value chosen is 0.5 at the base DF, decreasing to 0.3 at the top surface AC. At the top boundary AC and the slope boundary CD, a temperature of 25 °C and a volumetric moisture content of 0.2 are adopted. Other surfaces are defined as impermeable boundaries to both heat and moisture transfers.

Figure 2. 9 shows the results in contour plot of soil volumetric moisture content and temperature distributions at day 10. It can be observed that the two methods give the similar contour plots. The soil volumetric moisture content distribution presented in Figure 2. 9a clearly reflects the importance of a two-dimensional study. The soil volumetric moisture content contour lines are parallel to boundaries AC and CD. Specifically, different contour lines enable the soil volumetric moisture content to be different at the base line FD, varying gradually from 0.5 at point F to 0.2 at point D. The influence of the slope boundary seems significant on the volumetric moisture content distribution, which cannot be reflected in one-dimensional case. Similarly, the soil temperature distribution pattern is compatible as that of soil volumetric moisture content (Figure 2. 9b).

(a)



(b)

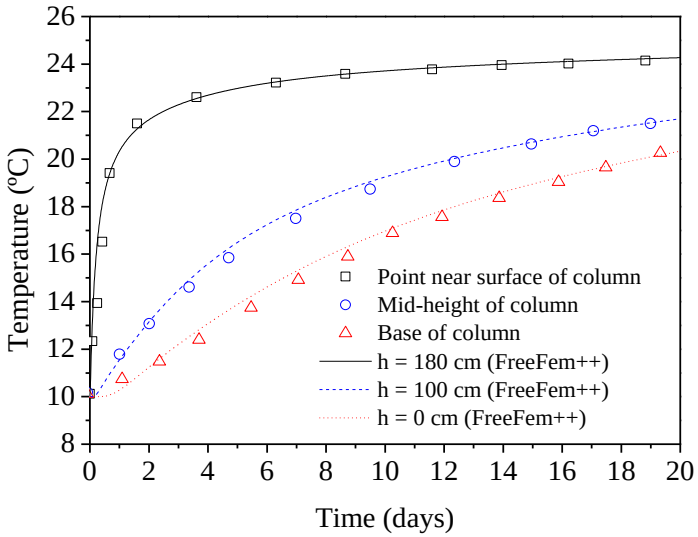
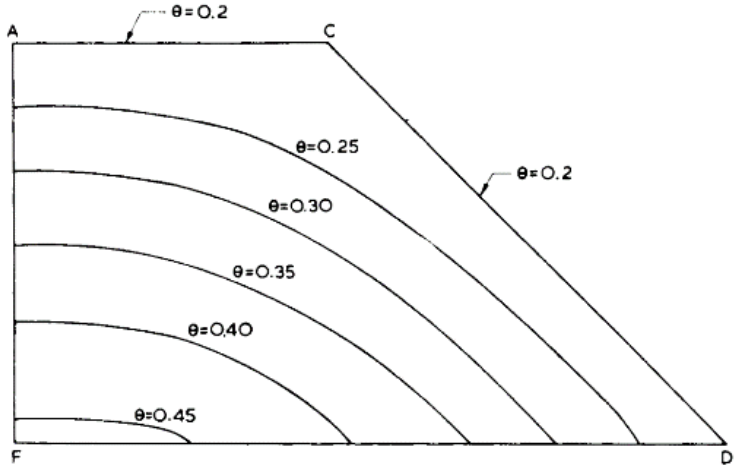


Figure 2. 8. Comparisons of computation results by two methods in Case 2: (a) volumetric moisture content variations at different positions; (b) temperature variations at different positions

With these three different cases, FreeFem++ code is validated. Furthermore, the significance of a fully coupled hydro-thermal soil model is illustrated.

(a)

Contour plot by Thomas (1985)

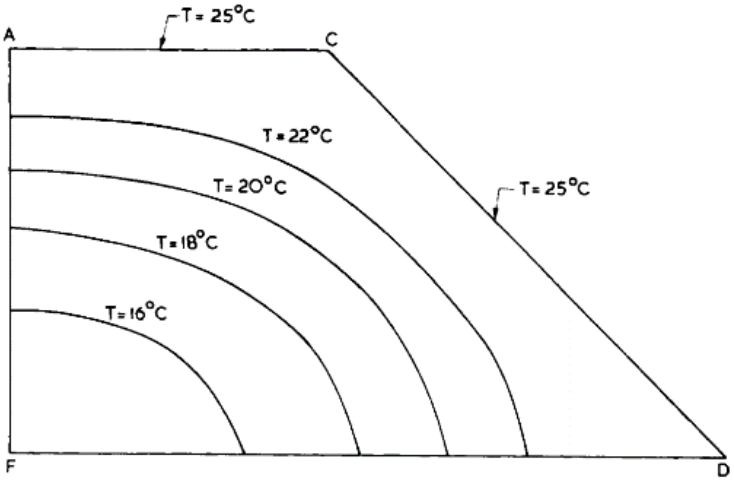


Contour plot by FreeFem++



(b)

Contour plot by Thomas (1985)



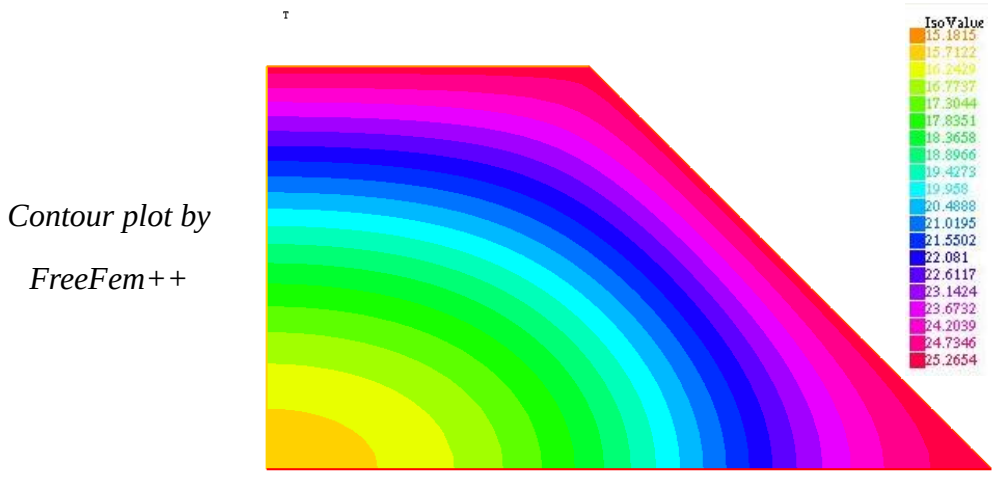


Figure 2. 9. Comparisons of computation results by the two methods in Case 3: (a) volumetric moisture content distribution at day 10; (b) temperature distribution at day 10

2.4.3 Discussion

As indicated above, Case 2 and Case 3 have the same initial and boundary conditions, but they are analyzed in one-dimensional and two-dimensional conditions, respectively. In order to show the effect of slope boundary, three points at different heights: h = 0 cm, 100 cm, 180 cm of section S used in Case 2 are also selected in Case 3 to record the change of soil volumetric water content and temperature. The corresponding soil volumetric water content and temperature variations in Case 2 and Case 3 are compared in Figure 2. 10. Figure 2. 10a shows the soil volumetric water content variations at different positions in the two cases. It is observed that the volumetric water content shows a steady decrease toward the equilibrium values under the gravity effect, as drying takes place on the surface AB. However, the differences at the middle and base points between the two cases appear at day 6 and increase gradually over time. Case 2 gives higher values of volumetric water content than Case 3. Besides, in terms of soil temperature variations, it can be observed that the soil temperature in Case 3 has a smaller value than that in Case 2, even though they have the same increasing tendency (Figure 2. 10b). Meanwhile, the soil volumetric water content and temperature at the top point have the same

variations in the two cases. Therefore, it proves that the one-dimensional and two-dimensional analyses give different results for the middle and base points. A full consideration of the effect of all boundary conditions is necessary in further two-dimensional analysis.

Overall, the feasibility with the FreeFem++ code is verified by analyzing heat flow and water flow in soil using a simple coupled hydro-thermal model. Furthermore, it is found that a fully coupled hydro-thermal model needs to be developed for better describing the soil hydro-thermal behavior. One-dimensional and two-dimensional studies should be selected depending on the objective of the study.

2.5 Fully coupled hydro-thermal model

2.5.1 Liquid flow and vapor flow

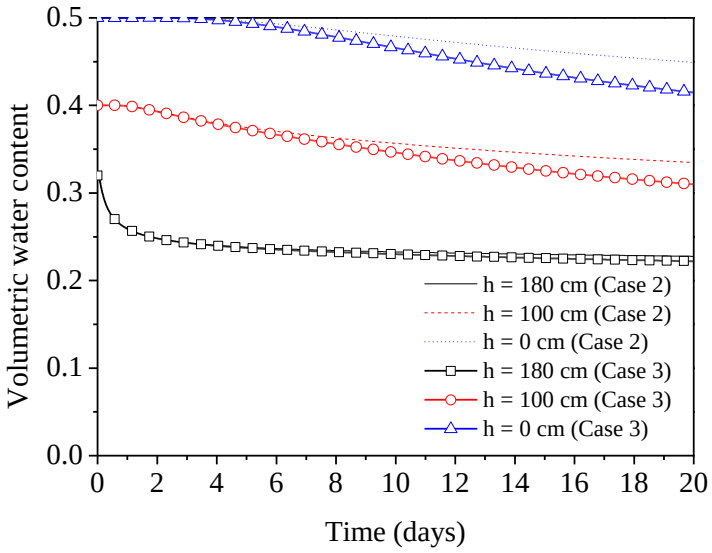
Darcy's law is extended to describe the non-isothermal liquid flow in unsaturated soils, relating the total potential to the liquid flux:

$$\mathbf{q}_l = -K\rho_l \nabla(\varphi + y) \tag{2.52}$$

where $\mathbf{q}_l$ (kg/(sm^2)) is the flux density of liquid; K (m/s) is the hydraulic conductivity of unsaturated soil; ρ_l (kg/m^3) represents the liquid density; φ (m) is the matric suction; y (m) is the elevation above a nominal datum. The water fluid is assumed to be incompressible and osmotic suction is not considered in the following study.

In unsaturated soils, the pore vapor flux is generally caused by two effects: one is the bulk flow of pore air and the other is the molecular diffusion. The mass flux of pore vapor due to molecular diffusion can be described by Fick's law. Without considering the pore air flow effect, the total flux of pore vapor is expressed as (Philip and De Vries 1957; Wilson 1990):

(a)



(b)

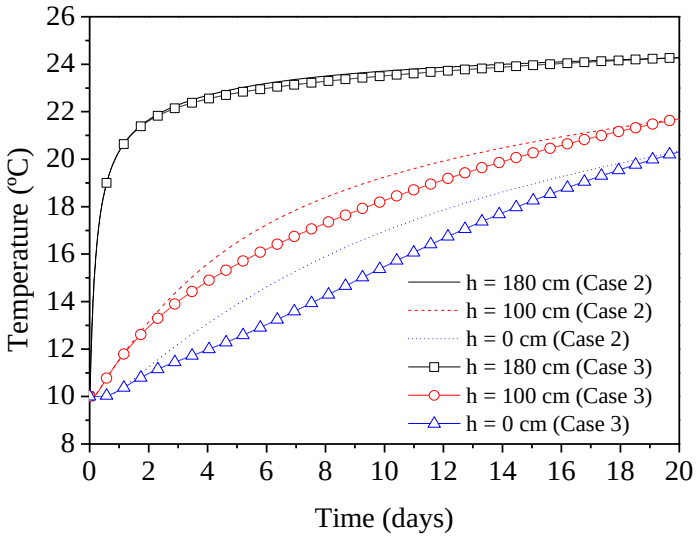


Figure 2. 10. Comparisons of computation results for the three studied points in Case 2 and Case 3: (a) volumetric moisture content variations over time; (b) temperature variations over time

$$\mathbf{q}_v = -D_{atm}\alpha\beta\nabla\rho_v \tag{2.53}$$

where $\mathbf{q}_v$ (kg/(sm^2)) is the flux density of vapor; D_{atm} (m^2/s) is the molecular diffusivity of vapor in the air; α is the tortuosity factor for soil; β is the cross-sectional area of soil in vapor flow;

ρ_v (kg/m^3) is the vapor density which is expressed in a system with a thermodynamic equilibrium between the liquid and vapor phases as (Philip and De Vries 1957):

$$\rho_v = \rho_0 \exp\left(\varphi g M_w / RT\right) \tag{2.54}$$

$$\begin{aligned} \nabla\rho_v &= \rho_0 \nabla h + h\nabla\rho_0 = \rho_0\left(\frac{\partial h}{\partial \varphi}\nabla\varphi + \frac{\partial h}{\partial T}\nabla T\right) + h\frac{\partial \rho_0}{\partial T}\nabla T \\ &= \rho_0 \frac{\partial h}{\partial \varphi}\nabla\varphi + \left(\rho_0 \frac{\partial h}{\partial T} + h\frac{\partial \rho_0}{\partial T}\right)\nabla T \end{aligned} \tag{2.55}$$

where ρ_0 (kg/m^3) is the saturated water vapor density (Thomas and King, 1991):

$$\rho_0 = \left\{194.4\exp\left[-0.06374\left(T-273\right) + 0.1634\times10^{-3}\left(T-273\right)^2\right]\right\}^{-1} \tag{2.56}$$

Based on Kelvin's equation, relative humidity of soil is calculated by:

$$h = \exp\left(\frac{\varphi g M_W}{RT}\right) \tag{2.57}$$

Thus:

$$\frac{\partial h}{\partial \varphi} = \frac{h g M_w}{RT} \tag{2.58}$$

$$\frac{\partial h}{\partial T} = -\frac{h\varphi g M_W}{RT^2} \tag{2.59}$$

Substituting equations (2.55), (2.58) and (2.59) into equation (2.53), the flux density of vapor can be expressed as:

$$\mathbf{q}_v = -\rho_l\left(D_{\varphi v}\nabla\varphi + D_{Tv}\nabla T\right) \tag{2.60}$$

where,

$$D_{\varphi v} = \frac{D_{atm}\alpha\beta\rho_0 hgM_W}{RT\rho_l} \tag{2.61}$$

$$D_{Tv} = \frac{D_{atm}\alpha\beta}{\rho_l}\left(-\frac{\rho_0 h\varphi gM_W}{RT^2} + h\frac{\partial\rho_0}{\partial T}\right) \tag{2.62}$$

Additionally, the mass transfer of water is the sum of liquid flow and vapor flow:

$$\mathbf{q} = \mathbf{q}_l + \mathbf{q}_v \tag{2.63}$$

The water mass conservation equation is expressed as:

$$\frac{\partial w}{\partial t} = -\nabla\cdot\mathbf{q} \tag{2.64}$$

where w (kg/m^3) is the moisture content which can be defined by both the vapor and liquid parts:

$$w = \theta\rho_l + (n-\theta)\rho_v \tag{2.65}$$

By substituting equations (2.52) and (2.60) into equation (2.63) and (2.64), the governing equation for water mass transfer is obtained:

$$C_\varphi\frac{\partial\varphi}{\partial t} + C_{\varphi T}\frac{\partial T}{\partial t} = \nabla\cdot\left[K_\varphi\nabla\varphi\right] + \nabla\cdot\left[K_{\varphi T}\nabla T\right] + \rho_l\nabla K \tag{2.66}$$

where,

$$C_\varphi = \left(\rho_l - \rho_v\right)\frac{\partial\theta}{\partial\varphi} + \left(n-\theta\right)\frac{\rho_0 hgM_W}{RT} \tag{2.67}$$

$$C_{\varphi T} = \left(n-\theta\right)\left(-\frac{\rho_0 h\varphi gM_W}{RT^2} + h\frac{\partial\rho_0}{\partial T}\right) \tag{2.68}$$

$$K_{\varphi T} = \rho_l D_{Tv} \tag{2.69}$$

$$K_{\varphi} = \rho_l D_{\varphi v} + K\rho_l \tag{2.70}$$

2.5.2 Heat flow

The heat transfer in unsaturated soils in terms of soil-atmosphere interaction mainly consists of heat conduction and latent heat processes. Generally, the thermal conduction is in accordance with Fourier's law. Latent heat is the heat consumed due to vapor/liquid transfer.

The heat energy flux per unit area can be written as:

$$\mathbf{Q} = -\lambda \nabla T + L_v \mathbf{q}_v \tag{2.71}$$

where $\mathbf{Q}$ (W/m^2) is the transferred heat flux through soil-atmosphere interface; λ (W/(mK)) is the soil thermal conductivity; L_v (J/kg) is the specific latent heat of vaporization.

Further, equation (2. 71) can be extended as:

$$\begin{aligned} \mathbf{Q} &= -\lambda \nabla T + L_v \left[-\rho_l \left(D_{\varphi v} \nabla \varphi + D_{Tv} \nabla T \right) \right] \\ &= -\left(\lambda + L_v \rho_l D_{Tv} \right) \nabla T - L_v \rho_l D_{\varphi V} \nabla \varphi \end{aligned} \tag{2.72}$$

The heat energy conservation equation is written as:

$$\frac{\partial (\Phi)}{\partial t} = -\nabla \cdot \mathbf{Q} \tag{2.73}$$

where, $\Phi = CT + \left(n - \theta \right) L_v \rho_v$.

The left of equation (2.73) is rewritten as:

$$\begin{aligned}
&\frac{\partial(\Phi)}{\partial t} = C\frac{\partial T}{\partial t} + T\frac{\partial C}{\partial t} + (n-\theta)L_v\frac{\partial \rho_v}{\partial t} - L_v\rho_v\frac{\partial \theta}{\partial t} \\
&= C\frac{\partial T}{\partial t} + (n-\theta)L_v\frac{\partial \rho_v}{\partial t} - L_v\rho_v\frac{\partial \theta}{\partial t} \\
&= C\frac{\partial T}{\partial t} + (n-\theta)L_v\left(\frac{\partial \rho_v}{\partial \varphi}\frac{\partial \varphi}{\partial t} + \frac{\partial \rho_v}{\partial T}\frac{\partial T}{\partial t}\right) - L_v\rho_v\frac{\partial \theta}{\partial \varphi}\frac{\partial \varphi}{\partial t} \\
&= \left(C + (n-\theta)L_v\frac{\partial \rho_v}{\partial T}\right)\frac{\partial T}{\partial t} + \left((n-\theta)L_v\frac{\partial \rho_v}{\partial \varphi} - L_v\rho_v\frac{\partial \theta}{\partial \varphi}\right)\frac{\partial \varphi}{\partial t} \\
&= C_T\frac{\partial T}{\partial t} + C_{T\varphi}\frac{\partial \varphi}{\partial t}
\end{aligned} \tag{2.74}$$

Meanwhile, the right of equation (2.73) is rewritten as:

$$\begin{aligned}
&-\nabla\cdot\mathbf{Q} \\
&= -\nabla\cdot\left[-(\lambda + L_v\rho_l D_{Tv})\nabla T - L_v\rho_l D_{\varphi V}\nabla\varphi\right] \\
&= \nabla\cdot(K_T\nabla T) + \nabla\cdot(K_{T\varphi}\nabla\varphi)
\end{aligned} \tag{2.75}$$

Thus, based on equations (2.71) and (2.73), the governing equation of heat flow can be expressed as:

$$C_T\frac{\partial T}{\partial t} + C_{T\varphi}\frac{\partial \varphi}{\partial t} = \nabla\cdot[K_T\nabla T] + \nabla\cdot[K_{T\varphi}\nabla\varphi] \tag{2.76}$$

where,

$$C_T = C + (n-\theta)L_v\frac{\partial \rho_v}{\partial T} \tag{2.77}$$

$$C = \rho_s C_{ps}(1-n) + \rho_l C_{pl}\theta + \rho_v C_{pv}(n-\theta) + \rho_a C_{pa}(n-\theta) \tag{2.78}$$

$$C_{T\varphi} = (n-\theta)L_v\frac{\partial \rho_v}{\partial \varphi} - L_v\rho_v\frac{\partial \theta}{\partial \varphi} \tag{2.79}$$

$$K_T = \lambda + L_v\rho_l D_{Tv} \tag{2.80}$$

$$K_{T\varphi} = L_v \rho_l D_{\varphi v} \tag{2.81}$$

Other related parameters and the corresponding values are listed in Table 2. 3.

In this study, the governing equations (2.66) and (2.76) for water mass transfer and energy transfer respectively are used for the analysis of soil hydro-thermal behavior with consideration of soil-atmosphere interaction using FreeFem++ code .

Table 2. 3. The values and definitions of the basic parameters

Parameter	*Value*	*Definition (unit)*
R	8.31432	Universal gas constant (J/(molK))
L_v	2.257×10^{6}	Latent heat of vaporization of water (J/kg)
β	n-θ	Cross-sectional area of soil that is available for the vapor flow
α	1.414	Tortuosity factor for soil
M_W	18.016×10^{-3}	Molecular mass of water vapor (kg/mol)
ρ_s	2700	Density of soil solid (kg/m^3)
C_{ps}	800	Specific heat capacity of soil solid (J/(kgK))
C_{pl}	4180	Specific heat capacity of water liquid (J/(kgK))
C_{pv}	1872	Specific heat capacity of water vapor (J/(kgK))
ρ_a	1.2	Density of air (kg/m^3)
C_{pa}	1005	Specific heat capacity of air (J/(kgK))
D_{atm}	$5.893\times10^{-11}\ T^{2.3}$	Molecular diffusivity of the pore vapor (m^2/s) (Hussain, 1997)

Compared with the simple coupled hydro-thermal model, the fully coupled model has the following developments:

1) An assumption that the mass of vapor is negligible compared with the mass of liquid is made in the simple coupled hydro-thermal model. However, vapor flow is considered as part of moisture flow in the fully coupled hydro-thermal model.
2) In the simple coupled model, the use of phase conversion factor simplifies the relationship between vapor and liquid phase change in moisture flow. Specifically, in the fully coupled hydro-thermal model, a system with a thermodynamic equilibrium between the liquid and vapor phases is applied to represent the vapor density. The relationship between vapor and

liquid fluxes is integrated in the water mass conservation equation.

3) In the simple coupled hydro-thermal model, merely the variable of soil moisture content θ (suction φ) is shown on the left of governing equation of moisture flow, the soil temperature T being on the left of governing equation of heat flow. However, in the fully coupled hydro-thermal model, the variables of soil suction φ and soil temperature T are both shown on the left of the governing equations of moisture flow and heat flow. Thus, these two variables are influenced by each other continuously.

2.6 Weak forms of fully coupled hydro-thermal model

Two governing equations of water flow (equation 2.66) and heat flow (equation 2.76) have been proposed. In order to implement them in FreeFem++ code, their weak forms are required to be developed.

2.6.1 Weak form of water flow

$$C_{\varphi}\frac{\partial \varphi}{\partial t}+C_{\varphi T}\frac{\partial T}{\partial t}=-\nabla\cdot\mathbf{q} \tag{2.82}$$

With the shape function N_r, the left side of equation (2.82) can be written as:

$$\int_{\Omega} N_r\left(C_{\varphi}\frac{\partial \varphi}{\partial t}+C_{\varphi T}\frac{\partial T}{\partial t}\right)d\Omega=\int_{\Omega} N_r\left(C_{\varphi}\frac{\varphi-\varphi_0}{\Delta t}+C_{\varphi T}\frac{T-T_0}{\Delta t}\right)d\Omega \tag{2.83}$$

Meantime, the right side of equation (2.82) is:

$$\begin{aligned}&-\nabla\cdot\mathbf{q}=-\nabla\cdot\left(\mathbf{q}_l+\mathbf{q}_v\right)\\&=\nabla\cdot\left[K\rho_l\nabla(\varphi+y)\right]+\nabla\cdot\left[\rho_l\left(D_{\varphi v}\nabla\varphi+D_{Tv}\nabla T\right)\right]\end{aligned} \tag{2.84}$$

With the shape function N_r, the first term of equation (2.84) can be extended with Green's theory by:

$$\begin{aligned}
&\int_{\Omega} N_r \nabla \cdot \left[K \rho_l \nabla (\varphi + y) \right] \\
&= \int_{\Omega} \nabla \cdot \left[N_r K \rho_l \nabla (\varphi + y) \right] d\Omega - \int_{\Omega} K \rho_l \nabla (\varphi + y) \nabla N_r d\Omega \\
&= -\int_{\tau} N_r \mathbf{q}_l d\tau - \int_{\Omega} K \rho_l \nabla (\varphi + y) \nabla N_r d\Omega \\
&= -\int_{\tau} N_r \mathbf{q}_l d\tau - \int_{\Omega} K \rho_l \nabla \varphi \nabla N_r d\Omega - \int_{\Omega} K \rho_l \frac{dN_r}{dy} d\Omega
\end{aligned} \tag{2.85}$$

Similarly, the second term of equation (2.84) is extended as:

$$\begin{aligned}
&\int_{\Omega} N_r \nabla \cdot \left[\rho_l \left(D_{\varphi v} \nabla \varphi + D_{Tv} \nabla T \right) \right] \\
&= \int_{\tau} N_r \rho_l D_{\varphi v} \nabla \varphi d\tau - \int_{\Omega} \rho_l D_{\varphi v} \nabla N_r \nabla \varphi + \int_{\tau} N_r \rho_l D_{Tv} \nabla T d\tau - \int_{\Omega} \rho_l D_{Tv} \nabla N_r \nabla T \\
&= -\int_{\tau} N_r \mathbf{q}_v d\tau - \int_{\Omega} \rho_l D_{\varphi v} \nabla N_r \nabla \varphi - \int_{\Omega} \rho_l D_{Tv} \nabla N_r \nabla T
\end{aligned} \tag{2.86}$$

Combing equation (2.83), (2.85), and (2.86) into (2.82), we have:

$$\begin{aligned}
&\int_{\Omega} N_r \left(C_{\varphi} \frac{\varphi - \varphi_0}{\Delta t} + C_{\varphi T} \frac{T - T_0}{\Delta t} \right) d\Omega \\
&+ \int_{\Omega} K \rho_l \nabla \varphi \nabla N_r d\Omega + \int_{\Omega} K \rho_l \frac{dN_r}{dy} d\Omega + \int_{\Omega} \rho_l D_{\varphi v} \nabla N_r \nabla \varphi d\Omega + \int_{\Omega} \rho_l D_{Tv} \nabla N_r \nabla T d\Omega \\
&+ \int_{\tau} N_r \mathbf{q}_l d\tau + \int_{\tau} N_r \mathbf{q}_v d\tau = 0
\end{aligned} \tag{2.87}$$

Finally, the weak form equation for water flow becomes:

$$\begin{aligned}
&\int_{\Omega} N_r \left(C_{\varphi} \frac{\varphi - \varphi_0}{\Delta t} + C_{\varphi T} \frac{T - T_0}{\Delta t} \right) d\Omega + \int_{\Omega} K_{\varphi} \nabla N_r \nabla \varphi d\Omega + \int_{\Omega} K_{\varphi T} \nabla N_r \nabla T d\Omega \\
&+ \int_{\Omega} K \rho_l \frac{dN_r}{dy} d\Omega + \int_{\tau} N_r L_{vn} d\tau + \int_{\tau} N_r V_{vn} d\tau = 0
\end{aligned} \tag{2.88}$$

where L_{vn} and V_{vn} represent the water flux and vapor flux respectively on the corresponding boundary.

2.6.2 Weak form of heat flow

$$C_T \frac{\partial T}{\partial t} + C_{T\varphi} \frac{\partial \varphi}{\partial t} = -\nabla \cdot \mathbf{Q} \tag{2.89}$$

With the shape function N_s, the left side of equation (2.89) can be written as:

$$\int_\Omega N_s \left(C_T \frac{\partial T}{\partial t} + C_{T\varphi} \frac{\partial \varphi}{\partial t} \right) d\Omega = \int_\Omega N_s \left(C_T \frac{T - T_0}{\Delta t} + C_{T\varphi} \frac{\varphi - \varphi_0}{\Delta t} \right) d\Omega \tag{2.90}$$

With the shape function N_s, the right side of equation (2.89) can be developed with Green's theory:

$$\begin{aligned}
&\int_\Omega N_s \nabla \cdot \mathbf{Q} d\Omega \\
&= \int_\Omega N_s \nabla \cdot \left[-\left(\lambda + L_v \rho_l D_{Tv} \right) \nabla T - L_v \rho_l D_{\varphi V} \nabla \varphi \right] d\Omega \\
&= \int_\tau N_s \left[-\left(\lambda + L_v \rho_l D_{Tv} \right) \nabla T - L_v \rho_l D_{\varphi V} \nabla \varphi \right] d\tau \\
&- \int_\Omega \left[-\left(\lambda + L_v \rho_l D_{Tv} \right) \nabla T d\Omega - L_v \rho_l D_{\varphi V} \nabla \varphi \right] \nabla N_s d\Omega \\
&= \int_\tau N_s \left[-\left(\lambda \right) \nabla T - \left(L_v \rho_l D_{Tv} \nabla T + L_v \rho_l D_{\varphi V} \nabla \varphi \right) \right] d\tau \\
&+ \int_\Omega \left(\lambda + L_v \rho_l D_{Tv} \right) \nabla T \nabla N_s d\Omega + \int_\Omega L_v \rho_l D_{\varphi V} \nabla \varphi \nabla N_s d\Omega \\
&= \int_\tau N_s \left[-\left(\lambda \right) \nabla T + L_v q_v \right] d\tau + \int_\Omega \left(\lambda + L_v \rho_l D_{Tv} \right) \nabla T \nabla N_s d\Omega + \int_\Omega L_v \rho_l D_{\varphi V} \nabla \varphi \nabla N_s d\Omega \\
&= \int_\tau N_s \left[\mathbf{Q} \right] d\tau + \int_\Omega \left(\lambda + L_v \rho_l D_{Tv} \right) \nabla T \nabla N_s d\Omega + \int_\Omega L_v \rho_l D \varphi_{\phi V} \nabla \varphi \nabla N_s d\Omega
\end{aligned} \tag{2.91}$$

Thereby, the final weak form for heat flow becomes:

$$\begin{aligned}
&\int_\Omega N_s \left(C_T \frac{T - T_0}{\Delta t} + C_{T\varphi} \frac{\varphi - \varphi_0}{\Delta t} \right) d\Omega + \int_\Omega K_T \nabla T \nabla N_s d\Omega \\
&+ \int_\Omega K_{T\varphi} \nabla \varphi \nabla N_s d\Omega + \int_\tau N_s T_{vn} d\tau = 0
\end{aligned} \tag{2.92}$$

where T_{vn} represents the heat flux on the corresponding boundary.

The weak forms for water (equation 2.89) and heat (2.92) governing equations will be applied in the numerical investigation of fully coupled hydro-thermal model in different cases, enabling the estimation of soil volumetric water content and temperature variations in time and in space.

2.7 Conclusions

This chapter introduces the numerical tool FreeFem++ code. In order to ensure the accuracy of the numerical solution using this code, it is necessary to compare the calculation results with the known theoretical solutions. Thereby, heat flow, and water flow in soil are adopted respectively to verify the accuracy of FreeFem++ code. With the simple coupled hydro-thermal model, the simulation results by FreeFem++ code present a high consistency with the known results in three assumed cases, in terms of soil volumetric water content and temperature variations. Afterwards, a fully coupled hydro-thermal model is developed and the weak forms of equations for water and heat flows are established. The main conclusions are summarized below:

1) Different cases involving heat flow and water flow in soil are considered to verify the accuracy of FreeFem++ code. The computation results by analytical methods are used for the purpose of comparison. An overall satisfactory agreement is obtained between the numerical calculation and analytical solution, indicating the accuracy of the numerical tool applying FreeFem++ code, despite some discrepancies caused by the limitation of the analytical solution;
2) The three cases investigated with the simple coupled hydro-thermal model allow further verification of the feasibility of FreeFem++ code in coupled conditions. The comparisons between the numerical results and the known solutions show a high consistency, indicating that the adopted numerical method is capable of determining the soil volumetric water content and temperature variations accurately;
3) A fully coupled hydro-thermal soil model is also developed. Meanwhile, the differences between the simple and the fully coupled hydro-thermal models are investigated, showing

the theoretical superiority of the latter. In order to make it usable directly in further study, the weak forms for water and heat governing equations are developed, respectively.

Chapter 3: Development and validation of the numerical approach adopted

A numerical approach is developed by combing the fully coupled hydro-thermal model and the soil-atmosphere interaction model. As the fully coupled hydro-thermal model has been presented in Chapter 2, only the details of soil-atmosphere interaction model are discussed in this chapter. Afterwards, this numerical approach is validated based on the column drying test by Wilson (1990).

3.1 Soil-atmosphere interaction

3.1.1 Balance equations used for the description of soil-atmosphere interaction

Soil-atmosphere interaction occurs at soil surface through water transfer and heat transfer (Blight 1997). Rainfall can be partitioned into infiltration and runoff. Meanwhile, evaporation happens at soil-atmosphere interface because of energy transfer and vapor pressure gradient exiting at the soil-atmosphere interface. Concerning the heat transfer, solar radiation is normally the only exterior heat resource. The net solar radiation can be partitioned into latent heat, soil heat and sensible heat. All these terms concerning the water transfer and heat transfer can be presented in mass balance and energy balance.

3.1.1.1 Mass balance

The mass balance at the soil surface is expressed as:

$$P = I_{nt} + R_{off} + E_a + I_{nf} \tag{3.1}$$

where P (m/s) is the rate of rainfall; I_{nt} (m/s) is the rate of water intercepted by canopy during

rainfall; R_{off} (m/s) represents the runoff rate on soil surface; E_a (m/s) is the actual evaporation rate; I_{nf} (m/s) is the infiltration rate. These components are illustrated in Figure 3. 1.

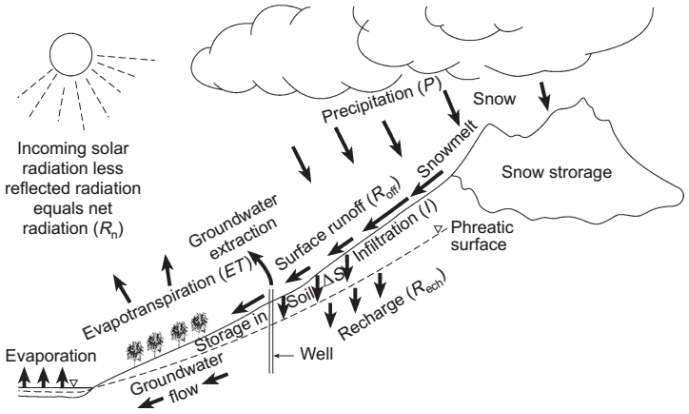


Figure 3. 1. Components in the mass balance of soil-atmosphere interaction (Blight 1997)

Rainfall and interception

The value of rainfall is easy to be measured using a standard rain gauge. Generally, field rainfalls are monitored half hourly or hourly in meteorological stations. For a vegetated surface, interception is the part of rainfall intercepted by the canopy and then evaporates without reaching the soil surface. Specifically, I_{nt} is zero for bare soil without canopy.

Runoff

Any rainfall exceeding soil infiltration capacity would have resulted in runoff. In fact, the estimation of runoff is not an easy task, because runoff depends not only on soil characteristics (type, initial water content, slope catchment size and surface vegetation), but also on rainfall rate and duration (Critchley and Siegert 1991; Chiew et al. 1993; Chiew and McMahon 1994; Rahardjo et al. 2004; USDA-SCS 2004; Bhadra et al. 2010; Gökbulak et al. 2015; Mu et al. 2015). According to literature, runoff can be either measured directly or predicted numerically. It can be estimated using either volumetric system (Pinson et al. 2004; Wei et al. 2014) or a continuous system (Rahardjo et al. 2004, 2008; Sajjan et al. 2013; Stewart et al. 2015). In the volumetric system, simple or complex tanks are used depending on the quantity of runoff. This tank system only collects "lump sum" runoff volume and provides no further hydrological information, which limits its applications (Miller 1994). In a continuous system, the evolution

of volume of water can be monitored using floating, counterweight recorders (Miller 1994), a capacitance water depth probe (Rahardjo et al. 2004) or a pressure transducer (Stewart et al. 2015). Information about flow durations, peak flows and the runoff starting time with respect to the start of rainfall can also be obtained.

Runoff can be also predicted by different models for different catchments and different rainfall conditions. According to Knapp et al. (1991) and Tedela (2009), there are two main models for rainfall runoff prediction: (i) the lumped-parameter model, and (ii) the spatially distributed model. The first model averages the total rainfall and ignores the spatial heterogeneity of the catchment response (Ponce and Hawkins 1996), while the second distributed model attempts to simulate most of the heterogeneous responses at a local scale (Beven 1989; O'Connell 1991; Garbrecht et al. 2001). One of the most widely used lumped-parameter models is the NRCS runoff model (USDA-SCS 2004). It allows estimating total runoff from total rainfall, without considering the evolution of runoff and rainfall rate. The soil antecedent water content was not considered clearly because this method is only designed for single rainfall event (Ponce and Hawkins 1996). Therefore, the estimation of runoff need be conducted by choosing the most suitable method based on the known conditions.

Evaporation

The amount of water that would be lost by evaporation and transpiration in case of abundant water is defined as potential evaporation. Actual evaporation is the quantity of water that is actually evaporated and transpired from a surface (Thornthwaite 1948; Gray 1970; Morton 1975; Brutsaert 1982; Wilson 1990; Wilson et al. 1994). Therefore, it is necessary to consider the condition of soil surface in the estimation of soil evaporation values. Obviously, the value of actual evaporation is smaller than that of potential evaporation. Various methods of estimating evaporation can be found in literature and they can be classified as direct measurement approaches and indirect prediction ones.

Actual evaporation of soil sample can be measured directly by sensitive weighing scales (Kondo et al. 1990, 1992; Wilson 1990; Qiu et al. 1998; Benson et al. 2001; Liu et al. 2002;

Benli et al. 2006) or weighing lysimeters (Bronswijk 1991; Qiu et al. 1998; Benson et al. 2001; Liu et al. 2002; Benli et al. 2006). By analyzing the recorded data of soil mass at regular intervals in these two approaches, the evaporation can be estimated with a high accuracy. Specifically, sensitive weighing scales are applied for soil sample in small size in the laboratory. The weighing lysimeters are used for measuring soil water evaporation of soil sample in a large scale in the field or in the laboratory. However, in these two approaches, the bottom of soil sample is isolated with the surrounding environment, limiting the accuracy of measurement results (Benson et al. 2001). Moreover, the estimation of evaporation can also be conducted by measuring the supplication of underground water under the control of water table through non-weighing lysimeter (Jensen et al. 1990).

In addition, different kinds of prediction models were also reported in literature allowing the estimation of potential evaporation and actual evaporation. For the potential evaporation, the mass transfer models are frequently applied because of their simplicity and reasonable accuracy (Dalton 1802; Meyer 1915; Penman 1948). In the mass transfer models, there are three governing factors: vapor pressure gradient, temperature and wind speed. A generalized equation of the mass transfer models was proposed as (Singh and Xu 1997):

$$E = f(u)\,g(e)\,h(T) \tag{3.2}$$

where $f(u)$, $g(e)$ and $h(T)$ are wind speed, vapor pressure and temperature functions, respectively. There are thirteen relatively simple and commonly used evaporation equations of this format. They are presented in Table 3. 1.

It is obvious that most of these equations are applicable for the estimation of monthly or daily evaporation. The equations proposed by Sverdrup (1946) and Thornthwaite and Holzman (1939) can be applied for calculating evaporation expressed in cm/s. However, the wind speed and vapor pressure at two different heights above soil surface need to be measured. Furthermore, these different equations can be classified in seven generalized categories (Table 3. 2).

Table 3. 1. Thirteen different equations of mass transfer model format (after Singh and Xu 1997)

Author	*Equation*	*Unit*	*Remark*
Dalton (1802)	$E = a(e_s - e_a)$	In. /month	a = 15 for small, shallow water; a = 11 for large, deep water
Fitzgerald (1886)	$E = (0.4 + 0.199u)(e_s - e_a)$	In. /month	
Meyer (1915)	$E = 11(1 + 0.1u)(e_s - e_a)$	In. /month	e_a is measured at 30 ft above the surface
Horton (1919)	$E = 0.4[2 - \exp(-2u)](e_s - e_a)$	In. /month	
Rohwer (1931)	$E = 0.77(1.465 - 0.0186p_b)(0.44 + 0.118u)(e_s - e_a)$	In. /day	p_b = barometric pressure in in. of Hg
Penman (1948)	$E = 0.35(1 + 0.24u_2)(e_s - e_a)$	In. /day	
Harbeck et al. (1954)	$E = 0.0578u_8(e_s - e_a)$ $E = 0.0728u_4(e_s - e_a)$	In. /day	
Kuzmin (1957)	$E = 6.0(1 + 0.21u_8)(e_s - e_a)$	In. /month	
Harbeck et al. (1958)	$E = 0.001813u(e_s - e_a)[1 - 0.03(T_a - T_w)]$	In. /day	T_a = average air temperature, °C+1.9°C; T_w = average water surface temperature, °C
Konstantinov (1968)	$E = 0.024[(t_w - t_2)/u_1 + 0.166u_1](e_s - e_a)$	In. /day	
Romanenko (1961)	$E = 0.0018(T_a + 25)^2(100 - h_n)$	cm/month	h_n = relative humidity
Sverdrup (1946)	$E = 0.623\rho K_0^2 u_8(e_0 - e_8)/\left(p(In(800/z))^2\right)$	cm/s	K_0 = von Karman's constant; ρ = air density; p = atmospheric pressure
Thornthwaite and Holzman (1939)	$E = 0.623\rho K_0^2(u_8 - u_2)(e_2 - e_8)/\left(p(In(800/200))^2\right)$	cm/s	

The wind speed (monthly mean) u is measured in miles per hour and vapor pressure e in inches of Hg. The subscripts attached to u and e refer to height in meters at which the measurements are taken; no subscript refers to wind speed measurements near the ground or water surface.

Table 3. 2. Generalized equations with easily measured parameters (after Singh and Xu 1997)

Number	*Generalized equations*
1	$E = a(e_0\text{-}e_a)$
2	$E = a\times u(e_0\text{-}e_a)$
3	$E = a(1\text{-}\exp(\text{-}u))(e_0\text{-}e_a)$
4	$E = a(1+b\times u)(e_0\text{-}e_a)$
5	$E = a\times u(e_0\text{-}e_a)(1\text{-}b(T_a\text{-}T_d))$
6	$E =a(T_a+25)^2(100\text{-}h_n)$
7	$E = a(1+b\times u)(e_0 - e_a)(1\text{-}c(T_a\text{-}T_d))$

where T_a is the air temperature, and T_d is the dew point temperature.

Overall, the mass transfer model is in a simple form with several measurable variables, allowing the estimation of potential evaporation. Besides, different models for the estimation of soil evaporation (actual evaporation) can be classified into three types: the resistance models, the vapor pressure models and the models considering energy exchanges.

1) The resistance models

As evaporation happens on the soil surface, soil water content in the region near soil surface decreases gradually and in some cases a dry soil layer could appear. With the presence of a dry layer, the evaporation begins to occur at the evaporation front, which is the bottom of the dry soil layer (van de Griend and Owe 1994; Yamanaka et al. 1997; Aluwihare and Watanabe 2003). Therefore, the process of water vapor moving from the evaporating surface to atmosphere will be restricted by three different resistances. The details are presented in Figure 3. 2:

- Water vapor is carried out from the water surface to the bottom of dry layer, and the corresponding resistance is noted as r_{sw};
- Water vapor is transported from the bottom of dry soil layer to the soil surface by vapor diffusion, and the corresponding resistance is termed as soil resistance r_d;
- Water vapor travels from the soil surface to the atmosphere under the restriction of aerodynamic resistance r_a.

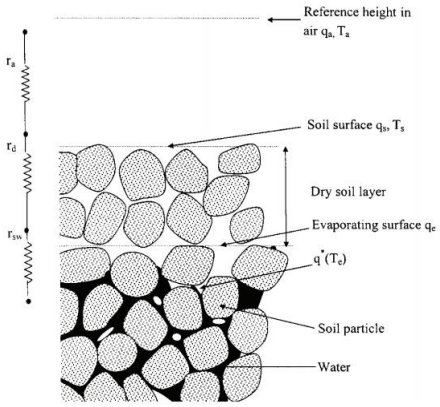


Figure 3. 2. The three stages of water vapor transportation from soil to atmosphere (Aluwihare and Watanabe 2003)

Correspondingly, a basic resistance model was proposed by Aluwihare and Watanabe (2003) as:

$$E = \rho_a \frac{q_{sat}(T_e) - h_a q_{sat}(T_a)}{r_{sw} + r_d + r_a} \tag{3.3}$$

$$r_d = z_d / \left(D_{atm} \partial_0 \theta_a v \right) \tag{3.4}$$

where q_{sat} (T_e) is the saturated specific humidity at the evaporating surface temperature T_e (ºC); h_a is the air relative humidity at the reference height; q_{sat} (T_a) is the saturated specific humidity at the air temperature of reference height T_a (ºC); r_{sw} (s/m) is the resistance imposed on the vapor flux when it travels from the pores of wet soil layer to the pores of dry soil layer; r_d (s/m)is the resistance imposed on vapor flux in the dry soil layer; r_a (s/m) is the aerodynamic resistance; D_{atm} (m^2/s) is the molecular diffusivity of water vapor in air; z_d (m) is the thickness of dry soil layer; v is the mass flow factor; α_0 is the tortuosity factor accounting for the extra path length and θ_a is the volumetric air content.

Through the assessment of field experiments, it is concluded that the resistance r_{sw} is much smaller compared with the resistance r_d, but cannot be neglected, especially at very dry conditions (Aluwihare and Watanabe 2003). The sum of r_{sw} and r_d can be considered as soil resistance r_s, which is intimately related to soil water content. Therefore, the determinations of

aerodynamic resistance r_a and soil resistance r_s are essential for this resistance model.

In literature, many studies have been conducted, attempting to estimate these resistances. Generally, the aerodynamic resistance is evaluated according to the aerodynamic principle and considering the atmospheric stability (Camillo and Gurney 1986; Choudhury and Monteith 1988; Daamen and Simmonds 1996; Xu and Qiu 1997; Xu et al. 1999; Aluwihare and Watanabe 2003). Several formulas used to estimate aerodynamic resistance are listed in Table 3. 3.

Table 3. 3. Several formulas used to estimate aerodynamic resistance (after Liu et al. 2007)

Author	*Equation*
Thom (1975)	$r_{ah}=\frac{1}{k^2u}\left[\ln\left(\frac{Z-d}{z_{0m}}\right)-\psi_m(\zeta)\right]\left[\ln\left(\frac{Z-d}{z_{0h}}\right)-\psi_h(\zeta)\right]$
Verma et al. (1975)	$r_{ah}=\frac{1}{k^2u}\left[\ln\left(\frac{Z-d}{z_{0m}}\right)\right]^2\left(1-16Ri_B\right)^{-1/4}$
Hatfield et al. (1983)	$r_{ah}=\frac{1}{k^2u}\left[\ln\left(\frac{Z-d}{z_{0m}}\right)\right]^2\left(1+\beta Ri_B\right)$
Mahrt and Ek (1984)	$r_{ah}=\frac{1}{k^2u}\left[\ln\left(\frac{Z-d}{z_{0m}}\right)\right]^2\left[\frac{1+c\left(-Ri_B\right)^{1/2}}{1+c\left(-Ri_B\right)^{1/2}-15Ri_B}\right]$
Choudhury et al. (1986)	$r_{ah}=\frac{1}{k^2u}\left[\ln\left(\frac{Z-d}{z_{0m}}\right)\right]\left[\ln\left(\frac{Z-d}{z_{0h}}\right)\right]\left(1-\beta Ri_B\right)^{-3/4}$
Xie (1988)	$r_{ah}=\frac{1}{k^2u}\left[\ln\left(\frac{Z-d}{z_{0m}}\right)\right]^2\left[1+\frac{\left[1-16Ri_B\ln\left(\frac{Z-d}{z_{0m}}\right)\right]^{-1/2}}{\ln\left(\frac{Z-d}{z_{0m}}\right)}\right]$
Viney (1991)	$r_{ah}=\frac{1}{k^2u}\left[\ln\left(\frac{Z-d}{z_{0m}}\right)\right]\left[\ln\left(\frac{Z-d}{z_{0m}}\right)\right]\left[a+b\left(-Ri_B\right)^c\right]^{-1}$
Yang et al. (2001)	$r_{ah}=\frac{1}{k^2u}\left[\ln\left(\frac{z}{z_{0m}}\right)-\psi_m(\zeta,\zeta_{0m})\right]\left[\ln\left(\frac{z}{z_{0h}}\right)-\psi_h(\zeta,\zeta_{0h})\right]$

Concerning the soil resistance, it is related to the water content of top soil layer and soil type. Many empirical equations have been proposed, allowing proper determination of soil resistance. A summary of these methods is presented in Table 3. 4.

The resistance model gives a clear description of physical process of water vapor traveling from soil to atmosphere. Theoretically, this method is able to estimate the value of actual evaporation with high precision. However, due to different experimental conditions (soil type, soil thickness, etc.), the value of soil resistance is difficult to be verified and hence restricts the use of this method.

Table 3. 4. Several formulas used to estimate soil resistance summarized after Mahfouf and Noilhan (1991) and Bittelli et al. (2008)

Author	*Equation*	*Remark*
Sun (1982)	$r_s = 3.5\left(\theta/\theta_{sat}\right)^{2.3} + 33.5$	θ and θ_{sat} are volumetric water content in 0~5 mm layer and saturated volumetric water content, respectively
Camillo and Gurney (1986)	$r_s = 4140\left(\theta_{sat} - \theta\right) - 805$	θ and θ_{sat} are volumetric water content in 0~1 cm layer and saturated volumetric water content, respectively
Passerat de Silans (1986)	$r_s = 38113\exp\left(-13.515\theta/\theta_{fc}\right)$	θ and θ_{fc} are volumetric water content of the near surface region and of the specific field capacity
Kondo et al. (1990)	$r_s = a\left(\theta_{sat} - \theta\right)^b / D_{atm}$ $D_{atm} = 0.229\times10^{-4}\left(T_s/273.16\right)^{1.75}$	θ and θ_{sat} are volumetric water content in 2 cm layer and saturated volumetric water content, respectively; a and b are parameters depending on soil type; T_s is the soil surface temperature (K)
van de Griend and Owe (1994)	$r_s = 10\exp\left[0.3563\left(15-\theta\right)\right]$	θ is volumetric water content in 1 cm layer

2) The vapor pressure models

The vapor pressure models indicate another direction to predict soil evaporation. Relying on the mass transfer model, the potential and actual evaporation can be presented as:

$$E_a = f(u)(e_s - e_a) \tag{3.5}$$

$$E_p = f(u)(e_0 - e_a) \tag{3.6}$$

where the function $f(u)$ is assumed to be the same for both soil surface and water surface; e_s (Pa) is the actual vapor pressure at the soil surface; e_0 (Pa) is the saturated vapor pressure at the water surface; and e_a (Pa) is the vapor pressure of air at the reference height.

Campbell (1985) proposed the basic model relating actual and potential evaporation, as follows:

$$\frac{E_a}{E_p} = \frac{e_s - e_a}{e_0 - e_a} \tag{3.7}$$

where,

$$e_s = \frac{h_s}{100} \times 610.8 \exp\left(\frac{17.27T_s}{T_s + 237.3}\right) \tag{3.8}$$

$$e_0 = 610.8 \exp\left(\frac{17.27T_0}{T_0 + 237.3}\right) \tag{3.9}$$

$$e_a = \frac{h_a}{100} \times 610.8 \exp\left(\frac{17.27T_a}{T_a + 237.3}\right) \tag{3.10}$$

$$h_s = \exp\left(\frac{\varphi g M_W}{R(T_s + 273.15)}\right) \tag{3.11}$$

where h_s (%) is the relative humidity at soil surface; h_a (%) is the relative humidity of air; T_s, T_0 and T_a (ºC) represent the soil surface temperature, the water surface temperature and the air temperature, respectively.

Furthermore, with the assumption that the temperatures at soil surface, water surface and in air are the same, e_0 can be considered as the saturated vapor pressure in these three cases. Thereby,

the ratio of E_a to E_p can be rewritten as (Wilson et al. 1997):

$$\frac{E_a}{E_p} = \frac{e_s / e_0 - e_a / e_0}{e_0 / e_0 - e_a / e_0} = \frac{h_s - h_a}{1 - h_a} \tag{3.12}$$

Using Kelvin equation, equation (3.12) can also be presented as:

$$\frac{E_a}{E_p} = \frac{\exp\left(\frac{\varphi g M_W}{R\left(T_s + 273.15\right)}\right) - h_a}{1 - h_a} \tag{3.13}$$

In this model, the influences of both soil and atmosphere parameters on evaporation are described clearly. Moreover, the used parameters to estimate soil evaporation (in equations 3.5~3.13) are very simple. The introduction of the surface suction in equation (3.13) makes it independent of soil properties such as soil texture and mineralogy, as well as the drying time. Nevertheless, the measurement of surface suction presents a big challenge for the application of this model.

3) The models considering energy exchange

Additionally, there are some approaches for evaluating potential evaporation and soil evaporation with consideration of energy exchange during soil-atmosphere interaction. They are listed in Table 3. 5.

In the coupled model proposed by Penman (1948), measurement of the surface temperature is not necessary because the potential evaporation is calculated without considering the surface temperature effect. Net radiation, air temperature, relative humidity and wind speed are required and can be measured easily. Generally, it is suitable for predicting the potential evaporation, rather than the actual evaporation of unsaturated soils (Wilson 1990; Wilson et al. 1994). The model proposed by Wilson et al. (1994) can be applied to estimate the actual evaporation of unsaturated soils, provided that the soil surface parameter is determined accurately (e.g., the value of B depending on the relative humidity at the soil surface). As far as the Penman-Monteith model (Monteith 1981) is concerned, it asks for the estimation of soil heat, which can

be measured directly using heat flux plates buried in the soil at a fixed depth (Gao 2005) or the calculation based on the energy balance (Blight 1997). Besides, the application of Penman-Monteith model also needs the determination of soil resistance, which is complex as discussed previously for the resistance models. Moreover, the three-temperature model gives a new direction of evaluating soil evaporation with considering temperatures at three different positions. In this method, the definition of the reference dry soil is essential and soil heat determination is also required.

Table 3. 5. The models for estimating soil evaporation considering energy exchange

Model	*Equation*	*Remark*
Coupled energy balance and mass transfer model (Penman 1948; Wilson et al. 1994)	Penman model: $E_{penman} = \left[\Delta R_n + \gamma E_p\right] / \left(\Delta + \gamma\right)$ $E_p = 0.35\left(1 + 9.8\times10^{-3} u\right)\left(e_0 - e_a\right)$ Wilson model: $E_w = \left[\Delta R_n + \gamma E_{aw}\right] / \left(\Delta + \gamma A\right)$ $E_{aw} = 0.35\left(1 + 0.146u\ \right) e_{aw}\left(B - A\right)$	γ is the pyschrometric constant; Δ is the slope of the saturation vapor pressure versus temperature curve at the mean temperature of the air; A is the inverse of the relative humidity at the soil surface; B is the inverse of the relative humidity in the air; e_{aw} is the water vapor pressure in air above the soil surface; u is the wind speed.
Coupled energy balance and resistance model (Monteith 1981)	Penman-Monteith model: $E_s = \dfrac{\Delta\left(R_n - G\right) + \rho_a c_p \left(e_0 - e_a\right) / r_a}{\left[\Delta + \gamma\left(1 + r_{sl} / r_a\right)\right]\rho_w L_e}$	r_{sl} is the bulk surface resistance that describes the resistance to flow of water vapor from inside the leaf, vegetation canopy or soil to outside the surface.
Three-temperature model (Qiu et al. 1998)	$E = \left[R_n - G - \left(R_{nd} - G_d\right)\dfrac{T_s - T_a}{T_{sd} - T_a} \right] \Big/ L_v$	R_{nd} is the net radiation of dry soil surface; G_d is the heat flux in dry soil; T_s is the drying soil surface temperature; T_a is the air temperature at the reference height; T_{sd} is the dry soil surface temperature.

Therefore, each prediction method of soil evaporation has its specific merits and drawbacks. The choice of method depends on the applicable conditions of these models and the known

parameters in the studied cases.

With the estimation of rainfall, runoff and actual evaporation in the mass balance during soil-atmosphere, the value of infiltration can be obtained and then applied as the water flux boundary condition at the soil-atmosphere interfaces. In the numerical calculation, the negative values of infiltration represent the water flux going out from soil. Conversely, the positive values mean the water flux going into soil.

3.1.1.2 Energy balance

The energy balance at the soil surface is expressed as:

$$R_n = G + L_E + H \tag{3.14}$$

where R_n (W/m^2) is the net radiation flux; G (W/m^2) means the soil heat flux; L_E (W/m^2) represents the latent heat flux which is the product of the evaporative flux E (m/s) and the latent heat of vaporization L_v (J/m^3); H (W/m^2) is the sensible heat flux.

Solar radiation consists of direct and diffuse radiations. Direct radiation is the part of solar radiation which spreads out without striking any obstacle and which reaches the earth's surface directly. The solar radiation which is diffused on its way through the atmosphere by clouds, water and dust particles, and reaches earth's surface, is termed as diffuse radiation. Both direct and diffuse radiations are short-wave radiation. Besides, the earth surface and atmosphere emit long-wave radiation. Net radiation includes the absorption and reflection of short-wave radiation, as well as the outgoing and incoming long-wave radiations, and can be expressed as follows

$$R_n = (1-\alpha_s) R_{si} - L\uparrow + L\downarrow \tag{3.15}$$

where R_{si} (W/m^2) is the solar radiation monitored normally by field meteorological station; $L\uparrow$ (W/m^2) is the long-wave radiation from the earth's surface; $L\downarrow$ (W/m^2) is the long-wave

radiation from the sky; α_s is soil surface albedo, depending on the soil water content, color and texture as well as the organic matter content and surface roughness. The suggested values for α for different soil surfaces are listed in Table 3. 6.

Table 3. 6. The values of soil albedo and surface emissivity at different soil surface (after Evett et al. (2011)

Soil surface	*Albedo*	*Emissivity*	*Source*
Soils, dark, wet to light, dry	0.05-0.50	0.90-0.98	Oke (1987)
Dry sandy soil	0.25-0.45		Rosenberg et al. (1983)
Sand, wet	0.09	0.98	Van Wijk (1963)
Sand, dry	0.18	0.95	Van Wijk (1963)
Dark clay, wet	0.02-0.08	0.97	Van Wijk (1963)
Dark clay, dry	0.16	0.95	Van Wijk (1963)
Fields, bare	0.12-0.25		Van Wijk (1963)
Grass, green	0.16-0.27	0.96-0.98	Van Wijk (1963)

In literature, depending on the consideration of soil temperature or not, two methods to estimate net solar radiation have been applied in different fields. They are summarized as follows:

1) The method without consideration of soil temperature (Method 1)

A. In hourly or half hourly

The method for calculating net solar radiation is expressed by:

$$R_n = (1-\alpha_s) R_{si} - \left[a_c \left(\frac{R_{si}}{R_{so}} \right) + b_c \right] \left(a_1 + b_1 e_d^{\,0.5} \right) \sigma \left(T_a^{\,4} \right) \tag{3.16}$$

where T_a (ºC) is the half-hourly mean air temperature; σ (5.67×10^{-8} W/(m^{2}K^4)) is Stefan-Boltzmann constant; a_c and b_c are could factors, taken equal to 1.35 and -0.35, respectively; a_1 and b_1 are emissivity factors, taken equal to 0.35 and -0.14, respectively, as suggested by Evett et al. (2011); R_{si}/R_{so} is the relative shortwave radiation, which is used to express the cloudiness of the atmosphere. When the sky is cloudier, its value is smaller. It varies in the range from 0.33 (dense cloud cover) to 1 (clear sky) (Allen et al. 1998). Specifically, its value is 0.7 for night

time (Evett et al. 2011).

Besides, e_d is calculated from mean daily dew point temperature T_d (ºC):

$$e_d = 0.611\exp\left(\frac{17.27T_d}{T_d + 237.3}\right) \tag{3.17}$$

Solar radiation in case of clear sky, R_{so}, is expressed as:

$$R_{so} = \left(0.75 + 0.00002EL_{msl}\right)R_{sa} \tag{3.18}$$

where EL_{msl} (m) is the site elevation above the mean sea level; the extraterrestrial solar radiation R_{sa} (W/m^2) is calculated by Evett et al. (2011) and Duffie and Beckman (1991):

$$R_{sa} = \left[\frac{24(60)}{2\pi}\right]G_{sc}d_r\left[\cos(\phi)\cos(\delta)\left[\sin(\omega_2) - \sin(\omega_1)\right] + (\omega_2 - \omega_1)\sin(\phi)\sin(\delta)\right] \tag{3.19}$$

where G_{sc} (-0.08202 MJ/(m^{2}min)) is the solar constant; J is the day of year; ϕ is latitude; δ is solar declination; the relative earth-sun distance d_r (m) is presented as:

$$d_r = 1 + 0.033\cos\left(\frac{2\pi J}{365}\right) \tag{3.20}$$

Additionally, w_1 and w_2 are the solar time angles at the beginning and ending of the considered period, respectively (all angles in radians), which need to be calculated as follows:

$$w_1 = w - \frac{\pi}{(24/\tau)} \tag{3.21}$$

$$w_2 = w + \frac{\pi}{(24/\tau)} \tag{3.22}$$

where w is the solar time angle at the center of the period in radians; τ is the length of the considered period in hours.

B. In daily

For the daily time scale studies, the method used for the half-hourly or hourly time scale needs to be modified. The equation (3.16) used to calculate net solar radiation is rewritten as:

$$R_n = (1-\alpha_s)R_{si} - \left[a_c\left(\frac{R_{si}}{R_{so}}\right)+b_c\right]\left(a_1+b_1 e_d^{\,0.5}\right)\sigma\left(\frac{T_m^{\,4}+T_n^{\,4}}{2}\right) \tag{3.23}$$

where T_m (ºC) and T_n (ºC) represent the maximum and the minimum air temperatures in one day; other parameters are the same as indicated for equation (3.16). Meantime, it is noted that the calculation of the extraterrestrial solar radiation R_{sa} for an entire day requires the knowledge of sunrise and sunset time. Therefore, the equation (3.19) needs to be transformed to:

$$R_{sa} = \left[\frac{24(60)}{\pi}\right]G_{sc}d_r\left[\cos(\phi)\cos(\delta)\sin(\omega_s)+\omega_s\sin(\phi)\sin(\delta)\right] \tag{3.24}$$

where w_s is the sunset time angle, the angel from solar noon to sunset (in radians). It is estimated as:

$$w_s = \cos^{-1}\left[-\tan(\phi)\tan(\delta)\right] \tag{3.25}$$

Other parameters have the same definitions as indicated above. Further details were presented by Evett et al. (2011), Jensen et al. (1990) and Duffie and Beckman (1991).

2) The method with consideration of soil temperature (Method 2)

Based on the Stefan-Boltzmann law, the outgoing and incoming long-wave radiations can be calculated respectively by:

$$L\uparrow = \varepsilon\sigma(T_s)^4 \tag{3.26}$$

$$L\downarrow = \varepsilon\sigma(T_a)^4 \tag{3.27}$$

Therefore, the net radiation becomes:

$$R_n = (1-\alpha_s) R_{si} - \varepsilon_s \sigma (T_s)^4 + \varepsilon_a \sigma (T_a)^4 \tag{3.28}$$

where ε_s is soil surface emissivity; ε_a is air emissivity.

Soil surface emissivity is mainly controlled by soil type and soil surface properties. It is not an easy task to determine this parameter with accuracy directly in the field (Humes et al. 1994; Rubio et al. 1997; ASTM 2006; Mira et al. 2010; López et al. 2012). Generally, it is determined based on the reference table (Table 3. 6) provided by Evett et al. (2011).

Besides, the methods for calculating air emissivity have also been studied widely. Several commonly used formulas are presented in Table 3. 7.

Table 3. 7. Different methods to estimate air emissivity

Author	*Equation*	*Remark*
Idso (1981)	$\varepsilon_a = 0.70 + 5.95\times10^{-4} e_a \exp\left[\frac{1500}{T_a + 273.1}\right]$ $e_a = \frac{h_a}{100} e_0$ $e_0 = 0.6107 \exp\left[\frac{17.269 T_a}{T_a + 273.1}\right]$	e_a (kPa) is the vapor pressure of air; h_a (%) is the relative humidity of air; e_0 (kPa) is the saturated vapor pressure at air temperature T_a (°C).
Brunt (1932)	$\varepsilon_a = 0.52 + 0.206 e_a^{0.5}$	
Brutsaert (1982)	$\varepsilon_a = 0.767 e_a^{1/7}$	

Howell et al. (1993) showed that all the three methods in Table 3.7 can give good predictions of air emissivity for clear sky condition. However, they may underestimate the values in cloudy and night time conditions. After the comparisons between several related methods, Hatfield et al. (1983) concluded that the method using only air temperature has a better performance than others considering vapor pressure or both vapor pressure and air temperature. With the superior performance, the method proposed by Idso (1981) is adopted in this study.

The selection of two methods (Method 1 and Method 2) to calculate net radiation depends on the adequacy of soil surface temperature. If the soil surface temperature is recorded continuously during the studied time period, the second method is preferred to be adopted because the effect of soil surface on net radiation is considered. Otherwise, the first method appears to be relatively more economical and more feasible than the second one.

Additionally, various methods to estimate sensible heat (Blight 1997, Voogt and Grimmond 2000, Cui et al. 2005) and latent heat (Bowen 1926; Choudhury et al. 1986; Jensen et al. 1990; Allen et al. 1994, 1998; Blight 1997) were proposed in literature. The common method used to determine sensible heat is given by Blight (1997):

$$H = -\rho_a C_{pa} K_H \left(\frac{\partial T}{\partial y} \right)_{air} \tag{3.29}$$

where ρ_a (kg/m^3) is the air density; C_{pa} (J/(kgK)) is the specific heat capacity of air; K_H (m^2/s) is the eddy diffusivity for heat through air; $\left(\frac{\partial T}{\partial y} \right)_{air}$ is the vertical temperature gradient in the air.

Because sensible heat is related to the gradient of air temperature, Cui et al. (2005) proposed a new equation for its determination:

$$H = -\lambda_a \left(\frac{\partial T}{\partial y} \right)_{air} \tag{3.30}$$

where λ_a (W/(mK)) is the air thermal conductivity. It is noted that at the soil and atmosphere interface, the gradients of air temperature and soil temperature are not continuous.

The latent heat represents the heat consumed for evaporation. It is related directly with the vapor gradient near soil surface. It can be calculated by (Blight 1997):

$$L_E = \frac{L_v \rho_a \varepsilon K_v}{P} \frac{\partial P_{va}}{\partial y} \tag{3.31}$$

where L_v (J/kg) is the latent heat of vaporization of water; ε is the ratio of the molecular mass of water to the molecular mass of dry air; P (Pa) is the atmospheric pressure; K_v (m^2/s) is the diffusivity for water vapor through air; and $\frac{\partial P_{va}}{\partial y}$ (Pa/m) is the vertical vapor pressure gradient in the air.

Furthermore, Bowen (1926) suggested a Bowen ratio β between sensible heat and latent heat. It was expressed by Blight (1997) as:

$$\beta = \frac{H}{L_E} = \frac{PC_{pa}\left(T_1 - T_2\right)}{L_V \varepsilon \left(P_{va1} - P_{va2}\right)} \tag{3.32}$$

where T_1 and T_2, P_{va1} and P_{va2} are the air temperature and vapor pressure, respectively at two different heights. Hence, latent heat can be expressed as:

$$L_E = \frac{R_n - G}{1 + \beta} \tag{3.33}$$

$$H = \beta L_E \tag{3.34}$$

The Bowen method asks for accurate estimation of the value of Bowen ratio β, which can be measured directly by Bowen ratio equipment (Blight 1997; Cui and Zornberg 2008). However, based on the comparison of four Bowen ratio systems, Dugas et al. (1991) concluded that the Bowen ratio equipment tends to underestimate the value of latent heat (Blad and Rosenberg 1974; Todd et al. 2000).

Relying on the definition of latent heat, it can be determined directly with the known value of actual evaporation:

$$L_E = L_v E_a \tag{3.35}$$

where E_a (m/s) is the value of actual evaporation. It is the simplest method for estimating the latent heat when the value of actual evaporation is provided.

Acquiring the values of net solar radiation, sensible heat and latent heat in the energy balance during soil-atmosphere interaction, the value of soil heat flux can be calculated and adopted as the heat flux boundary condition at the soil-atmosphere interfaces.

3.1.2 Initial and boundary conditions

In numerical modelling with fully coupled hydro-thermal model, the definitions of initial conditions of soil temperature and volumetric water content are essential. Generally, the initial conditions are defined based on the direct measurements at the starting moment.

With the fully coupled hydro-thermal model proposed in Chapter 2, it is necessary to define the corresponding hydraulic and thermal boundary conditions. For the studied cases, the bottom boundary conditions are normally defined based on the measured values of soil temperature and volumetric water content. The lateral boundary conditions can be estimated depending on the corresponding situations of hydraulic and thermal transfers.

For the hydraulic and thermal conditions at the soil-atmosphere interfaces, they are estimated respectively relying on the mass and energy balance presented in section 3.1. For bare soil, with the rainfall, runoff and actual evaporation estimated in equation (3.1), I_{nf} can be estimated and set as water flux boundary condition at soil-atmosphere interfaces. The negative value of water flux boundary condition refers to evaporation happening at the soil-atmosphere interfaces. Conversely, the positive value of water flux boundary condition represents the infiltration situation. Correspondingly, the evaporation/infiltration boundary conditions will lead to the decreasing/increasing of soil volumetric water content.

With the estimations of net solar radiation R_n, sensible heat H and latent heat L_E, the energy

balance (equation 3.14) can be used to determine the value of soil heat flux *G* and then set as the heat flux boundary condition at the interfaces of soil and atmosphere. When the soil heat flux is in negative value, the soil is sending out energy to the surrounding environment. Conversely, the positive value of soil heat flux represents the heating soil phenomenon.

Due to the factors involved in mass and energy balance equations, the calculations of water flux I_{nf} and heat flux *G* boundary conditions need to be performed by iteration considering both the atmosphere condition (net solar radiation, wind speed, air relative humidity, air temperature, etc.) and soil surface situation (soil suction and temperature) during the studied period. Consequently, the climate effect on soil hydro-thermal performance is considered in the determination of soil boundary conditions through soil-atmosphere interaction model.

Therefore, a numerical approach is proposed by combing the fully coupled hydro-thermal model and the soil-atmosphere interaction model. It can be adopted to study soil hydro-thermal behavior under climate effect.

3.2 Validation of the proposed numerical approach based on a column drying test

3.2.1 Introduction of column drying test (Wilson, 1990)

A simulation work of the column drying test carried out by Wilson (1990) is conducted to study the soil hydro-thermal behavior during evaporation, allowing the validation of the proposed numerical approach. As shown in Figure 3. 3 and Figure 3. 4, two columns of soil with diameter of 153.7 mm and height of 300 mm were designed to have a continuous evaporation for 42 days in a hot arid chamber. A water filled evaporation pan of 100 mm diameter using the same PVC casing as for the soil column was also prepared for the measurement of potential evaporation. Beaver Creek sand was selected as the studied soil in the column drying test due to its great potential for rapid desaturation, limited volume change and distinct liquid/vapor water flow. The whole test was conducted in an environmental chamber with temperature 38.0±1.0 °C.

Meanwhile, the relative humidity of the chamber was maintained between 11% and 23% with a mean value of 15%. As stated by Wilson (1990), this combination of temperature and relative humidity resulted in a potential evaporative flux from 7.2 mm/day to 8.3 mm/day from the water filled evaporation pan. In order to collect water content of soil samples, several series of vertical sampling ports in diameter of 10 mm were drilled in a vertical distance of 20 mm. Besides, six thermocouples were installed along the center axis of Column A and Column B for the measurements of soil temperature profile. They were positioned at the soil surface and different depths 10 mm, 25 mm, 50 mm, 100 mm and 250 mm. Electronic scales were used for two soil filled columns and a mechanical balance was used for the water filled pan, allowing the recording of variations of samples' weight (±0.01 g). Hence, the value of evaporation can be obtained directly. The column was filled with saturated Beaver Creek sand initially. After draining to get a hydrostatic situation, it was sealed at the base and the circumference. The surface of column was allowed to evaporate freely. The details about column drying test A are shown in Figure 3. 4.

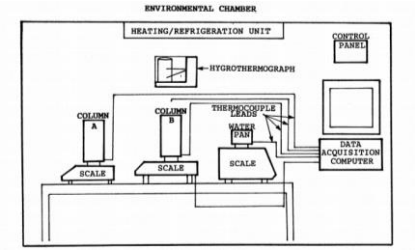


Figure 3. 3. Column drying test by Wilson (1990)

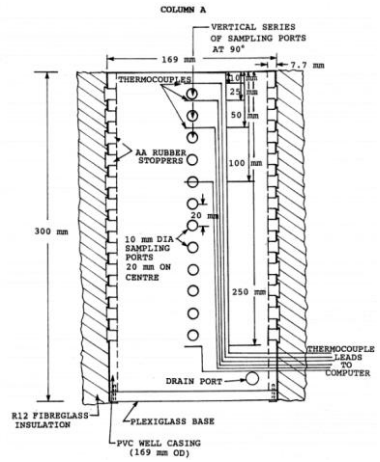


Figure 3. 4. Details about drying test of column A (Wilson 1990)

3.2.2 Model dimensions, initial and boundary conditions

Aiming at the numerical analysis of the soil column drying test, the model dimensions are set as shown in Figure 3. 5.

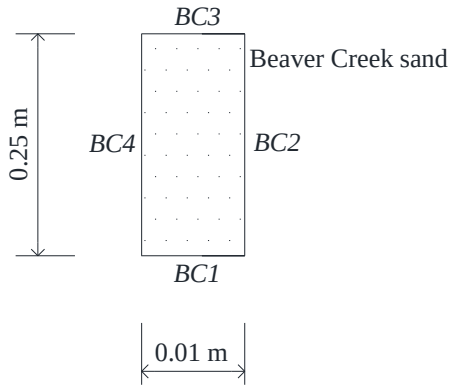


Figure 3. 5. Model dimensions of column drying test

The definitions of the initial conditions of soil temperature and suction are based on the direct measurements of soil temperature and volumetric water content. At the initial moment, the soil temperature is in a constant temperature distribution at 38 °C (Figure 3. 6a). Figure 3. 6b presents the initial distribution of soil volumetric water content. It shows that in the region deeper than 0.2 m, the soil is in the saturated state. The value of soil volumetric water content is becoming less as it approaches the soil surface. In the numerical modelling, the initial soil volumetric water content values are transferred to soil suction values.

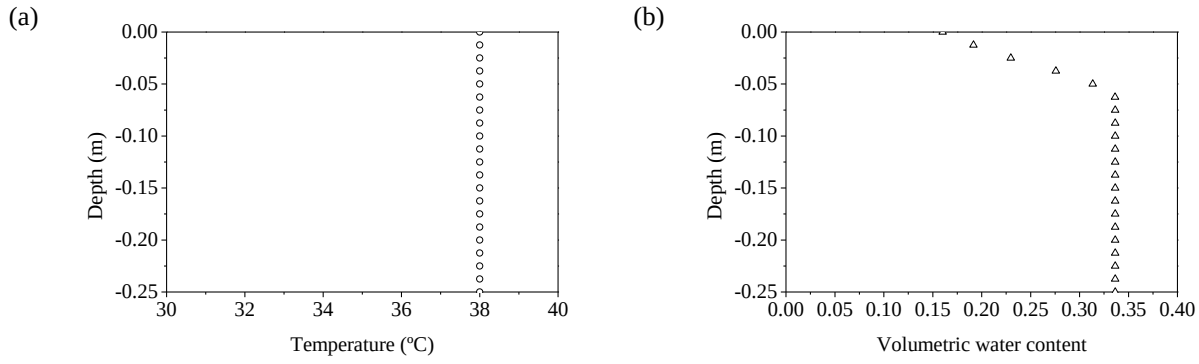


Figure 3. 6. The initial conditions of (a) soil temperature and (b) volumetric water content

As the column drying test was studied under a continuous evaporation process, evaporation is the only factor existing in mass balance (equation 3.1). Thereby, evaporation is the water flux boundary condition applied at the top surface in the numerical modelling. The evaporation of two parallel columns A and B was measured by Wilson (1990) (Figure 3. 7). On the other hand, in the energy balance (equation 3.10), net solar radiation is zero in the environmental chamber. With the calculation of sensible heat (equation 3.29) and latent heat (equation 3.35), soil heat can be determined easily, allowing the estimation of heat flux boundary condition.

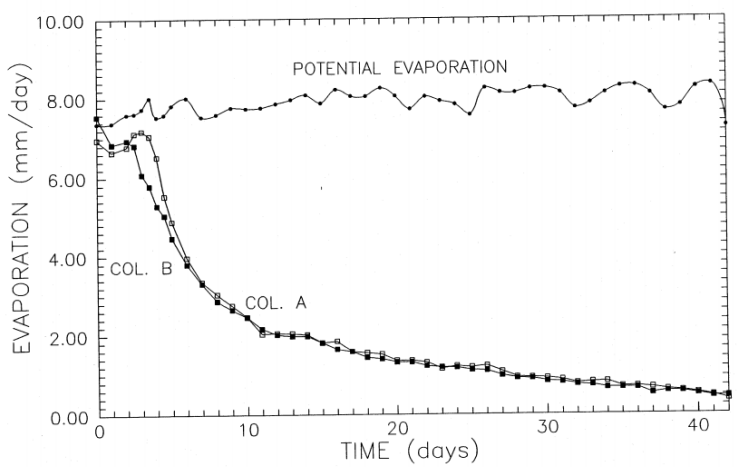


Figure 3. 7. The evaporation measured by Wilson (1990)

Besides, it is assumed that no water and heat transfers happened at the lateral boundaries of soil column during the test. The measured soil temperature and volumetric water content values are used directly as the bottom boundary conditions in the numerical modelling.

3.2.3 Soil parameters

In the numerical analysis of evaporation in the column drying tests, the parameters of the studied soil are required. For Beaver Creek sand used in the column drying test, the soil thermal conductivity, soil water retention, and hydraulic conductivity curves are determined based on the studies by Wilson (1990) and Cui et al. (2005), and presented in Figure 3. 8, Figure 3. 9 and Figure 3. 10, respectively.

A liner relationship between soil thermal conductivity and volumetric water content is adopted.

When soil temperature varies in the range of 30~38 ºC, soil thermal conductivity is estimated by (Figure 3. 8):

$$\lambda = 4.44\theta + 1 \tag{3.36}$$

where λ (W/(mK)) is the soil thermal conductivity; θ is the soil volumetric water content.

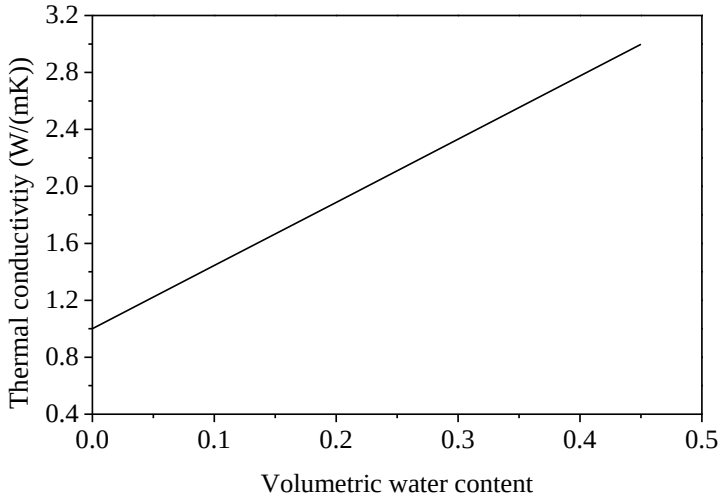


Figure 3. 8. Thermal conductivity curve versus volumetric water content for Beaver Creek sand

The soil water retention curve is expressed as (Figure 3. 9):

$$\theta = \frac{\theta_s - \theta_r}{1 + \left\{1 + \left[\left(\theta_s - \theta_r\right)/\left(\theta_1 - \theta_r\right) - 1\right]\right\}\left(s/s_1\right)^{\xi_1}} + \theta_r \tag{3.37}$$

where θ, θ_s, and θ_1 are the volumetric water content at suction s, null suction and suction s_1, respectively; the values of θ_s and θ_1 equal 0.45 and 0.2, respectively; the value of s_1 equals 6 kPa; the coefficient of proportionality ξ_1 equals 1.98; the residual volumetric water content θ_r is taken as equal to 0.008.

In addition, the relationship between hydraulic conductivity and suction is shown as follows (Figure 3. 10):

$$K = \frac{K_s}{1+\left[\left(K_s/K_1\right)-1\right]\left(s/s_1\right)^{\zeta_2}} \tag{3.38}$$

where the saturated soil hydraulic conductivity K_s equals 3.9×10^{-6} m/s; the suction value s_1 equals 2 kPa; the value of soil hydraulic conductivity K_l at suction s_1 equals 9.63×10^{-8} m/s; the coefficient of proportionality ξ_2 equals 3.

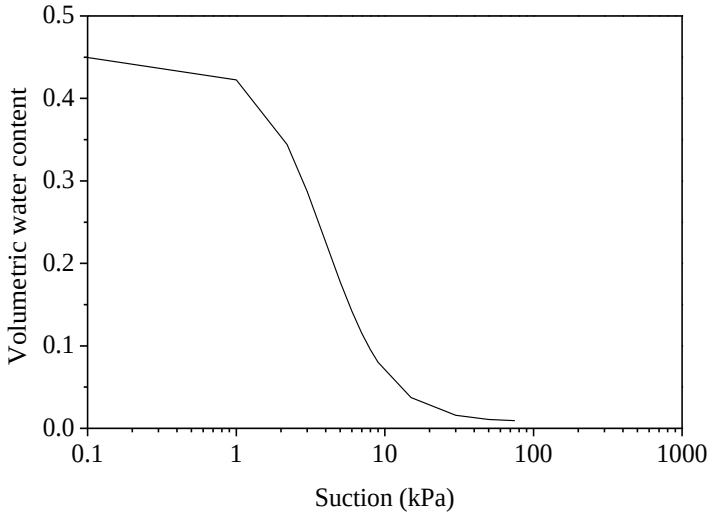


Figure 3. 9. Water retention curve for Beaver Creek sand

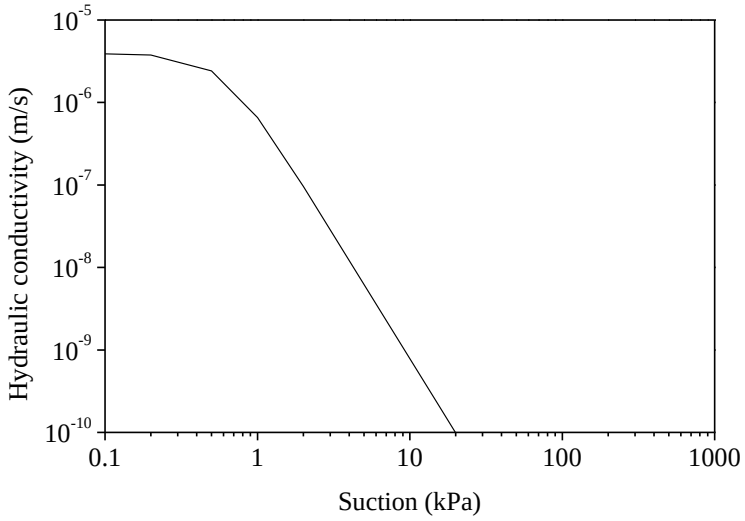


Figure 3. 10. Hydraulic conductivity curve versus suction for Beaver Creek sand

3.2.4 Results and analysis

With the initial and boundary conditions and soil parameters, the numerical analysis of column drying test is conducted by FreeFem++ code. The tests of column A and column B were conducted in parallel, giving the similar results (Wilson 1990). Therefore, only the results of column A are selected for the further comparison with the numerical results. The comparisons of simulation results with the measured data in terms of soil temperature and volumetric water content in the first day are presented in Figure 3. 11 and Figure 3. 12, respectively.

Figure 3. 11 presents a good agreement between the calculated data and the measured data of soil temperature in the first day. The soil temperature shows a decreasing tendency over time. Initially, the whole soil column holds a nearly constant temperature value of 38 °C. Afterwards, under the effect of the soil heat flux boundary condition at the top surface, soil temperature decreases more rapidly in the region near soil surface than that of the deeper zone. In this case, the soil heat flux keeps positive values at the soil surface due to the evaporation taking the soil heat out from soil. The consumption of soil heat leads the decreasing of soil temperature. Hence, the soil surface temperature decreases down to 34.31 °C (1 h), 33.33 °C (2 h), 32.20 °C (4 h), 31.13 °C (8 h), 30.51 °C (16 h) and 30.35 °C (1 day). For the points at the middle region of soil column, the soil temperature decreases but still owing higher values than the surface points. The temperature at the bottom of soil column has a slight decreasing, from 38 °C at the initial moment to 36.85 °C at the first day. Overall, it is proved that the simulation results of soil temperature variation are in good agreement with the measured data.

Figure 3. 12 shows the same overall variation tendency between the calculated data and the measured data of soil volumetric water content. In the first day, the soil volumetric water content of the whole column decreases gradually. The water content in the region near soil surface decreases more rapidly than that of the deeper region because of the top water flux boundary condition (evaporation). The variations of soil volumetric water content at t = 0 h, 1 h, 2 h, 4 h, 8 h, 16 h and 24 h are calculated. Even though the comparison cannot be conducted for these moments because the soil volumetric water content was only measured at moment t = 0 h and t

= 24 h, the simulation results show the consistent variation tendency as the measurements.

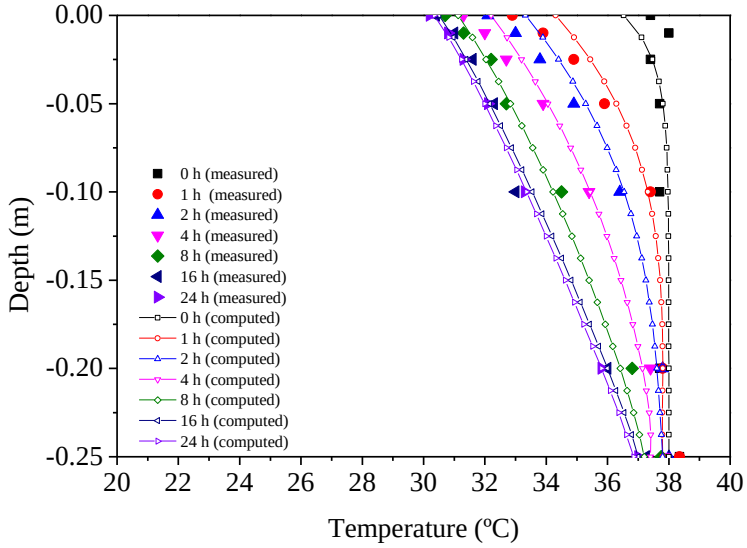


Figure 3. 11. Comparisons of soil temperature between the calculated and measured results at different moments: *t* = 0 h, 1 h, 2 h, 4 h, 8 h, 16 h, and 24 h

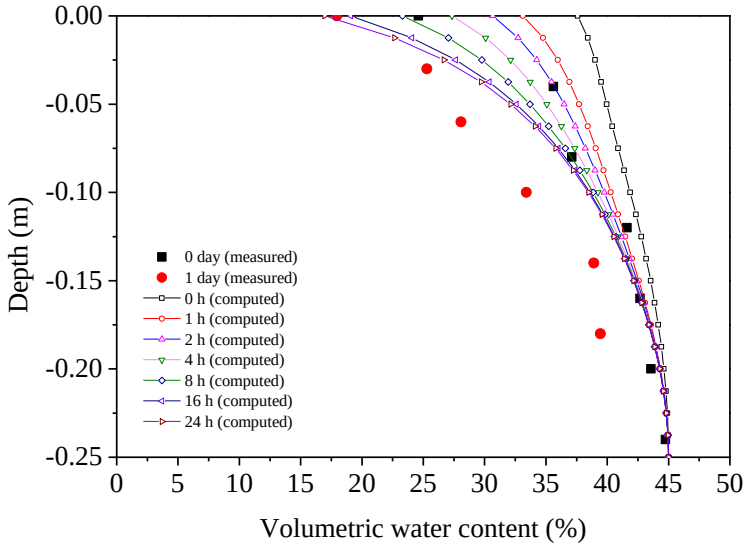


Figure 3. 12. Comparisons of soil volumetric water content between the calculated and measured results at different moments: *t* = 0 h, 1 h, 2 h, 4 h, 8 h, 16 h, and 24 h for computed results; *t* = 0 h and 24 h for measured results

3.3 Conclusions

This chapter describes the mass and energy balances in soil-atmosphere interaction. By combining the coupled hydro-thermal model and the soil-atmosphere interaction model, a numerical approach for studying soil hydro-thermal behavior under climate effect is developed. This approach is further validated through a column drying test carried out by Wilson (1990). The main conclusions are summarized below:

1) The interaction between soil and atmosphere is discussed in this chapter, by considering water and heat transfers through the mass and energy balances, respectively. In the mass balance equation, the value of rainfall can be partitioned into infiltration, runoff and actual evaporation. Rainfall value is normally recorded in meteorological stations, and runoff value can be determined by either direct measurement using suitable devices or prediction using appropriate methods. The value of actual evaporation can be estimated by direct measurements or empirical formulas, depending on the conditions of the studied cases. On the other hand, in the energy balance equation, the value of net solar radiation is the sum of sensible heat, latent heat and soil heat. Various methods for estimating net solar radiation, sensible heat and latent heat are presented with their application conditions. It is suggested to select the method to calculate these heat fluxes according to the known parameters and the conditions of the studied cases;
2) Based on the mass and energy balance equations, the estimation of infiltration I_{nf} and soil heat G can be conducted. They will be set as water and heat flux boundary conditions at soil-atmosphere interfaces in the fully coupled hydro-thermal model. The values of these two boundary conditions are influenced continuously by the atmosphere condition (net solar radiation, wind speed, air relative humidity, air temperature, etc.) and the soil surface situation (the value of soil temperature and suction). They must be determined by iteration calculations;
3) To verify the proposed approach combining the fully coupled hydro-thermal model and the soil-atmosphere interaction model, the experimental results from a column drying test

carried out by Wilson (1990) are adopted to do the comparison with the numerical results. A high consistency is obtained between the numerical and experimental results, indicating that the adopted numerical method is capable of determining the soil temperature and volumetric water content variations accurately provided that soil parameters and the initial and boundary conditions are well determined.

Chapter 4: Modelling of evaporation tests in environmental chamber

4.1 Environmental chamber

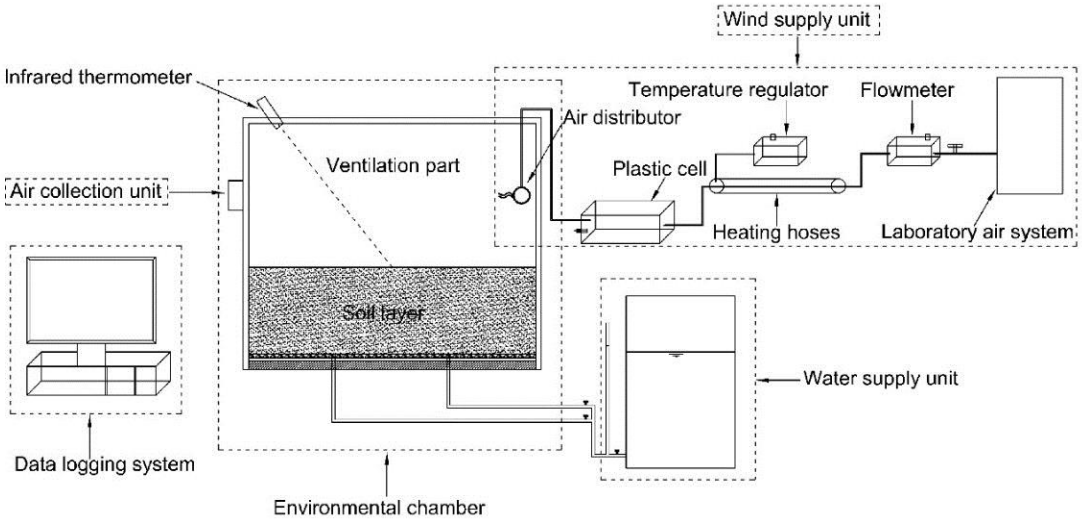
An environmental chamber has been developed (Cui et al. 2013; Song 2014; Song et al. 2014; Ta 2009) in the laboratory, as shown in Figure 4. 1a. The whole experimental setup includes an environmental chamber, a wind supply unit, an air collection unit, a photograph collection unit, a water supply unit and a data logging system. The chamber has a top cover of 8 mm thick, wall of 20 mm thick, an internal width of 800 mm and an internal length of 1000 mm. Figure 4. 1b presents the outlook of the environmental chamber system. Figure 4. 2 shows a simplified three dimensional view.

In order to estimate the soil temperature and volumetric water content variations during a test, different sensors were installed at various depths during the sample preparation by compaction (Figure 4. 3). In this study, the temperature of the soil grains, water and air are assumed to be in an equilibrium sate, having the same values. The drainage layer is a compacted gravel layer 15 mm thick (grain diameter: 2~4 mm) and sandwiched between two layers of geotextile 1 mm thick (Figure 4. 3). In addition, two outlets were set up at the bottom of the drainage layer for soil saturation, drainage and water supply.

Further details of the used sensors are presented in Table 4. 1. Theta Probes were used to measure the soil volumetric water content, and they were buried at different depths (25 mm, 40 mm, 55 mm, 125 mm and 225 mm below the soil surface. Six PT1000 soil temperature sensors were installed every 50 mm along the soil column (0 mm, 25 mm, 75 mm, 125 mm, 175 mm, 225 mm and 275 mm) under the soil surface. Besides, an infrared thermometer was fixed at the top of environmental chamber to measure soil surface temperature. Additionally, thermistors were fixed at different elevations along one side of the wall in the ventilation part, allowing the data recording of air temperature (80 mm, 185 mm, 275 mm, 380 mm and 465 mm above the

soil surface).

(a)



(b)

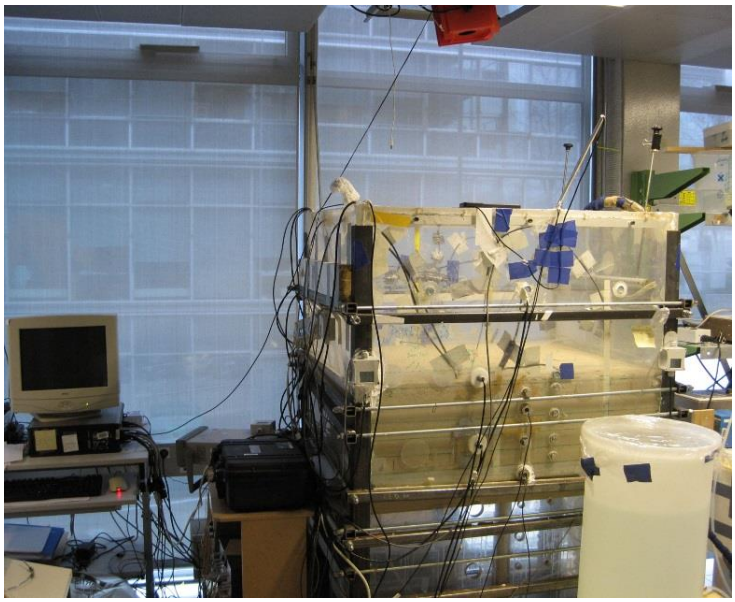


Figure 4. 1. (a) Sketch of the environmental chamber test system; (b) Outlook of the environmental chamber system (Song at al. 2014)

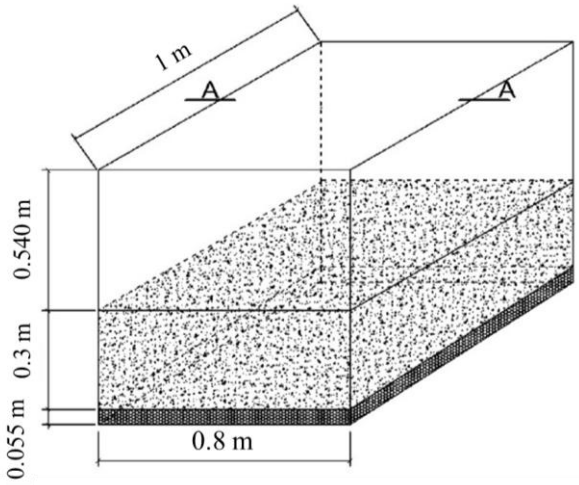


Figure 4. 2. Three-dimensional view of the environmental chamber (Song at al. 2014)

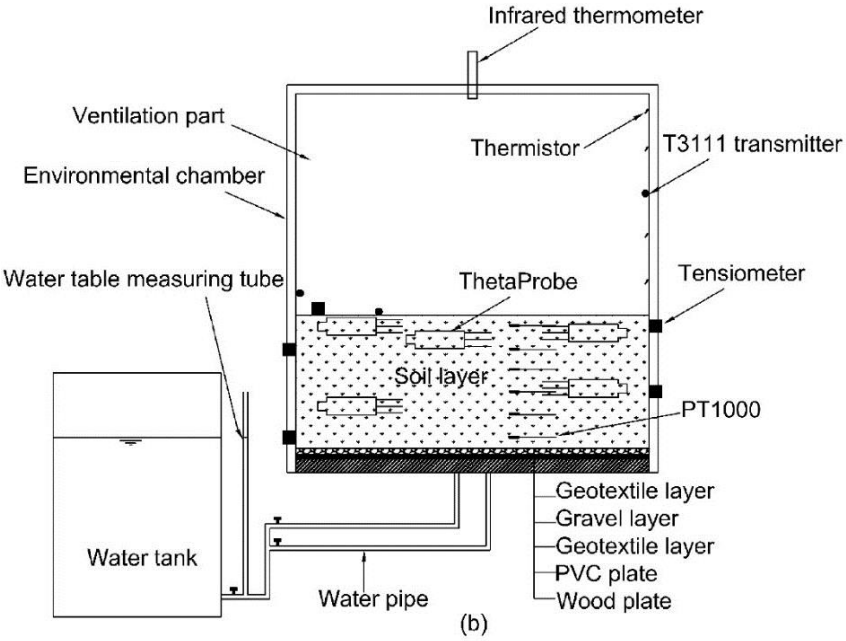


Figure 4. 3. Environmental chamber sensors and details of the schematic cross section (A-A) (Song at al. 2014)

The air flow rate was controlled by a regulator and was monitored by a flowmeter. One anemometer was fixed on one edge of the chamber for measuring wind speed at 50 mm above the center of soil surface. Note that the wind speed at this position was considered as representative of its values in the chamber.

Four soil water evaporation tests were conducted with various air flow rates and heating tube

temperatures. The details of conditions in four tests are presented in Table 4. 2. Note that the heating tube temperature is much higher than the air temperature in the environmental chamber.

Table 4. 1. Details of the used sensors

Sensor	*Model / Manufacturer*	*Parameter measured*	*Range*	*Accuracy*	*Number*
Theta Probe	ML2x / Delta-T	Volumetric Water Content	0~100%	±1.0%	5
PT1000	PT1000 / Correge	Soil Temperature	0~100 °C	±0.3 °C	6
Infrared Thermometer	Pyropen-D / Calex	Soil Surface Temperature	-20~250 °C	±1.0%	1
Thermistors	DO-35 / Radiospare	Air Temperature	-40~250 °C	±1.0%°	5
Anemometer	435-2 / Testo	Wind velocity	0~20 m/s	±(0.03 m/s + 5% measured value)	1
Flowmeter	MAS-2130/ Kobold	Air flow rate	0~500 L/min	±1.5 % full scale	1
Transmitter	T3111 / Elcowa	Relative humidity Temperature	0~100 % -30~-150 °C	±2.5 % ±0.4 °C	6

Table 4. 2. Four tests under different conditions of evaporation

Test number	*Air flow rate (L/min)*	*Temperature in heating tube (°C)*	*Test duration (days)*
Test 1	185	50	11.5
Test 2	172	200	11.5
Test 3	130	50	17.5
Test 4	130	200	30

Fontainebleau sand was selected for the evaporation experiment. It is a natural, fine, white siliceous sand (Figure 4. 4a). Its specific gravity, maximum density and minimum density are 2.64 Mg/m^3, 1.75 Mg/m^3, and 1.39 Mg/m^3, respectively. Its effective grain size D_{10} is 0.14 mm and the coefficient of uniformity, $C_u = D_{60}/D_{10}$, equals 1.6 (Delfosse Ribay et al. 2004). The grain size distribution curve determined by sieving is shown in Figure 4. 4b.

(a)



(b)

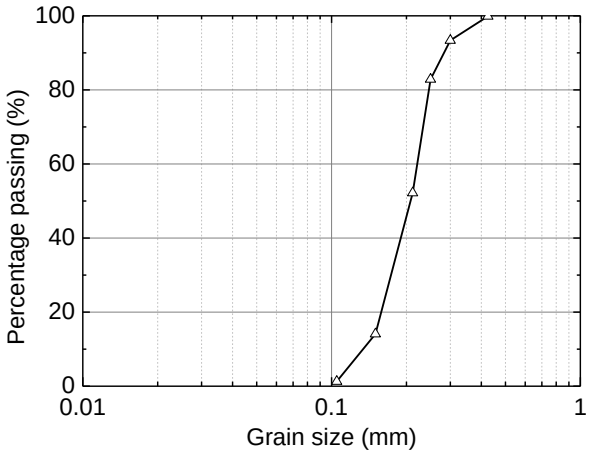


Figure 4. 4. Fontainebleau sand: (a) picture of Fontainebleau sand; (b) grain size distribution curve

4.2 Definition of numerical model

4.2.1 Model dimensions, initial and boundary conditions

Based on the three-dimensional view of the environmental chamber presented in Figure 4. 2, the numerical model is assumed to be two-dimensional with 1 m width, and 0.3 m height (Figure 4. 5). The different boundaries are also named in the numerical modelling: BC1 is the bottom boundary; BC2 and BC4 are the lateral boundaries; BC3 is the top boundary which is the soil-atmosphere interface.

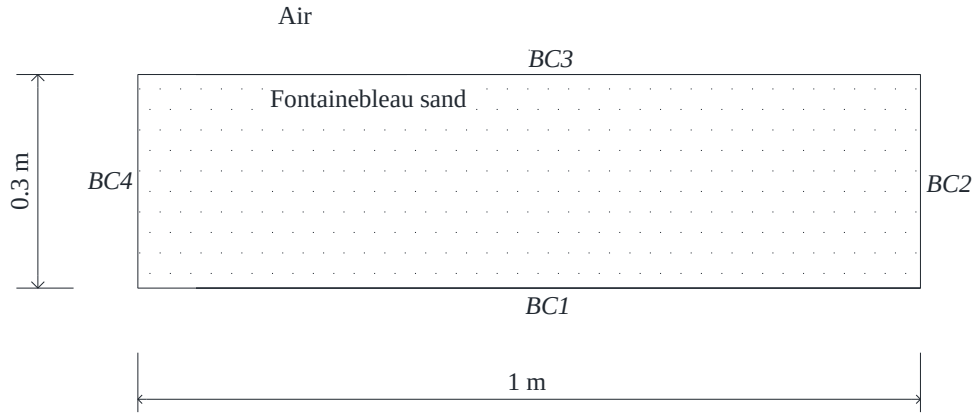


Figure 4. 5. Model dimensions in the numerical modelling of environmental chamber

In addition, the measured values of soil temperature and volumetric water content at the beginning of each test are defined as the initial conditions. Considering water and heat transfers between soil and atmosphere, the water and heat flux conditions at the top boundary are estimated as follows.

Mass balance

The mass balance at the soil surface is expressed by equation (3.1). In the environmental chamber tests, the value of rainfall (P), runoff (R_{off}), interception (I_{nt}) and infiltration (I_{nf}) are equal to zero. As a result, the evaporation represents the water flux boundary condition on the soil top surface in the drying tests.

Four drying tests were implemented in environmental chamber through air flows at different rates and different temperatures. The values of the corresponding evaporation were determined by Song et al. (2014):

$$E_a = 86400Q\left(h_{a-outlet} - h_{a-inlet}\right)/\left(\rho_l A\right) \tag{4.1}$$

where E_{a} (mm/day) is the actual evaporation rate; Q (L/s) is the air flow rate through the chamber; $h_{\text{a-outlet}}$ and $h_{\text{a-inlet}}$ (Mg/m^3) are the absolute humidity values at the outlet and inlet, respectively; ρ_{l} (Mg/m^3) is the water liquid density; A (m^2) is the area of the exposed

evaporative surface in the chamber.

The evaporation process in the four tests continued for 11.5 days, 11.5 days, 17.5 days, and 30 days, as presented in Figure 4. 6a, Figure 4. 6b, Figure 4. 6c, Figure 4. 6d, respectively:

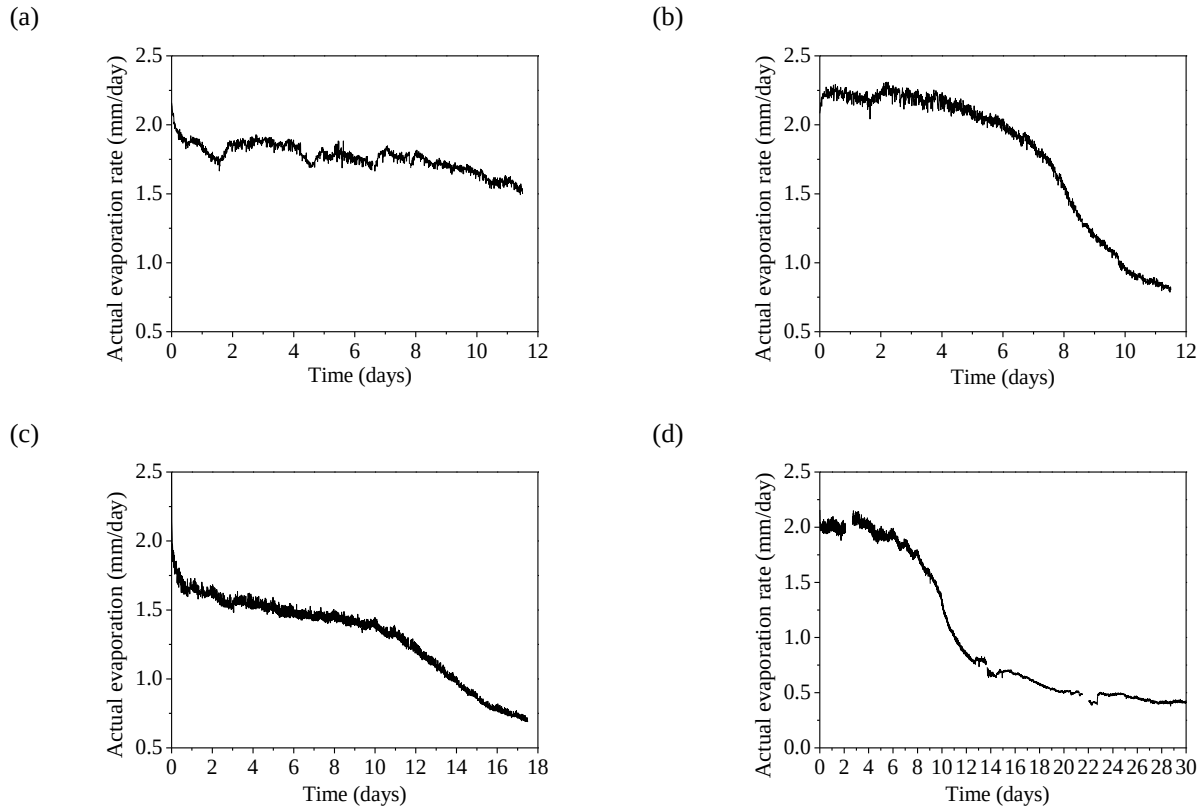


Figure 4. 6. Evolutions of actual evaporation rate: (*a*) Test 1; (*b*) Test 2; (*c*) Test 3; (*d*) Test 4

In terms of heat transfer at the soil surface, the energy balance is presented by equation (3.14). In this environmental chamber, the value of net radiation is zero because of the absence of solar radiation. As a result, equation (3.14) can be rewritten as:

$$H = G + L_E \tag{4.2}$$

Due to the convection of air flow during soil-atmosphere interaction, the sensible heat can be estimated based on equation (3.29).

With the known actual evaporation, the latent heat can be calculated by:

$$L_E = L_v E_a \tag{3.35}$$

where L_v is the latent heat of water vaporization; the actual evaporation E_a in the four tests are presented in Figure 4. 6. Based on the energy balance, the value of soil heat flux G is calculated and applied as the heat flux boundary condition at the interfaces of atmosphere and soil.

All the details of initial conditions and boundary conditions in the numerical modeling are listed in Table 4. 3.

Table 4. 3. Initial and boundary conditions used

Initial conditions		Measurement data at the starting moment	
	Boundary number	*Thermal boundary conditions*	*Hydraulic boundary conditions*
Boundary conditions	BC1	Measured soil temperature	$\varphi = 0$
	BC2, BC4	$G = 0$	$L_{vn} = 0$
	BC3	$G = H - L_E$ $H = f(T_3)$	$L_{vn} = E_a$
where T_3 is the soil surface temperature at "BC3" boundary as shown in Figure 4. 5. Other terms are explained in Chapter 3.			

4.2.2 Soil parameters

Fontainebleau sand is assumed to be homogeneous and isotropic. The hydro-thermal properties of Fontainebleau sand are required in the numerical modeling. Its thermal conductivity, water retention curve, and hydraulic conductivity are determined and presented respectively as follows.

KD2 analyzer (see Figure 4. 7) is used to measure the soil thermal conductivity (Tang et al. 2008; Buongiorno et al. 2009; Teng et al. 2010). According to the methods proposed by Côté and Konrad (2005) (Figure 4. 8), an analytical relationship between soil thermal conductivity and volumetric water content for medium and fine sand is chosen to express the thermal

conductivity of Fontainebleau sand:

$$\lambda = (\lambda_{sat} - \lambda_{dry}) \cdot \lambda_r + \lambda_{dry} \tag{4.3}$$

$$\lambda_r = \frac{3.55 \cdot S_r}{1 + (3.55 - 1) \cdot S_r} \tag{4.4}$$

where λ (W/(mK)) is the soil thermal conductivity; λ_{sat} and λ_{dry} are the soil volumetric water content in saturated state and dry state, equal 2.903 (W/(mK)) and 0.276 (W/(mK)), respectively; λ_r is the Kersten number; S_r is the degree of saturation. The analytical curve of soil thermal conductivity versus volumetric water content is drawn in Figure 4. 9. Specifically, the thermal conductivity of the surface region (0~-0.025 m) is assumed to be 0.05 (W/(mK)).

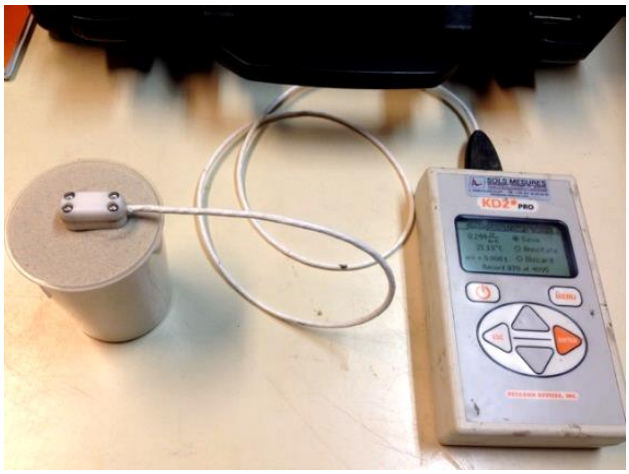


Figure 4. 7. KD2 Analyzer used to measure thermal conductivity for Fontainebleau sand

The volumetric water content variations with suction have been measured by Doussan and Ruy (2009), Mbonimpa et al. (2004) and Song (2014) (Figure 4. 10). Based on van Genuchten model (van Genuchten 1980), the fitting curve of soil water retention is drawn (Figure 4. 10) with the following expression:

$$S_e = \frac{\theta - \theta_r}{\theta_s - \theta_r} = \left[\frac{1}{1 + (\alpha_s \varphi)^n} \right]^m \tag{4.5}$$

where S_e is the effective saturation; θ_s is the saturated volumetric water content, equals 0.356; θ_r is the residual volumetric water content, equals 0.04; α_s, m and n are the soil constants, equal 0.2 kPa^{-1}, 0.8, 3.0, respectively.

Additionally, the saturated hydraulic conductivity of Fontainebleau sand was measured through constant water head test. Based on the soil water retention curve determined previously, the hydraulic conductivity at unsaturated state is estimated using van Genuchten model (van Genuchten 1980) considering residual hydraulic conductivity (Figure 4. 11),

$$K = \left(K_s - K_r\right) S_e^{0.5} \left[1 - \left(1 - S_e^{1/m_1}\right)^{m_1}\right]^2 + K_r \tag{4.6}$$

where $m_1 = 0.5$; saturated hydraulic conductivity $K_s = 1.36\times10^{-5}$ m/s; residual hydraulic conductivity $K_r = 3.75\times10^{-9}$ m/s; other parameters have the same values as in equation (4.5). Note that the hysteresis in terms of soil water retention and hydraulic conductivity behavior was neglected in this study.

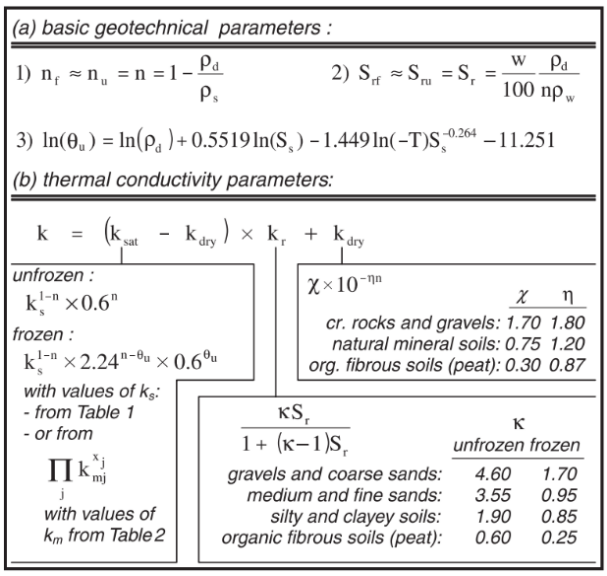


Figure 4. 8. Analytical relationship between soil thermal conductivity and volumetric water content summarized by Côté and Konrad (2005)

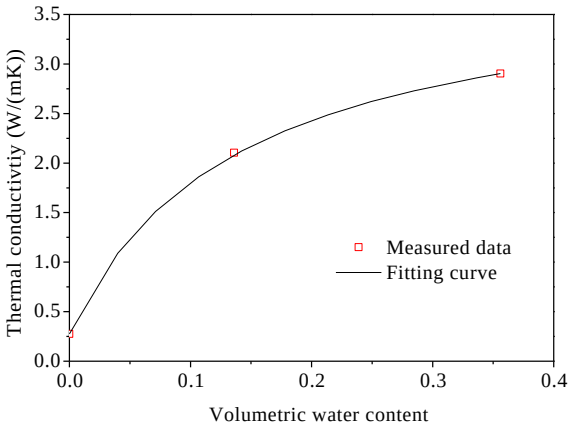


Figure 4. 9. Thermal conductivity curve versus volumetric water content for Fontainebleau sand

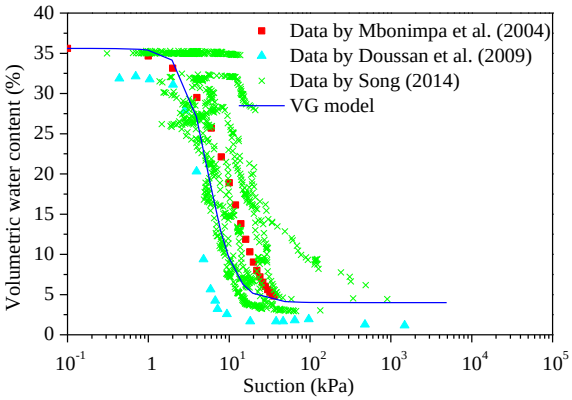


Figure 4. 10. Water retention curve for Fontainebleau sand

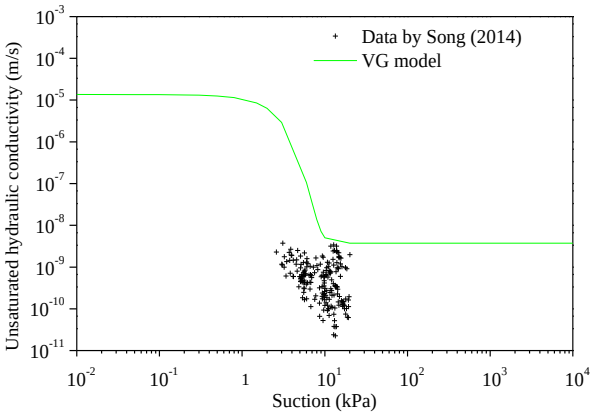


Figure 4. 11. Hydraulic conductivity curve versus suction for Fontainebleau sand

4.3 Results and analysis

The numerical investigation of soil-atmosphere interaction in the four tests is conducted by finite element method through FreeFem++ code (Hecht 2010). The comparisons between calculated and measured results of soil hydro-thermal behavior are analyzed as follows.

4.3.1 Test 1

Figure 4. 12 presents the calculated and measured variations of soil temperature over depth in Test 1. Overall, soil temperature in deep region (-0.025~-0.300 m) shows a liner relationship with depth, varying in a small range. In the region near the soil surface (0~-0.025 m), soil temperature increases sharply as depth increases, presenting a much larger gradient compared with that of deep region. Thereby, the variations of soil temperature profile are discussed in two parts: near surface region (0~-0.025 m) and deep region (-0.025~-0.300 m). On the other hand, it is observed that soil temperature goes down from the initial moment to reach the minimum value at the second day. Afterwards, it begins to go up gradually, showing a temperature rebounding phenomenon. Hence, the variations of soil temperature are divided into two phases: declining phase: t = 0~2 days (Figure 4. 12a) and rebounding phase: t = 2~11.5 days (Figure 4. 12b).

The measurements of soil temperature at the moment t = 0 day corresponds to the initial condition. At this moment, soil temperature goes down quickly from 18.00 °C to 13.80 °C as depth decreases in the near surface region, while it keeps nearly stable at 18 °C in the region deeper than -0.025 m.

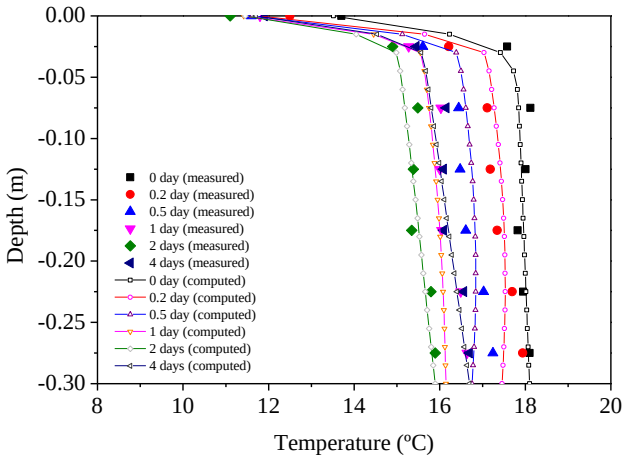
In the first declining phase (Figure 4. 12a), the calculated soil surface temperature declines quickly from the initial value 13.52 °C to 11.76 °C at t = 0.2 day, followed by a slight decrease up to 11.45 °C at the second day. In the deep region, the average calculated soil temperature goes down from the initial value 17.93 °C to 17.47 °C at t = 0.2 day and then reduces to 15.43 °C at t = 2 days.

Concerning the rebounding phase, the calculated value of soil surface temperature shows an increasing tendency, varying from 11.45 °C at t = 2 days to 11.70 °C at t = 4 days, 12.21 °C at t = 6 days, 12.82 °C at t = 8 days and 13.82 °C at t = 11.5 days. The increasing tendency is also observed in the variations of the average soil temperature of the deep region, increasing from 15.43 °C at t = 2 days to 16.11 °C at t = 4 days, 15.99 °C at t = 6 days, 16.52 °C at t = 8 days, and 16.70 °C at t = 11.5 days.

Figure 4. 12b shows that the calculated soil temperatures at the surface point are a little larger than the measured data in the second phase. It is caused by the assumed value of soil thermal conductivity. As a dry layer may appear and become deeper as the evaporation continues (Aluwihare and Watanabe 2003), it is not easy to define the accurate values of soil thermal conductivity in this zone. Nevertheless, as the identified value differences are less than 2.00 °C, the comparisons of soil temperature between simulated and measured results still provide satisfactory agreement.

Figure 4. 13 illustrates the evolution of soil volumetric water content, revealing an overall consistency between the calculation and measurement results. Both of them show a continuous decrease as a result of evaporation. Moreover, it can be identified that the soil volumetric water content in the region near the soil surface decreases more quickly than that in the deep region. There is no comparison of soil volumetric water content at the surface point due to the absence of measurements. The numerical results of soil volumetric water content at surface point decrease gradually from the initial value 21.00% to 9.75% at t = 11.5 days. Note that a water tank was connected to the bottom of soil sample during the whole test, keeping the soil bottom in a saturated situation.

(a)



(b)

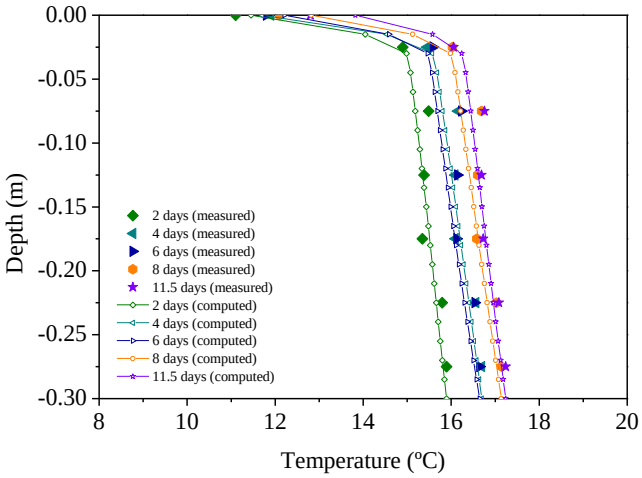


Figure 4. 12. Comparisons between the calculated and measured soil temperature profiles at different moments in Test 1: (a) *t* = 0 day, 0.2 day, 0.5 day, 1 day, 2 days, 4 days; (b) *t* = 2 days, 4 days, 6 days, 8 days, 11.5 days

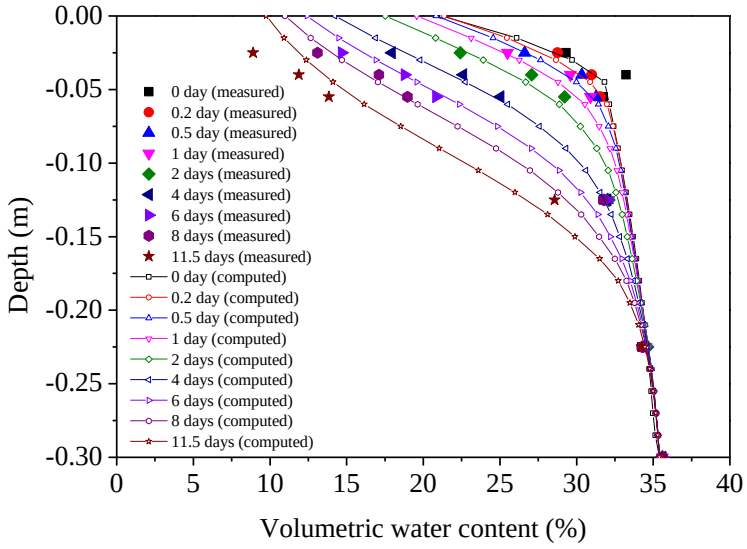


Figure 4. 13. Comparisons between the calculated and measured soil volumetric water content profiles at different moments in Test 1: *t* = 0 day, 0.2 day, 0.5 day, 1 day, 2 days, 4 days, 6 days, 8 days and 11.5 days

4.3.2 Test 2

The evolutions of soil temperature at different moments *t* = 0 day, 0.2 day, 0.5 day, 1 day, 2 days, 4 days, 8 days, and 11.5 days, are presented in Figure 4. 14. The initial condition of the numerical modelling is set based on the measurements at *t* = 0 day, presenting a steady temperature distribution around 18.00 °C. The soil temperature shows a continuous increase in Test 2. Specifically, it is noticed that the surface soil temperature rises up more quickly than those at deeper points, showing a larger gradient of soil temperature distribution in the near surface region (0~-0.025 m) than that in deep region (-0.025~-0.300 m).

At the surface point, the measured soil temperature increases from 18.80 °C at *t* = 0 day to 20.10 °C at *t* = 0.2 day, 20.30 °C at *t* = 0.5 day, 20.50 °C at *t* = 1 day, 22.10 °C at *t* = 4 days, 22.30 °C at *t* = 6 days, 24.20 °C at *t* = 8 days, 29.60 °C at *t* = 11.5 days, respectively. For the deep region (-0.025~-0.300 m), consistent temperature variations are observed at different moments, varying from 18.21 °C at *t* = 0 day to 18.44 °C at *t* = 0.2 day, 18.77 °C at *t* = 0.5 day, 19.20 °C at *t* = 1 day, 19.67 °C at *t* = 2 days, 20.46 °C at *t* = 4 days, 20.47 °C at *t* = 6 days,

21.27 °C at t = 8 days, 23.87 °C at t = 11.5 days.

The calculated results keep an overall consistency with the measured values, giving the value of soil surface temperature as 18.72 °C at t = 0 day, 19.66 °C at t = 0.2 day, 19.76 °C at t = 0.5 day, 20.02 °C at t = 1 day, 20.69 °C at t = 2 days, 21.28 °C at t = 4 days, 21.52 °C at t = 6 days, 23.51 °C at t = 8 days and 25.86 °C at t = 11.5 days. Besides, the average values of calculated soil temperature at the deep region (-0.025~-0.300 m) are 18.29 °C at t = 0 day to 18.55 °C at t = 0.2 day, 18.88 °C at t = 0.5 day, 19.43 °C at t = 1 day, 20.02 °C at t = 2 days, 20.94 °C at t = 4 days, 20.92 °C at t = 6 days, 21.70 °C at t = 8 days and 24.23 °C at t = 11.5 days.

It is identified that the values of calculated soil temperature at soil surface become lower than those of measurements since day 4 until the end of the test. The comparison of soil temperature at deep region also shows several minor differences, less than 0.5 °C. Similar to the case of Test 1, the value differences exist mainly at the surface point. It is attributed to the assumed value of soil thermal conductivity in the near surface region.

Figure 4. 15 shows the consistent tendency of soil volumetric water content variation between calculated and measured data in Test 2. However, the comparison is not conducted for the surface point due to the absence of measured data. Along with the saturated condition at the bottom of soil sample, the soil volumetric water distribution in the soil sample is mainly affected by the surface evaporation. Thereby, the soil volumetric water content at the near surface region decreases more quickly than in the deep region.

Some differences are identified since day 6: the measured data shows a continuous decrease, while the calculated results decline at one moment and then start to go up. This phenomenon suggests that more water is supplied by deep region after day 6. For instance, the calculated soil surface volumetric water content at t = 11.5 days is 11.07%, larger than 9.83% at t = 8 days. It is attributed to the adopted values of soil hydraulic conductivity, leading to different water flow and water content distribution in soil.

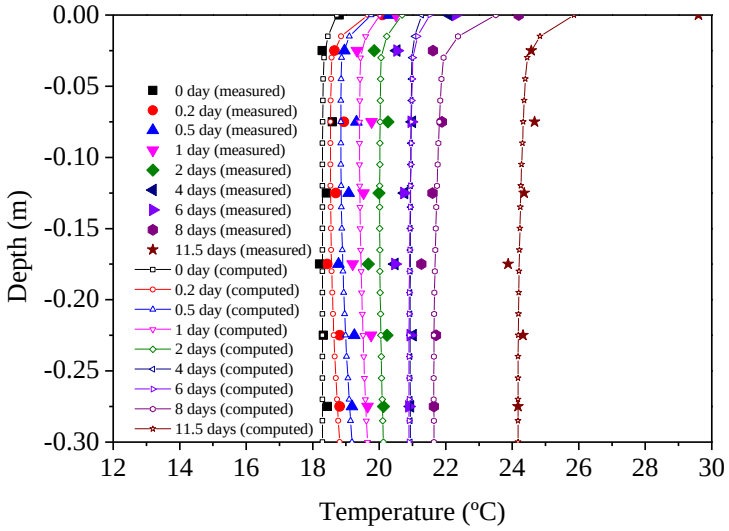


Figure 4. 14. Comparisons between the calculated and measured soil temperature profiles at different moments in Test 2: *t* = 0 day, 0.2 day, 0.5 day, 1 day, 2 days, 4 days, 6 days, 8 days, and 11.5 days

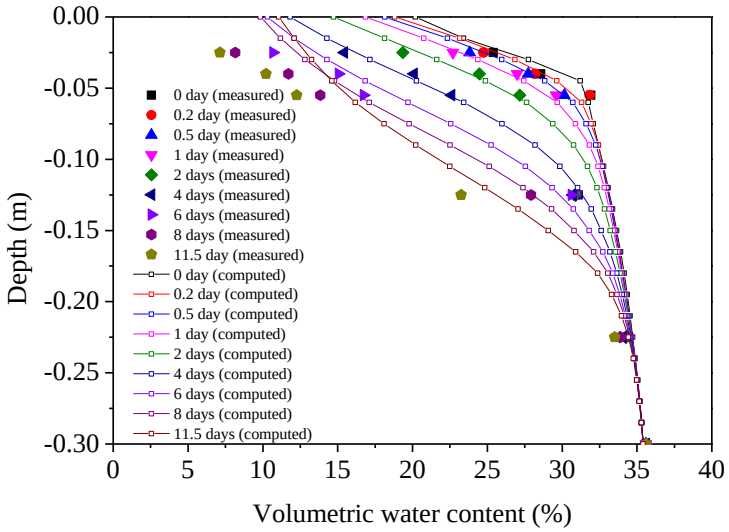


Figure 4. 15. Comparisons between the calculated and measured soil volumetric water content profiles at different moments in Test 2: *t* = 0 day, 0.2 day, 0.5 day, 1 day, 2 days, 4 days, 6 days, 8 days, and 11.5 days

4.3.3 Test 3

Similar to the case of Test 1, the variation of soil temperature profile in Test 3 is discussed in two separate parts: near surface region (0~-0.025 m) and deep region (-0.025~-0.300 m). The process of soil temperature variations in Test 3 can also be divided into two phases: declining phase (Figure 4. 16a) and rebounding phase (Figure 4. 16b).

At the initial moment, the calculated soil temperature in the near surface region increases sharply from 16.01°C (0 m) to 20.22 °C (-0.025 m). In the deep region, the soil temperature keeps a constant value of 20.00 °C.

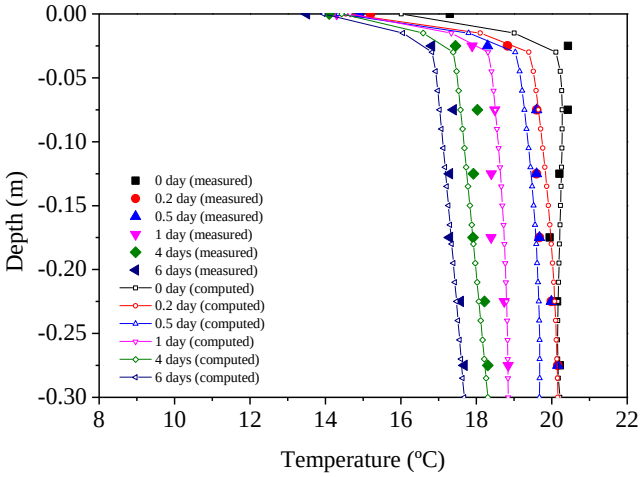
In the first declining phase, the calculated soil surface temperature decreases quickly from 16.01 °C at t = 0 day to 14.54 °C at t = 0.2 day, then decreases slightly from 14.54 °C (0.2 day) to 13.95 °C at t = 6 days. The average soil temperature of deep region goes down from the initial value 20.18 °C to 20.05 °C at t = 0.2 day, 17.43 °C at t = 6 days, respectively. After day 6, the soil temperature begins to go up gradually: the value of soil surface temperature is 13.95 °C, 14.69 °C, 15.52 °C, 16.62 °C, and 17.57 °C at t = 6 days, 8 days, 11.5 days, 15 days, and 17.5 days, respectively; the average value in the deep region is 17.29 °C, 17.63 °C, 17.59 °C, 17.31 °C, and 18.62 °C at t = 6 days, 8 days, 11.5 days, 15 days, and 17.5 days, respectively.

An overall satisfactory agreement can be observed in the comparisons between the calculated and measured data in terms of soil temperature, albeit some minor differences. At the surface point, the calculated soil temperatures are slightly larger than the measured ones since day 6 until the end of test. It is attributed to the differences of soil thermal conductivity between the assumed value and the real one. On the other hand, the differences of soil temperature at deep region are negligible as they are identified to be less than 0.50 °C.

Additionally, Figure 4. 17 presents the same variation tendency between the calculated and measured results of soil volumetric water content in Test 3. Along with the saturated condition at the bottom of soil sample, evaporation serves as the top water flux boundary condition for 17.5 days. Consequently, the whole soil volumetric water of soil sample decreases continuously.

The calculated temperatures fit well with the measured data in the first six days, followed by some differences between them. The values of calculated results are larger than those of measured data, indicating that more water is allowed to be transported to the surface region since day 6 to day 17.5. Thus, it is inferred that the assumed soil hydraulic conductivity in the near surface region is larger than the real value, which requires further investigation.

(a)



(b)

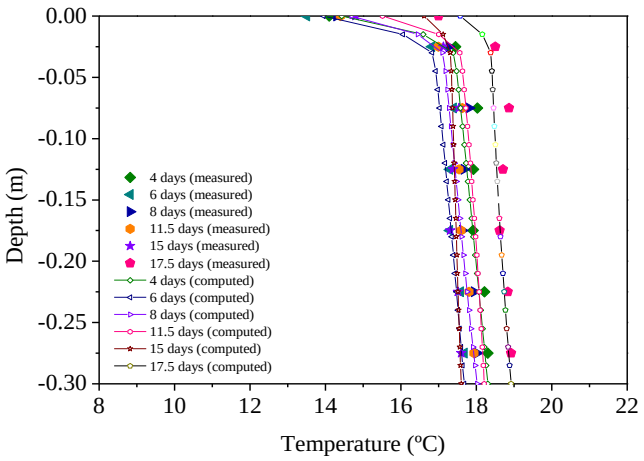


Figure 4. 16. Comparisons between the calculated and measured soil temperature profiles at different moments in Test 3: (a) *t* = 0 day, 0.2 day, 0.5 day, 1 day, 4 days, and 6 days; (b) *t* = 4 days, 6 days, 8 days, 11.5 days, 15 days, and 17.5 days

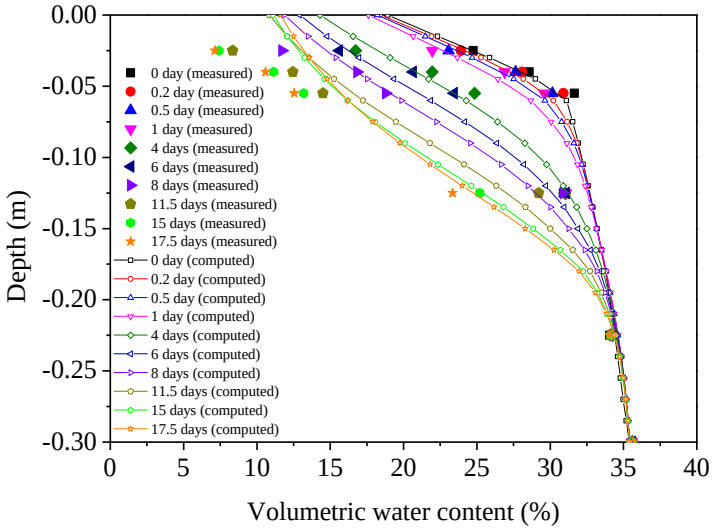


Figure 4. 17. Comparisons between the calculated and measured soil volumetric water content profiles at different moments in Test 3: *t* = 0, 0.2 day, 0.5 day, 1 day, 4 days, 6 days, 8 days, 11.5 days, 15 days, and 17.5 days

4.3.4 Test 4

The evolutions of soil temperature at different moments *t* = 0 day, 0.2 day, 0.5 day, 1 day, 2 days, 4 days, 6 days, 8 days, 12 days, 18 days, 20 days and 30 days in Test 4 are presented in Figure 4. 18. The initial conditions in the numerical modelling are set based on the measurements at *t* = 0 day, presenting a steady temperature distribution around 21 °C with the surface point at a specific value of 18.80 °C. In the whole period, the soil temperature shows a continuous increase as in the case of Test 2. Moreover, it is observed that the calculated surface soil temperature rises up more quickly in the near surface region (0~-0.025 m), leading to a larger gradient of temperature than that in the deep region (-0.025~-0.300 m).

At the surface point, the measured soil temperature increases from 18.80 °C at *t* = 0 day to 21.50 °C at *t* = 0.25 day, 21.70 °C at *t* = 0.5 day, 22.30 °C at *t* = 1 day, 22.80 °C at *t* = 2 days, 23.00 °C at *t* = 4 days, 23.00 °C at *t* = 6 days, 23.10 °C at *t* = 8 days, 24.90 °C at *t* = 12 days, 30 °C at *t* = 18 days, 30.4 °C at *t* = 20 days, and 33.3 °C at *t* = 30 days, respectively. For the deep region (-0.025~-0.300 m), consistent temperatures are observed at different moments:

20.29 °C at t = 0 day to 20.57 °C at t = 0.25 day, 20.89 °C at t = 0. 5 day, 21.29 °C at t = 1 day, 21.62 °C at t = 2 days, 22.19 °C at t = 4 days, 21.66 °C at t = 6 days, 21.36 °C at t = 8 days, 22.01 °C at t = 12 days, 23.74 °C at t = 18 days, 23.50 °C at t = 20 days and 27.88 °C at t = 30 days.

The calculated surface soil temperature varies from 18.72 °C at t = 0 day to 22.91 °C at t = 0.25 day, 21.84 °C at t = 0. 5 day, 22.29 °C at t = 1 day, 22.75 °C at t = 2 days, 23.10 °C at t = 4 days, 23.09 °C at t = 6 days, 23.49 °C at t = 8 days, 25.39 °C at t = 12 days, 26.84°C at t = 18 days, 26.96 °C at t = 20 days, and 27.44 °C at t = 30 days. In the deep region, soil keeps the consistent temperature during the whole period of test, varying from 20.81 °C at t = 0 day to 20.74 °C at t = 0.25 day, 20.98 °C at t = 0. 5 day, 21.42 °C at t = 1 day, 21.87 °C at t = 2 days, 22.68 °C at t = 4 days, 22.05 °C at t = 6 days, 21.85 °C at t = 8 days, 21.22 °C at t = 12 days, 24.30 °C at t = 18 days, 24.09 °C at t = 20 days and 25.22 °C at t = 30 days.

Concerning the comparison of soil temperatures by calculations and measurements, the calculated value at surface point is smaller than the measured data since day 12 until the end of test. It is caused by the estimated values of soil thermal conductivity in the surface region, being different with its real value. Thereby, the importance to study the soil thermal conductivity in this region is revealed again. Besides, a satisfactory agreement between the calculated and measured soil temperatures is obtained in the deep region.

The overall consistent tendency between the calculated and measured data of soil volumetric water content is identified in Figure 4. 19. In the first six days, the calculated data at the selected moments are nearly consistent with the measured data. As evaporation continues, the calculated soil volumetric water content begins to show larger values than the measured data, suggesting that more water is transferred from deep region than in the real situation. This phenomenon is inferred as the result of the differences between the assumed soil hydraulic conductivity and the real one.

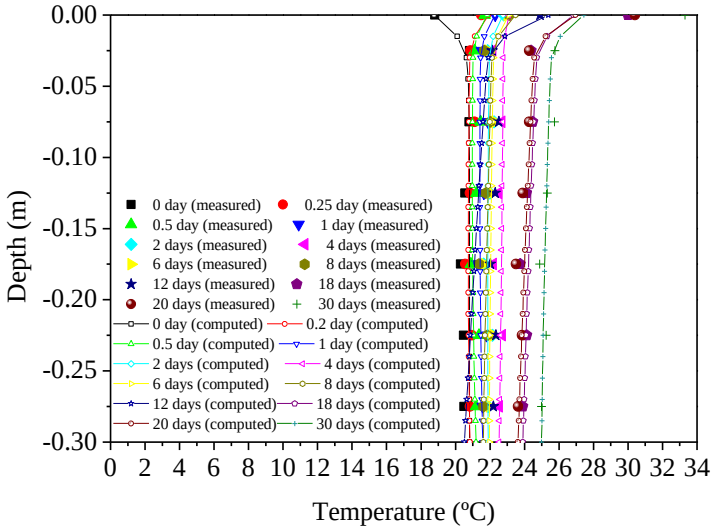


Figure 4. 18. Comparisons between the calculated and measured soil temperature profiles at different moments in Test 4: *t* = 0 day, 0.25 day, 0.5 day, 1 day, 2 days, 4 days, 6 days, 8 days, 12 days, 18 days, 20 days, and 30 days

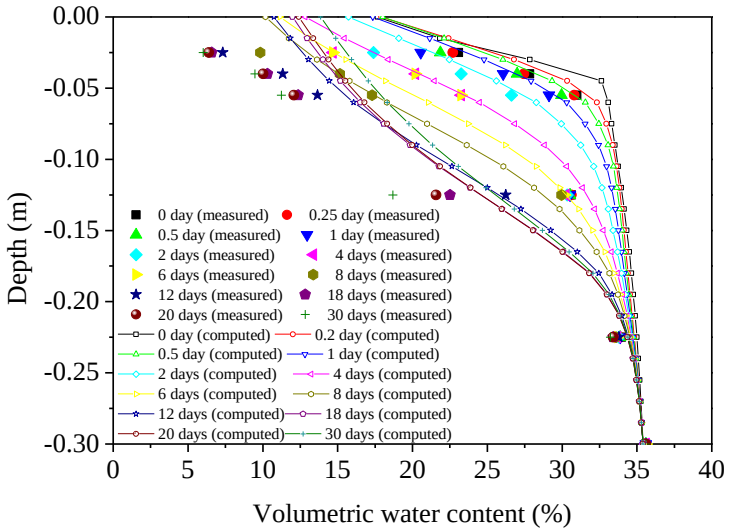


Figure 4. 19. Comparisons between the calculated and measured soil volumetric water content profiles at different moments in Test 4: *t* = 0 day, 0.25 day, 0.5 day, 1 day, 2 days, 4 days, 6 days, 8 days, 12 days, 18 days, 20 days, and 30 days

4.4 Discussion

4.4.1 Definition of typical evaporation stages

According to the air temperature in the chamber (Table 4. 2), the four tests carried out can be summarized as two groups: Group 1 with low air temperature (heating tube temperatures 50 °C) (Test 1 and Test 3) and Group 2 with high air temperature (heating tube temperatures 200 °C) (Test 2 and Test 4).

The evaporation process was recorded for 11.5 days, 11.5 days, 17.5 days and 30 days in Test 1, Test 2, Test 3 and Test 4, respectively. Two phases in the evaporation process can be identified in Test 1 (Figure 4. 20a): first falling stage (0~2 days) and constant-rate stage (2~11.5 days). Figure 4. 20c reveals three phases of evaporation process in Test 3: first falling stage (0~6 days), constant-rate stage (6~11.5 days) and slow-rate stage (11.5~17.5 days). On the other hand, the same three-phases are observed in Test 2 (Figure 4. 20b) and Test 4 (Figure 4. 20d): the evaporation in Test 2 consists of a constant-rate stage (0~6 days), a falling-rate stage (6~10 days) and a slow-rate stage (10~11.5 days); the evaporation in Test 4 involves a constant-rate stage (0~6 days), a falling-rate stage (6~14 days) and a slow-rate stage (14~30 day).

In literature, the three-phase evaporation process has been summarized (Wilson et al. 1994; Yanful and Choo 1997; Hillel 2003; Lal and Shukla 2005; Qiu and Ben-Asher 2010) and presented as (Figure 4. 21): constant-rate stage; falling-rate stage; slow-rate stage. This general definition is defined for evaporation along with three conditions:

(1) A continuous supply of evaporative energy;

(2) A vapor pressure gradient existing between the evaporating surface and atmosphere;

(3) A continual supply of water from the interior of soil to the evaporating surface.

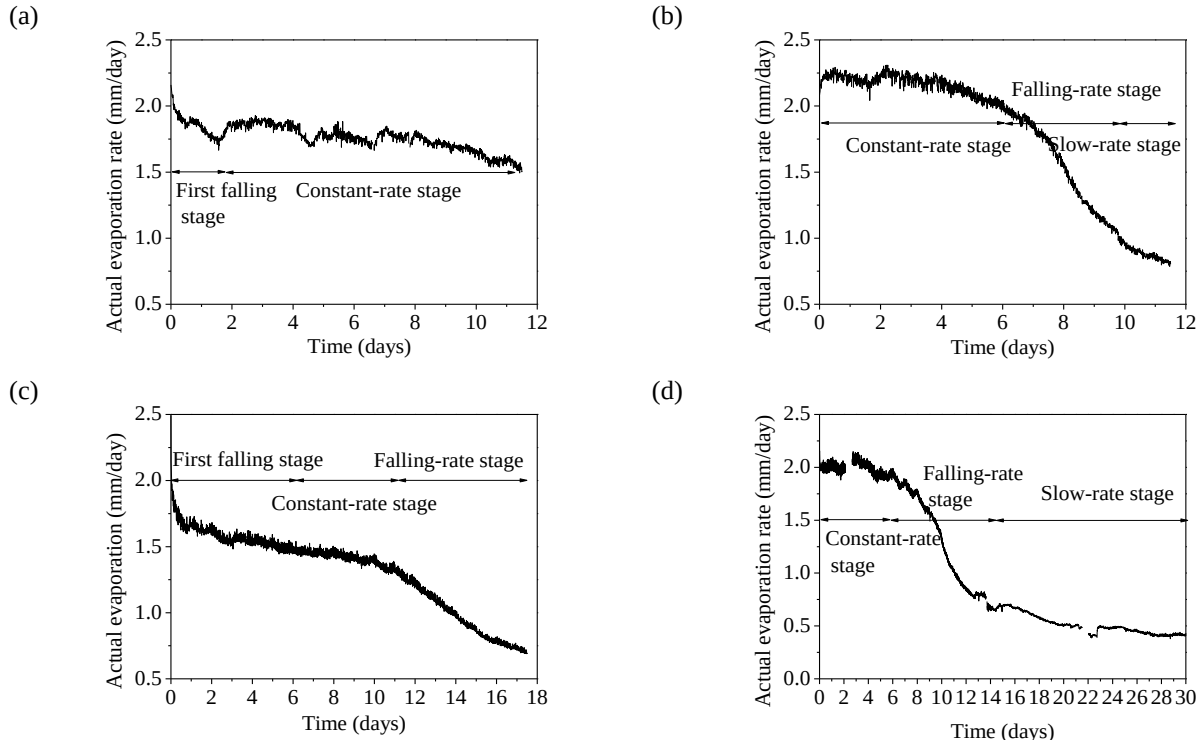


Figure 4. 20. Definition of the evaporation process for the four tests carried out: (a) Test 1; (b) Test 2; (c) Test 3; (d) Test 4

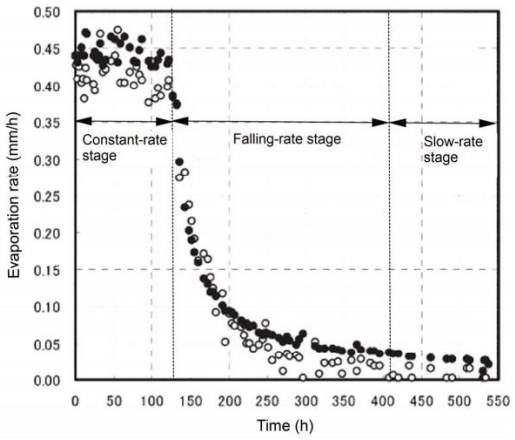


Figure 4. 21. The general three stages of evaporation process (Qiu and Ben-Asher 2010)

However, a sudden down rate stage during the period of 0~2 days and 0~6 days are identified in Test 1 and Test 3 respectively before the general first stage of evaporation. This specific stage is most likely caused by the non-sufficient supply of evaporative energy. As the air temperature is low (heating tube temperatures 50 °C) in Test 1 and Test 3, it is difficult to keep the evaporation at a high rate as its initial value, leading to the sudden drop of evaporation rate.

In terms of soil temperature variations, two phases are identified in Test 1 and Test 3: a declining phase and a rebounding phase. Along with the first falling stage of evaporation, the soil temperatures decrease firstly, reaching the minimum value at the end of the first phase. At the second phase, the soil temperature starts to go up, approaching the initial temperature at the end of test. The turning points of these two phases in Test 1 and Test 3 are day 2 and day 6, respectively. Correspondingly, the evaporation finishes its first falling stage and begins the constant-rate stage at day 2 and day 6 in Test 1 and Test 3, respectively.

As the soil temperature variation is mainly governed by soil heat flux boundary condition that depends on the sensible heat and latent heat, it can be inferred that the evaporation takes energy from both air and soil in the first falling stage, hence the soil temperature decreases gradually. In other words, the value of the latent heat is equal to the sum of sensible and soil heat during the period of 0~2 day in Test 1 and 0~6 days in Test 3. Afterwards, the evaporation with lower rates obtains energy merely from air, indicating that air is able to provide energy for both evaporation and soil heating. It means that the sensible heat is partitioned into latent heat and soil heat in the following days.

Figure 4. 20b and Figure 4. 20d depict the evolutions of evaporation in Test 2 and Test 4, respectively. They have the general three phases of evaporation: constant-rate stage, falling-rate stage, slow-rate stage. Meantime, the soil temperature shows continuous increases in Test 2 and Test 4. Therefore, it is inferred that the process of evaporation is ensured by sufficient energy from air at high temperature (heating tube temperatures 200 °C), illustrating that air is able to provide energy for both evaporation and soil heating. In other words, the sensible heat is the sum of latent heat and soil heat during the whole period considered in Test 2 and Test 4.

4.4.2 Dry soil layer

As evaporation continues, the surface soil is becoming dry, followed by the appearance of a dry layer in the near surface zone. Consequently, the evaporation front will move from the soil surface to the bottom of dry layer as presented in Figure 4. 22. On the whole, the soil water

evaporation presents three stages (Aluwihare and Watanabe 2003): (1) water vapor is carried out from the water surface to the bottom of dry layer; (2) water vapor is transported from the bottom of dry soil layer to the soil surface by vapor diffusion; and (3) water vapor travels from the soil surface to atmosphere.

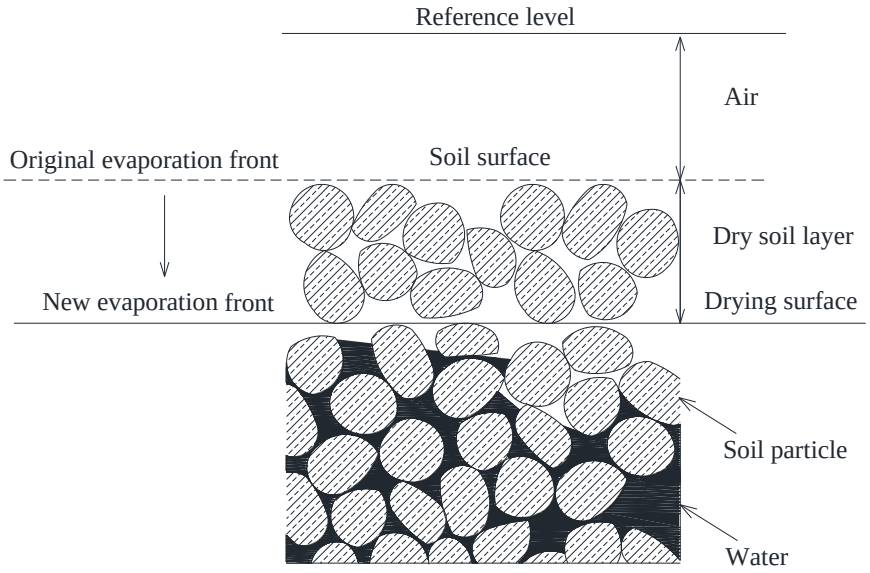


Figure 4. 22. The diagram of dry soil layer in the evaporation process modified after Aluwihare and Watanabe (2003) and Song (2014)

Concerning the variations of soil volumetric water content, an overall consistency is observed between the calculated and measured data, along with some minor differences at the end of each test. As explained in section 4.3, these differences of soil volumetric water content are inferred as the result of the assumed soil hydraulic conductivity in the near surface region. In addition, evaporation in the environment chamber tests may also lead the appearance of a dry layer, and result in the movement of evaporation front. This layer will change the location of the actual top water flux boundary condition. Due to the absence of soil volumetric water content measurements in this zone, it is not easy to determine the variations of the depth of dry layer. In the numerical modeling, this phenomenon is not considered; the evaporation front is assumed to be at the top of soil surface. Thereby, the numerical results of soil volumetric water variations may also be affected by the neglecting of this layer. The consideration of the movement of

evaporation front is required in further study.

4.4.3 The application of Gardner model

In the numerical modelling of the four tests in environmental chamber, the soil water retention and the hydraulic conductivity curves are proposed based on van Genuchten model (van Genuchten 1980). Teng et al. (2016) applied a new set of soil water retention curve (Figure 4. 23) and hydraulic conductivity curve (Figure 4. 24) based on Gardner model (Gardner 1958) for the same Fontainebleau sand:

$$\theta = \theta_r + (\theta_s - \theta_r) e^{-\alpha_u \varphi} \tag{4.7}$$

$$K = K_s e^{-\alpha_u \varphi} \tag{4.8}$$

where α_u is the desaturation coefficient, equals 3.53; θ_s is the saturated volumetric water content, equals 0.356; θ_r is the residual volumetric water content, equals 0.044; the saturated hydraulic conductivity K_s is taken equal to 7.4×10^{-9} m/s.

Similar to the numerical modelling presented in section 4.2, new simulations of the four tests are conducted using the soil parameters deduced from Gardner model. The calculation results of soil temperature and volumetric water content are thus discussed, respectively.

Figure 4. 25a, Figure 4. 25b, Figure 4. 25c, and Figure 4. 25d present the results of soil temperature distribution at different moments in Test 1, Test 2, Test 3 and Test 4, respectively. The conclusion similar to the numerical modelling with van Genuchten model (van Genuchten 1980) can be achieved. The general tendencies of soil temperature variations are consistent between the calculated and measured results in the four tests. The differences are mainly observed at the surface points. Therefore, it is concluded that the changes of soil water retention and the hydraulic conductivity curves do not affect the variations of soil temperature significantly.

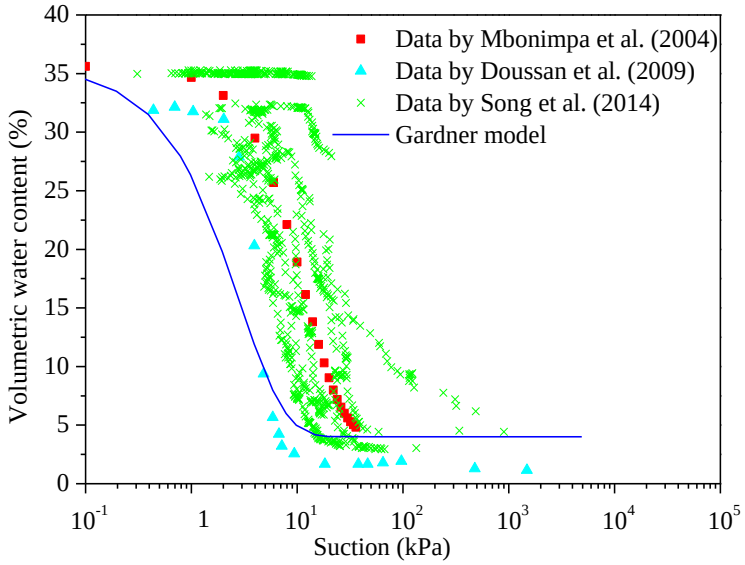


Figure 4. 23. Soil water retention curve versus suction based on Gardner model

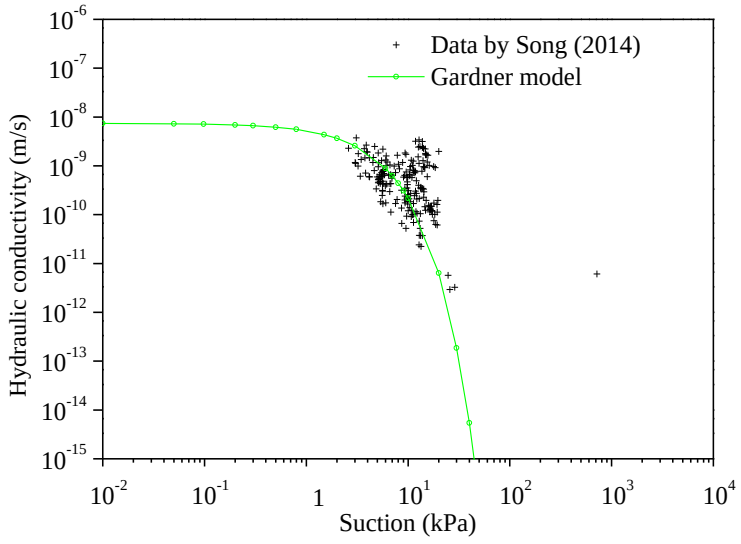
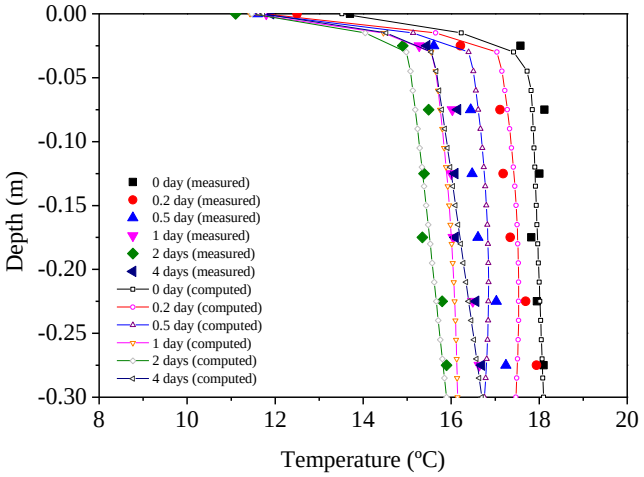
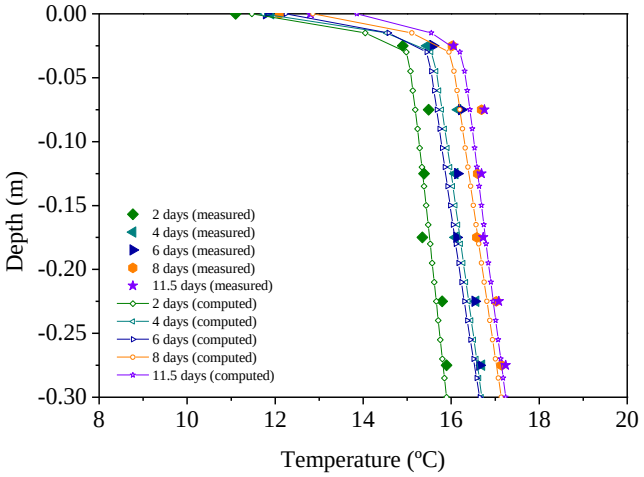


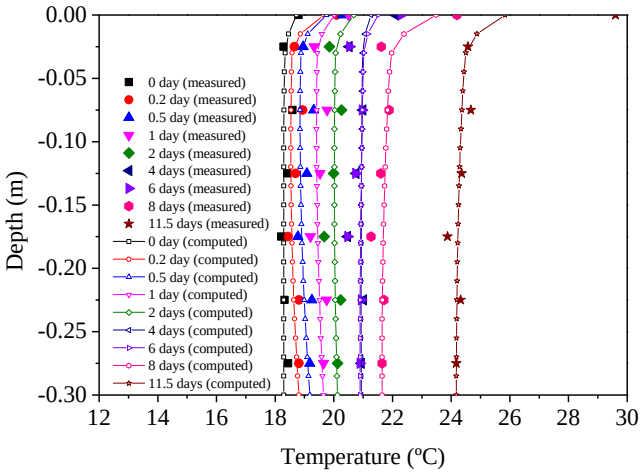
Figure 4. 24. Soil hydraulic conductivity curve versus suction based on Gardner model

(a)

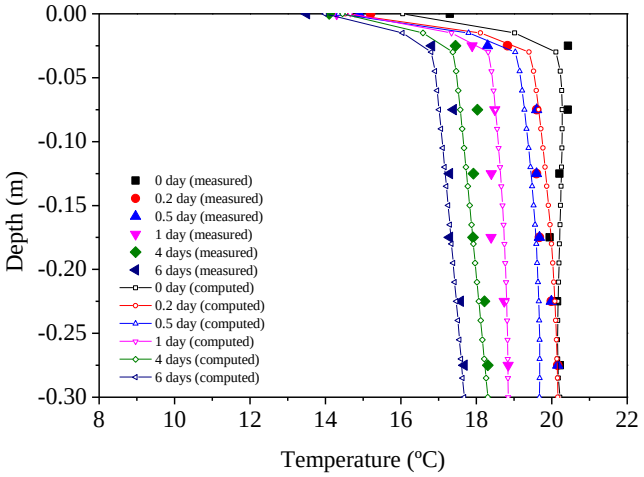

Depth (m)
Temperature (ºC)
0 day (measured)
0.2 day (measured)
0.5 day (measured)
1 day (measured)
2 days (measured)
4 days (measured)
0 day (computed)
0.2 day (computed)
0.5 day (computed)
1 day (computed)
2 days (computed)
4 days (computed)

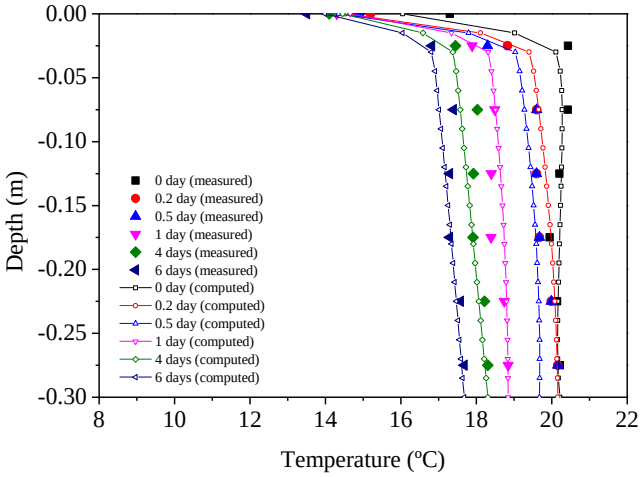

Depth (m)
Temperature (ºC)
2 days (measured)
4 days (measured)
6 days (measured)
8 days (measured)
11.5 days (measured)
2 days (computed)
4 days (computed)
6 days (computed)
8 days (computed)
11.5 days (computed)

(b)


Depth (m)
Temperature (ºC)
0 day (measured)
0.2 day (measured)
0.5 day (measured)
1 day (measured)
2 days (measured)
4 days (measured)
6 days (measured)
8 days (measured)
11.5 days (measured)
0 day (computed)
0.2 day (computed)
0.5 day (computed)
1 day (computed)
2 days (computed)
4 days (computed)
6 days (computed)
8 days (computed)
11.5 days (computed)

(c)





(d)

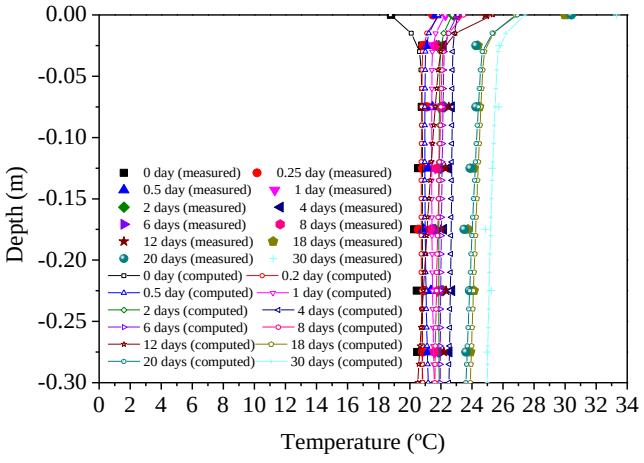
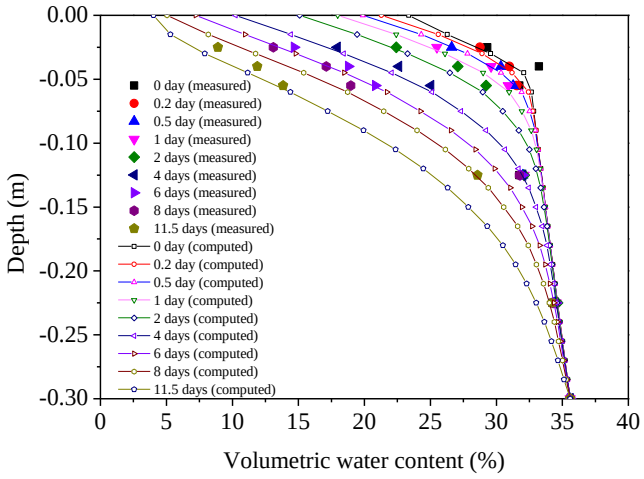


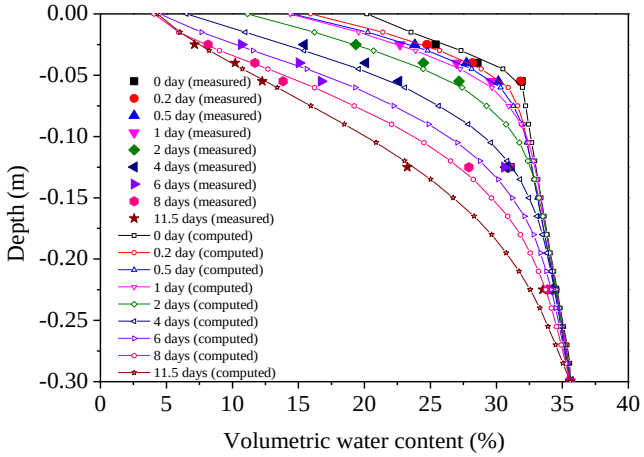
Figure 4. 25. Comparisons of soil temperature between the measured and calculated results at different moments: (a) Test 1; (b) Test 2; (c) Test 3; (d) Test 4.

Figure 4. 26 shows the calculations and measurements of soil volumetric water content at different moments in the four tests. In Test 1and Test 2, evaporation was recorded for 11.5 days. It is observed that the calculated results of soil volumetric water content fit well with the measured data at the studied moments (Figure 4. 26a and Figure 4. 26b). Besides, evaporation continued for 17.5 days and 30 days in Test 3 and Test 4 (Figure 4. 26c and Figure 4. 26d), respectively. Even though the overall variation tendency of the calculated results is consistent with the measured data, some differences can be identified since day 8 to the end of tests: the calculated values are becoming lower than the measured values in the deep region; some calculated data are larger than the measured values in the near surface zone. Specifically, the soil volumetric water content is becoming linear with depth at the end of Test 4. As the soil hydraulic conductivity is much smaller compared to the value adopted in van Genuchten model (van Genuchten, 1980), water transfers at a lower rate in the soil sample with the saturated bottom boundary, leading to smaller values of soil water content.

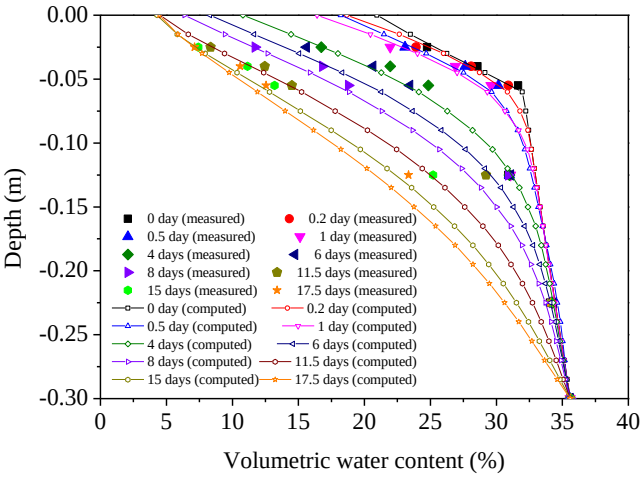
(a)



(b)



(c)



(d)

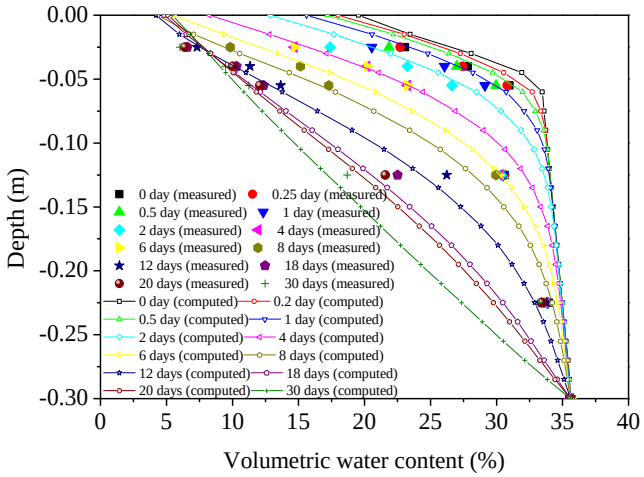


Figure 4. 26. Comparison of soil volumetric water content between the measured and calculated results at different moments: (a) Test 1; (b) Test 2; (c) Test 3; (d) Test 4

It proves that the selection of soil volumetric water content curve and soil hydraulic conductivity during evaporation greatly affects the estimation of soil volumetric water content variations. Moreover, it is observed that the numerical modelling based on van Genuchten model (van Genuchten 1980) and Gardner model (Gardner 1958) both can provide satisfactory estimation of soil volumetric water content variations. However, the numerical investigation by van Genuchten model (van Genuchten 1980) with higher saturated hydraulic conductivity can give better performance in the deep region than that by Gardner model (Gardner 1958) with lower saturated hydraulic conductivity. By contrast, the performance of Gardner model (Gardner 1958) is superior in the near surface zone. These results indicate that it is difficult to obtain an ideal numerical results of soil volumetric water content based on van Genuchten model (van Genuchten 1980) or Gardner model (Gardner 1958). The model to define the soil volumetric water content curve and hydraulic conductivity curve during evaporation requires further study.

4.5 Conclusions

In this chapter, four evaporation tests carried out by Song (2014) in environmental chamber are introduced. This environmental chamber was richly instrumented, with a wind and water supply unit, specific sensors for recording air flow rate and relative humidity in various positions, and buried sensors for the measurements of soil temperature and volumetric water content at different depths, etc. It enables the study of soil-atmosphere interaction and its effect on soil temperature and volumetric water content variations. Overall, the numerical modelling of the four tests shows that the proposed approach combining a fully coupled hydro-thermal soil model and a soil-atmosphere interaction model is suitable for the estimation of soil temperature and volumetric water content variations.

In terms of soil temperature variations, a rebounding phenomenon is observed in both Test 1 and Test 3. This result indicates that soil participates in providing energy for the evaporation in the first falling stage and the heated air (heating tube temperatures 50 °C) provides energy for

both evaporation and soil heating in the following stages. In Test 2 and Test 4, a steady increase tendency is identified in the variations of soil temperature. It means that the heated air (heating tube temperatures 200 °C) is able to support evaporation and soil heating for the whole period. Note that the heating tube temperatures affect the values of air temperature, rather than impose the same value for air temperature. Concerning the variations of soil volumetric water content, they show a continuous decrease as a result of evaporation serving as the water flux boundary condition at soil surface in the four tests.

The differences in terms of soil temperature and volumetric water content are mainly observed at the surface points. They can be attributed to the assumed values of soil parameters. In addition, Gardner model (Gardner 1958) for soil water retention and soil hydraulic conductivity curves is adopted in the new numerical calculation. It is difficult to obtain better results of soil volumetric water content variations with this model compared with the van Genuchten model (van Genuchten 1980). It proves that the variations of soil properties during evaporation need to be studied further, especially in terms of the effects of soil thermal conductivity, water retention and hydraulic conductivity curves in the near surface region. On the other hand, along with evaporation, the surface soil is becoming dry leading to the appearance of a dry layer. This layer moves from the top soil surface to the bottom of dry layer, modifying the evaporative surface. In other words, the appearance of dry layer indicates the change of the top boundary in numerical modelling. However, this is not considered in the numerical investigation conducted.

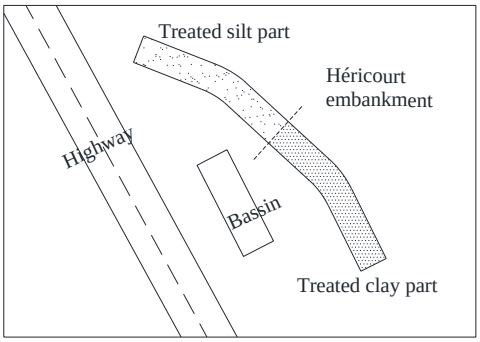
On the whole, the satisfactory agreement obtained between the calculated and measured data in terms of soil temperature and volumetric water content in the four tests shows that this numerical approach is appropriate provided that suitable soil parameters and boundary conditions are adopted in the numerical investigation.

Chapter 5: Modelling of Héricourt embankment

5.1 Héricourt embankment

Within the national "ANR-07-PCGU-006-10-TerDOUEST" project, an embankment was constructed at Héricourt in Franche-Comté region in the north east of France. This region is characterized by a continental climate influenced by ocean. The embankment is constructed in two parts, one with lime/cement treated silt and another with lime/cement treated clay, each part being 53.5 m long. The field site plan and a view of the embankment are presented in Figure 5. 1a and Figure 5. 1b, respectively.

(a)



(b)



Figure 5. 1. (a) Héricourt embankment plan with two parts in different kinds of treated soil: lime/cement treated silt and lime/cement treated clay; (b) Field site view in 06/2011

The construction started in 07/2009 and ended in 09/2010. The main objectives of this experimental embankment are:

1) Understanding the coupling between chemical and geotechnical behavior of treated soils;
2) Understanding the long term behavior of treated soils;
3) Having a reference embankment to study the construction and monitoring with treated soils;
4) Studying the effects of the environment and various operations during the earthwork.

A weather station was installed on the top of the embankment, recording meteorological data half-hourly: solar radiation, rainfall, wind speed, air relative humidity and temperature at the height of 0.5 m, etc. Besides, runoff appears when rainfall rate exceeds the infiltration capacity

of surface soil. It was recorded hourly by a continuous measurement system on the slope surface (Figure 5. 2).

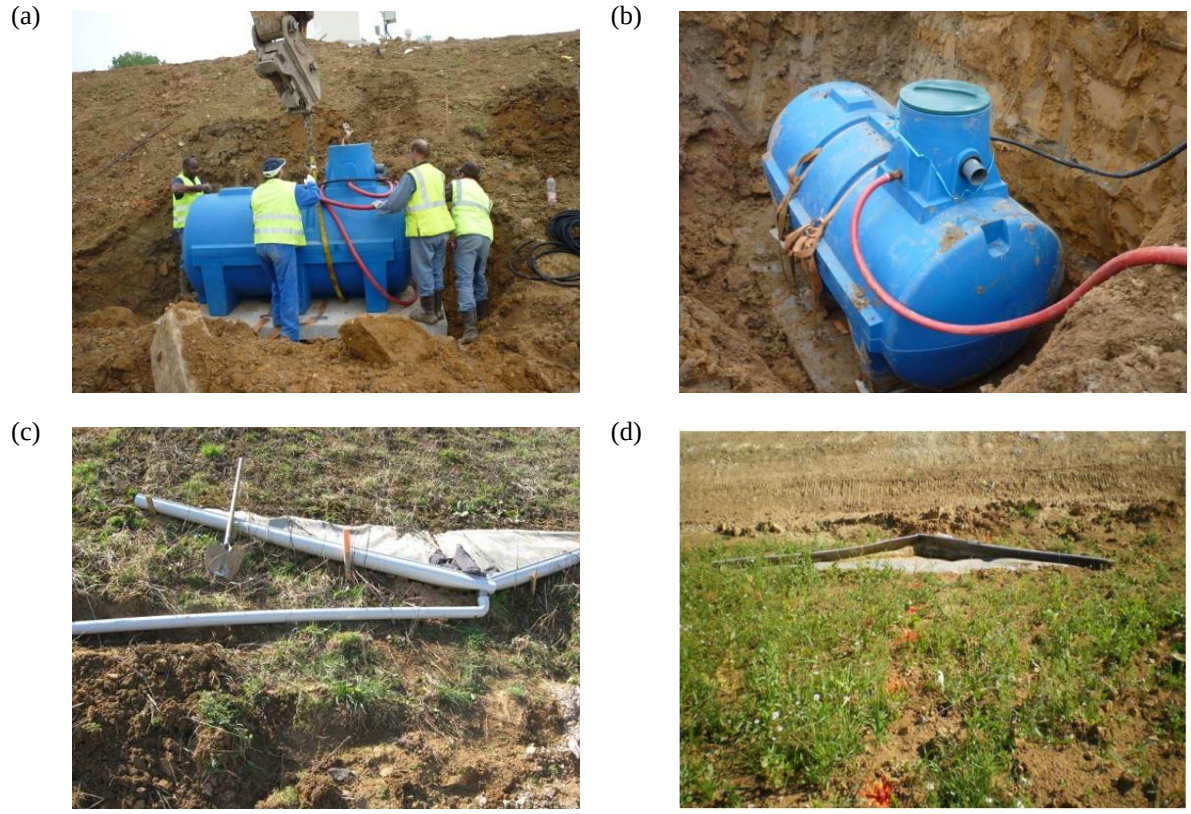


Figure 5. 2. Details of runoff measurement system on the slope surface of Héricourt embankment: (a) the installation process of tank; (b) the installed tank on the prefabricated concrete elements; (c) the structure of collector on the slope; (d) the view of the runoff collector from the embankment top

Soil temperature and volumetric water content at different positions in embankment were measured by TDR probes each three hours. In terms of soil slope surface temperature, temperature sensor PT100 was adopted for recording its temperature variation every three hours. During construction, a soil layer with a thickness of 20 cm was added on the slopes to maintain the slope surface sensors. Moreover, an individual soil temperature probe ST1 was set for monitoring the temperature variation at the top surface of embankment every 30 min. These sensors were installed at different layers during the construction as shown in Figure 5. 3. More information of this embankment construction and monitoring can be found in the report by

Froumentin (2012).

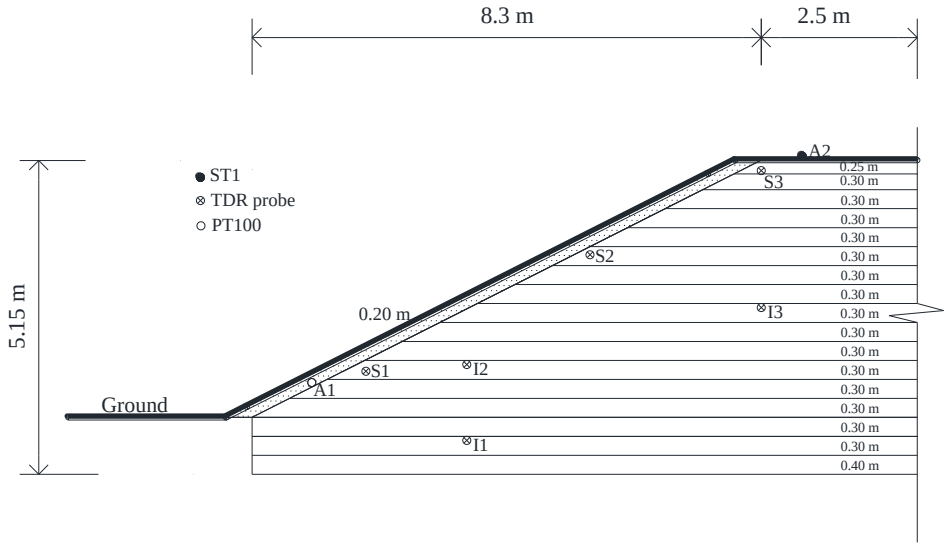


Figure 5. 3. Embankment instrumentation: TDR sensors for recording soil volumetric water content variations and temperature variations (I1~3, S1~3) in the embankment; PT100 for recording slope surface temperature variations (A1); ST1 for recording top surface temperature variations (A2)

In this study, only the lime/cement treated silt part is chosen to investigate the soil-atmosphere interaction. This part of embankment is 53 m long with a slope of 1:2 (Vertical: Horizontal) for the two sides. The width of the bottom and top of the selected section are 21.6 m and 5 m respectively as presented in Figure 5. 4. Different treatments conducted for silt are summarized as follows:

1) For roadbed fill part (R0~R11): with 2% CaO;
2) For PST part (PST0~PST2): with 3% Cement;
3) For CDF part (CDF0): with 1% CaO+ 5% Cement;
4) For surface layer part (ASS0): with GNT 0/31.5 mm.

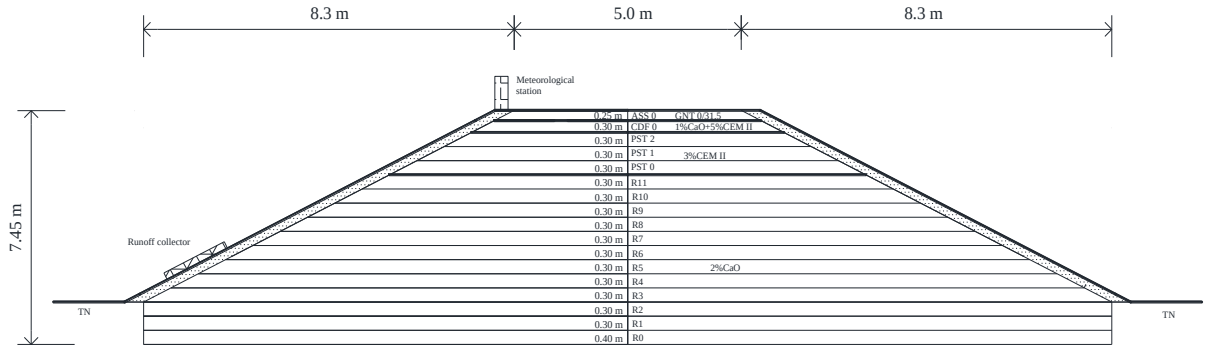


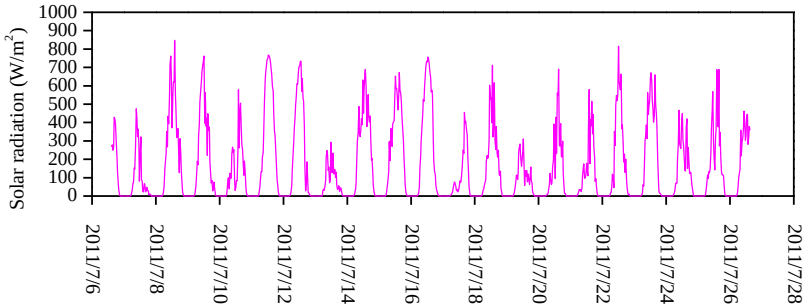
Figure 5. 4. Studied cross section of Héricourt embankment with soil treatment information

Data recorded from 06/07/2011 to 26/07/2011 is complete including all meteorological data, runoff and soil variables (volumetric water content/temperature). Thus, this period of 20 days is chosen in this study. Figure 5. 5 presents the monitoring data of solar radiation (Figure 5. 5a), rainfall (Figure 5. 5b), wind speed (Figure 5. 5c), air relative humidity (Figure 5. 5d) and temperature (Figure 5. 5e) at 0.5 m elevation as well as the runoff information (Figure 5. 5f) during the studied period.

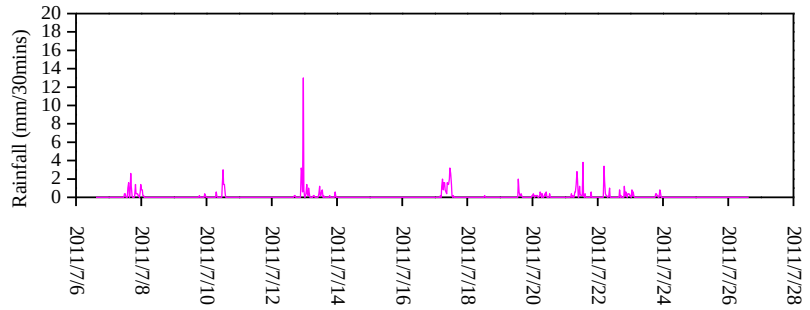
In the numerical modeling of Héricourt embankment, several assumptions are made for simplification:

1) Soil is assumed to be homogeneous and isotropic in the whole embankment, except the 20 cm surface slope layer;
2) The positions of sensors for recording soil temperature and volumetric water content are assumed to be at the right place shown in Figure 5. 3; no offset of sensors during the construction happened;
3) The heat flux and water flux boundary conditions are assumed to be the same for all points at the same surface boundary;
4) The surface of field embankment is bare; no vegetation effect is considered.

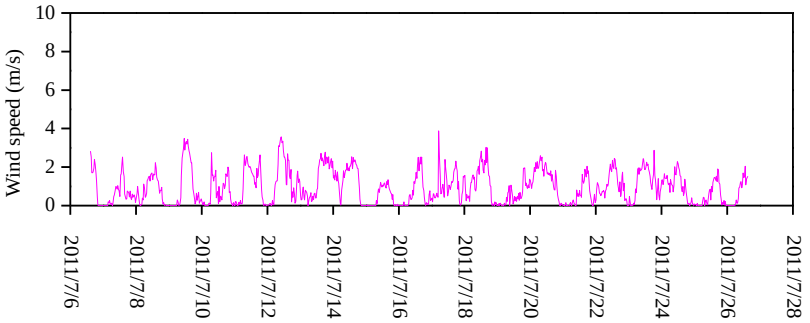
(a)


Solar radiation (W/m²)
1000
900
800
700
600
500
400
300
200
100
0
2011/7/6
2011/7/8
2011/7/10
2011/7/12
2011/7/14
2011/7/16
2011/7/18
2011/7/20
2011/7/22
2011/7/24
2011/7/26
2011/7/28

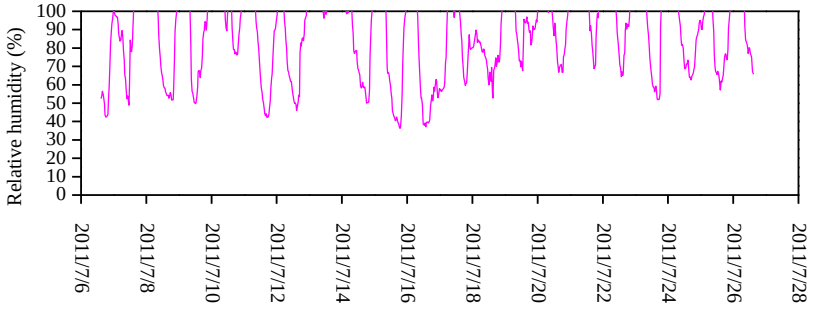
(b)


Rainfall (mm/30mins)
20
18
16
14
12
10
8
6
4
2
0
2011/7/6
2011/7/8
2011/7/10
2011/7/12
2011/7/14
2011/7/16
2011/7/18
2011/7/20
2011/7/22
2011/7/24
2011/7/26
2011/7/28

(c)


Wind speed (m/s)
10
8
6
4
2
0
2011/7/6
2011/7/8
2011/7/10
2011/7/12
2011/7/14
2011/7/16
2011/7/18
2011/7/20
2011/7/22
2011/7/24
2011/7/26
2011/7/28

(d)


Relative humidity (%)
100
90
80
70
60
50
40
30
20
10
0
2011/7/6
2011/7/8
2011/7/10
2011/7/12
2011/7/14
2011/7/16
2011/7/18
2011/7/20
2011/7/22
2011/7/24
2011/7/26
2011/7/28

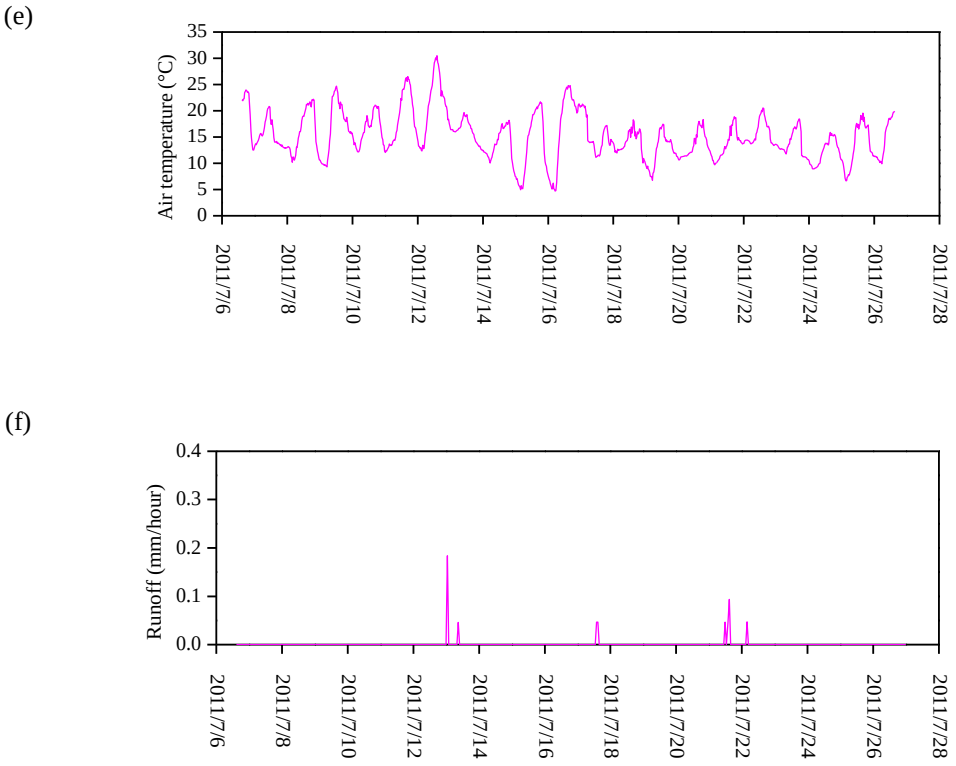


Figure 5. 5. Field meteorological data from 06/07/2011 to 26/07/2011: (a) solar radiation; (b) rainfall; (c) wind speed; (d) relative humidity at 0.5 m above the embankment surface; (e) air temperature at 0.5 m above the embankment surface; (f) runoff measured on the slope surface

5.2 Definition of numerical model

5.2.1 Soil parameters

The hydro-thermal properties of treated silt are required in the numerical analysis. The thermal conductivity, soil water retention curve and hydraulic conductivity of the studied treated silt are determined and presented below.

KD2 Analyzer is used to measure thermal conductivity of treated soil (Tang et al. 2008; Buongiorno et al. 2009; Teng et al. 2010). For numerical simplicity, a linear relationship between soil thermal conductivity and volumetric water content proposed by De Vries (1963)

and Cui et al. (2005) is chosen for the studied treated silt (Figure 5. 6):

$$\lambda = 2.1818\theta + 0.808 \tag{5.1}$$

where λ (W/(mK)) is the thermal conductivity; θ is the volumetric water content.

Field soil sample was taken and tested to obtain water retention curve using "WP4 method" (Scanlon et al. 2002; Thakur et al. 2006). Based on van Genuchten model (van Genuchten 1980), the expression for the soil water retention curve is built:

$$S_e = \frac{\theta - \theta_r}{\theta_s - \theta_r} = \left[\frac{1}{1 + (\alpha_s \varphi)^n} \right]^m \tag{5.2}$$

where the saturated volumetric water content $\theta_s = 0.4$; the residual volumetric water content $\theta_r = 0.004$; parameters $\alpha_s = 0.003$ kPa^{-1}, $m = 0.18$ and $n = 1.8$. With the measurement data, a fitting curve is drawn as shown in Figure 5. 7.

Field soil samples are tested and their saturated hydraulic conductivities are measured using triaxle cell. The values obtained on two samples are quite close, being equal to 8×10^{-10} m/s and 1×10^{-9} m/s respectively. Therefore, the value of 1×10^{-9} m/s is chosen in the numerical modeling. Based on the soil water retention curve determined previously, the hydraulic conductivity at unsaturated state can be estimated using van Genuchten model (van Genuchten 1980):

$$K = K_s S_e^{0.5} \left[1 - \left(1 - S_e^{1/m_1} \right)^{m_1} \right]^2 \tag{5.3}$$

where $m_1 = 0.5$; the saturated hydraulic conductivity $K_s = 1\times10^{-9}$ m/s; other parameters have the same values as for equation (5. 3). The curve of soil hydraulic conductivity versus suction is plotted in Figure 5. 8. Note that the hysteresis in terms of soil water retention and hydraulic conductivity behavior was ignored in this study.

As for the 20 cm soil layer added on the slope of embankment, its thermal conductivity is assumed to be 0.25 W/(mK) and its hydraulic conductivity is taken equal to 1×10^{-8} m/s. Its soil

water retention curve is regarded as the same as that of the treated silt.

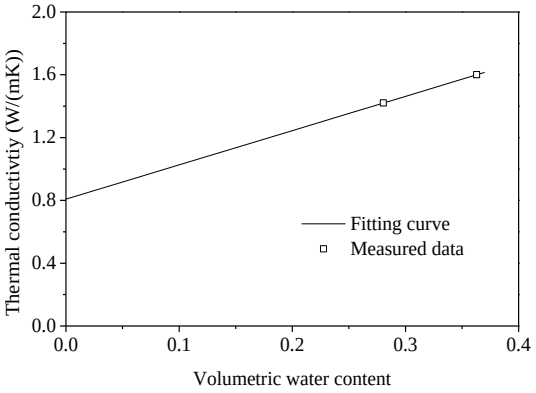


Figure 5. 6. Thermal conductivity curve versus volumetric water content for the treated silt

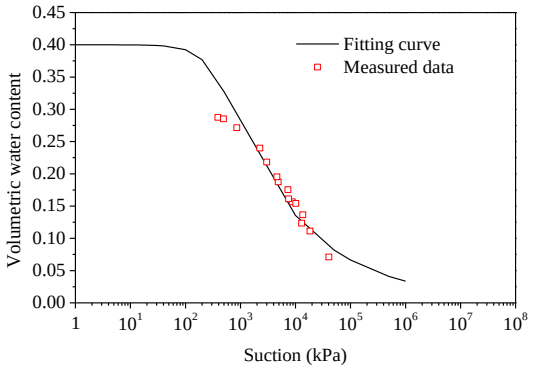


Figure 5. 7. Water retention curve versus suction for the treated silt

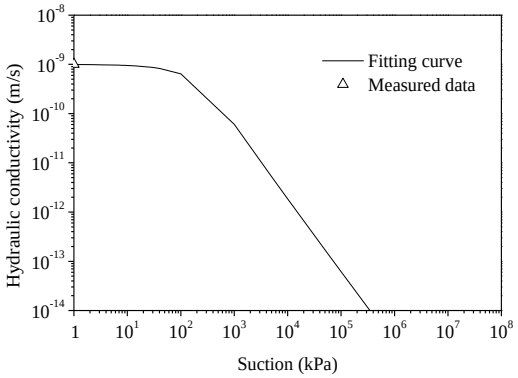


Figure 5. 8. Hydraulic conductivity curve versus suction for the treated silt

5.2.2 Model dimensions

In numerical modelling, it is essential to set suitable dimensions to simulate the real cases. In literature (Azizi 1999; Yue 2008; Cui et al. 2010; Kalliainen and Kolisoja 2011; Rujikiatkamjorn et al. 2012), the effect of model dimensions was specifically analyzed, showing the importance of model dimensions in the numerical results in terms of variations of soil water content, strain and stress over time. However, for the coupled hydro-thermal soil models, no suggestions of model dimensions have been made in the case of two-dimensional embankment.

In order to adopt the appropriate model dimensions in the numerical modelling of Héricourt embankment, four different dimensions are analyzed respectively (Table 5. 1 and Figure 5. 9). Dimensions 1 is the original embankment size considering the basement of 5 m depth. Dimensions 2, 3 and 4 are extended to different sizes. Besides, six points are selected at depths 0 m (point P1), 0.25 m (point P2), 0.50 m (point P3), 0.75 m (point P4), 1.00 m (point P5) and 1.50 m (point P6) in sections A and B to record soil temperature and volumetric water content variations over time (Figure 5. 9). The groundwater table is assumed to be at the depth of 5 m below the ground. The bottom boundary condition is set at 10 ºC temperature. It is assumed that no water and heat transfers happen at the left and right boundaries.

The top boundaries of this embankment consist of top, slope surfaces of the embankment and ground surface. Two cases with different top boundary conditions are considered for the dimensions' analysis. It is assumed that the embankment has a uniform initial temperature of 10 ºC. The soil above the groundwater table is in unsaturated state and its initial suction profile is expressed by $U_0 = -y$, where U_0 and y are soil initial suction and soil depth from the embankment top surface, respectively (Figure 5. 9). Using the adopted soil parameters, the initial and boundary conditions, numerical calculation are conducted in two cases, as follows:

5.2.1.1 Case 1

In Case 1, it is assumed that evaporation (1×10^{-7} m/s) and infiltration (5×10^{-8} m/s) happen alternately during six days on the top boundaries (Figure 5. 10). Meantime, zero heat flux is applied on the top boundaries.

Figure 5. 11 shows that the numerical results of volumetric water content variations at each point in sections A and B are nearly consistent for the four different dimensions (1-P1 represents point 1 in Dimensions 1, 2-P2 represents point 2 in Dimensions 2, etc.). In Figure 5. 11a, the volumetric water content at the selected points in section A shows a regular increasing/decreasing trend with the occurring of infiltration/evaporation. When evaporation happens in the first day, the volumetric water content at the surface point P1 decreases to 0.323 firstly then goes up to a nearly saturated situation as rainfall continues in the second day. Afterwards, it drops to 31.2% and 30.1% in the third and fifth day and rebounds to 38.7% and 38.1% in the fourth and last day, respectively. For point P2, the soil volumetric water content shows the variations similar to that of the surface point P1. As points P3, P4, P5 and P6 are situated far from the top surface, they have much smaller variation amplitudes compared with point P1 and P2, indicating that they are not sensitive to the water flux boundary conditions. Similar variations of soil volumetric water content can be identified at the six points in section B (Figure 5. 11b). Meanwhile, the soil temperatures at these points are stable, keeping the same value as their initial value because the heat flux is zero.

Table 5. 1 The details of four model dimensions

Item	*Ground width L_e*	*Soil depth H_e*
Dimensions 1	0	5 m
Dimensions 2	0.5L	5 m
Dimensions 3	1.5L	3H
Dimensions 4	$\approx$ 3L	$\approx$ 5H

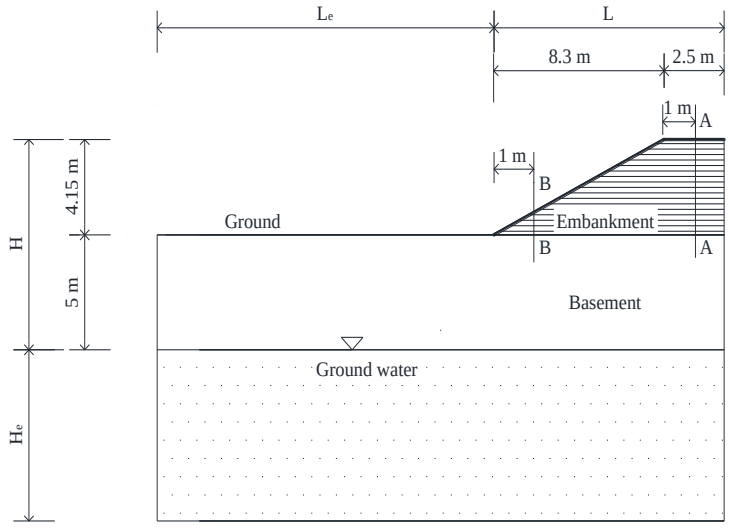


Figure 5. 9. Héricourt embankment dimension

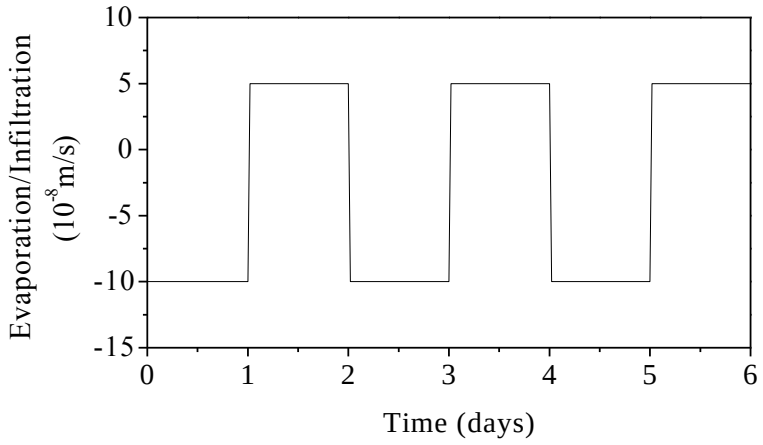


Figure 5. 10. Water flux conditions on the top boundaries in six days in Case 1

Figure 5. 12 shows that the contour lines of volumetric water content are always parallel to the surface lines of embankment for the four dimensions. Moreover, it is observed that the influenced region of the top boundary condition of water flux is limited to the depth of 1 m below the surface. However, the neglecting of the left ground region in dimension1 leads to different volumetric water content distribution in the region near the slope toe, compared with those in three other dimensions. Therefore, it is suggested to consider the left ground region in the model dimension.

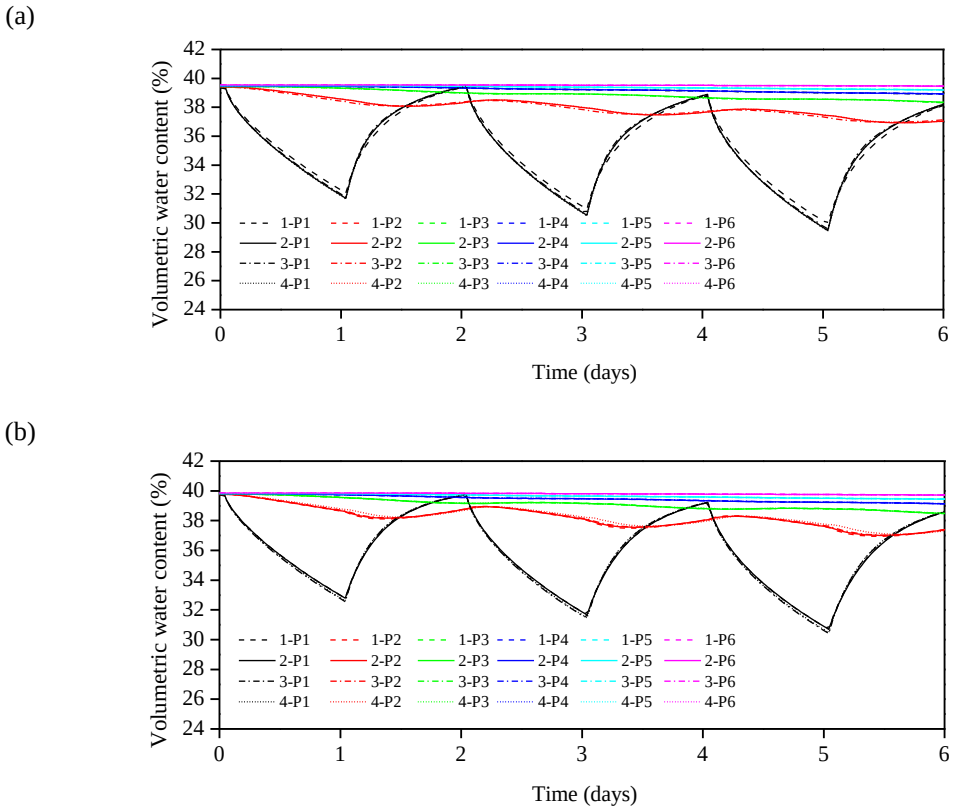


Figure 5. 11. Volumetric water content variations at six points in the four dimensions: (a) in section A; (b) in section B

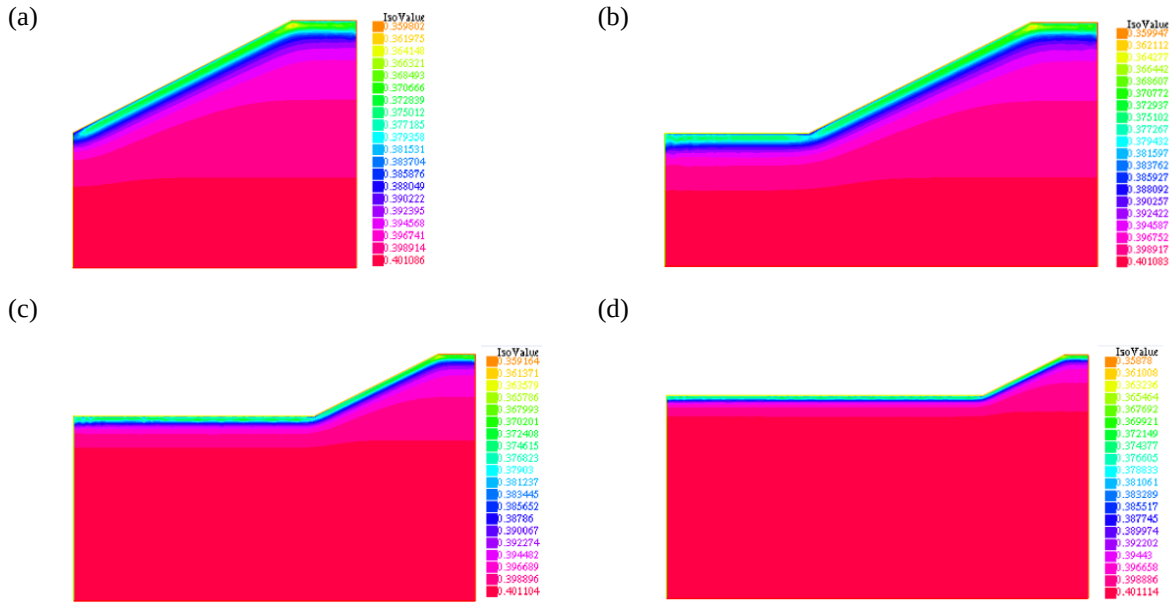


Figure 5. 12. Volumetric water content distributions in the four dimensions at day 6: (a) Dimensions 1; (b) Dimensions 2; (c) Dimensions 3; (d) Dimensions 4

5.2.1.2 Case 2

In Case 2, based on the value of solar radiation, the heat flux top boundary conditions are assumed as 45 (W/m^2) for 6 hours during day time (Figure 5. 13a) and -15 (W/m^2) for 18 hours during night time (Figure 5. 13b). The water fluxes at the top boundaries are assumed as zero.

The variations of soil temperature at six points in sections A and B show high consistency for the four different dimensions (Figure 5. 14). Figure 5. 14a shows that the temperature at surface point P1 decreases quickly from 10.00 °C to 8.69 °C in the first 9 hours during night time when soil heat is -15 (W/m^2), then it goes up to 12.65 °C when soil heat is 45 (W/m^2) during day time. The variations of soil temperature at the surface point P1 repeat the same daily decreasing/increasing cycles during the six days. Similar variation tendency of soil temperature is observed at point P2, along with a variation amplitude of 9.80~10.20 °C. Moreover, obvious time delay of 2.4 to 4.8 hours is identified at point P2 because of its deeper position compared with point P1. Points P3, P4, P5 and P6 keep nearly constant temperature as their initial values, indicating that they are not situated in the influenced zone of surface heat flux. This influence depth is intimately related to the thermal conductivity of treated soil. Figure 5. 14b reveals that the soil temperatures at the six points in section B have nearly the same variations as in section A. On the other hand, the initial volumetric water content variations in section A and section B are governed by the gravity effect, then keep stable during the six days due to zero water flux top boundary conditions.

The contour lines of soil temperature distribution are presented in Figure 5. 15. They are parallel to the surface lines of embankment for the four dimensions. It is observed that the soil temperature distributions are nearly consistent for the four dimensions. During the six days, the influenced region of heat flux top boundary conditions is limited in the depth of 0.5 m below the surface.

In this study, overall consistent results for the four dimensions in terms of soil volumetric water content and temperature variations are obtained, except the volumetric water content

distribution in the region near the slope toe for Dimensions 1. Therefore, it is concluded that the effect of model dimensions is not significant for the soil hydro-thermal behavior in two-dimensional embankments.

Nevertheless, it is suggested to consider the effect of the left ground surface on soil volumetric water content distribution. Considering the accuracy, computing time, and computer memory requirements, Dimensions 3 is adopted in the further study. The adopted model dimensions are presented in Figure 5. 16.

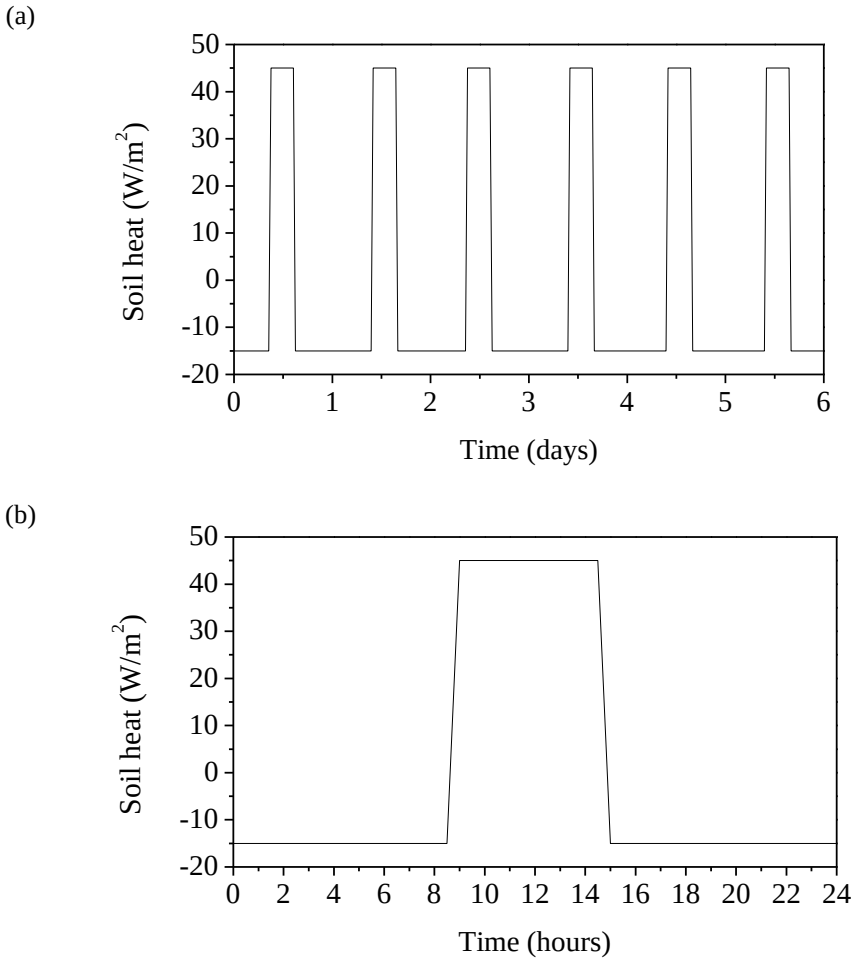


Figure 5. 13. In Case 2: (a) heat flux conditions on the top boundaries in six days; (b) details of the heat flux variations in 24 hours

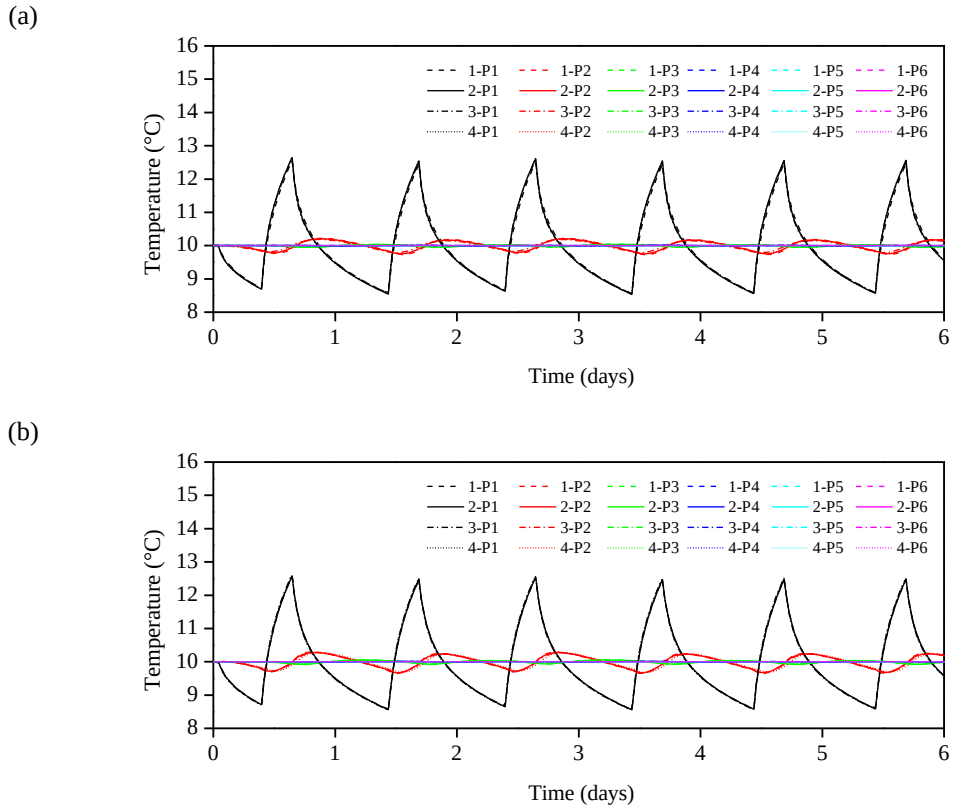


Figure 5. 14. Temperature variations at six points in the four dimensions: (a) in section A; (b) in section B

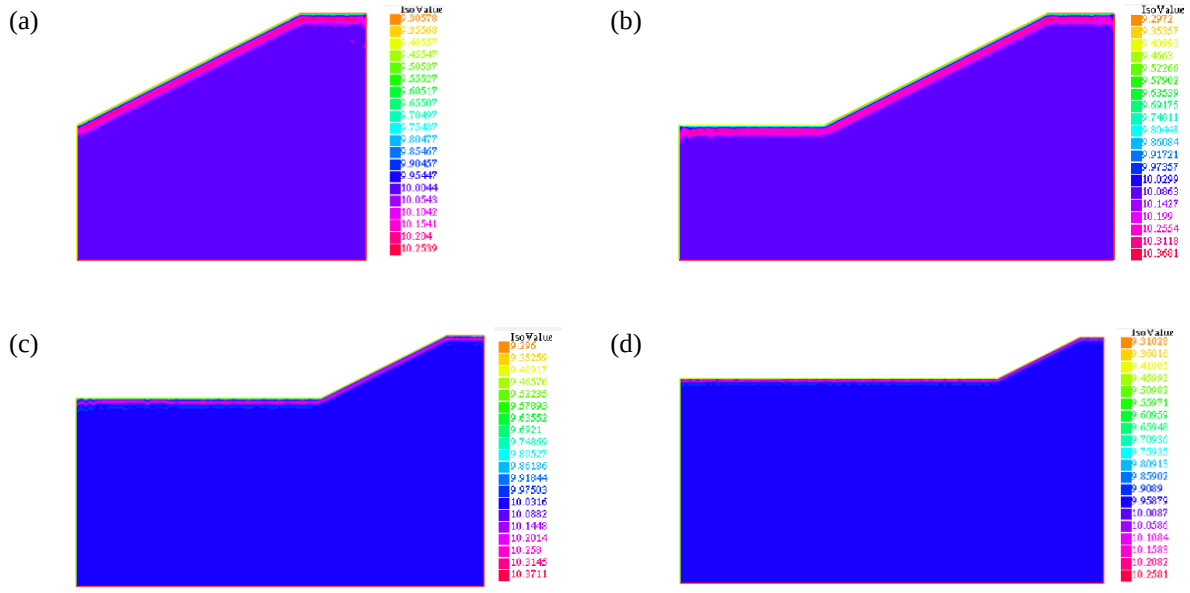


Figure 5. 15. Temperature distributions in the four dimensions at day 6: (a) Dimensions 1; (b) Dimensions 2; (c) Dimensions 3; (d) Dimensions 4

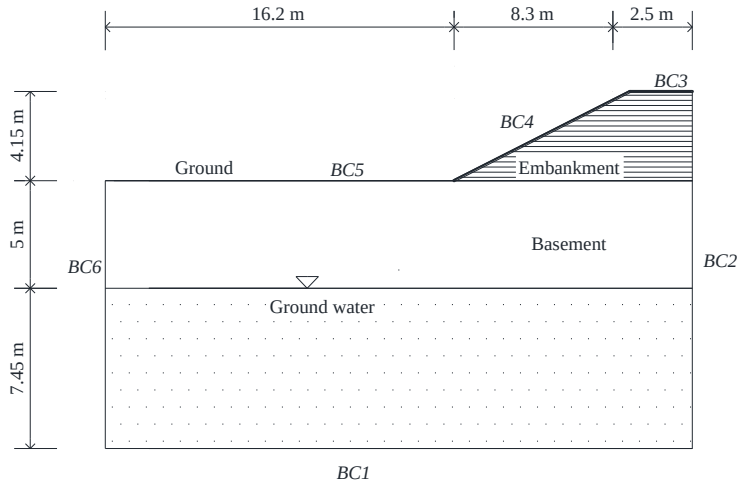


Figure 5. 16. Numerical model dimensions for Héricourt embankment

5.2.3 Initial and boundary conditions

The measurements of soil temperature and volumetric water content at the beginning of the studied period (06/07/2011, 14:42:52) are defined as initial conditions of the coupled hydro-thermal model. For bare soil, as rainfall happens, part of water will infiltrate into soil. The rest of rainfall becomes runoff on soil surface. Meanwhile, evaporation happens at soil-atmosphere interface because of energy transfer and vapor pressure gradient exiting near the soil surface and its value is normally negligible during rainfalls. As far as the heat transfer is concerned, solar radiation is the only exterior heat resource. The net solar radiation is equal to the sum of latent heat, soil heat and sensible heat. Thus, mass and energy balances during soil-atmosphere interaction are used to determine the water and heat boundary conditions (Blight 1997).

Mass balance

The mass balance at the soil surface is expressed by equation (3.1). In Héricourt embankment, field rainfall was monitored half hourly by the weather station (Figure 5. 5b). Runoff was collected hourly as shown in Figure 5. 5f. Evaporation is estimated using the method developed by Song (2014), based on the models proposed by Campbell (1985), Wilson et al. (1994) and Ta (2009):

$$\frac{E_a}{E_p} = \frac{e_s - e_a}{e_0 - e_a} \tag{3.7}$$

$$E_p = \left(a_1 u + a_2\right)\left(100 - h_a\right) \tag{5.4}$$

where E_p (m/s) represents potential evaporation; u (m/s) is wind speed; h_a (%) is air relative humidity; a and b are empirical parameters: a = 0.022, b = 0.031 (Song 2014). The soil surface vapor pressure e_s, saturated vapor pressure at water surface e_0 and air vapor pressure e_a can be calculated as indicated in Chapter 3. As there is no canopy in Héricourt embankment, I_{nt} is equal to zero. With all these parameters estimated, the water flux boundary condition I_{nf} at soil surface can be determined continuously.

Energy balance

The energy balance at the soil surface is expressed by equation (3.14). The method to determine net solar radiation in half hourly without soil temperature is adopted here (equations (3.16~3.22)). The measured solar radiation R_{si} (W/m^2) is shown in Figure 5. 5a and the recorded air temperature in Figure 5. 5e. Besides, the sensible heat and latent heat are calculated respectively based on equations (3.29) and (3.35). Based on the energy balance, the value of soil heat flux G is calculated and applied as the heat flux boundary condition at the soil and atmosphere interfaces.

All these details of initial conditions and boundary conditions are listed in Table 5. 2.

In order to explain the boundary conditions determined through considering soil-atmosphere interaction, heat and water fluxes on the top surface (BC3) are presented in Figure 5. 17 and Figure 5. 18, respectively. Other boundaries interacted with atmosphere (BC4, BC5) own the similar boundary conditions. Note that these boundary conditions are calculated iteratively.

As presented in Figure 5. 17, the soil heat is governed by the net solar radiation with positive values during day time and negative values during night time. Latent heat represents the energy consumed by evaporation and is in negative values. Sensible heat represents the energy to heat

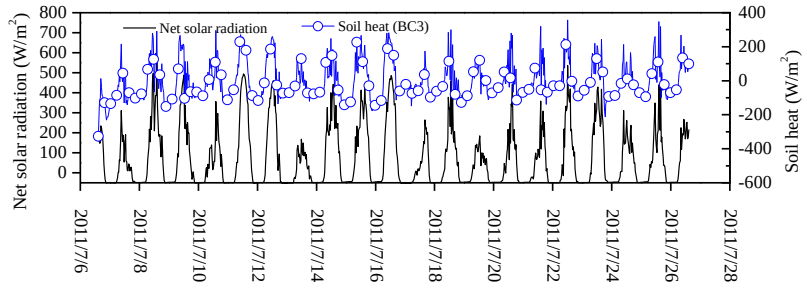
air. When it is in negative value, soil temperature is higher than air temperature. By contrast, air temperature is higher than soil temperature. Relying on the energy balance, soil heat can be estimated effectively by net solar radiation, latent heat and sensible heat.

The runoff value is measured by the runoff collector system (see Figure 5. 5e). As shown in Figure 5. 18, the evaporation and runoff are in the same order of magnitude 10^{-8} m/s, much smaller than that of rainfall and infiltration (10^{-6} m/s). Therefore, it is obvious that rainfall is able to affect the water flux boundary effectively. The infiltration represents the values of water boundary condition on soil surface. Its positive value means that water flows into soil. By contrast, evaporation happens at soil surface.

Table 5. 2. Initial and boundary conditions used for numerical modelling of Héricourt embankment

Initial conditions		Measurement data at the starting moment	
	Boundary number	*Thermal boundary conditions*	*Hydraulic boundary conditions*
Boundary conditions	BC1	Measured soil temperature	$\varphi = 0$
	BC2, BC6	$G = 0$	$I_{nf} = 0$
	BC3	$G = R_n - L_E - H$ $H = f\left(T_3\right)$ $L_E = f\left(T_3, \varphi_3\right)$	$I_{nf} = \left(P - R_{off} - E_a\right)\rho_l$ $E_a = f\left(T_3, \varphi_3\right)$
	BC4	$G = R_n - L_E - H$ $H = f\left(T_4\right)$ $L_E = f\left(T_4, \varphi_4\right)$	$I_{nf} = \left(P - R_{off} - E_a\right)\rho_l$ $E_a = f\left(T_4, \varphi_4\right)$
	BC5	$G = R_n - L_E - H$ $H = f\left(T_5\right)$ $L_E = f\left(T_5, \varphi_5\right)$	$I_{nf} = \left(P - R_{off} - E_a\right)\rho_l$ $E_a = f\left(T_5, \varphi_5\right)$
where T_i and φ_i mean soil temperature (°C) and suction (m) at the surface point chosen at the "BCi" boundary as shown in Figure 5. 16. Other terms are explained in Chapter 3.			

(a)



(b)

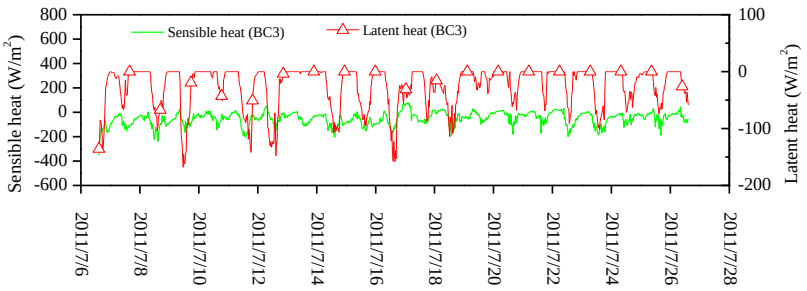
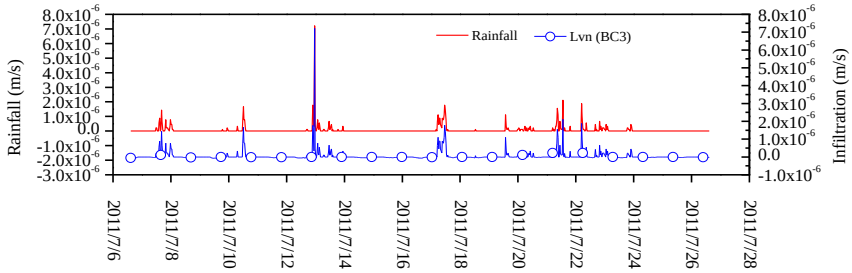


Figure 5. 17. Heat fluxes at the top surface of Héricourt embankment (BC3): (a) net solar radiation and soil heat; (b) sensible heat and latent heat

(a)



(b)

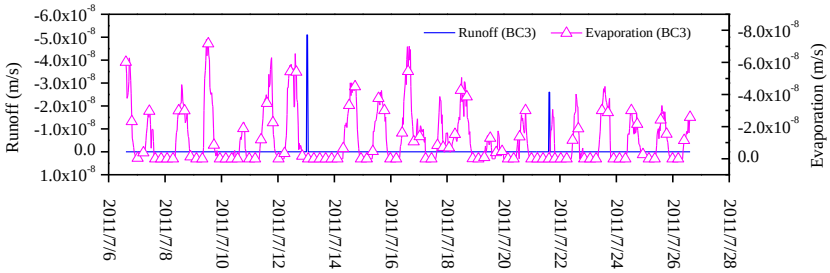


Figure 5. 18. Water fluxes at the top surface of Héricourt embankment (BC3): (a) rainfall and infiltration; (b) runoff and evaporation

5.3 Results and analysis

5.3.1 Soil hydro-thermal behavior

With soil parameters, initial and boundary conditions as introduced above, the modelling of Héricourt embankment with consideration of soil-atmosphere interaction can be performed by finite element method using FreeFem++ code (Hecht 2010). Thereby, the variations of volumetric water content and temperature are analyzed in three groups as follows.

5.3.1.1 Interior points (Points I1, I2 and I3)

The numerical results at three interior points (I1, I2 and I3) are compared with measurements in Figure 5. 19. It appears that the temperatures change slightly during the period of monitoring considered: all curves keep nearly stable. This suggests that even though heat transfer and mass transfer occur at soil surface, these three points are not significantly influenced. Comparison between the measurement data and the simulation results of soil temperature shows a good agreement (Figure 5. 19a). Similar variation tendency is observed for soil volumetric water content at these three points, and the simulation results also fit well with the corresponding measurement data (Figure 5. 19b). The small variations of temperature and volumetric water content can be explained by the relatively far positions from the top and slope surfaces of these points.

5.3.1.2 Near soil surface points (S1, S2 and S3)

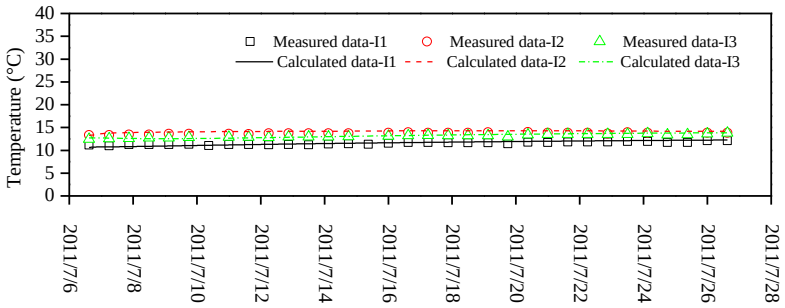
Three different points near soil surface, S1, S2 and S3, are chosen for analyzing the effect of soil-atmosphere interaction. These three points have the vertical distances of 40 cm, 33 cm and 15 cm respectively to the soil surface (Figure 5. 20). In terms of soil temperature variations, points S1 and S2 show a good agreement between the measurement data and the simulation results, with slight variations around 17 °C (Figure 5. 20a). For point S3, the measured

temperature increased at day time and decreased at night time, showing daily cyclic changes. The same tendency is also observed in simulation result even though there are significant differences between simulation and measurement. These differences may be due to the soil heterogeneity at the junction of slope and top boundary of field embankment. The real soil characteristics may differ from the assumed soil parameters in the numerical calculation.

Examination of the simulation result of volumetric water content at these three points shows an increase during a rainfall event and a decrease during evaporation. This is consistent with the measurement results. Indeed, no variation of volumetric water content is identified at points S1 and S2 during the first six days (Figure 5. 20b), which can be explained by the delayed reaction of the sensors because of the 20 cm layer of soil added on the slope surface. Thereby, comparison is conducted only from the 6th day. For point S2, its simulation result shows a good agreement with the measurement data (Figure 5. 20b). By contrast, for point S1, differences between two results can be observed. The measurement data keeps stable around 0.36 from the 6th day to the 9th day then goes down sharply. In the following days, it only shows a slight increase when the rainfall arrives again and always keeps stable for more than one day. The simulation result reaches the same value as the measured one at the 6th day, then decreases gradually with evaporation and increases with rainfall. As far as the rainfall information presented in Figure 5. 5b, it is noticed that discontinuous rainfall exists during 12/07/2011 to 14/07/2011 then appears again on 17/07/2011. The simulation results show that the volumetric water content decreases gradually from the 7th day to the 11th day then has the increase-decrease variation in the following days. Therefore, it can be inferred that the simulation results of gradual decrease during the 7th day to the 11th day are more rational compared with the values of sharp decrease at the 9th day in measurements. This suggests that some unexpected problems may happen during the field measurement, and the simulation results can help identify and correct the sensor problems during the field measurement. For point S3, it appears that the response of volumetric water content is consistent with the surface water flux boundary condition (evaporation/infiltration) from the beginning, proving a good agreement between the measurement and the simulation results. This evidences the effect of slope surface boundary

condition on the volumetric water content variations. Furthermore, at points S1 and S2, the soil temperatures keep stable, but the volumetric water contents show variations over time. These results indicate that soil-atmosphere interaction is characterized by different depths of influence for soil temperature and volumetric water content.

(a)



(b)

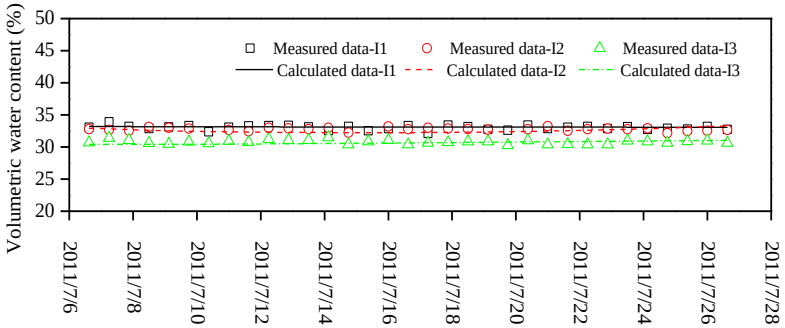
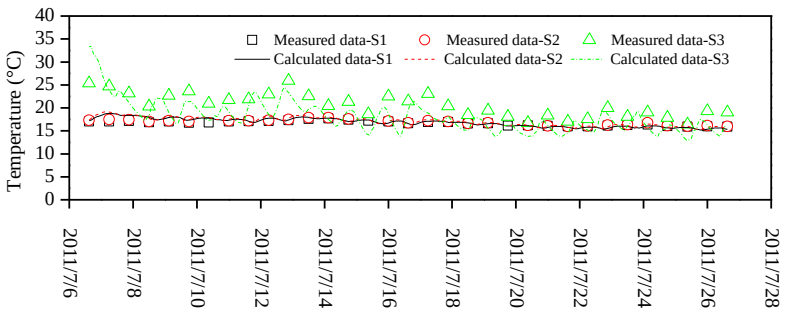


Figure 5. 19. Comparisons between the measured data and calculated data for interior points I1, I2, and I3: (a) temperature variations; (b) volumetric water content variations

(a)



(b)

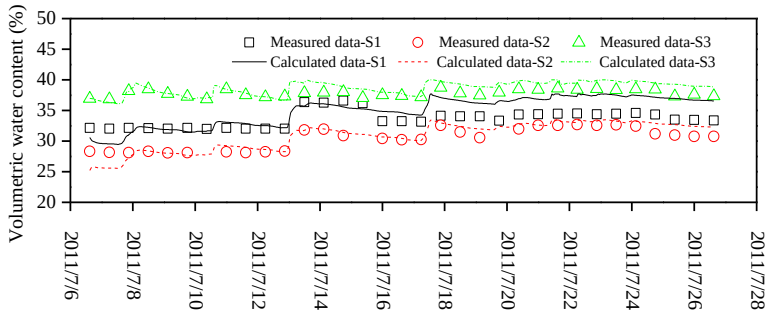


Figure 5. 20. Comparisons between the measured data and calculated data for the near soil surface points S1, S2, and S3: (a) temperature variations; (b) volumetric water content variations

5.3.1.3 Soil surface points (A1 and A2)

In the field measurements, only temperature variations over time were recorded for the top soil surface at point A1 and for the slope surface at point A2 (10 cm below the soil surface). Thereby, only the temperature variations are considered for comparison. In Figure 5. 21a, a good agreement can be identified between measurement and simulation in terms of the temperature variation at point A1. In Figure 5. 21b, the temperature variation of the slope surface point A2 is compared. A satisfactory agreement is also observed between measurement and simulation: the differences between both are limited to 2 ºC.

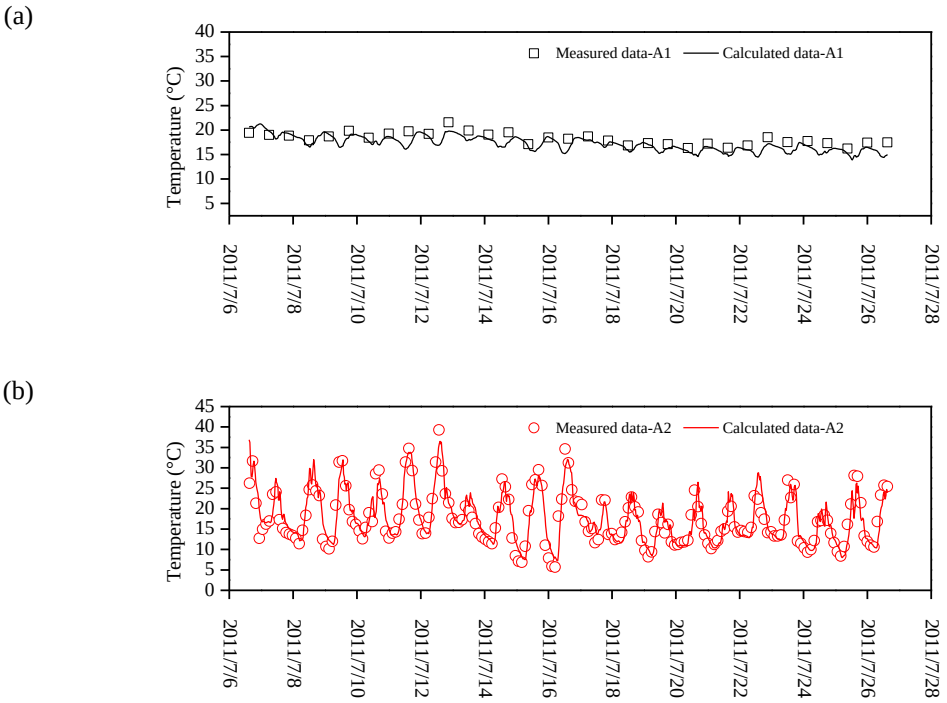
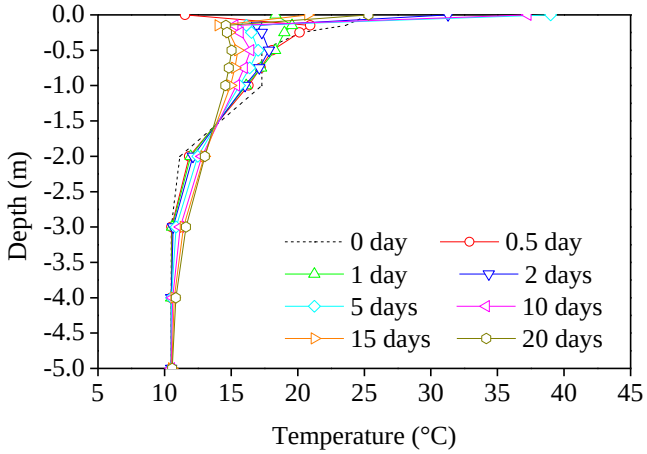


Figure 5. 21. Temperature comparisons between the measured data and simulation data: (a) for slope surface point A1; (b) for top surface point A2

5.3.2 Influence depths of soil temperature and volumetric water content by climate conditions

The overall good agreement between the measurements and the simulations validates the adopted fully coupled hydro-thermal soil model and the surface boundary conditions deduced from the soil-atmosphere interaction model. Furthermore, it proves that the soil temperature and volumetric water content are both greatly influenced by the soil-atmosphere interaction, but within different limited depths. For the temperature variations, the field data at points S1 and S2 shows a variation lower than 1.0 ºC (Figure 5. 20a). However, the measured volumetric water content at both points S1 and S2 shows significant variations due to evaporation/infiltration process (Figure 5. 20b).

(a)



(b)

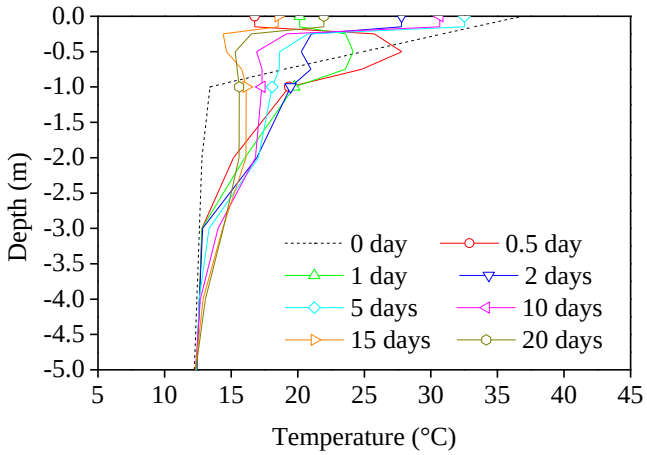
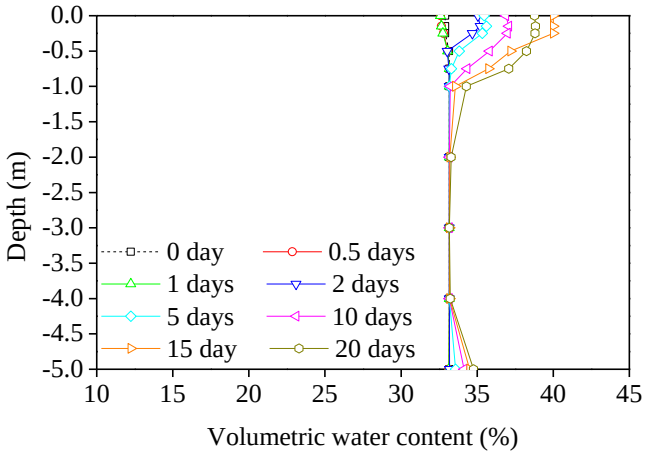


Figure 5. 22. Soil temperature profiles at different times: (a) below point A1; (b) below point A2

In order to further explore the influence depth of soil-atmosphere interaction, the simulated soil temperature and volumetric water content profiles below points A1 and A2 are presented in Figure 5. 22a and Figure 5. 22b, respectively. It can be observed that, the soil temperatures at the depth of 4 m below point A1 and point A2 keep nearly stable and are not influenced by the surface boundary conditions. Larger variations can be identified for the temperatures below point A2 as compared to those below point A1, showing the contribution of the slope surface boundary conditions. Nevertheless, the influence depths in terms of soil volumetric water content below point A1 and point A2 are estimated at 2 m and 3 m respectively as shown in Figure 5. 23a and Figure 5. 23b. The soil volumetric water content at the depth of 4 m below

point A1 is influenced by the underground water table as shown in Figure 5. 16. The results indicate that the slope surface boundary conditions have a smaller effect on the volumetric water content variation than on the temperature variation. On the other hand, heat is transferred homogeneously in all directions in a homogeneous material while soil volumetric water content variation is dominantly controlled by the vertical water flow due to the gravity effect. Therefore, it is recommended to investigate the influence depths of temperature and volumetric water content separately in different zones of the two-dimensional embankment, because the temperature changes are related to the thermal boundary conditions while the volumetric water content changes are governed by the hydraulic boundary conditions.

(a)



(b)

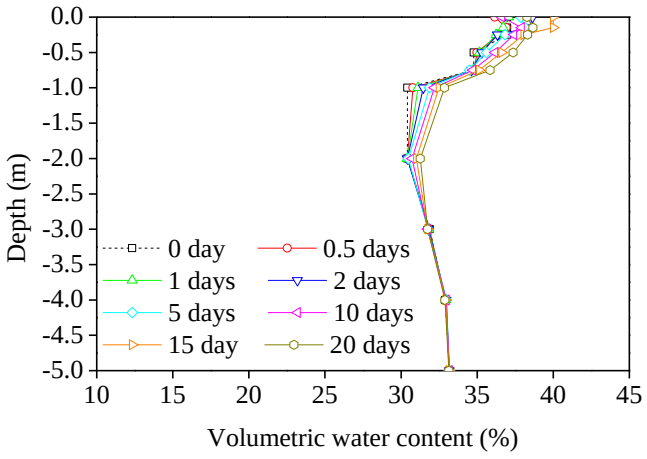


Figure 5. 23. Soil volumetric water content profiles at different times: (a) below point A1; (b) below point A2

5.4 Sensitivity analysis about initial condition effect

A sensitivity study on initial condition effect is useful to understand how initial setup of the system impacts the final numerical results. Specifically, it is important to study the effect of influencing factors in initial condition on the final results and the time required for the error disappears, which can be defined as calibration time. As stated by Daniel (2013), with an initial isothermal state defined by a reference depth temperature, his model needs to be run for 4~7 days in order to generate a realistic soil temperature profile. This could also be achieved by cycling 4~7 times during the first day for producing a relatively realistic initial soil temperature profile. In contrary, the initial water content profile needs to be measured accurately. In literature, the study of initial condition effect only involves heat flow in soil, water flow being not discussed. Furthermore, few studies of initial conditions effect have been conducted in the numerical analysis of geotechnical constructions. Based on the abundant information collected in Héricourt embankment, numerical experiments can be designed for this purpose. As a coupled hydro-thermal soil model is applied, the numerical experiments are conducted in two parts: initial conditions in terms of soil temperature and in terms of volumetric water content.

5.4.1 Initial condition of soil temperature

In terms of temperature changes, soil in all depths will be influenced by climate conditions when the studied period is long enough. In a limited studied period, the climate effect on soil temperature will be restricted in a shallow depth. Generally, due to the fact that the surface sensors are not easy to be installed and in addition, they are frequently influenced by the environment near soil surface, error in the estimation of soil initial temperature may appear. It is essential to well understand the initial soil temperature effect on the final calculation results.

5.4.1.1 Three cases with different soil initial temperatures

In Héricourt embankment, a much larger temperature gradient has been observed in the region

near soil surface (Figure 5. 24). Three different initial conditions of soil temperature profile are proposed for numerical investigation. They are defined in a reasonable range based on the measurements and are presented in Table 5. 3. Below point A2 (Figure 5. 3), five points are selected at depths of 0.00 m (point P1), 0.15 m (point P2), 0.25 m (point P3), 0.50 m (point P4), 0.75 m (point P5) for monitoring soil temperature variations over time.

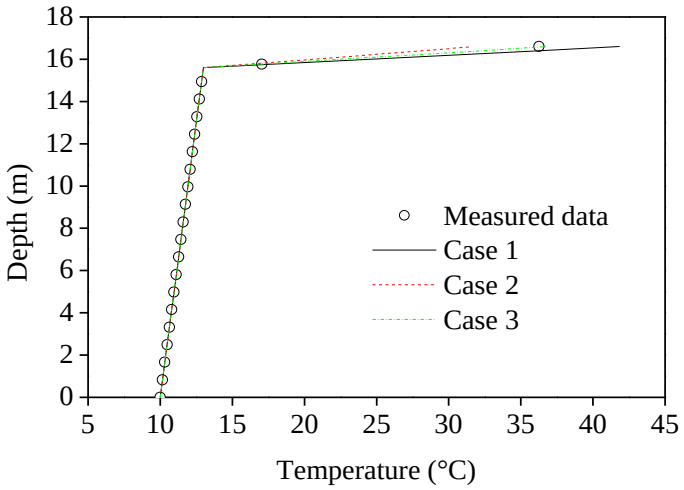


Figure 5. 24. Soil temperature measurement profile and assumed three initial soil temperature conditions below point A2

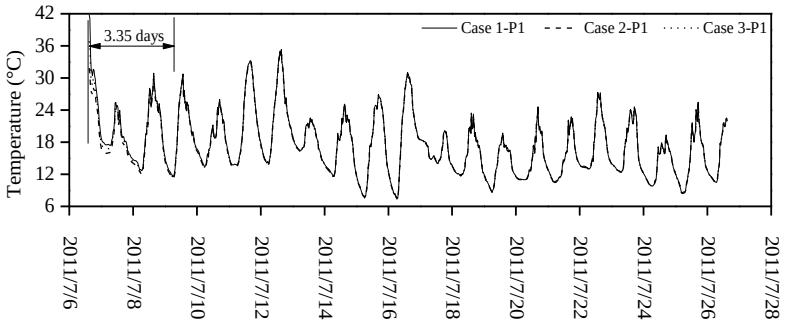
Table 5. 3. Soil initial temperature in three different cases

Soil depth	*Initial condition of soil temperature (°C)*
y >= 15.6m	Case 1: T_0 = 13+(y-15.6)×28.85
	Case 2: T_0 = 13+(y-15.6)×18.85
	Case 3: T_0 = 13+(y-15.6)×23.85
y < 15.6m	T_0 = 10+0.24×y

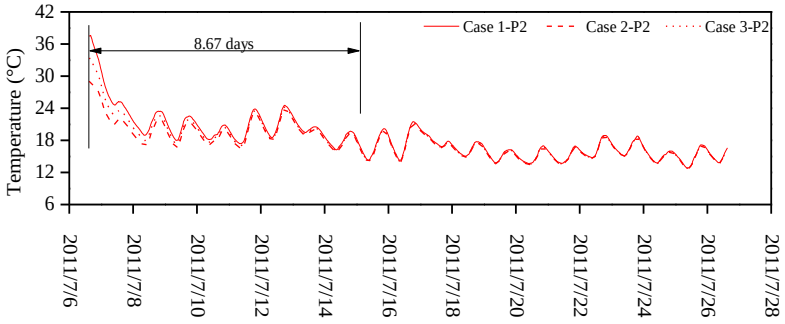
Other required information is assumed to be the same as that adopted in section 5.2. The soil temperature variations at the five points in the three cases are presented in Figure 5. 25. In this study, calibration time is defined as the period from the starting moment to the moment when the differences in the three cases are smaller than 0.2 ºC. In Figure 5. 25, from point P1 to P5, the calibration time is 3.35 days, 8.67 days, 10.96 days, 15.29 days, 18.40 days, showing that

longer calibration time is required for deeper points. Meantime, it is observed that the variation range of soil temperature is smaller as the depth increases.

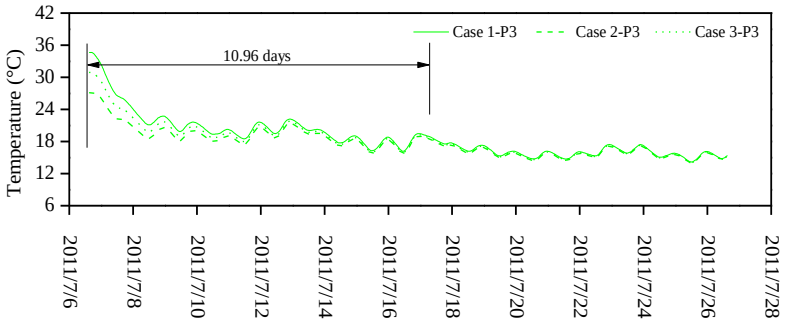
(a)



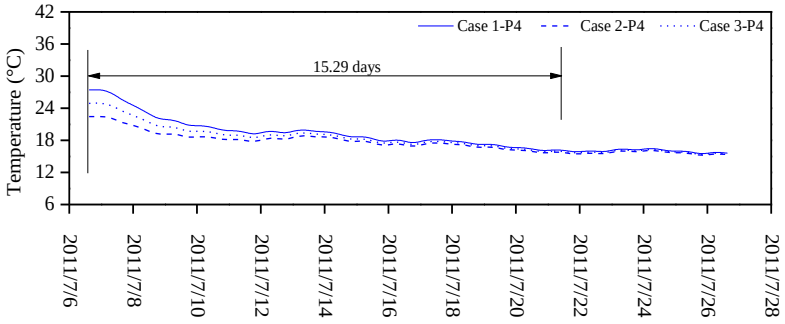
(b)



(c)



(d)



(e)

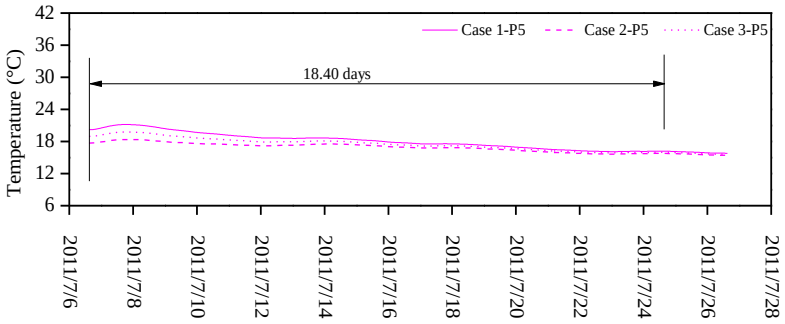


Figure 5. 25. Soil temperature variations in the three cases with different initial temperature conditions: (a) at point P1; (b) at point P2; (c) at point P3; (d) at point P4; (e) at point P5

In the three cases with different soil temperature initial conditions, the reasons to lead the final consistent value after a calibration time might be questioned. As presented in section 5.2.3, heat flux boundary conditions influence significantly the variations of soil temperature. In Figure 5. 26, heat fluxes at the top boundary (BC3) are presented to explain the dissipation process of soil temperature differences caused by different soil initial conditions.

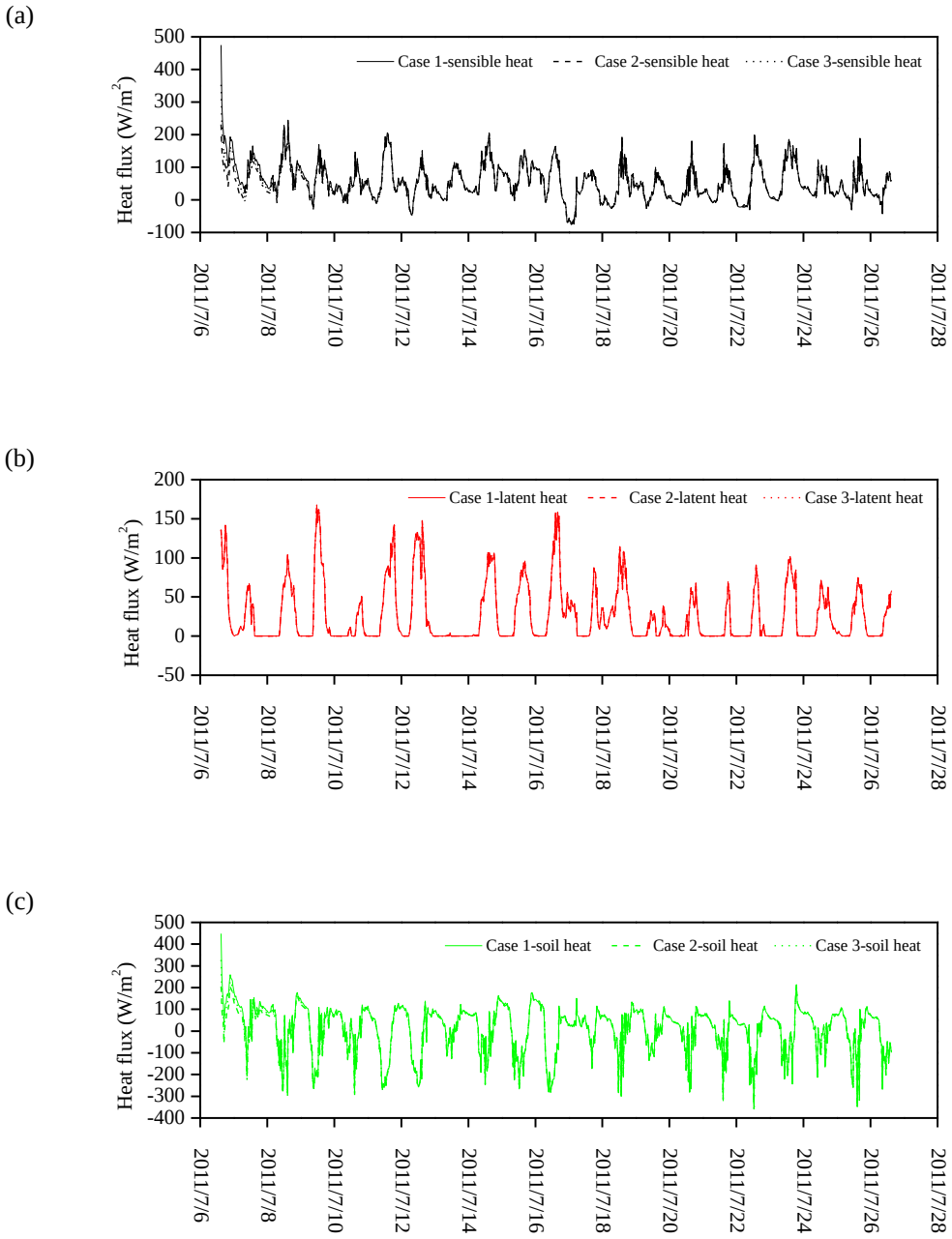


Figure 5. 26. Heat flux variations during the studied time period: (a) sensible heat; (b) latent heat; (c) soil heat

Based on equation (3.14), net solar radiation is the same input data as the only exterior heat source in the three cases. Soil heat flux G is applied as heat flux boundary condition and needs to be estimated using latent heat L_E and sensible heat H. The determination of sensible heat H

(equation 3.29) is intimately related with the soil surface temperature, while the latent heat L_E is related with the soil surface temperature and volumetric water content because of evaporation. For the surface points, their initial temperatures will be modified iteratively by heat flux boundary conditions during the interaction with atmosphere. For the three cases, during soil-atmosphere interaction, the sensible heat values are different initially but reach the same value finally as shown in Figure 5. 26a. However, Figure 5. 26b shows that the latent heat results in the three cases are nearly the same during all the studied period. Finally, as the heat flux boundary condition on the soil surface, soil heat flux G in the three cases reaches the same value after the calibration time (Figure 5. 26c). Hence, it is inferred that the sensible heat is the predominant and direct reason to lead the variation of soil heat flux, further affecting the dissipation process of soil temperature differences.

Additionally, some influencing factors in initial temperature condition can lead different calibration time. In the further sensitivity analysis, soil thermal conductivity and time scale of boundary conditions are tested respectively.

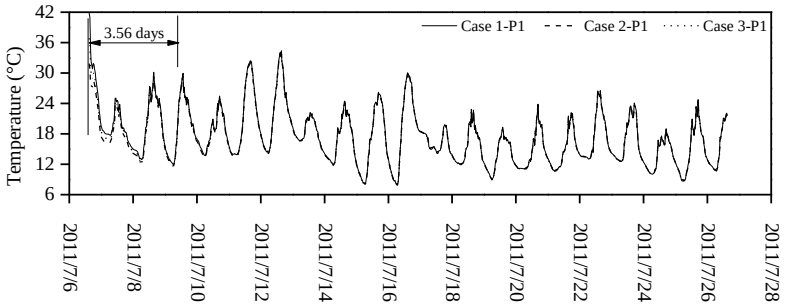
5.4.1.2 Effect of soil thermal conductivity

The effect of soil thermal conductivity on soil temperature variation is naturally significant because conduction is the most important form of heat transfer in soil. Different values of soil thermal conductivity are adopted respectively for the three different cases presented above, aiming at studying the effect of soil thermal conductivity on calibration time. As the common value of soil thermal conductivity is 0.15~4.00 (W/(mK)), soil thermal conductivity values are assumed to be $\lambda = \lambda_{original}+0.5$ and $\lambda = \lambda_{original}+1$ in the two other cases.

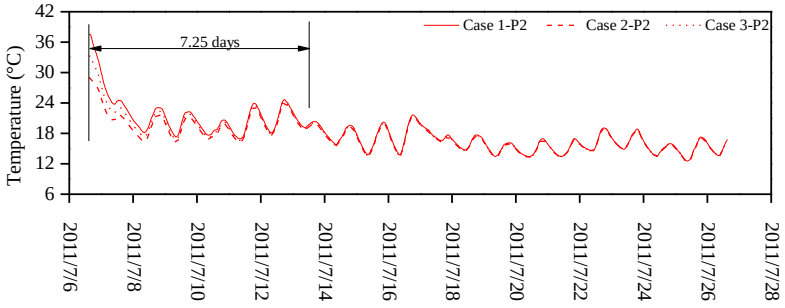
Firstly, three cases with different initial temperature conditions are tested with soil thermal conductivity $\lambda = \lambda_{original}+0.5$. As presented in Figure 5. 27, for each point, the differences between the three cases are decreasing over time. The calibration time is found to be 3.56 days, 7.25 days, 8.98 days, 12.31 days and 14.75 days for points P1, P2, P3, P4, and P5, respectively. As depth increases, longer calibration time is required because of heat conduction. Meantime,

soil temperature of deeper points shows much smaller fluctuations than that in the near surface zone.

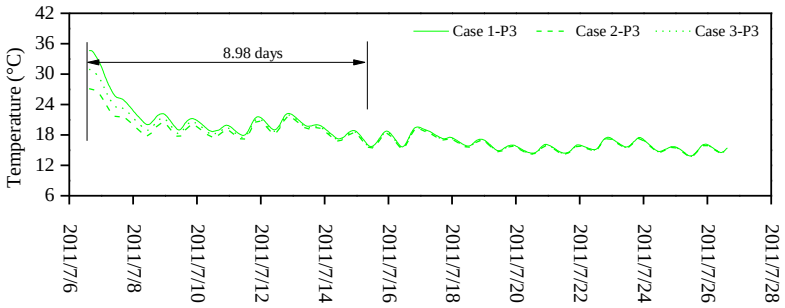
(a)



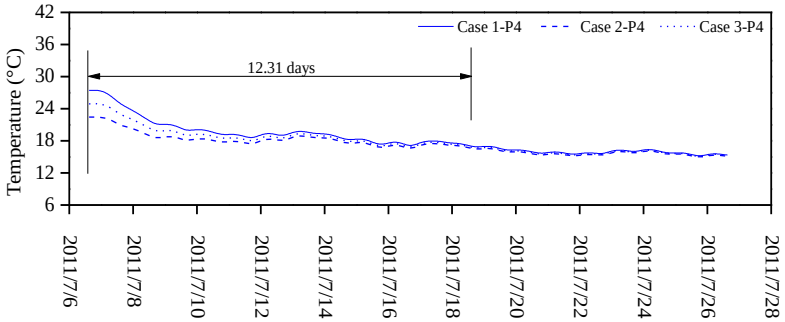
(b)



(c)



(d)



(e)

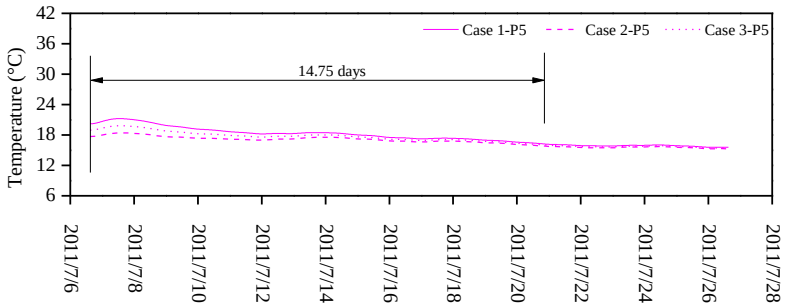


Figure 5. 27. Soil temperature variations with soil thermal conductivity $\lambda = \lambda_{original}+0.5$ in the three cases with different initial temperatures: (a) at point P1; (b) at point P2; (c) at point P3; (d) at point P4; (e) at point P5

Secondly, the soil thermal conductivity of $\lambda = \lambda_{original}+1$ is applied for the three cases. Figure 5. 28 presents the calculation results of the five points, indicating that the differences between the three cases in terms of each point are decreasing over time. The calibration phase takes 3.52 days, 6.35 days, 7.75 days, 10.50 days and 12.48 days at points P1, P2, P3, P4, and P5, respectively. It suggests that the calibration time is longer for deeper positions. Meanwhile, as depth increases, the fluctuation range of soil temperature becomes smaller.

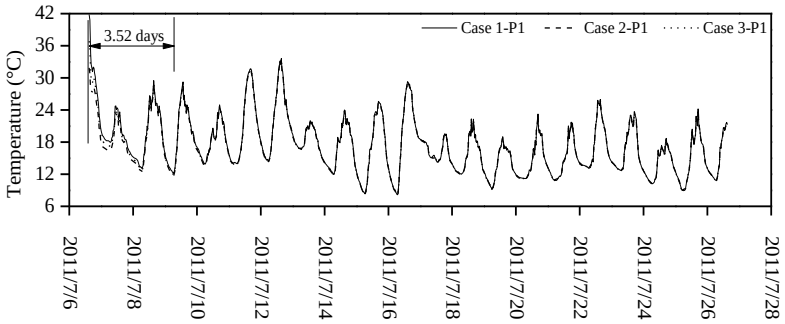
The information of calibration time for soil with different thermal conductivities is summarized in Table 5. 4. As soil surface temperature is directly influenced by heat flux boundary condition and is involved in sensible heat and latent heat, the calibration times at the surface points are nearly the same for soil with different thermal conductivities. For other studied points, as soil thermal conductivity increases, shorter calibration time is needed. In addition, at deeper position, the effect of soil thermal conductivity on calibration time is more obvious, suggesting that longer calibration time is saved with larger thermal conductivity. For instance, at point P2, the calibration time is 8.67 days for soil with original thermal conductivity $\lambda_{original}$, and 7.25 days for soil with thermal conductivity $\lambda_{original}+0.5$. It indicates that nearly one day of calibration time is saved for higher soil thermal conductivity. However, at point P5, the calibration time is reduced from 18.40 days to 14.75 days, nearly 3.75 days being saved when the soil thermal conductivity increases from $\lambda_{original}$ to $\lambda_{original}+0.5$. This clearly shows the importance of soil

thermal conductivity for the calibration time and the determination of soil temperature initial conditions.

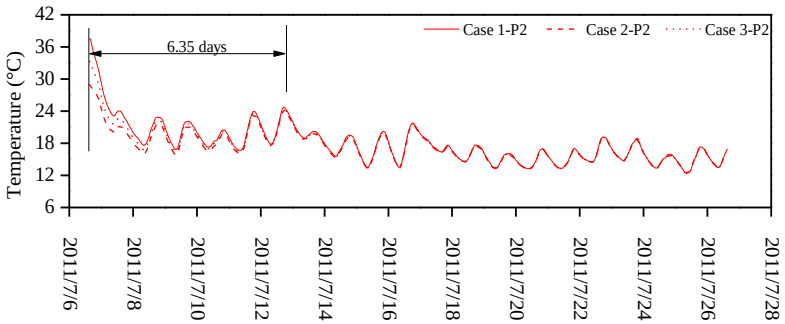
Table 5. 4. Calibration time for five points at different depths with different soil thermal conductivities

Points / *Thermal conductivity*	*Calibration time (days) (when difference < 0.2°C)*				
	P1	P2	P3	P4	P5
Original value $\lambda_{original}$	3.35	8.67	10.96	15.29	18.40
$\lambda = \lambda_{original}+0.5$	3.56	7.25	8.98	12.31	14.75
$\lambda = \lambda_{original}+1$	3.52	6.35	7.75	10.50	12.48

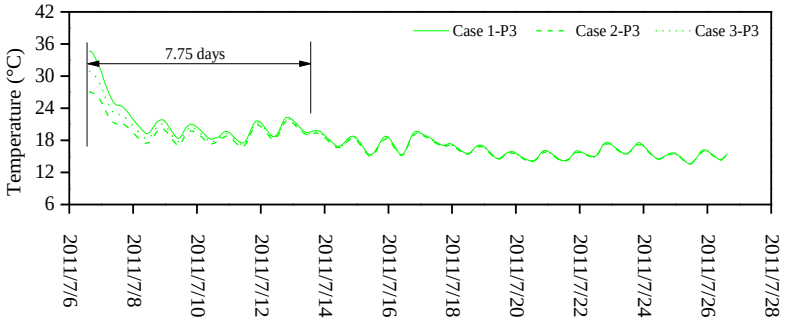
(a)



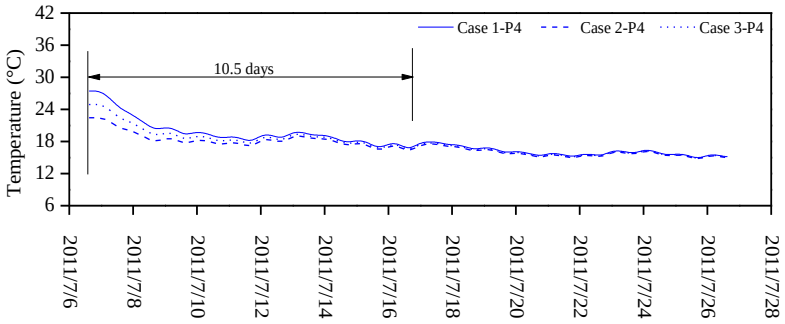
(b)



(c)



(d)



(e)

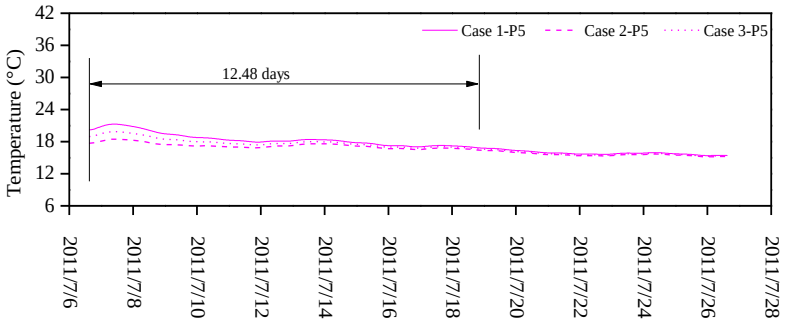


Figure 5. 28. Soil temperature variations with soil thermal conductivity $\lambda = \lambda_{original}+1$ in the three cases with different initial temperatures: (a) at point P1; (b) at point P2; (c) at point P3; (d) at point P4; (e) at point P5

5.4.1.3 Effect of time scale of boundary conditions

Through the above analysis, it appears interesting to further explore the effect of time scale of boundary conditions on the calibration time. With the meteorological information provided at

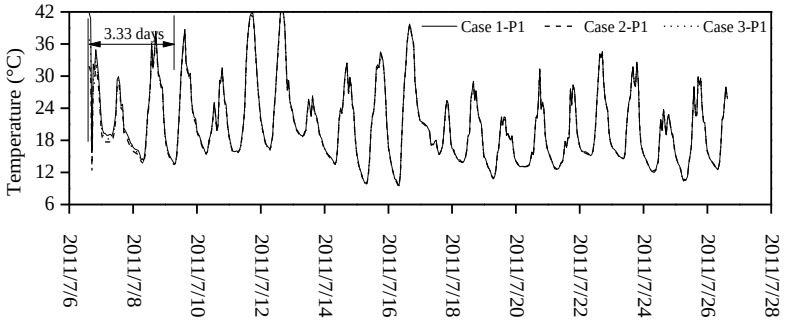
the site of Héricourt embankment, the heat flux boundary conditions are integrated and calculated in different time scales: 30 min, 1 hour, 6 hours, and 1 day. It means that different time steps are considered in the three cases. The results of numerical analysis in different time scales of 1 hour, 6 hours and 1 day are respectively presented in Figure 5. 29, Figure 5. 30, and Figure 5. 31. In all time scales, longer calibration time is required as depth increases. For instance, in the calculation results with a time step of 1 hour (Figure 5. 29), the calibration time is 3.33 days, 8.75 days, 11.00 days, 15.33 days, and 18.50 days for points P1, P2, P3, P4 and P5, respectively. Whilst the soil temperatures of deeper points always show much smaller fluctuation than those of near soil surface points.

All information about calibration time in different time scales is summarized in Table 5. 5. The calibration time can be obtained for all the points when the time scale is 30 min or 1 hour. However, when the time scale is 6 hours or 1 day, the soil temperature at some deep points (P4 and P5 for 6 hours, P3, P4 and P5 for 1 day) cannot be calibrated during 20 days and longer calibration time is required.

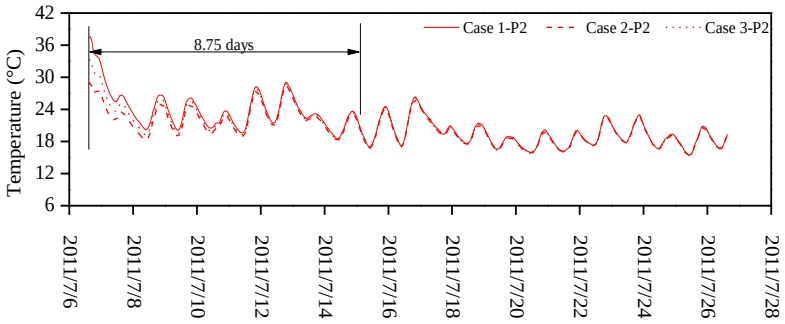
Table 5. 5. Calibration time for five points at different depths with different time scales

Points / *Time scale*	*Calibration time (days) (when differences < 0.2°C)*				
	P1	P2	P3	P4	P5
30 min	3.35	8.67	10.96	15.29	18.40
1 hour	3.33	8.75	11	15.33	18.5
6 hours	9.75	14	16.5	>20	>20
1 day	16.0	20	>20	>20	>20

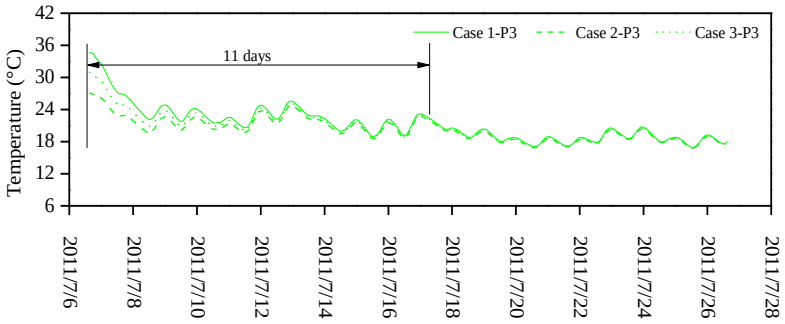
(a)


Case 1-P1
Case 2-P1
Case 3-P1
3.33 days
Temperature (°C)
42
36
30
24
18
12
6
2011/7/6
2011/7/8
2011/7/10
2011/7/12
2011/7/14
2011/7/16
2011/7/18
2011/7/20
2011/7/22
2011/7/24
2011/7/26
2011/7/28

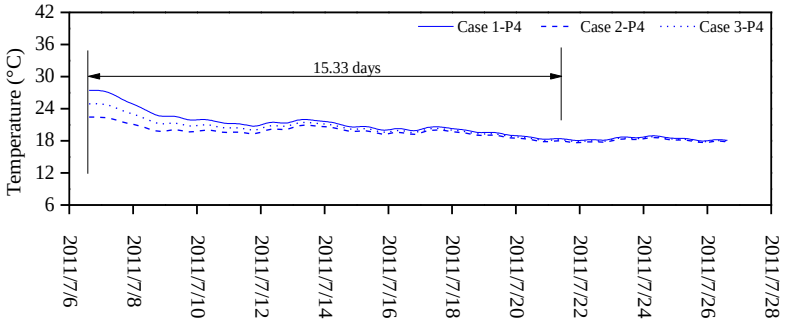
(b)


Case 1-P2
Case 2-P2
Case 3-P2
8.75 days
Temperature (°C)
42
36
30
24
18
12
6
2011/7/6
2011/7/8
2011/7/10
2011/7/12
2011/7/14
2011/7/16
2011/7/18
2011/7/20
2011/7/22
2011/7/24
2011/7/26
2011/7/28

(c)


Case 1-P3
Case 2-P3
Case 3-P3
11 days
Temperature (°C)
42
36
30
24
18
12
6
2011/7/6
2011/7/8
2011/7/10
2011/7/12
2011/7/14
2011/7/16
2011/7/18
2011/7/20
2011/7/22
2011/7/24
2011/7/26
2011/7/28

(d)


Case 1-P4
Case 2-P4
Case 3-P4
15.33 days
Temperature (°C)
42
36
30
24
18
12
6
2011/7/6
2011/7/8
2011/7/10
2011/7/12
2011/7/14
2011/7/16
2011/7/18
2011/7/20
2011/7/22
2011/7/24
2011/7/26
2011/7/28

(e)

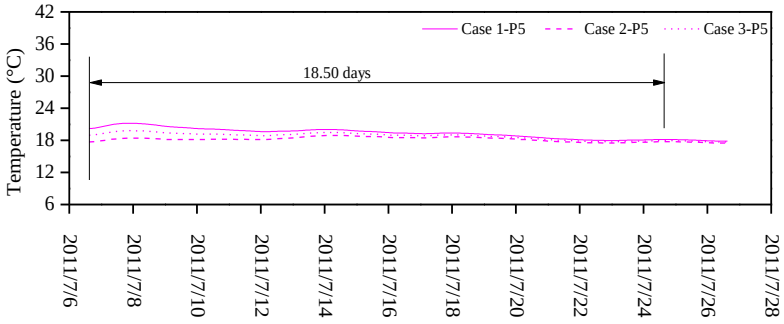
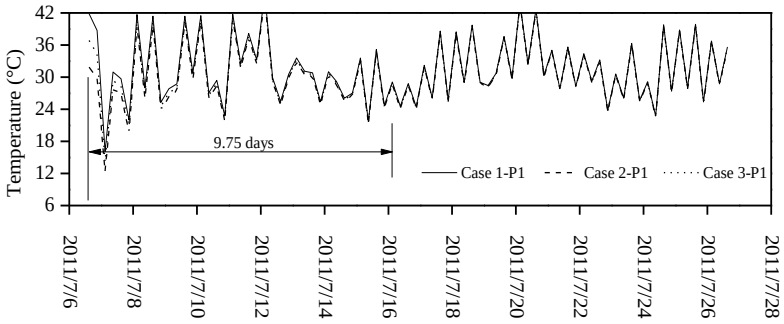
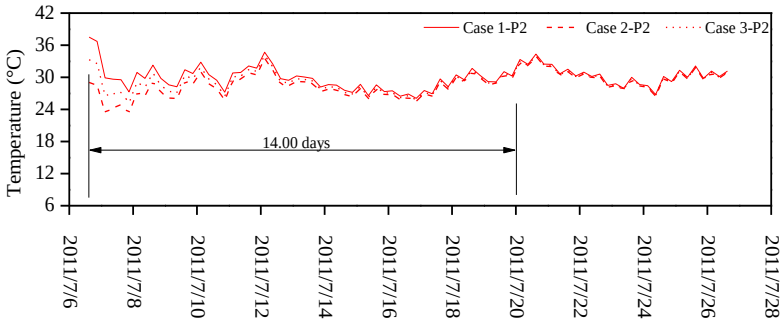


Figure 5. 29. Soil temperature variations when the time step is one hour: (a) at point P1; (b) at point P2; (c) at point P3; (d) at point P4; (e) at point P5

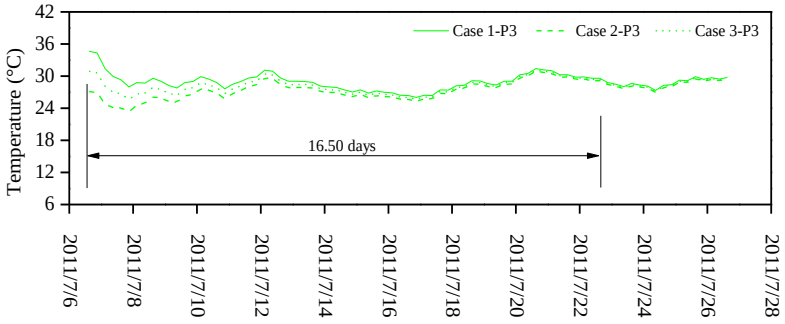
(a)



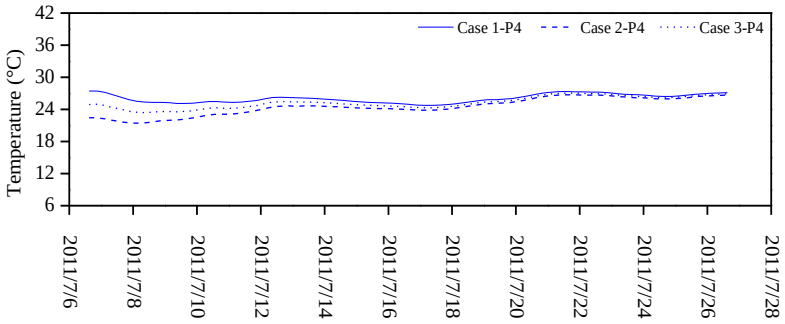
(b)



(c)



(d)



(e)

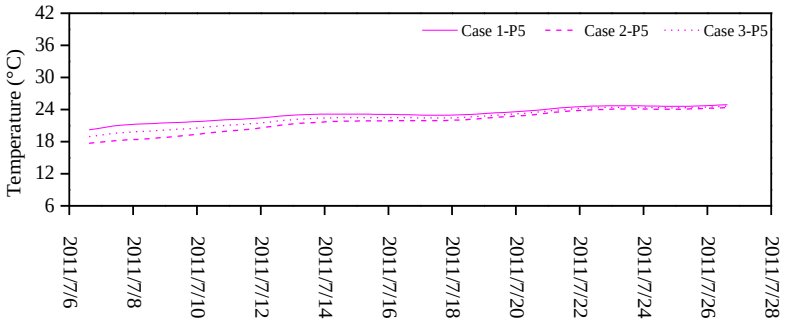
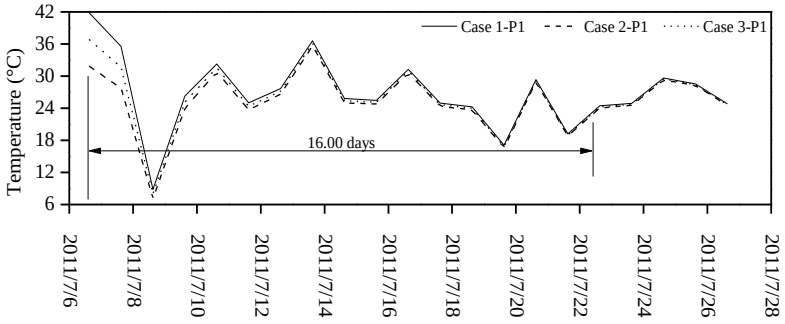
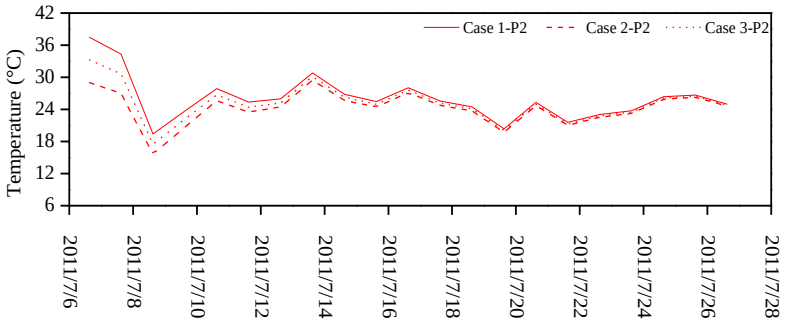


Figure 5. 30. Soil temperature variations when the time step is six hours: (a) at point P1; (b) at point P2; (c) at point P3; (d) at point P4; (e) at point P5

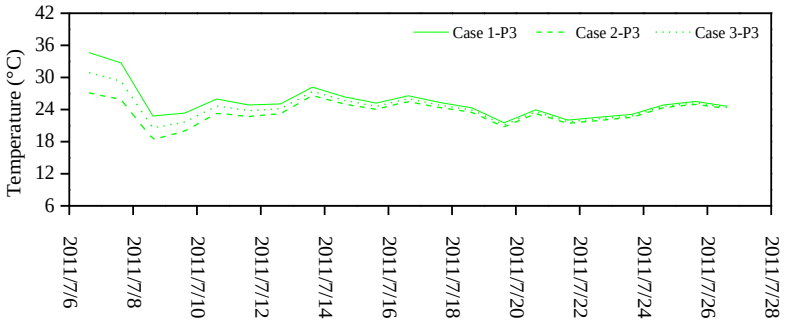
(a)


Case 1-P1
Case 2-P1
Case 3-P1
Temperature (°C)
16.00 days
42
36
30
24
18
12
6
2011/7/6
2011/7/8
2011/7/10
2011/7/12
2011/7/14
2011/7/16
2011/7/18
2011/7/20
2011/7/22
2011/7/24
2011/7/26
2011/7/28

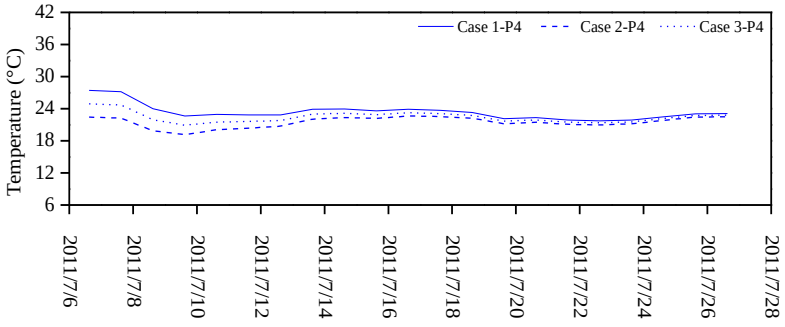
(b)


Case 1-P2
Case 2-P2
Case 3-P2
Temperature (°C)
42
36
30
24
18
12
6
2011/7/6
2011/7/8
2011/7/10
2011/7/12
2011/7/14
2011/7/16
2011/7/18
2011/7/20
2011/7/22
2011/7/24
2011/7/26
2011/7/28

(c)


Case 1-P3
Case 2-P3
Case 3-P3
Temperature (°C)
42
36
30
24
18
12
6
2011/7/6
2011/7/8
2011/7/10
2011/7/12
2011/7/14
2011/7/16
2011/7/18
2011/7/20
2011/7/22
2011/7/24
2011/7/26
2011/7/28

(d)


Case 1-P4
Case 2-P4
Case 3-P4
Temperature (°C)
42
36
30
24
18
12
6
2011/7/6
2011/7/8
2011/7/10
2011/7/12
2011/7/14
2011/7/16
2011/7/18
2011/7/20
2011/7/22
2011/7/24
2011/7/26
2011/7/28

(e)

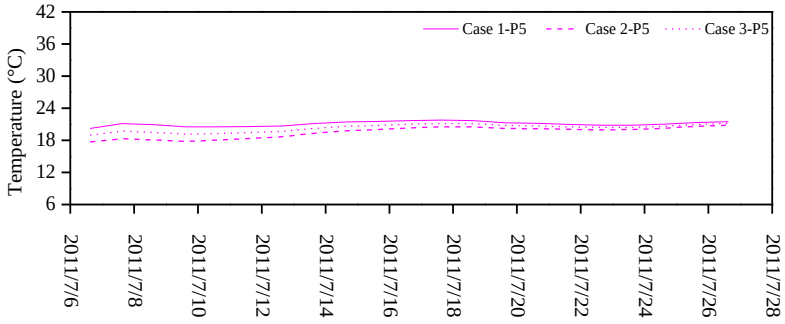


Figure 5. 31. Soil temperature variations when the time step is one day: (a) at point P1; (b) at point P2; (c) at point P3; (d) at point P4; (e) at point P5

As the surface point P1 is directly influenced by the heat flux boundary conditions, the soil surface temperatures are involved effectively in the determination of sensible heat. The calibration time at this point is nearly the same for the time scales of 30 min and 1 hour. When the numerical calculation is conducted every 6 hours or daily, much longer calibration time is needed. Regarding the results obtained at point P2, the calibration time increases with the increase of time step. The effect of time step at other points cannot be studied because the calibration time is expected to be longer, but the similar conclusion can be inferred as that for point P2. It can then be concluded that shorter time scale reduces the calibration time by accelerating the iteration rate of soil-atmosphere interaction.

5.4.2 Initial condition of soil volumetric water content

Based on the measurements of soil volumetric water content, three different cases are assumed in order to study the effect of soil volumetric water content initial conditions on the final results (Figure 5. 32). The details of soil initial volumetric water content expressions are expressed in Table 5. 6.

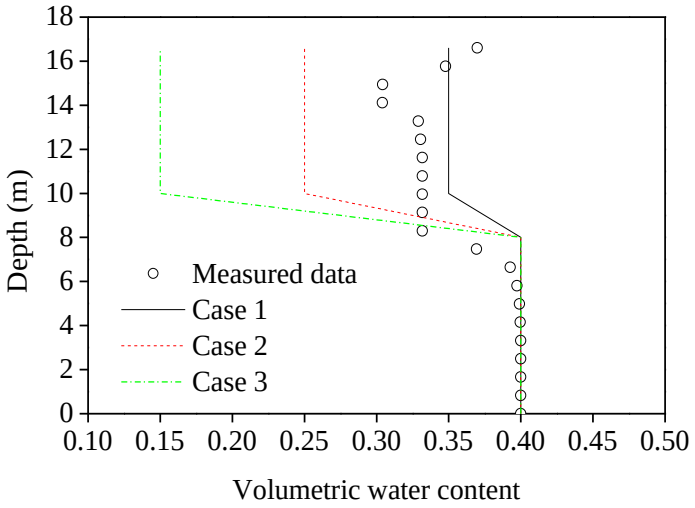


Figure 5. 32. Soil volumetric water content profile measured and three initial soil volumetric water content conditions assumed below point A2

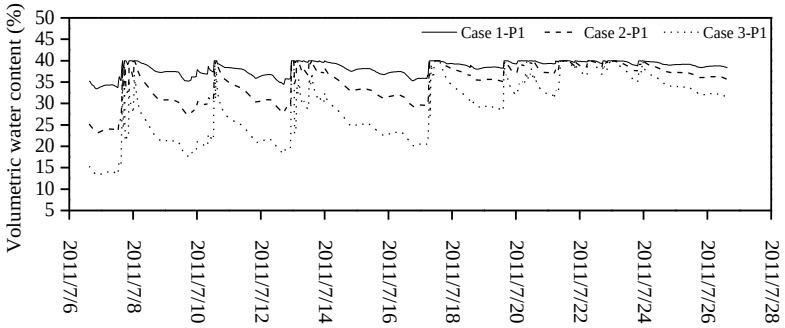
Other required information is assumed to be the same as that adopted in section 5.2. The five studied points are the same as chosen in section 5.4.1. The results of soil volumetric water content variation at these points in the three cases are presented in Figure 5. 33. It is observed that the soil volumetric water content in the region near soil surface (Point P1) in three cases all show a slight increasing trend over time, varying in a much larger range than those at other deeper points. However, the values in the three cases cannot reach the same value after a period of time. Similarly, deeper points also present a slight growth trend with certain fluctuations and this growth trend becomes weaker as depth increases. For all studied points in the three cases, the same value of soil volumetric water content cannot be reached after a period of time. It means that no calibration time exists for the soil volumetric water content in these three cases.

Table 5. 6. Soil initial volumetric water contents in three different cases

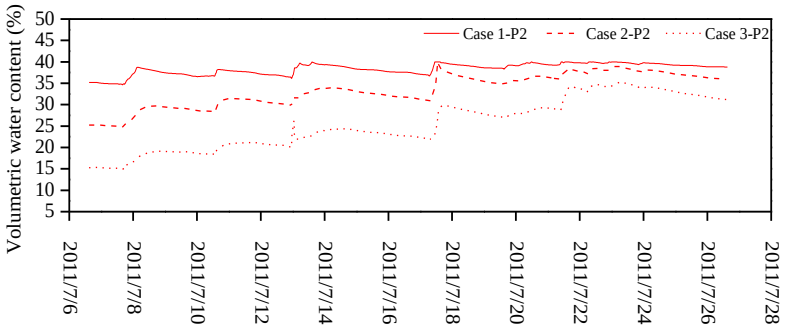
Soil depth	***Initial condition of soil volumetric water content***
y >= 5 m	Case 1: w_0 = 0.35 Case 2: w_0 = 0.25 Case 3: w_0 = 0.15
y < 5 m	w_0 = 0.4

As the water flux boundary condition on the top surface will be infiltration or evaporation, dominantly controlled by rainfall, runoff and evaporation and rainfall and evaporation will not show regular daily cycles as temperature, water flux boundary conditions are relatively independent of the variations of soil surface volumetric water content. Besides, the soil surface temperature and volumetric water content are only involved in the estimation of evaporation during numerical modelling. Therefore, the differences of soil volumetric water contents caused by different initial conditions are not easy to be corrected automatically.

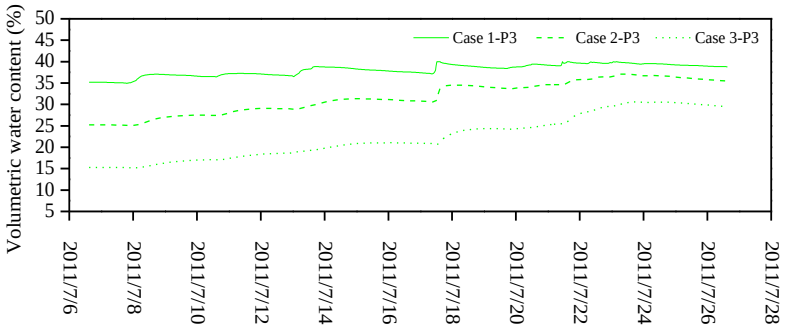
(a)



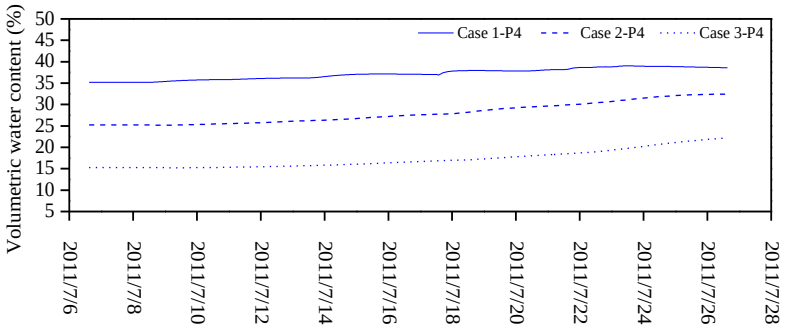
(b)



(c)



(d)



(e)

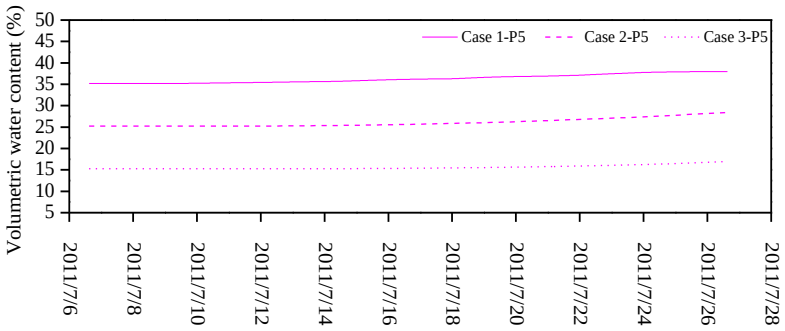


Figure 5. 33. Soil volumetric water content variations in the three cases with different initial volumetric water content conditions: (a) at point P1; (b) at point P2; (c) at point P3; (d) at point P4; (e) at point P5

5.4.3 Suggestions for determining soil initial conditions

According to the above analyses, it is observed that in the definition of soil initial temperature conditions, longer calibration time is required and smaller fluctuation of temperature variation exists as depth increases. As soil thermal conductivity increases, heat is conducted more quickly to deeper region from soil surface. Correspondingly, the influenced region by boundary conditions is becoming deeper and shorter calibration time is required at the same position. On the other hand, different calibration time is obtained when different time scales of boundary conditions are considered. Shorter time scale helps renew the boundary conditions more effectively, allowing the calibration time to be reduced. Conversely, the calibration phase does not exist for the soil volumetric water content in this study.

Relying on the numerical analyses, it can be concluded that the initial conditions of soil temperature and volumetric water content need to be treated in different ways. Regarding initial soil temperature condition, the value can be regulated within a certain influence depth. But for the deeper region out of this influence depth, accurate measurement data is necessary. In practice, this method can also be applied to verify the accuracy of soil temperature measurements.

Because rainfall and evaporation do not show regular daily cycles as the heat flux, water flux boundary conditions are relatively independent of the variation of soil surface volumetric water content. Therefore, no calibration time exists for volumetric water content. Hence, accurate measurements are required for defining initial conditions of soil volumetric water content.

5.5 Conclusions

The Héricourt embankment constructed in Franche-Comté region is studied in this chapter. This embankment was richly instrumented, with a weather station on the embankment surface, specific sensors for the measurements of soil temperature and volumetric water content in various positions. This enables the study of soil-atmosphere interaction and its effect on soil temperature and volumetric water content variations. The comparison between simulation results and filed measurements shows that an approach combining a fully coupled hydro-thermal soil model and soil-atmosphere interaction model is suitable for analyzing the soil temperature and volumetric water content in two-dimensional embankments. The good agreement between measurements and calculations also proves that suitable boundary conditions and soil parameters have been adopted for the numerical analyses.

During the studied period of 20 days, the soil temperature and volumetric water content variations show different influence depths of soil-atmosphere interaction: 4 m below the slope surface (below point A1) and below the top surface (below point A2) for temperature; 2 m below point A1 and 3 m below point A2 for volumetric water content. Note however that a larger temperature variation is identified below point A2 as compared to that below point A1,

showing the contribution of the slope surface boundary conditions. This suggests that the soil temperature in the region below the top surface is more sensitive to the slope boundary conditions than the soil volumetric water content.

Furthermore, numerical tests are conducted for a better understanding of initial condition effect on the final results. It appears that in terms of initial temperature conditions, longer calibration time is required and less fluctuation of soil temperature variation exists as depth increases. The effects of soil thermal conductivity and time scale are also investigated. It is observed that heat is conducted more quickly to deeper region from soil surface when soil thermal conductivity is larger, leading the deeper influence zone of boundary conditions and shorter calibration time at the same position. On the other hand, when different time scales of boundary conditions are considered, the numerical calculations are conducted in different time steps. It indicates that shorter time scale helps renew the boundary conditions more effectively, allowing the calibration time to be reduced. By contrast, the calibration phase does not exist for soil volumetric water content in this study.

Therefore, it is suggested that the initial conditions of soil temperature and volumetric water content need to be treated in different ways. Regarding initial soil temperature condition, the value can be regulated within a certain influence depth. But for the deeper region out of this influence depth, accurate measurement data is necessary. Besides, accurate measurements are required in the definition of initial conditions of soil volumetric water content.

Chapter 6: Modelling of Rouen embankment

6.1 Rouen embankment

In the project “Digues et Ouvrages Fluviaux, Érosion Affouillements et Séismes (DOFEAS)”, an experimental embankment was constructed in Rouen, France. This region is characterized by a continental climate influenced by ocean. The field site plan is presented in Figure 6. 1. The surface and slope situations of the embankment are shown in Figure 6. 2a and Figure 6. 2b, respectively. The construction of experimental embankment was conducted from 26/09/2011 to 26/10/2011. The embankment is 21 m long, 1.8 m high, consisting of six layers of 0.3 m each, with two different slopes 2:3 (left) and 1:2 (right) (Vertical: Horizontal) as shown in Figure 6. 3. The soil used for the embankment construction is a silt treated by 2% CaO. In terms of untreated silt, its plastic limit w_p is 23%, liquid limit w_l is 37%, plasticity index *IP* is 14, and methylene blue value *VBS* is 2.38. More information about the embankment construction can be found in the report by Charles and Froumentin (2013).

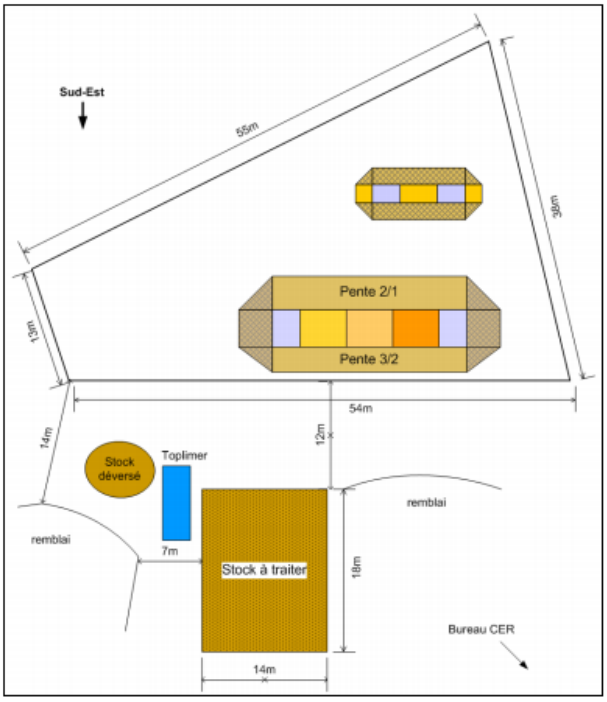


Figure 6. 1. Field site plan of Rouen experimental embankment

(a) (b)



Figure 6. 2. Field view of Rouen embankment: (a) embankment surface situation in 10/2011; (b) the slope situation of embankment in 07/2015

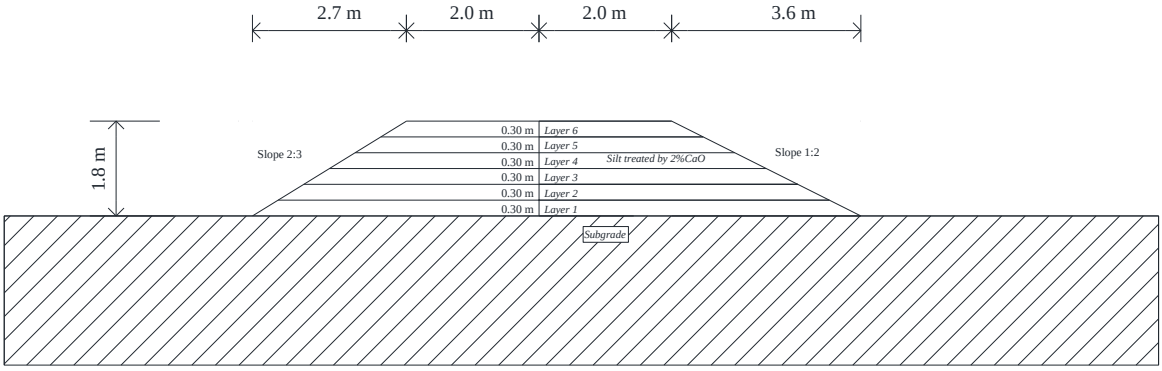


Figure 6. 3. Cross section of Rouen embankment

Figure 6. 4 presents the instrumentation of the field embankment and indicates the number of each layer. The soil temperature and volumetric water content were recorded by PT 100 and TDR sensors, respectively. These sensors were designed to be installed at different layers during the construction as follows:

1) 1C0 to 4C0 were sited on the interface between supportive soil and the first soil layer;
2) 1C2 to 3C2 were sited on the second layer;
3) 1C4 to 3C4 were sited on the fourth layer;
4) 1C5 and 2C5 were sited on the interface between the sixth and fifth layer.

The outlook of sensors used for the temperature measurement (PT 100) and volumetric water content measurement (TDR) are presented in Figure 6. 5. The soil temperature was recorded

every two hours from 10/07/2011 to 03/02/2015 by a central automatic acquisition system. For the soil volumetric water content, it was measured every six hours from 25/10/2011 to 12/12/2014 by a multiplexer and trace acquisition system.

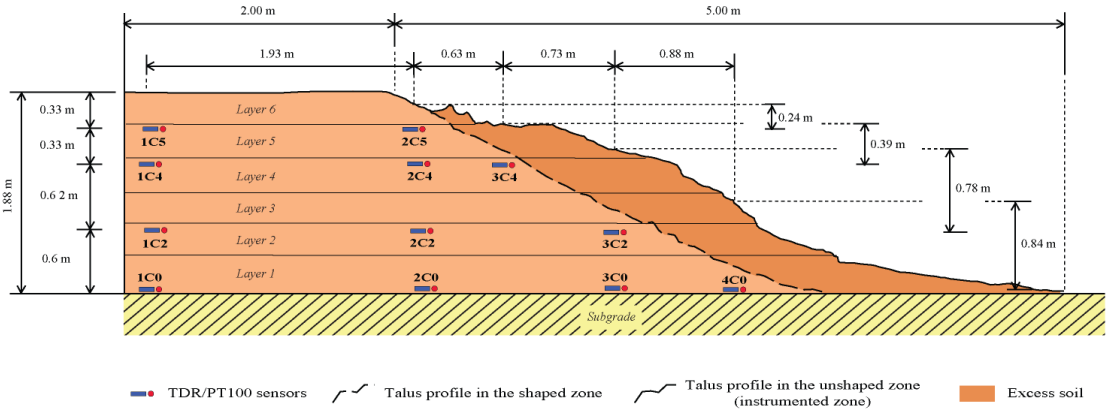


Figure 6. 4. Field instrumentation profile of Rouen embankment, providing information about the number and position of each sensor



Figure 6. 5. PT100 sensor for soil temperature measurement (left) and TDR sensor for soil volumetric water content measurement (right)

During 10/07/2014-13/01/2015 (187 days), hourly meteorological data such as solar radiation, rainfall, wind speed, air relative humidity, air temperature and dew temperature were successfully recorded by a "ECTOT LES BAONS" station of METEO FRANCE, which is 30 km away from Rouen embankment. Moreover, during 27/10/2011-17/11/2012 (387 days), precise hourly information about air temperature and air relative humidity, rainfall and dew temperature information were measured by a field meteorological station (20 m away from

Rouen embankment). The information of solar radiation and wind speed during the same period (387 days) can be collected from "ECTOT LES BAONS" station. Thereby, these two different periods (187 days+387 days) were chosen with complete metrological data, soil temperature and soil volumetric water content at different points, enabling the evaluation of climate effect on treated soil embankment.

In the numerical modeling of Rouen embankment, several assumptions are made for simplification:

1) Soil is assumed to be homogeneous and isotropic in the whole embankment;
2) The positions of sensors for recording soil temperature and volumetric water content are assumed to be at the right place shown in Figure 6. 4; no offset of sensors during the construction happened;
3) The heat flux and water flux boundary conditions are assumed to be the same for all points at the same surface boundary;
4) The surface of field embankment is bare; no vegetation effect is considered.

6.2 Definition of numerical model

6.2.1 Soil parameters

The hydro-thermal properties of the studied silt treated by 2% CaO are required for the numerical analysis. Its thermal conductivity, soil water retention and hydraulic conductivity curves are determined and presented below.

As for the Héricourt embankment, the soil thermal conductivity was measured by KD2 Analyzer (Tang et al. 2008; Buongiorno et al. 2009; Teng et al. 2010). As proposed by De Vries (1963) and Cui et al. (2005), a linear relationship between soil thermal conductivity and volumetric water content is chosen (Figure 6. 6) and expressed by:

$$\lambda = 2.1818\theta + 0.808 \tag{5.1}$$

where λ is the thermal conductivity (W/(mK)), θ is the volumetric water content.

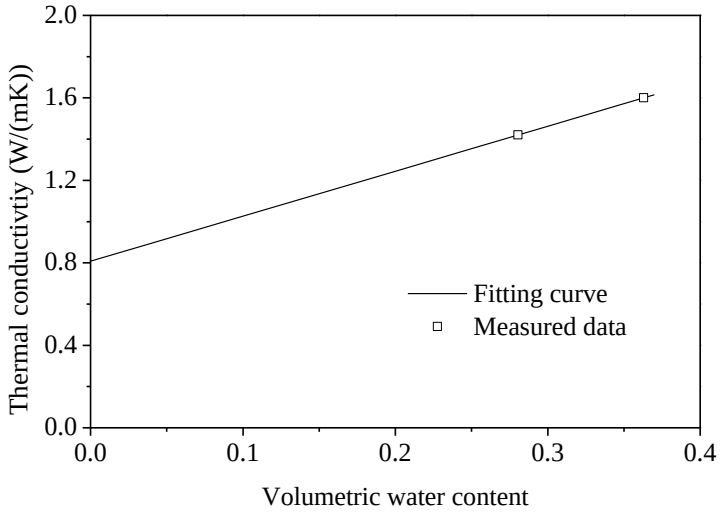


Figure 6. 6. Thermal conductivity curve versus volumetric water content for the silt treated by 2% CaO

Three field soil samples are taken and tested to obtain the water retention curve using "WP4 method" (Scanlon et al. 2002; Thakur et al. 2006). Besides, the porosity of treated silt is also determined, being equal to 0.37. Based on van Genuchten model (van Genuchten 1980), the expression for the soil water retention curve is built:

$$S_e = \frac{\theta - \theta_r}{\theta_s - \theta_r} = \left[\frac{1}{1 + (\alpha_s \varphi)^n} \right]^m \tag{5.2}$$

where the saturated volumetric water content $\theta_s = 0.37$; the residual volumetric water content $\theta_r = 0.00$; parameter $\alpha_s = 0.0025$ kPa^{-1}, $m = 0.18$ and $n = 2.2$. With the measurement data, a fitting curve is drawn in Figure 6. 7.

As stated by Charles and Froumentin (2013), the saturated permeability of treated silt has been measured in-situ at different positions and at different times: 2.8×10^{-9} m/s (28 days), 1.2×10^{-9}

m/s, 3.9×10^{-8} m/s, 9.4×10^{-9} m/s (180 days), and 1.2×10^{-8} m/s (365 days). It means that during the construction and service period, the soil hydraulic properties vary slightly, keeping the value in the range from 1.0×10^{-8} to 1.0×10^{-9} m/s. Therefore, the value of 1.0×10^{-9} m/s is chosen in the numerical modeling. Based on the soil water retention curve determined previously, the hydraulic conductivity in unsaturated state can be estimated using van Genuchten model (van Genuchten 1980):

$$K = K_s S_e^{0.5}\left[1-\left(1-S_e^{1/m_1}\right)^{m_1}\right]^2 \tag{5.3}$$

where $m_1 = 0.5$; saturated hydraulic conductivity $K_s = 1.0\times10^{-9}$ m/s; other parameters take the same values as explained for equation (5.2). The curve of soil hydraulic conductivity versus suction is plotted in Figure 6. 8.

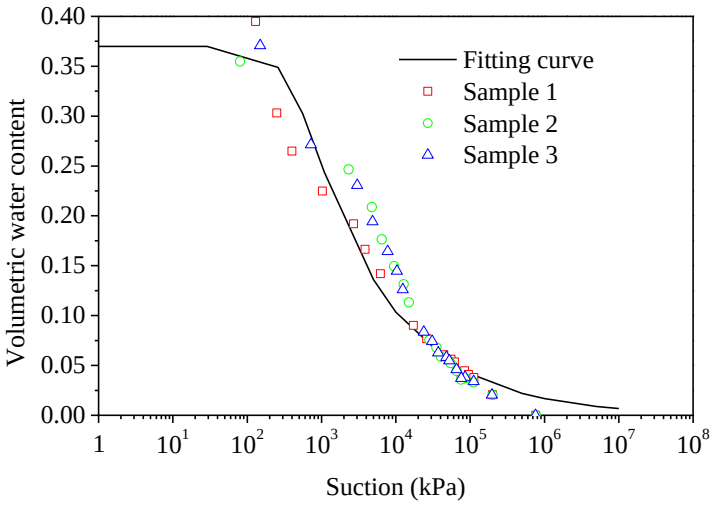


Figure 6. 7. Water retention curve versus suction for the silt treated by 2% CaO

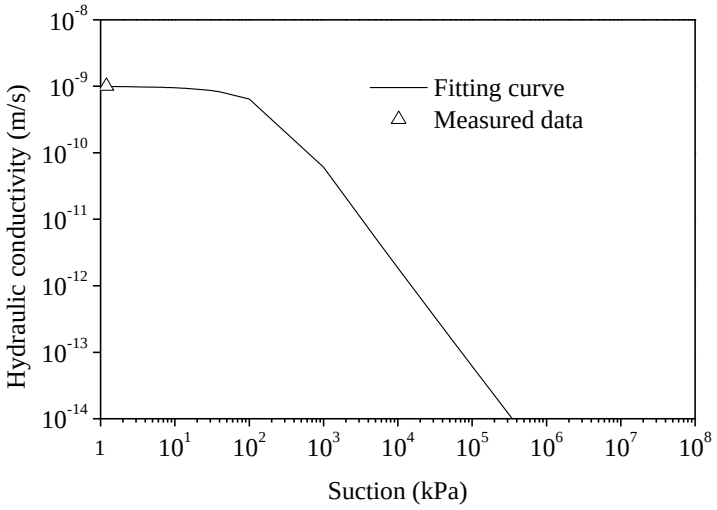


Figure 6. 8. Hydraulic conductivity curve versus suction for the silt treated by 2% CaO

6.2.2 Model dimensions, initial and boundary conditions

Based on the field embankment profile (Figure 6. 4) and the suggested model dimensions of Héricourt embankment in Chapter 5, the numerical model dimensions of Rouen embankment are defined as shown in Figure 6. 9 .

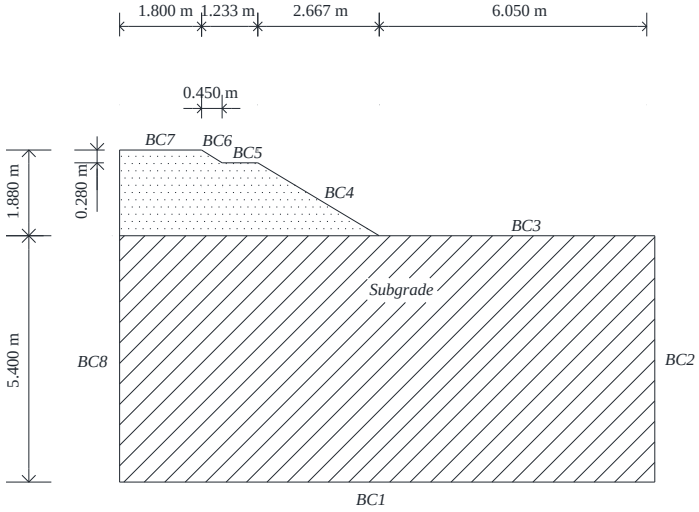


Figure 6. 9. Model dimensions adopted for Rouen embankment

The initial conditions of the coupled hydro-thermal soil model are determined by the measurement data of soil temperature and volumetric water content at the starting time

10/07/2014, 16:00 for 187 days and 27/10/2011, 16:00 for 387 days, respectively.

For bare soil, as rainfall happens, part of water will infiltrate into the soil. The rest of rainfall becomes runoff on soil surface. Based on the measurements of runoff in Héricourt embankment, runoff is assumed as zero for Rouen embankment. Meanwhile, evaporation happens at soil-atmosphere interface because of energy transfer and vapor pressure gradient existing near the soil surface. As far as the heat transfer is concerned, solar radiation is the only exterior heat resource. The net solar radiation is equal to the sum of latent heat, soil heat and sensible heat. As for the Héricourt embankment, the mass and energy balances during soil-atmosphere interaction are used to determine the water and heat boundary conditions (Blight, 1997). These details of initial conditions and boundary conditions are listed in Table 6. 1.

In order to explain the boundary conditions estimated through considering soil-atmosphere interaction, heat and water fluxes on the top surface (BC7) in the studied period of 187 days are presented in Figure 6. 10 and Figure 6. 11, respectively. Other boundaries interacted with atmosphere (BC6, BC5, BC4, and BC3) have the similar conditions. Note that these boundary conditions are calculated iteratively. Furthermore, the same method is applied to estimate the boundary conditions for the studied period of 387 days.

As presented in Figure 6. 10, the soil heat is dominated by the net solar radiation which is the energy from the sun to soil and its value keeps positive during the day and negative during the night. Latent heat represents the energy consumed by evaporation and is in negative values. Sensible heat represents the energy to heat air. When it is in negative value, soil temperature is higher than air temperature. Conversely, air temperature is higher than soil temperature. Relying on the energy balance, soil heat can be estimated effectively by net solar radiation, latent heat and sensible heat. Moreover, the seasonal variations are also reflected by the variations of net solar radiation, soil heat and sensible heat fluxes: the absolute values of net solar radiation and soil heat decrease gradually from summer to winter; the sensible heat varies from negative values in summer to positive values in winter, indicating that soil temperature is higher than air temperature in summer but lower than air temperature in winter.

Table 6. 1. Initial conditions and boundary conditions used for numerical modelling of Rouen embankment

Initial conditions		Measurement data at the starting moment	
Boundary conditions	*Boundary number*	*Thermal boundary conditions*	*Hydraulic boundary conditions*
	BC1	Measured soil temperature	$\varphi = 0$
	BC2, BC8	$G = 0$	$I_{nf} = 0$
	BC7	$G = R_n - L_E - H$ $H = f(T_7)$ $L_E = f(T_7, \varphi_7)$	$I_{nf} = (P - R_{off} - E_a)\rho_l$ $E_a = f(T_7, \varphi_7)$
	BC6	$G = R_n - L_E - H$ $H = f(T_6)$ $L_E = f(T_6, \varphi_6)$	$I_{nf} = (P - R_{off} - E_a)\rho_l$ $E_a = f(T_6, \varphi_6)$
	BC5	$G = R_n - L_E - H$ $H = f(T_5)$ $L_E = f(T_5, \varphi_5)$	$I_{nf} = (P - R_{off} - E_a)\rho_l$ $E_a = f(T_5, \varphi_5)$
	BC4	$G = R_n - L_E - H$ $H = f(T_4)$ $L_E = f(T_4, \varphi_4)$	$I_{nf} = (P - R_{off} - E_a)\rho_l$ $E_a = f(T_4, \varphi_4)$
	BC3	$G = R_n - L_E - H$ $H = f(T_3)$ $L_E = f(T_3, \varphi_3)$	$I_{nf} = (P - R_{off} - E_a)\rho_l$ $E_a = f(T_3, \varphi_3)$
Equation (5.4)			187 days: $a_1 = 0.031$; $a_2 = 0.022$ 387 days: $a_1 = 0.0155$; $a_2 = 0.03$
where T_i and φ_i mean soil temperature (°C) and suction (m) of the surface point chosen at the "BCi" boundary as shown in Figure 6. 9. Other terms are explained in Chapter 3.			

In the case of Héricourt embankment, runoff rate is smaller than 3.3% rainfall, corresponding to 0.5% in volumetric water content. Thereby, considering the similarities between the two embankments, in Rouen embankment, the runoff value is assumed as zero without field measurement. Its values may affect the calculation results, but this effect is believed to be limited in comparison with the rainfalls. As shown in Figure 6. 11, the evaporation values are

mainly in the order of magnitude of 10^{-8} m/s, much smaller compared with that of rainfall and infiltration in 10^{-6} m/s. Thereby, it is obvious that rainfall affects the water flux boundary effectively. The infiltration represents the value of water boundary condition on soil surface. Its positive value means that water flows into the soil. By contrast, evaporation is in negative value, showing water going out from the soil surface.

(a)

(b)

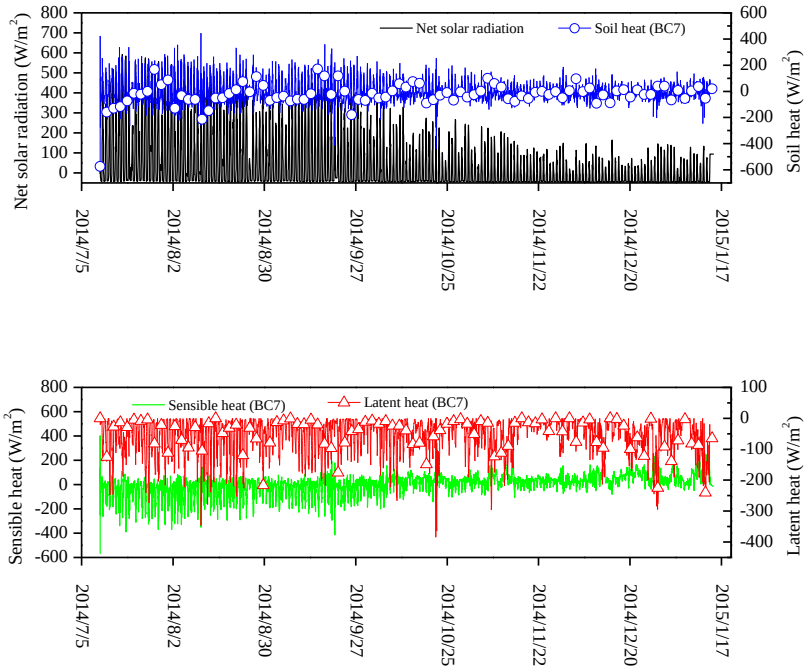


Figure 6. 10. Heat fluxes at the top surface of Rouen embankment (BC7): (a) net solar radiation and soil heat; (b) sensible heat and latent heat

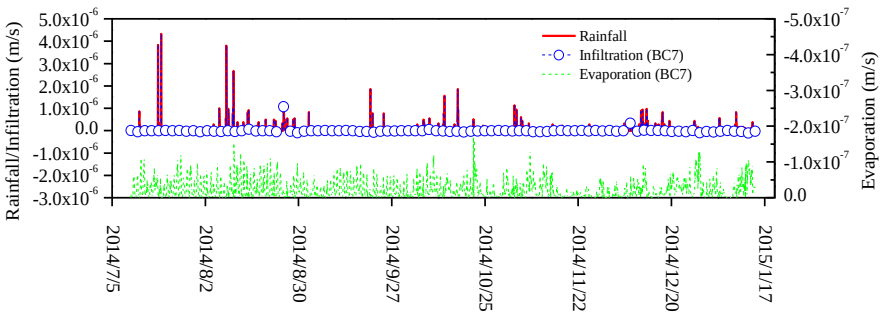


Figure 6. 11. Water fluxes at the top surface of Rouen embankment (BC7): rainfall, infiltration, and evaporation

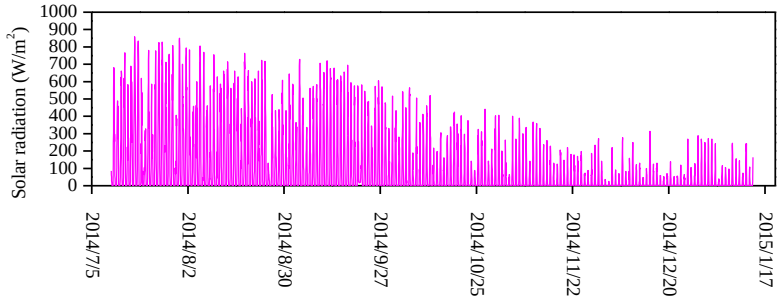
With the soil parameters, initial and boundary conditions as introduced above, the modelling of Rouen embankment with consideration of soil-atmosphere interaction can be performed by finite element method using FreeFem++ code (Hecht 2010).

6.3 Modelling of Rouen embankment for 187 days

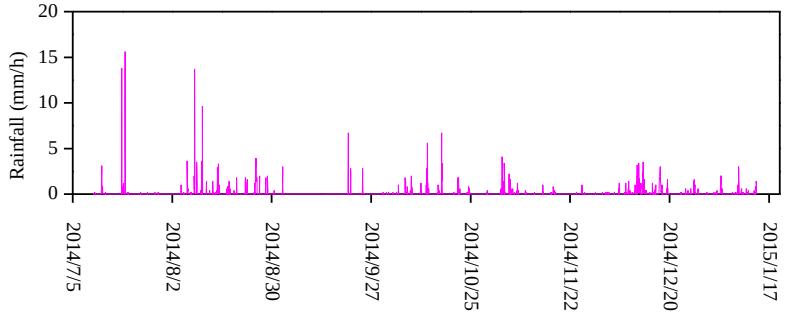
6.3.1 Presentation of meteorological data

At meteorological station "ECTOT LES BAONS", the hourly meteorological data including solar radiation (Figure 6. 12a), rainfall (Figure 6. 12b), wind speed (Figure 6. 12c), relative humidity (Figure 6. 12d), air temperature (Figure 6. 12e) and dew temperature (Figure 6. 12f) during 10/07/2014~13/01/2015 (187 days) are recorded. It is observed that solar radiation, air and dew temperatures present obvious decreasing tendency as season changes from summer to winter. These data are used to calculate the heat and water flux boundary conditions with consideration of the surface soil temperature and suction as discussed in section 6. 2.

(a)



(b)



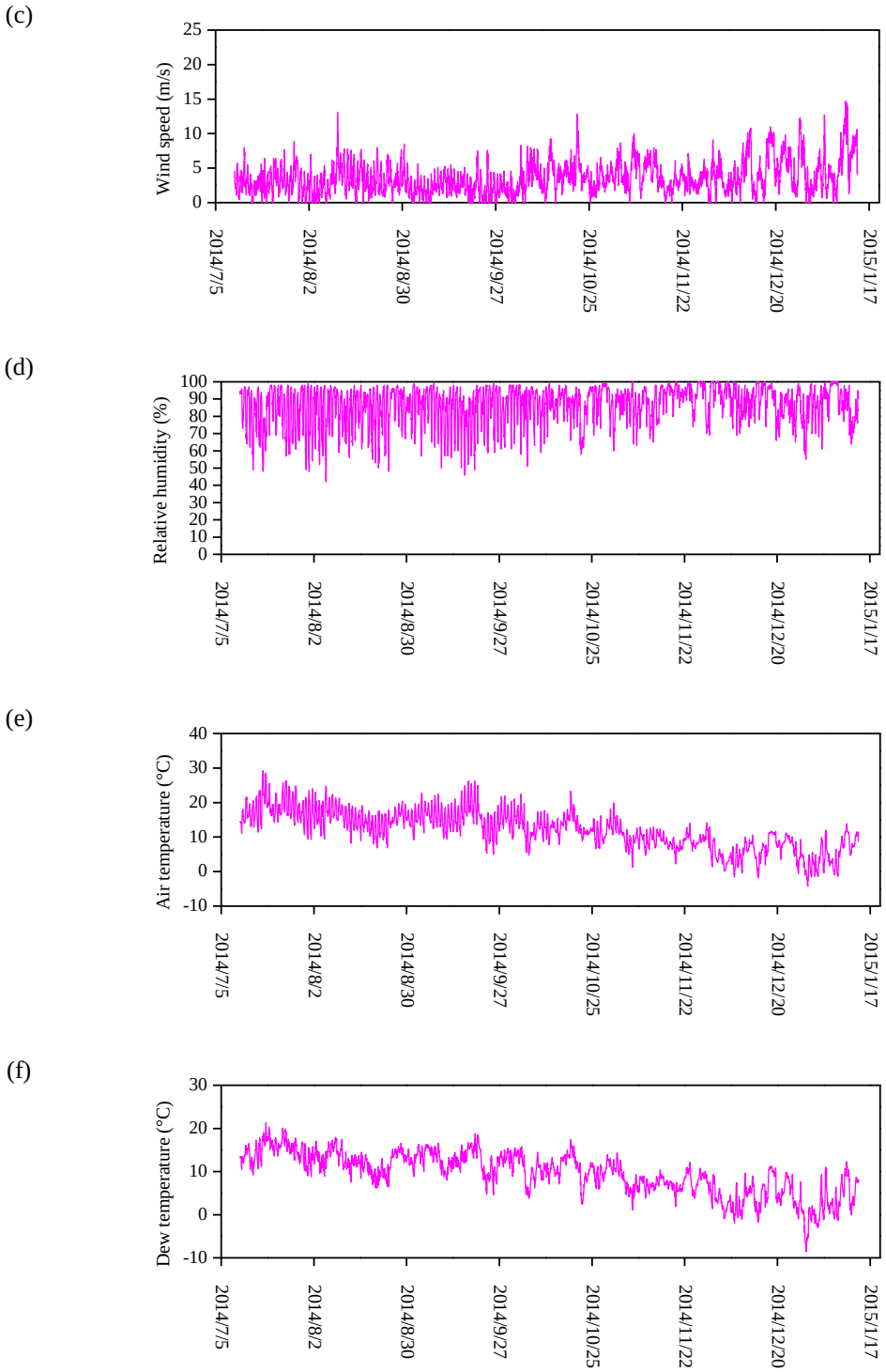


Figure 6. 12. Meteorological data recorded at meteorological station of METEO FRANCE from 10/07/2014 to 13/01/2015: (a) solar radiation; (b) rainfall; (c) wind speed; (d) relative humidity; (e) air temperature; (f) dew temperature

6.3.2 Results and discussions

6.3.2.1 Variations of soil temperature

All PT100 sensors worked well during the studied period form 10/07/2014 to 13/01/2015 (187 days), involving four groups of points: near top surface points (point 1C5 and 2C5), near slope surface points (point 3C4, 3C2 and 4C0), interior points (point 2C4, 2C2 and 2C0), and interior middle points (point 1C4, 1C2 and 1C0). These points are situated at different layers as shown in Figure 6. 4. The comparisons of soil temperature variations between calculation and measurement at these points are made.

Firstly, points 1C5 and 2C5 sited on the interface between the top layer and the second layer are studied. Point 1C5 is in the middle of the field embankment, while point 2C5 is under the juncture of the top surface and the slope surface of the embankment. They hold different vertical distances from the top surface boundary (BC7) and the slope surface one (BC6): 0.38 m for point 1C5 and 0.24 m for point 2C5. In Figure 6. 13, satisfactory agreement between measured and calculated data of soil temperature at these two points is obtained. At points 1C5 and 2C5, soil temperature shows a declining tendency following the seasonal change from summer to winter in 2014. At point 1C5, soil temperature increases to reach the maximum value of 25.6 °C on 19/07/2014, then it goes down continuously to the minimum value of 3.73°C on 31/12/2014, along with several decrease-increase fluctuations. The similar seasonal variations of soil temperature are also observed at point 2C5. Meanwhile, daily variations of soil temperature at these two points can be observed, along with the seasonal variations.

For the near slope surface points 3C4, 3C2 and 4C0, they hold different vertical distances of 0.39 m, 0.78 m, 0.84 m to the slope surface, respectively. Satisfactory consistency is obtained between calculation and measurement for these points (Figure 6. 14). They keep the similar decreasing tendency over time, showing the similar seasonal changes as the two points in the first group. Besides, daily variations of soil temperature at these points can also be identified. As point 3C4 is located closer to the slope surface than the others, it is more sensitive to the

climate conditions, showing significant variations. However, deeper points 3C2 and 4C0 vary more smoothly with less daily variations.

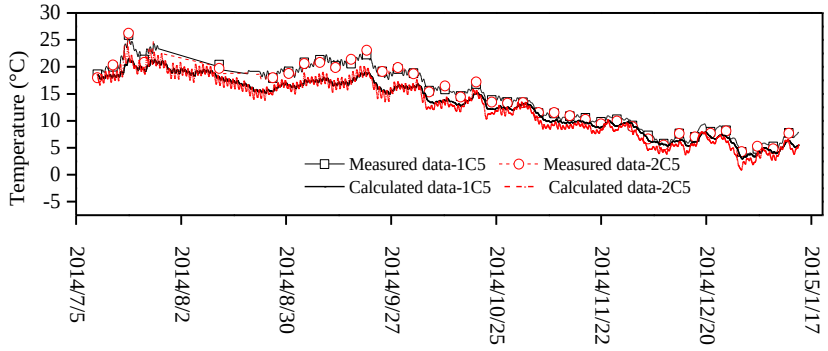


Figure 6. 13. Soil temperature comparisons between the calculation and measurement for points 1C5 and 2C5 during the studied period

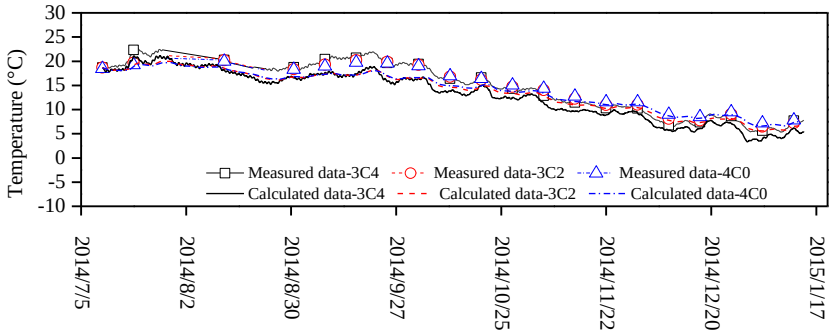


Figure 6. 14. Soil temperature comparisons between the calculation and measurement for points 3C4, 3C2 and 4C0 during the studied period

The points of the third group, 2C4, 2C2 and 2C0, are at depths of 0.59 m, 1.19 m, and 1.79 m below the top boundary, respectively. All the calculated data of the interior points fit the measured data very well during the studied period as shown in Figure 6. 15. They show the similar temperature variation tendency as season changes. As the closest one to the top boundary among three points, point 2C4 shows more significant temperature variation than other points. Less daily variations appear at deeper points. Compared with point 2C4, points 2C2 and 2C0 have more smooth variations.

Regarding the interior central points, 1C4, 1C2 and 1C0, they are situated in the middle vertical axe of the field embankment at different depths: 0.68 m, 1.28 m and 1.88 m respectively. The calculated results also show a good agreement with the measured data (Figure 6. 16). Due to its higher position, point 1C4 shows a larger seasonal variation than points 1C2 and 1C0. Moreover, minor daily variations can be also identified at point 1C4. But it is difficult to observe the daily variations at points 1C2 and 1C0 because of their deeper positions.

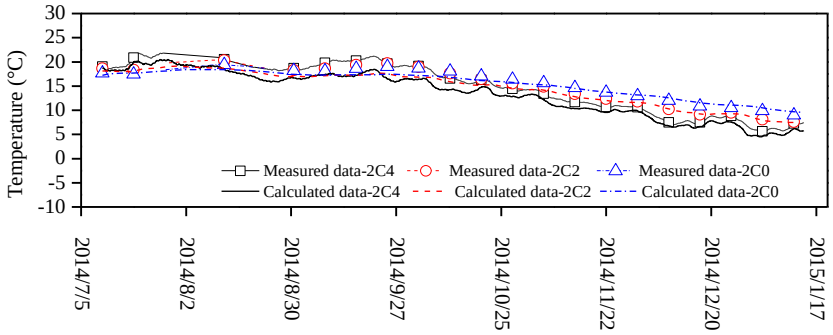


Figure 6. 15. Soil temperature comparisons between the simulation results and measurement data of points 2C4, 2C2 and 2C0 during the studied period

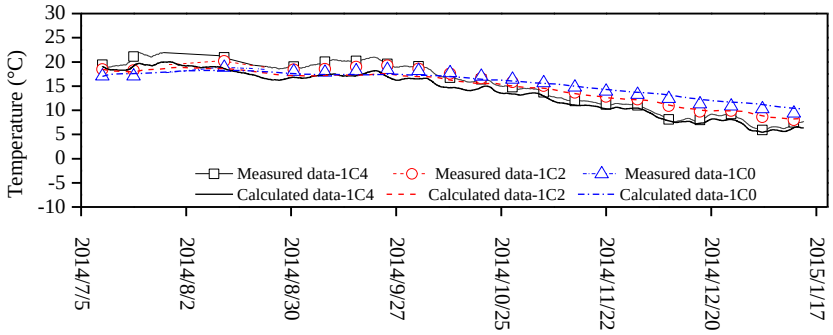


Figure 6. 16. Soil temperature comparisons between the simulation results and measurement data of points 1C4, 1C2 and 1C0 during the studied period

6.3.2.2 Variations of soil volumetric water content

Soil volumetric water content was recorded every six hours from 10/07/2014 to 12/12/2014

with a short period of data missing during the period from 30/08/2014 to 30/09/2014. The studied points with measurements are divided in three groups: near top surface points (points 1C5 and 2C5), near slope surface points (points 3C4, 3C2 and 4C0), interior points (points 3C0, 2C0 and 1C0). The comparisons of soil volumetric water content between simulation and measurement for these three groups are shown in Figure 6. 17, Figure 6. 18, Figure 6. 19, respectively.

In Figure 6. 17, the calculated volumetric water content variations for points 1C5 and 2C5 show large variations under the effects of infiltration/evaporation. A similar tendency between the calculated and measured data can be observed, despite some differences from time to time. For instance, the calculated data at point 1C5 is consistent with the measured data from July to October in 2014. Specifically, the calculated value decreases to 0.30 as the measured value on 01/10/2014 even though the measured data is missing in the period from 30/08/2014 to 30/09/2014. Afterwards, the calculated values are smaller than the measured values. Nevertheless, they present the similar tendency during the whole studied period. Furthermore, compared with point 1C5, point 2C5 is more sensitive to infiltration/evaporation due to its position nearer to the surface boundaries. A larger value variation amplitude of soil volumetric water content is also observed at point 2C5.

Regarding the near slope surface points 3C4, 3C2 and 4C0, their calculated data are highly consistent with the measured data except some differences of point 3C4 in the last month. As for the points in the first group (points 1C5 and 2C5), a decreasing tendency is found by simulation for the period form 30/08/2014 to 30/09/2014 when the measurements are missing. In particular, due to the closet distance to the slope boundary among the three points, point 3C4 is more sensitive to infiltration/evaporation, showing more significant variations compared with the two others.

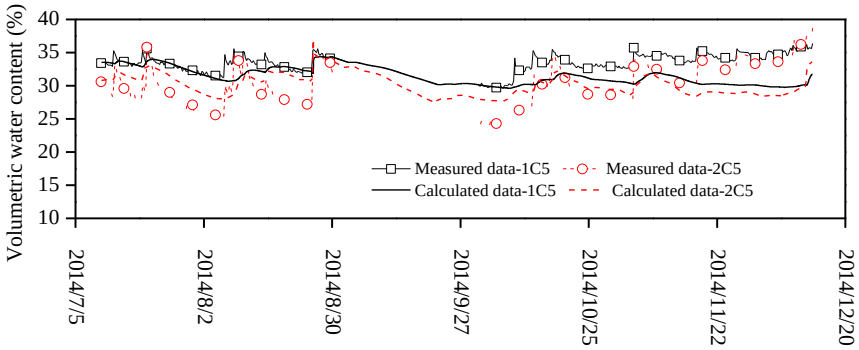


Figure 6. 17. Soil volumetric water content comparisons between the simulation results and measurement data of points 1C5 and 2C5 during the studied period

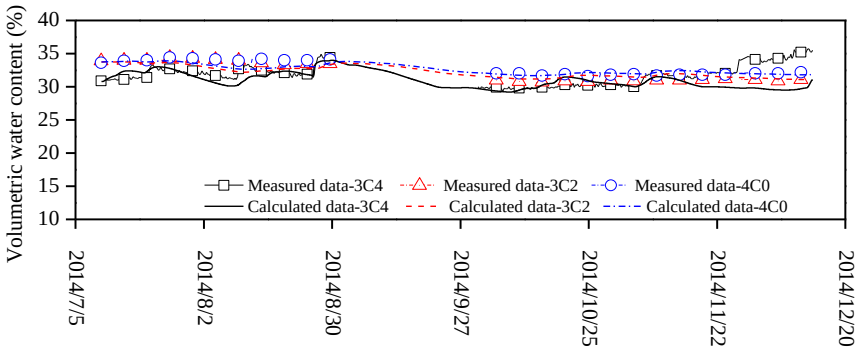


Figure 6. 18. Soil volumetric water content comparisons between the simulation results and measurement data of points 3C4, 3C2 and 4C0 during the studied period

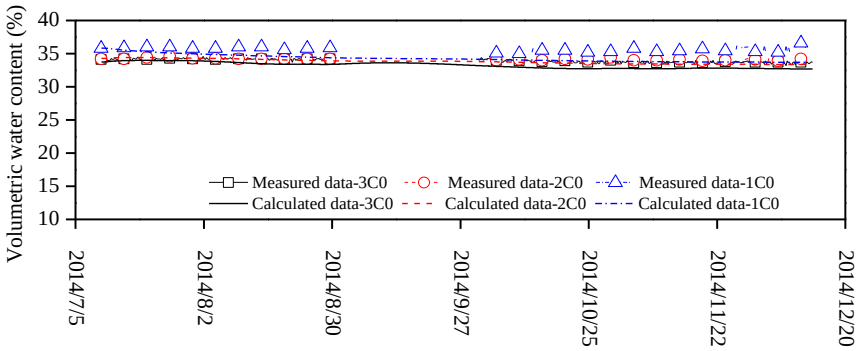


Figure 6. 19. Soil volumetric water content comparisons between the simulation results and measurement data of points 3C0, 2C0 and 1C0 during the studied period

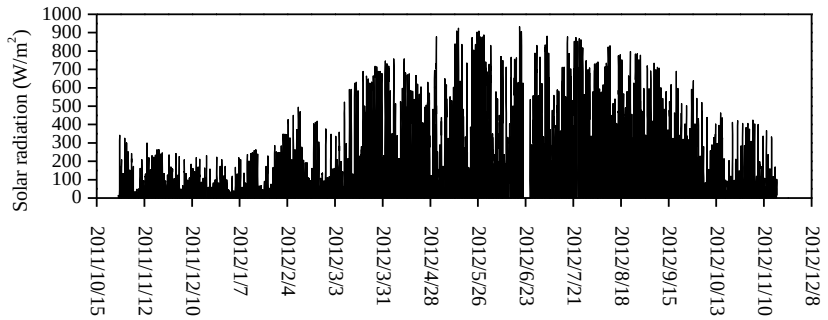
For the interior points 3C0, 2C0 and 1C0, a good agreement can be observed between the calculated and measured data (Figure 6. 19). The calculated results keep constant values over time as the measured data. The measured soil volumetric water content at these points are stable as their initial values during the whole studied period, suggesting that these points are out of the influence zone of the hydraulic boundary conditions. Furthermore, no seasonal effects are observed for the soil volumetric water content variations. It suggests that the effects of climate conditions on soil temperature and volumetric water content need to be studied individually. As in the case of points 2C0 and 1C0, soil temperature may vary significantly but the volumetric water content can keep constant.

6.4 Modelling of Rouen embankment for 387 days

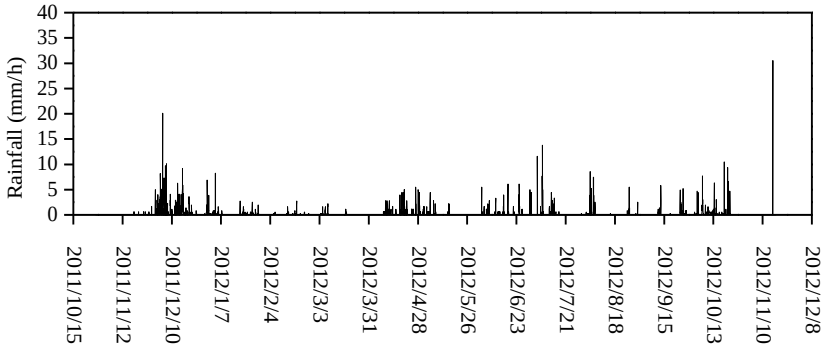
6.4.1 Presentation of meteorological data

In order to have a better understanding of soil hydro-thermal behavior under climate effect, the numerical investigation of Rouen embankment during the period from 27/10/2011 to 17/11/2012 (387 days) is also conducted. The information of hourly solar radiation provided by "ECTOT-LES-BAONS" station of METEO FRANCE (30 km away from the embankment) is used. Wind speed recorded at the same station is adopted. Other hourly meteorological data come from a nearby meteorological station (20 m away from the embankment) with some short periods of data missing. The records of wind speed at this station are not reliable due to some technique problems. The solar radiation, rainfall, wind speed, air temperature, air relative humidity and dew temperature information are presented respectively in Figure 6. 20 (a~f). Seasonal variations can be clearly observed in relative humidity, air temperature, dew temperature and solar radiation.

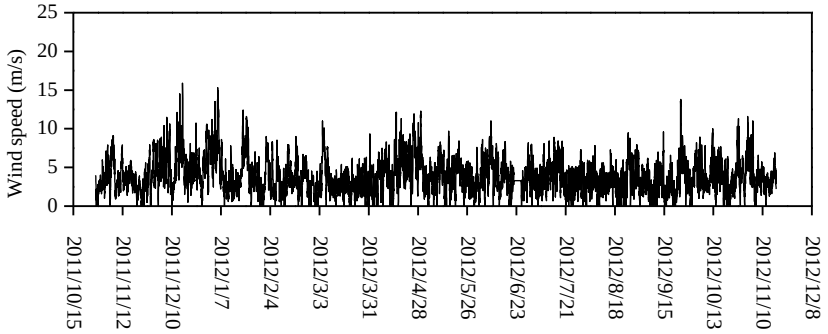
(a)


Solar radiation (W/m²)
1000
900
800
700
600
500
400
300
200
100
0
2011/10/15
2011/11/12
2011/12/10
2012/1/7
2012/2/4
2012/3/3
2012/3/31
2012/4/28
2012/5/26
2012/6/23
2012/7/21
2012/8/18
2012/9/15
2012/10/13
2012/11/10
2012/12/8

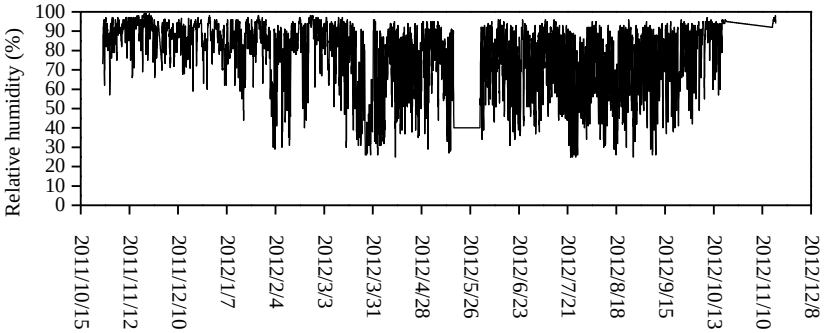
(b)


Rainfall (mm/h)
40
35
30
25
20
15
10
5
0
2011/10/15
2011/11/12
2011/12/10
2012/1/7
2012/2/4
2012/3/3
2012/3/31
2012/4/28
2012/5/26
2012/6/23
2012/7/21
2012/8/18
2012/9/15
2012/10/13
2012/11/10
2012/12/8

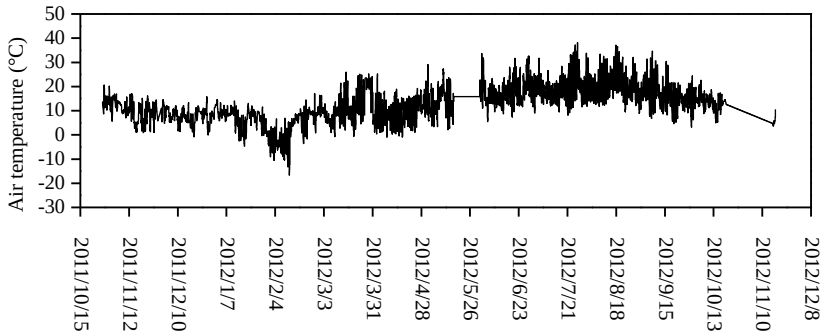
(c)


Wind speed (m/s)
25
20
15
10
5
0
2011/10/15
2011/11/12
2011/12/10
2012/1/7
2012/2/4
2012/3/3
2012/3/31
2012/4/28
2012/5/26
2012/6/23
2012/7/21
2012/8/18
2012/9/15
2012/10/13
2012/11/10
2012/12/8

(d)


Relative humidity (%)
100
90
80
70
60
50
40
30
20
10
0
2011/10/15
2011/11/12
2011/12/10
2012/1/7
2012/2/4
2012/3/3
2012/3/31
2012/4/28
2012/5/26
2012/6/23
2012/7/21
2012/8/18
2012/9/15
2012/10/13
2012/11/10
2012/12/8

(e)



(f)

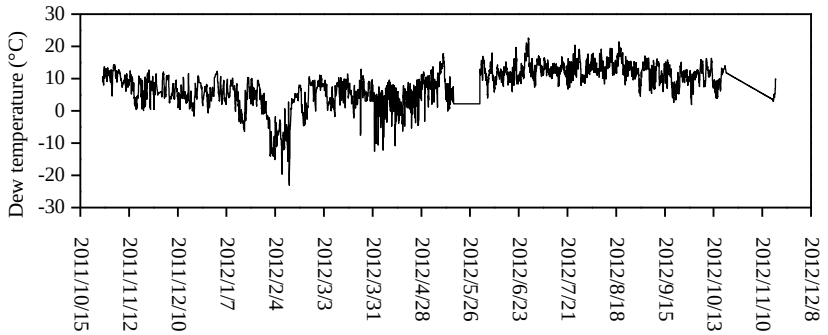


Figure 6. 20. Field meteorological data from 27/10/2011 to 17/11/2012: (a) solar radiation; (b) rainfall; (c) wind speed; (d) relative humidity; (e) air temperature; (f) dew temperature

6.4.2 Results and discussions

The variations of soil temperature and volumetric water content are calculated for 387 days. As in the case of 187 days, the points selected for analyzing the soil temperature and volumetric water content variations are defined in four and three groups respectively. Based on the energy and mass balance equations, the soil surface heat flux and water flux boundary conditions are estimated. Thereby, using the proposed fully coupled hydro-thermal soil model with the treated silt soil parameters, the variations of soil volumetric water content and temperature can be calculated.

6.4.2.1 Variations of soil temperature

In the first group, a good agreement is obtained between the calculated data and the measured data at points 1C5 and 2C5 (Figure 6. 21). At point 1C5, the soil temperature decreases gradually following the seasonal change from summer to winter, reaching the minimum temperature in February of 2012. Afterwards, it begins to increase from winter to summer, reaching the highest value in August of 2012. The similar seasonal variations of soil temperature are observed at point 2C5. Meantime, there were obvious and continuous daily fluctuations of soil temperature at these two points along with the seasonal variations.

High consistency is obtained between the measured and calculated data for the three points in the second group (Figure 6. 22). They keep the similar variation tendency over time, showing seasonal changes as the two points in the first group. The values reach the minimum (1.67 °C) during the winter and the maximum (23.16 °C) during the summer. Besides, daily variations of soil temperature at these points can be observed. As point 3C4 is located closer to the slope boundary than the others, its temperature variation is more sensitive to the climate conditions, varying more significantly.

As shown in Figure 6. 23, the calculated data fit the measured data well for the points of the third group, 2C4, 2C2 and 2C0. They show the similar temperature variation tendency, varying properly as season changes. As the closest one to the top boundary among three points, point 2C4 shows the minimum value of 1.93 °C in winter and the maximum value of 22.14 °C in summer. Less daily variations appear at deeper points. Compared with point 2C4, the values at points 2C2 and 2C0 vary more smoothly all over the year.

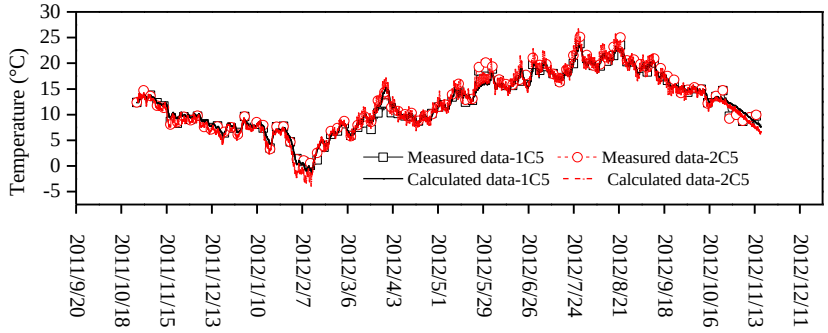


Figure 6. 21. Soil temperature comparisons between the simulation results and measurement data of points 1C5 and 2C5 during the studied period

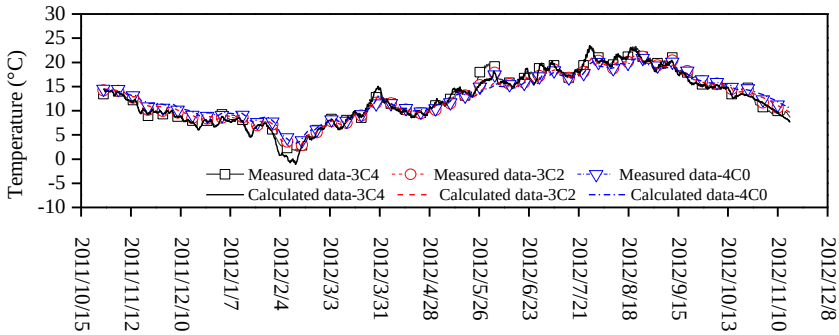


Figure 6. 22. Soil temperature comparisons between the simulation results and measurement data of points 3C4, 3C2 and 4C0 during the studied period

Regarding the interior central points, 1C4, 1C2 and 1C0, they are situated in the middle vertical axe of field embankment at different depths. The calculated results also show a good agreement with the measured data (Figure 6. 24). Point 1C4 shows a larger seasonal variation than points 1C2 and 1C0 because of its higher position. Moreover, minor daily variations can be also identified at point 1C4. It is not the case for points 1C2 and 1C0 due to their deeper positions.

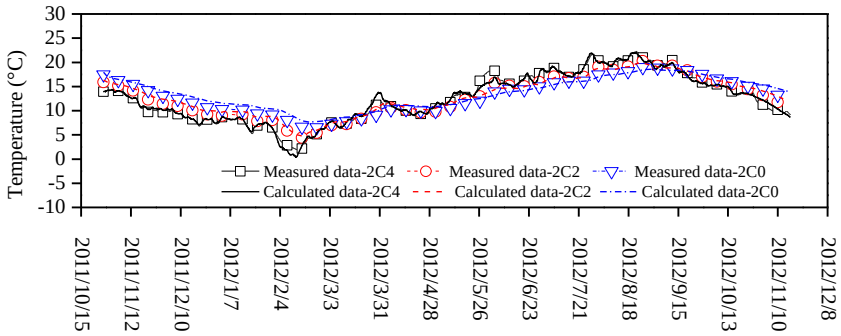


Figure 6. 23. Soil temperature comparisons between the simulation results and measurement data of points 2C4, 2C2 and 2C0 during the studied period

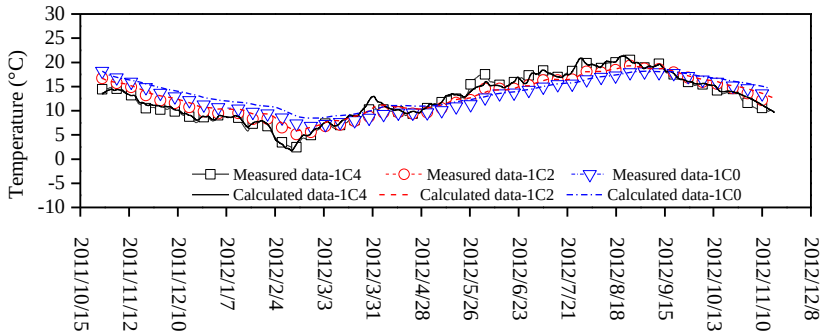


Figure 6. 24. Soil temperature comparisons between the simulation results and measurement data of points 1C4, 1C2 and 1C0 during the studied period

6.4.2.2 Variation of soil volumetric water content

In Figure 6. 25, the calculated volumetric water contents of both points 1C5 and 2C5 show large variations under the effects of infiltration/evaporation. On the whole, the calculated and measured data have a similar tendency, despite some differences from time to time. For instance, at point 2C5, the calculated soil volumetric water contents are relatively constant in the beginning, then increase up to the value corresponding to the saturated state (0.37) after a series of intensive rainfall events in December of 2011. Afterwards, the values decrease down to the minimum but with rebounds occurring in case of rainfalls. The saturated values were reached

again with rainfall events at the end of April of 2012, and the volumetric water content remained almost constant at the saturated value after October of 2012. Meanwhile, the measured soil volumetric water contents show the same trend of variations as the calculated ones, but significantly differ in values at some times. Furthermore, compared with point 1C5, point 2C5 is closer to the embankment surface and is also influenced by both the top and slope boundary conditions. Thereby, the soil volumetric water content at point 2C5 has larger value variation amplitude, suggesting a higher sensitivity to infiltration/evaporation.

Regarding the near slope surface points, 3C4, 3C2 and 4C0, similar to the case of points in the first group (points 1C5 and 2C5), the similar tendency can be observed for the calculated data and the measured data despite some minor differences (Figure 6. 26). For the calculation results, they keep stable initially, then increase to approach the saturated value in December of 2011, finally go down to the minimum value in June of 2012. Going through several variations in spring/summer, they finally increase again to reach the saturated value in October of 2012. In particular, due to the closest distance to the slope boundary among the three points, point 3C4 shows more significant changes than the two others.

The interior points 3C0, 2C0 and 1C0 in the third group show a good agreement between the calculated and measured data (Figure 6. 27). Slight decrease-increase variations can be identified in the calculated data. Meanwhile, the measured data of these points are stable around 34% during the whole period, suggesting that these points are out of the influence zone of the hydraulic boundary conditions. Moreover, it can be seen that unlike the temperature variations, the variations of soil volumetric water do not reflect the seasonal changes at these points. This suggests that the effects of climate conditions on soil temperature and volumetric water content need to be considered respectively. At the same point, the temperature may vary significantly but the soil volumetric water content can keep stable. This is the case for points 2C0 and 1C0.

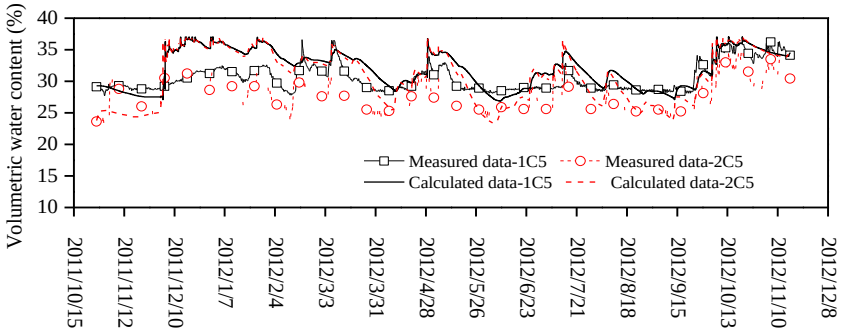


Figure 6. 25. Soil volumetric water content comparisons between the simulation results and measurement data of points 1C5 and 2C5 during the studied period

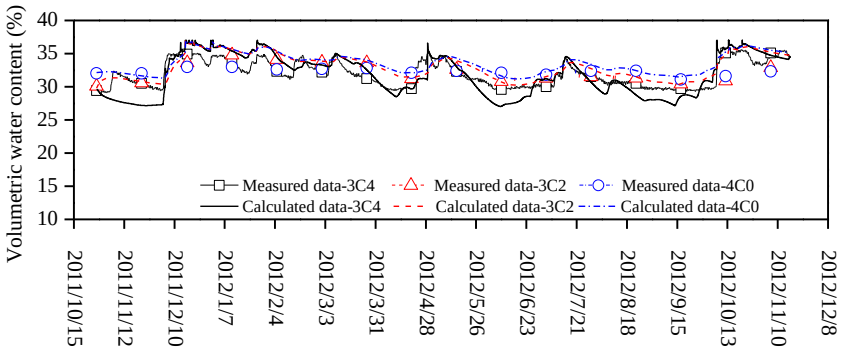


Figure 6. 26. Soil volumetric water content comparisons between the simulation results and measurements data of points 3C4, 3C2 and 4C0 during the studied period

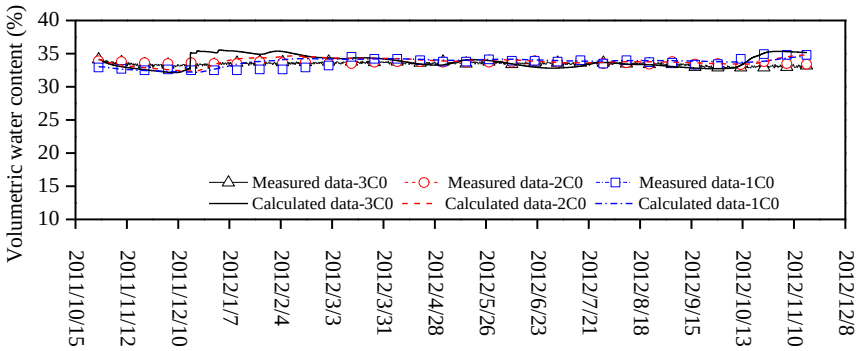


Figure 6. 27. Soil volumetric water content comparisons between the simulation and measurement for points 3C0, 2C0 and 1C0 during the studied period

6.5 Discussions

6.5.1 Soil temperature variations

A good agreement between the calculated and measured data of soil temperature has been obtained for two different periods: from 10/07/2014 to 13/01/2015 (187 days) and from 27/10/2011 to 17/11/2012 (387 days). In fact, the estimation of soil temperature is relying on the heat flux boundary condition (soil heat). In the energy balance, soil heat is conditioned by net solar radiation, sensible heat and latent heat. As the only heat source, net solar radiation is the most influencing parameter in heat transfer on soil-atmosphere interface. Normally, it can be estimated based on the recorded solar radiation in metrological data. The numerical results obtained in two studied cases (187 days+387 days) prove that the solar radiation recorded by the weather station of METEO FRANCE (30 km away) is appropriate for satisfactorily estimating the soil temperature variations in Rouen embankment. Therefore, it is considered as one feasible solution when field measurement of solar radiation is not available. Specifically, during the period from 27/10/2011 to 17/11/2012, some differences appeared between the calculated and measured data in February of 2012 when soil temperatures are negative. These differences can be attributed to neglecting the water liquid/solid phase change in this study. On the other hand, these calculated values are negative because of the input negative air and dew temperatures during the same period.

6.5.2 Soil volumetric water content variations

The differences between the calculated and measured data of soil volumetric water content deserve further investigations. In fact, soil volumetric water content variation is controlled directly by the hydraulic boundary conditions (infiltration/evaporation). In the mass balance, the infiltration term is governed by rainfall, runoff and actual evaporation.

In the period from 10/07/2014 to 13/01/2015, rainfall is recorded by “ECTOT LES BAONS” station (30 km away), evaporation is estimated by theoretical method and runoff is assumed as

zero. As shown in Figure 6. 11, it is obvious that rainfall is able to affect the water flux boundary effectively. Thereby, the comparisons between the calculated and measured results at points 1C5, 3C4 and 3C0 are presented along with the rainfall information in Figure 6. 28, Figure 6. 29 and Figure 6. 30, respectively. In Figure 6. 28, several significant increases of soil volumetric water content can be observed in the measured data at 08/10/2014, 17/11/2014 and 25/11/2014, which are inferred to be caused by heavy rainfall events. But no such pronounced increases can be observed in the calculation data, suggesting that the input rainfall data do not represent the real values at the studied embankment due to the fact that the weather station is 30 km far away. Similar results can be identified at point 3C4 (Figure 6. 29), indicating the importance of using precise rainfall information. The situation of point 3C0 is also presented with rainfall information in Figure 6. 30. The constant value of soil volumetric water content indicates again that this point is out of the influence region of hydraulic boundary conditions.

In the period from 27/10/2011 to 17/11/2012, as the rainfall data used was recorded by a weather station 20 m away from the embankment, some minor differences may exist compared with the real rainfall data at the embankment. For the top and slope boundaries (BC4~BC7 in Figure 6. 9), the term of evaporation was calculated based on the wind speed from "ECTOT LES BAONS" station (30 km away), and runoff was neglected. The values of evaporation and runoff may also affect the calculation results, but their effects are believed to be limited in comparison with the rainfalls.

In order to illustrate the effect of rainfalls at 20 m away from the embankment, points 1C5, 3C4, 3C0 are selected for analyzing the variations of volumetric water content with rainfalls. In Figure 6. 31, the recorded rainfall data are presented along with the soil volumetric water content variation at point 1C5. For the intensive rainfall events from 03/12/2011 to 20/12/2011, the calculated soil volumetric water contents increase more significantly than the measured ones. Afterwards, only slight rainfalls occurred from 20/12/2011 to 16/02/2012, the calculated data shows a consistent variation mode as the measured data but with higher values over time, illustrating the effect of the last rainfall events. In particular, two significant increases appeared

in the calculated data on 19/02/2012 and 08/03/2012, which are inferred to be caused by heavy rainfall events. But no such pronounced increases are identified by the measurements. Moreover, from 12/04/2012 to 25/09/2012, several increases are identified by calculation but the measured data have a less increases or remain relatively stable. After 25/09/2012, there is a good agreement between measurement and calculation, the values approaching the saturated one. Figure 6. 32 compares the calculated volumetric water contents with the measured ones at point 3C4, along with the rainfall data. Before 02/12/2011, the values of volumetric water content keep stable in the calculation, while the measured data shows a peak on 06/11/2011. Afterwards, it can be observed that the variations of volumetric water contents between calculated data and measured data are nearly consistent with minor differences at several moments as presented in point 1C5. The analysis of the situation of point 3C4 indicates that the input rainfall from 20 m away of the embankment is able to lead the overall satisfactory results, even though some minor differences exist between measurements and calculations.

In Figure 6. 28 and Figure 6. 29, the measured soil volumetric water content at point 3C4 varies more smoothly than that at point 1C5, meaning that point 1C5 is influenced by climate more effectively. Nevertheless, pronounced increases can be identified in the measurements at point 3C4 (from 03/12/2011 to 20/12/2011, etc.), but not at point 1C5 (Figure 6. 31and Figure 6. 32), indicating some problems of the measurements at point 1C5 during the period from 27/10/2011 to 17/11/2012.

The situation of point 3C0 is presented in Figure 6. 33. The calculation evidences a slight variation over time for the volumetric water content, but the measurement rather shows stable values. Even though the input rainfall data may be a little different from the real one at the investigated site, the differences of soil volumetric water content are smaller than 0.02. The limited variations of volumetric water content are attributed to the deeper position of point 3C0. In other words, this point is out of the influence zone of infiltration/evaporation hydraulic boundary conditions.

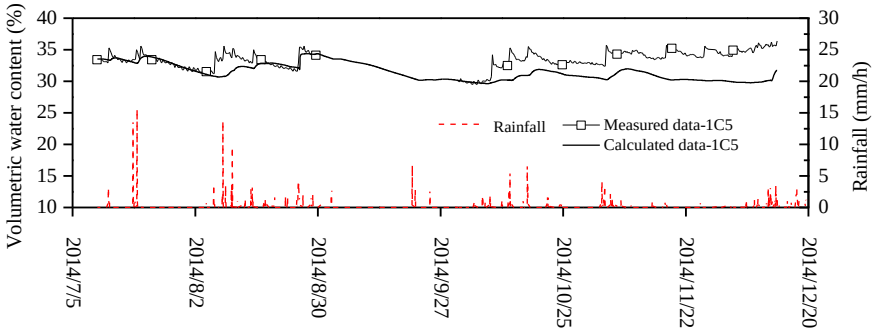


Figure 6. 28. Comparison of soil volumetric water content variations between the simulated and measured data of point 1C5 along with rainfall information (187 days)

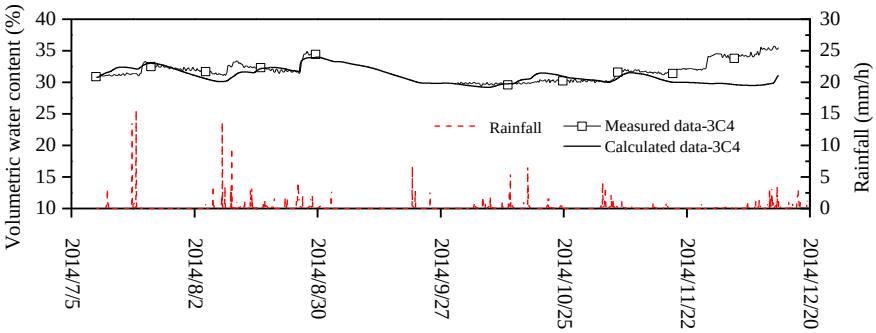


Figure 6. 29. Comparison of soil volumetric water content variations between the simulated and measured data of point 3C4 along with rainfall information (187 days)

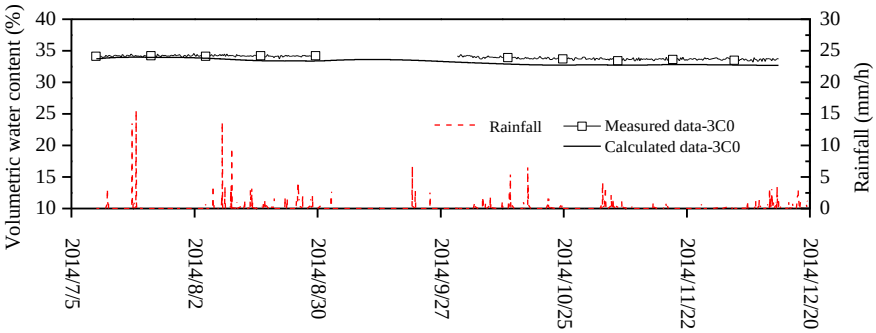


Figure 6. 30. Comparison of soil volumetric water content variations between the simulated and measured data of point 3C0 along with rainfall information (187 days)

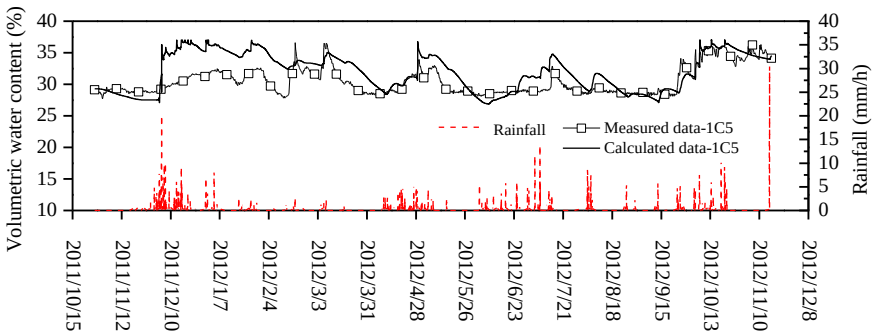


Figure 6. 31. Comparison of soil volumetric water content variations between the simulated and measured data of point 1C5 along with rainfall information (387 days)

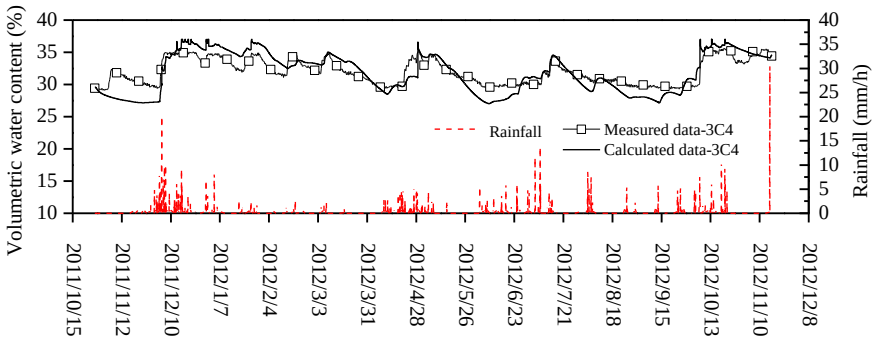


Figure 6. 32. Comparison of soil volumetric water content variations between the simulated and measured data of point 3C4 along with rainfall information (387 days)

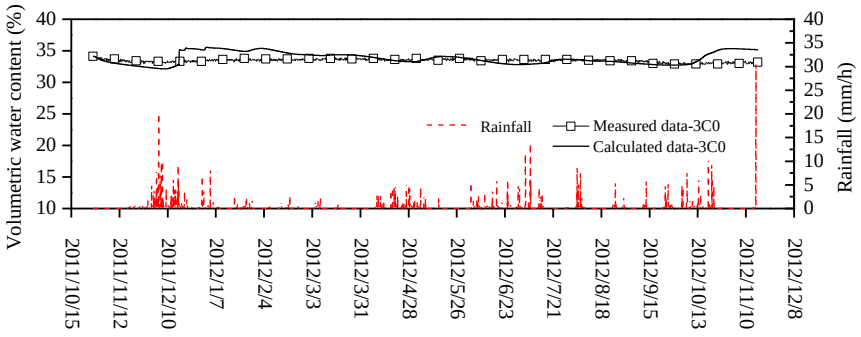


Figure 6. 33. Comparison of soil volumetric water content variations between the simulated and measured data of point 3C0 along with rainfall information (387 days)

As indicated above, the effect of evaporation on the soil volumetric water content is not as significant as rainfall. However, when wind speed data recorded by "ECTOT LES BAONS" station (30 km away) are used, the empirical parameters a_1 and a_2 in the formula of potential evaporation (equation 5.4) should be determined specifically. To illustrate this point, Point 3C4 is chosen for evaluating the fitting values of the two parameters a_1 and a_2. From equation (5.4) that describes the relationship between potential evaporation and wind speed, it can be observed that parameter a_1 can significantly affect the evaporation when the wind speed is high, while parameter a_2 affects the evaporation constantly whatever the wind speed. Thereby, different values of a_1 and a_2 will lead to different soil volumetric water contents. To further evaluate the effects of these two parameters, five different cases with different values of a_1 and a_2 listed in Table 6. 2 are considered. The calculated volumetric water content variations are presented in Figure 6. 34 and Figure 6. 35.

Table 6. 2. Different cases with different values of a_1 and a_2

Studied cases	*Value of a_1*	*Value of a_2*
Case 1 (adopted for 387 days)	0.0155	0.03
Case 2	0.03	0.03
Case 3	0.00775	0.03
Case 4	0.0155	0.06
Case 5	0.0155	0.015

Figure 6. 34 compares the measured data and the calculated results of soil volumetric water content at point 3C4 in Case 1, Case 2 and Case 3, along with the information of wind speed. In the three cases, the values of a_2 are kept the same, equals 0.03, while the values of a_1 are taken equal to 0.0155, 0.03 and 0.00775, respectively. As evaporation is higher with a larger value of a_1, soil volumetric water content will be lower. As a result, the overall soil volumetric water content in Case 1 and Case 3 are higher than that in Case 2 (Figure 6. 34). Moreover, larger differences between the three cases can be identified during the period with higher wind speed, illustrating the significant influence of a_1.

On the other hand, the effect of a_2 is depicted in Figure 6. 35. In Case 1, Case 4 and Case 5, the values of a_1 are the same, equals 0.0155, while the values of a_2 are taken equal to 0.03, 0.06 and 0.0015, respectively. It is observed that the overall differences of soil volumetric water content in these three cases are less than those between the three cases with different values of a_1 (Figure 6. 34). In particular, soil volumetric water contents in Case 1, Case 4 and Case 5 are nearly consistent in the period from 16/12/2011 to 21/01/2012. This is attributed to the high wind speeds existing in this period, suggesting the pronounced effect of a_1 in case of high wind speed. The overall results in five cases show that the effect of a_1 is more significant than the effect of a_2 on soil volumetric water content variations, especially in the period with high wind speed.

The analysis above indicates that the rainfall data recorded at "ECTOT LES BAONS" station (30 km away) with proper assumptions of evaporation and runoff can be used to define the water flux boundary conditions, allowing proper estimation of soil volumetric water content variations. Furthermore, the rainfall data provided by a weather station 20 m away from the embankment allow a better estimation of soil volumetric water content variations, indicating the importance of using precise rainfall information in this kind of analysis. On the other hand, even though the effect of evaporation on soil volumetric water content is not as significant as rainfall, it is essential to well determine the fitting parameters a_1 and a_2 in equation (5.4) because evaporation is strongly dependent on wind speed. In other words, the variation of soil volumetric water content can be well estimated when precise measurements of rainfall and proper evaluations of evaporation are conducted.

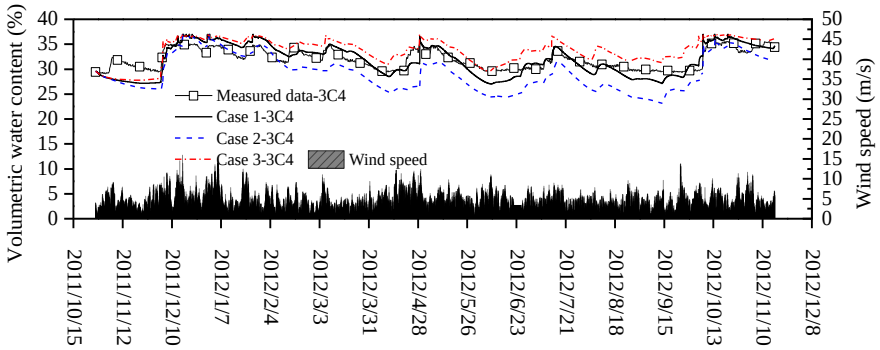


Figure 6. 34. Calculated soil volumetric water content variations in Case 1, Case 2, Case 3 and measured data of point 3C4 along with wind speed information

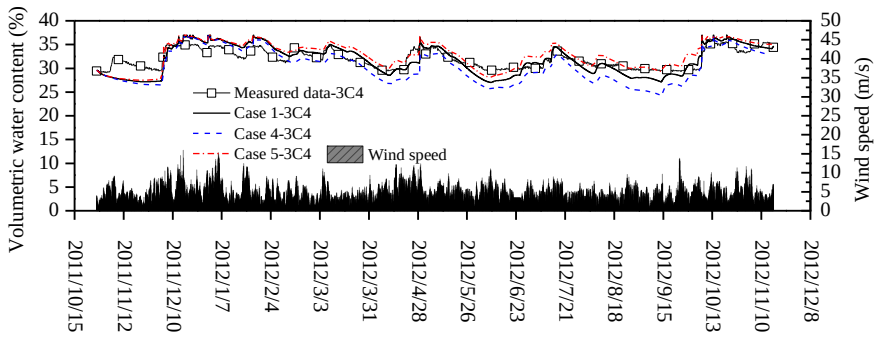


Figure 6. 35. Calculated soil volumetric water content variations in Case 1, Case 4, Case 5 and measured data of point 3C4 along with wind speed information

6.6 Conclusions

In this chapter, an instrumented embankment with treated silt in Rouen, France, is analyzed. Different devices were mobilised in the embankment, providing rich data that allows interaction between the embankment and atmosphere to be investigated. The devices employed mainly include a nearby weather station (20 m away) and the sensors for soil temperature and soil volumetric water content measurements at different positions. Some meteorological information provided by ECTOT-LES-BAONS station of METEO FRANCE (30 km away) is also used to complete the data in the investigation. Based on the meteorological data and soil

parameters, the numerical modelling of Rouen embankment is conducted for two different periods: from 10/07/2014 to 13/01/2015 (187 days) and from 27/10/2011 to 17/11/2012 (387 days).

Comparisons between simulations and measurements of soil temperature and volumetric water content show that the proposed approach that combines the fully coupled hydro-thermal model and a soil-atmosphere interaction model is suitable for estimating soil hydro-thermal behaviour in two-dimensional embankments. The good agreement between calculations and measurements also proves that the thermal and hydraulic boundary conditions defined as well as the adopted soil parameters are appropriate. Seasonal variations are observed in the variations of soil temperature but not for the variations of volumetric water content. At the same point, the temperature may vary significantly but the soil volumetric water content can keep stable, illustrating the necessity of separate consideration of the effects of climate conditions on soil temperature and volumetric water content.

This approach can be also applied to predict soil temperature and volumetric water content variations in long term when the corresponding meteorological data is available. Based on the numerical investigation of soil temperature and volumetric water content of Rouen embankment and discussions in this study, several suggestions can be proposed for the collection of input data:

1) As in the estimation of the soil temperature variations, net solar radiation is the most influencing parameter in heat transfer on soil-atmosphere interface and relying on solar radiation, it is feasible to adopt the measurements of solar radiation from other meteorological stations in the same region when field measurements are not available;
2) As the significant input factor, rainfall is recommended to be recorded at the same site;
3) This study also shows that for the wind speed, when field data are not available, data from a further weather station can be used if the parameters a_1 and a_2 in the formula of potential evaporation are well calibrated. The differences of wind speed between the studied site and the site of wind speed measurement will not significantly affect the calculation results, as

the solar radiation data.

General conclusions

This study is devoted to the numerical investigation of interaction between soil and atmosphere. Firstly, a fully coupled hydro-thermal model is developed, allowing the numerical estimation of soil temperature and volumetric water content variations. Then, a soil-atmosphere interaction model is introduced and all the related factors are studied respectively. By combining the fully coupled hydro-thermal model and the soil-atmosphere interaction model, a numerical approach is proposed allowing the soil hydro-thermal behavior under climate effect to be investigated.

This approach is firstly validated by the column drying tests conducted by Wilson (1990). Afterwards, four evaporation tests carried out by Song (2014) on Fontainebleau sand in environmental chamber equipped with various sensors is introduced. The numerical modelling of these four tests are conducted using the proposed approach, allowing further verification of its performance in the estimation of soil temperature and volumetric water content variations in different evaporation processes. After that, the meteorological information for 20 days and the soil parameters (soil thermal conductivity, water retention and hydraulic conductivity curves) for Héricourt embankment are collected/determined, enabling the numerical investigation of soil hydro-thermal behavior in two-dimensional conditions. Moreover, another application of the proposed approach is presented involving Rouen embankment with the meteorological information during two different periods (187 and 387 days) and the soil parameters determined (thermal conductivity, soil water retention and soil hydraulic conductivity curves). The results allow the following conclusions to be drawn:

Environmental chamber

The numerical investigations of four drying tests in environmental chamber are conducted. The satisfactory agreement obtained between simulations and measurements shows that the proposed approach is relevant for estimating the variations of soil temperature and volumetric water content in environmental chamber. The soil volumetric water content presents a continuous decrease tendency in the four evaporation tests. However, the soil temperature

shows different variations in the cases of low air temperature (Test 1 and Test 3) and high air temperature (Test 2 and Test 4). In Test 1 and Test 3, the soil temperature decreases in the first short period and then goes up until the end of test, showing a rebounding phenomenon. This result indicates that soil participates to provide energy for evaporation in the first short period due to the high evaporation rate and then air is able to support both evaporation and soil heating as the decline of evaporation rate. In Test 2 and Test 4, as air flow with high temperature can provide sufficient energy for both evaporation and soil heating, soil temperature increase continuously. This application verifies the good performance of the proposed approach in the estimation of coupled soil hydro-thermal behavior.

Héricourt embankment

The proposed approach is applied to Héricourt embankment, allowing the estimations of soil temperature and volumetric water content at the points classified in three groups (interior, near soil surface, soil surface points) from 06/07/2011 to 26/07/2011 (20 days). Comparison between simulation results and filed measurements shows that this approach is suitable for analyzing the soil temperature and volumetric water content in two-dimensional embankments under the real climate effect. The good agreement between measurements and calculations also proves that suitable boundary conditions and soil parameters have been adopted for the numerical investigation. Moreover, the influenced depths of climate effect are further estimated to be 4 m for soil temperature, and about 2~3 m for volumetric water content, respectively. The simulation results suggest that the soil temperature in the region below the top surface is more sensitive to the slope boundary conditions than the soil volumetric water content.

Rouen embankment

A second application of the proposed approach is done involving Rouen embankment. The numerical investigation in this embankment provides the estimations of soil temperature at different points classified in four groups (near top surface, near slope surface, interior, and interior middle points) and volumetric water content at the points in three groups (near top surface, near slope surface, and interior points) for two different periods: from 10/07/2014 to

13/01/2015 (187 days) and from 27/10/2011 to 17/11/2012 (387 days). Comparison between simulations and measurements in terms of soil temperature and volumetric water content shows that the proposed approach has a good performance in the estimation of soil hydro-thermal behaviour in two-dimensional embankments under the real climate effect. The good agreement between calculations and measurements also reveals that the thermal and hydraulic boundary conditions defined as well as the adopted soil parameters are appropriate. Besides, seasonal variations are observed in variations of soil temperature (with daily fluctuations for near surface points) but not for variations of volumetric water content. At the same point, the temperature may vary significantly but the soil volumetric water content can keep stable, illustrating the necessity of separate consideration of the effects of climate conditions on soil temperature and volumetric water content.

Furthermore, it is proposed to apply this approach in the prediction of soil hydro-thermal behaviour in long term when the corresponding meteorological data is available. Several suggestions are made for the collection of input data:

1) The information of solar radiation is feasible to be collected from other meteorological stations in the same region when field measurements are not available;
2) As the significant input factor, rainfall is recommended to be recorded at the same site;
3) In the case without field data, the wind speed data from a further weather station can be used if the parameters a_1 and a_2 in the formula of potential evaporation are well calibrated.

Perspectives

1) Accurate estimation of soil hydro-thermal properties in the region concerning soil-atmosphere interaction and the consideration of the movement of evaporation front in numerical modeling

Based on the study of the tests using environmental chamber, it is inferred that the adopted approach does not properly consider the soil water retention and the hydraulic conductivity curves in the near surface region. Further experimental work is required to study the variations of soil hydro-thermal properties in the zone influenced by the soil-atmosphere interaction. On the other hand, as the evaporation front is governed by the depth of dry layer, the top boundary condition will change depending on the movement of evaporation front. Hence, further study is also necessary to consider the movement of evaporation front in the soil-atmosphere interaction model.

2) Extension to deformable materials

It is noted that the proposed approach is for non-deformable materials: Fontainebleau sand for environmental chamber, treated silt soil for Héricourt and Rouen embankment. Coupled hydro-thermal model is developed without considering soil deformation. Specifically, this model needs to be extended to take the soil volume change behavior into account in order to deal with deformable materials (e.g. clay).

3) Further applications for the soil long term behavior under climate effect

In this study, the proposed approach is used to estimate the soil hydro-thermal behavior in embankments using proper estimations of soil parameters and boundary conditions. As the determination of boundary conditions is intimately related to the climate conditions, it is proposed to apply this approach to predict the variations of soil temperature, volumetric water content/suction in long term when the corresponding meteorological data is available. It allows the further applications:

- Because of the sensitivity of plants generation to the conditions of soil moisture and

temperature, this approach can be used to provide guidance for plants management.

- Because the infrastructure is unavoidably subjected to the climate effect, this proposed approach can also be adopted to further study the existing engineering damages and to predict the potential engineering problems induced by climate conditions, such as soil desiccation/shrinkage, soil erosion and collapse, slope stability problems, the long term performance of barriers materials for waste disposal, etc.
- Concerning the natural site where trenches must be excavated or the spatial heterogeneity needs to be taken into account, the model dimensions need to be defined properly depending on the real situation.
- In order to make this approach more applicable in practice, it will be of paramount importance to develop a practical platform for integrating climate information into the design, construction and maintenance of geotechnical infrastructures.

Nomenclature

Symbol	*Definition*
C	Volumetric heat capacity of the soil (J/(m^{3}K))
$C_{T\varphi}$	Volumetric isothermal capacity of the structure (J/m^4)
C_T	Volumetric thermal capacity of the structure (J/(m^{3}K))
$C_{\varphi T}$	Volumetric thermal capacity of moisture (kg/(m^{3}K))
C_φ	Volumetric isothermal capacity of moisture (kg/m^4)
C_{pl}	Specific heat capacity of water liquid (J/(kgK))
C_{ps}	Specific heat capacity of soil solid (J/(kgK))
C_{pv}	Specific heat capacity of water vapor (J/(kgK))
C_{pa}	Specific heat capacity of air (J/(kgK))
d_r	Relative earth-sun distance (m)
D_{atm}	Molecular diffusivity of the pore vapor (m^2/s)
D_{TV}	Thermal vapor diffusivity (m^2/(sK))
$D_{\varphi V}$	Isothermal vapor diffusivity (m/s)
E_a	Actual evaporation rate (m/s)
E_p	Potential evaporation (m/s)
EL_{msl}	Site elevation above the mean sea level (m)
e_s	Saturated vapor pressure at the water surface (Pa)
e_a	Vapor pressure of air at the reference height (Pa)
e_0	Actual vapor pressure at the soil surface (Pa)
e_d	Mean daily saturated vapor pressure (Pa)
G	Soil heat flux (W/m^2)
G_{sc}	Solar constant (MJ/(m^{2}min))
H	Sensible heat flux (W/m^2)
h_a	Relative humidity of air (%)
h_s	Relative humidity at soil surface (%)
I_{nf}	Infiltration rate (m/s)

I_{nt}	Rate of water intercepted by canopy during rainfall (m/s)
J	The day of year
K_H	Eddy diffusivity for heat through air (m^2/s)
K_T	Thermal soil structure diffusivity (W/(mK))
$K_{T\varphi}$	Isothermal soil structure diffusivity (W/m^2)
$K_{\varphi T}$	Thermal moisture diffusivity (kg/(msK))
K_φ	Isothermal moisture diffusivity ($kg/(sm^2)$)
K	Unsaturated soil hydraulic conductivity (m/s)
K_s	Saturated soil hydraulic conductivity (m/s)
L_E	Latent heat flux (W/m^2)
L_v	Latent heat of vaporization of water (J/kg)
P	Rate of rainfall (m/s)
Q	Transferred heat flux through soil-atmosphere interface (W/m^2)
q	Flux density of total moisture ($kg/(sm^2)$)
q_l	Flux density of liquid ($kg/(sm^2)$)
q_v	Flux density of vapor ($kg/(sm^2)$)
q_h	Flux density of heat (W/m^2)
R	Universal gas constant (J/(molK))
R_{sa}	Extraterrestrial solar radiation (W/m^2)
R_{s0}	Solar radiation in clear sky (W/m^2)
R_{si}	Solar radiation (W/m^2)
R_{off}	Runoff rate on soil surface (m/s)
R_n	Net radiation flux (W/m^2)
T	Absolute temperature (K)
T_a	Air temperature (ºC)
T_d	Mean daily dew point temperature (ºC)
T_s	Soil surface temperature (ºC)
T_0	Water surface temperature (ºC)

M_W	Molecular mass of water vapor (kg/mol)
w	Moisture content (kg/m^3)
α_s	Soil surface albedo
u	Wind speed (m/s)
y	Elevation above a nominal datum (m)
α	Tortuosity factor for soil
β	Cross-sectional area of the soil that is available for vapor flow
n	Soil porosity
θ	Volumetric water content
θ_s	Saturated volumetric water content
θ_r	Residual volumetric water content
φ	Matric suction (m)
λ	Thermal conductivity of soil (W/(mK))
ρ_0	Density of saturated water vapor (kg/m^3)
ρ_l	Density of water liquid (kg/m^3)
ρ_v	Density of water vapor (kg/m^3)
ρ_s	Density of soil solid (kg/m^3)
ϕ	Latitude (m)
δ	Solar declination
ε_s	Soil surface emissivity
ε_a	Air emissivity
r_a	Aerodynamic resistance (s/m)
r_s	Soil resistance (s/m)

References

Allen, R.G., Pereira, L.S., Raes, D., and Smith, M. 1998. Crop evapotranspiration: guidelines for computing crop water requirements. *In* Irrigation and Drainage Paper 56. Rome, Italy.

Allen, R.G., Smith, M., Perrier, A., and Pereira, L.S. 1994. An update for the definition of reference evapotranspiration. Bulletin of the International Commission on Irrigation and Drainage, **42**(1): 35–92.

Alonso, E.E. 2003. Exploring the limits of unsaturated soil mechanics: the behavior of coarse granular soil and rockfill. The Eleventh Spencer J. Buchanan Lecture,: 1–53.

Alonso, E.E., Gens, A., and Josa, A. 1990. A constitutive model for partially saturated soils. Géotechnique, **40**(3): 405–430. doi:10.1680/geot.1990.40.3.405.

Alonso, E.E., Gens, A., and Delahaye, C.H. 2003. Influence of rainfall on the deformation and stability of a slope in overconsolidated clays: a case study. Hydrogeology Journal, **11**(1): 174–192. doi:10.1007/s10040-002-0245-1.

Alsherif, N.A., and McCARTNEY, J.S. 2015. Thermal behaviour of unsaturated silt at high suction magnitudes. Géotechnique, **65**(9): 703–716. doi:10.1680/geot.14.P.049.

Aluwihare, S., and Watanabe, K. 2003. Measurement of evaporation on bare soil and estimating surface resistance. Journal of Environmental Engineering, **129**(12): 1157–1168. doi:10.1061/(ASCE)0733-9372(2003)129:12(1157).

ASTM. 2006. Standard test methods for measuring and compensating for emissivity using infrared imaging radiometers. ASTM: West Conshohocken., PA, USA. doi:10.1520/E1933-99AR10.2.

Azizi, F. 1999. Applied analyses in geotechnics. CRC Press.

Barnett, T.P., Adam, J.C., and Lettenmaier, D.P. 2005. Potential impacts of a warming climate on water availability in snow-dominated regions. Nature, **438**(7066): 303–309.

Nature Publishing Group. doi:10.1038/nature04141.

Bárta, D., Fortunato, E., and Barbars, J. 2016. Call 2012: Road owners adapting to Climate Change ROADAPT and CliPDaR projects.

Benli, B., Kodal, S., Ilbeyi, A., and Ustun, H. 2006. Determination of evapotranspiration and basal crop coefficient of alfalfa with a weighing lysimeter. Agricultural Water Management, **81**(3): 358–370. doi:10.1016/j.agwat.2005.05.003.

Benson, C., Abichou, T., Albright, W., Gee, G., and Roesler, A. 2001. Field Evaluation of Alternative Earthen Final Covers. International Journal of Phytoremediation, **3**(1): 105–127. doi:10.1080/15226510108500052.

Beven, K. 1989. Changing ideas in hydrology- the case of physically-based models. Journal of Hydrology, **105**: 157–172. doi:10.1016/0022-1694(89)90101-7.

Bhadra, A., Bandyopadhyay, A., Singh, R., and Raghuwanshi, N.S. 2010. Rainfall-runoff modeling: comparison of two approaches with different data requirements. Water Resources Management, **24**: 37–62. doi:10.1007/s11269-009-9436-z.

Bishop, A.W. 1959. The principle of effective stress. Teknisk Ukeblad, **106**(39): 859–863.

Bishop, A.W., and Blight, G.E. 1963. Some aspects of effective stress in saturated and unsaturated soils. Géotechnique, **13**(3): 177–197.

Bittelli, M., Ventura, F., Campbell, G.S., Snyder, R.L., Gallegati, F., and Pisa, P.R. 2008. Coupling of heat, water vapor, and liquid water fluxes to compute evaporation in bare soils. Journal of Hydrology, **362**(3–4): 191–205. Elsevier B.V. doi:10.1016/j.jhydrol.2008.08.014.

Blad, B.L., and Rosenberg, N.J. 1974. Lysimetric calibration of the Bowen ratio-energy balance method for evapotranspiration estimation in the central great plains. Journal of Applied Meteorology, **13**(2): 227–236. doi:10.1175/1520-0450(1974)013<0227:LCOTBR>2.0.CO;2.

Blight, G.E. 1965. A study of effective stresses for volume change. *In* in Moisture Equilibria and Moisture Changes in Soils Beneath Covered Areas, A Symp. *Edited by* E. G. D. Aitchison. Australia: Butterworths. pp. 259–269.

Blight, G.E. 1997. Interactions between the atmosphere and the Earth. Géotechnique, **47**(4): 715–767. doi:10.1680/geot.1997.47.4.713.

Blight, G.E. 2002. Measuring evaporation from soil surfaces for environmental and geotechnical purposes. Water SA, **28**(4): 381–394. doi:10.4314/wsa.v28i4.4911.

Blight, G.E. 2003. The vadose zone soil-water balance and transpiration rates of vegetation. Géotechnique, **53**(1): 55–64. doi:10.1680/geot.2003.53.1.55.

Blight, G.E. 2009. Solar heating of the soil and evaporation from a soil surface. Géotechnique, **59**(4): 355–363. doi:10.1680/geot.2009.59.4.355.

Boldini, D., Comegna, L., Rianna, G., and Tommasi, P. 2014. Evapotranspiration estimate in a clayey slope affected by landslide phenomena. Rivista Italiana Di Geotecnica, **1**: 21–33.

Bowen, I.S. 1926. The ratio of heat losses by conduction and by evaportion from any water surface. Physical Review, **27**: 779–787.

Brand, E.W. 1984. State-of-the-art report of landslides in Southeast Asian. *In* Proceedings of the 4th International Symposium on landslides. Toronto, Canada. pp. 17–37.

Brand, E.W. 1992. Slope instability in tropical areas. *In* Proceedings of the 6th International Symposium on Landslides. Christchurch, New Zealand. pp. 2031–2051.

Brunt, D. 1932. Notes on radiation in the atmosphere. Quarterly Journal of the Royal Meteorological Society, **58**: 389–418. doi:10.1002/qj.49705824704.

Bronswijk, J.J.B. 1991. Drying, cracking, and subsidence of a clay soil in a lysimeter. Soil Science, **152**(2): 92–99.

Brutsaert, W. 1982. Evaporation into the atmosphere. Theory, History and Applications. *In* D.

Riedel Publishing Company. D. Reidel publishing Company., Dordrecht, Holland. doi:10.1007/978-94-017-1497-6.

Buckingham, E. 1907. Studies on the movement of soil moisture. U.S.D.A. Bureau of Soils Bulletin, **38**. Department of Agriculture.

Buongiorno, J., Venerus, D.C., Prabhat, N., McKrell, T., Townsend, J., Christianson, R., Tolmachev, Y. V., Keblinski, P., Hu, L.W., Alvarado, J.L., Bang, I.C., Bishnoi, S.W., Bonetti, M., Botz, F., Cecere, A., Chang, Y., Chen, G., Chen, H., Chung, S.J., Chyu, M.K., Das, S.K., Di Paola, R., Ding, Y., Dubois, F., Dzido, G., Eapen, J., Escher, W., Funfschilling, D., Galand, Q., Gao, J., Gharagozloo, P.E., Goodson, K.E., Gutierrez, J.G., Hong, H., Horton, M., Hwang, K.S., Iorio, C.S., Jang, S.P., Jarzebski, A.B., Jiang, Y., Jin, L., Kabelac, S., Kamath, A., Kedzierski, M.A., Kieng, L.G., Kim, C., Kim, J.H., Kim, S., Lee, S.H., Leong, K.C., Manna, I., Michel, B., Ni, R., Patel, H.E., Philip, J., Poulikakos, D., Reynaud, C., Savino, R., Singh, P.K., Song, P., Sundararajan, T., Timofeeva, E., Tritcak, T., Turanov, A.N., Van Vaerenbergh, S., Wen, D., Witharana, S., Yang, C., Yeh, W.H., Zhao, X.Z., and Zhou, S.Q. 2009. A benchmark study on the thermal conductivity of nanofluids. Journal of Applied Physics, **106**(9). doi:10.1063/1.3245330.

Cahill, A., and Parlange, M. 1998. On water vapour transport in field soils. Water Resources Research, **34**(4): 731–739.

Camillo, P.J., and Gurney, R.J. 1986. A resistance parameter for bare-soil evaporation models. Soil Science, **141**(2): 95–106.

Campbell, G.S. 1985. Soil physics with BASIC: transport models for soil-plant systems. Elsevier, Amsterdam.

Carslaw, H.S., and Jaeger, J.C. 1959. Conduction of heat in solids. Oxford University Press.

Cary, J.W. 1965. Water flux in moist soil: thermal versus suction gradients. Soil Science, **100**(3): 168–175.

Charles, I., and Froumentin, M. 2013. Digue expérimentale en limon traité à la chaux Campagnes d'essais au CER Opération de recherche DOFEAS.

Chiew, F., and McMahon, T. 1994. Application of the daily rainfall-runoff model MODHYDROLOG to 28 Australian catchments. Journal of Hydrology, **153**: 383–416. doi:10.1016/0022-1694(94)90200-3.

Chiew, F.H.S., Stewardson, M.J., and McMahon, T. a. 1993. Comparison of six rainfall-runoff modelling approaches. Journal of Hydrology, **147**: 1–36. doi:10.1016/0022-1694(93)90073-I.

Childs, E.C., and George, N.C. 1950. The permeability of porous materials. *In* Proceedings of the Royal Society of London A: Mathematical, Physical and Engineering Sciences. pp. 392–405.

Chipp, P.N., Henkel, D.J., Clare, D.G., and Pope, R.G. 1982. Field measurement of suction in colluvium covered slopes in Hong Kong. *In* Proceedings of 7th Southeast Asian Geotechnical conference. pp. 49–62.

Choudhury, B., and Monteith, J. 1988. A four layer model for the heat budget of homogenous land surfaces. Quarterly Journal of the Royal Meteorological Society, **114**: 373–398.

Choudhury, B.J., Reginato, R.J., and Idso, S.B. 1986. An analysis of infrared temperature observations over wheat and calculation of latent heat flux. Agricultural and Forest Meteorology, **37**: 75–88.

Chowdhury, R., and Flentje, P. 2007. Perspectives for the future of Geotechnical Engineering. *In* Proceedings of the International Conference on Civil Engineering For the New Millennium: Opportunities and Challenges. Bengal Engineering College, Shibpur, India.

Collins, B.D., and Znidarcic, D. 2004. Stability analyses of rainfall induced landslides. Journal of Geotechnical and Geoenvironmental Engineering, **130**(4): 362–372. American Society of Civil Engineers. doi:10.1061/(ASCE)1090-0241(2004)130:4(362).

Corey, A.T. 1957. Measurement of water and air permeability in unsaturated soil. Soil

Science Society of America Journal, **21**(1): 7. Soil Science Society of America. doi:10.2136/sssaj1957.03615995002100010003x.

Côté, J., and Konrad, J.M. 2005. A generalized thermal conductivity model for soils and construction materials. Canadian Geotechnical Journal, **42**(2): 443–458. doi:10.1139/t04-106.

Critchley, W., and Siegert, K. 1991. A manual for the design and construction of water harvesting schemes for plant production. Rome.

Cui, Y.J., and Delage, P. 1996. Yielding and plastic behaviour of an unsaturated compacted silt. Géotechnique, **46**(2): 291–311. doi:10.1680/geot.1996.46.2.291.

Cui, Y.J., Delage, P., and Sultan, N. 1995. An elasto-plastic model for compacted soils. *In* Proceedings of the first international conference on unsaturated soils. Volume 2. *Edited by* E.E. Alonso and P. Delage. Presses de l'École nationale des ponts et chaussées. pp. 703–709.

Cui, Y.J., Duong, T.V., Tang, A.M., Dupla, J.C., Calon, N., and Robinet, A. 2013a. Investigation of the hydro-mechanical behaviour of fouled ballast. Journal of Zhejiang University SCIENCE A, **14**(4): 244–255. doi:10.1631/jzus.A1200337.

Cui, Y.J., Gao, Y.B., and Ferber, V. 2010. Simulating the water content and temperature changes in an experimental embankment using meteorological data. Engineering Geology, **114**(3–4): 456–471. doi:10.1016/j.enggeo.2010.06.006.

Cui, Y.J., Lu, Y.F., Delage, P., and Riffard, M. 2005. Field simulation of in situ water content and temperature changes due to ground–atmospheric interactions. Géotechnique, **55**(7): 557–567. doi:10.1680/geot.2005.55.7.557.

Cui, Y.J., Ta, A.N., Hemmati, S., Tang, A.M., and Gatmiri, B. 2013b. Experimental and numerical investigation of soil-atmosphere interaction. Engineering Geology, **165**: 20–28. Elsevier B.V. doi:10.1016/j.enggeo.2012.03.018.

Cui, Y.J., and Tang, A.M. 2013. On the chemo-thermo-hydro-mechanical behaviour of

geological and engineered barriers. Journal of Rock Mechanics and Geotechnical Engineering, **5**(3): 169–178. doi:10.1016/j.jrmge.2013.05.001.

Cui, Y.J., and Zornberg, J.G. 2008. Water balance and evapotranspiration monitoring in geotechnical and geoenvironmental engineering. Geotechnical and Geological Engineering, **26**(6): 783–798. doi:10.1007/s10706-008-9198-z.

Daamen, C.C., and Simmonds, L.P. 1996. Measurement of evaporation from bare soil and its estimation using surface resistance. Water Resources Research, **32**(5): 1393–1402.

Dakshanamurthy, V., and Fredlund, D.G. 1981. A mathematical model for predicting moisture flow in an unsaturated soil under hydraulic and temperature gradients. Water Resources Research, **17**(3): 714–722. doi:10.1029/WR017i003p00714.

Dalton, J. 1802. Experimental essays on the constitution of mixed gases on the force of steam or vapour from water and other liquids in different temperatures, both in a Torricellian vacuum and in air; on evaporation ; and on the expansion of gases. Manchester Literary and Philosophical Society,: 535–602.

Daniel, H. 2013. Advances in Irrigation. Elsevier.

Daniel, J.S., Jacobs, J.M., Asce, M., Douglas, E., Mallick, R.B., and Hayhoe, K. 2014. Impact of climate change on pavement performance: preliminary lessons learned through the infrastructure and climate network (ICNet). *In* International Symposium of Climatic Effects on Pavement and Geotechnical Infrastructure 2013. pp. 1–9.

Darcy, H. 1856. Les fontaines publiques de la ville de Dijon, exposition et application. *Edited by*Victor Dalmon. Paris.

Dehn, M., Bürger, G., Buma, J., and Gasparetto, P. 2000. Impact of climate change on slope stability using expanded downscaling. Engineering Geology, **55**(3): 193–204. doi:10.1016/S0013-7952(99)00123-4.

Deng, Y.F., Tang, A.M., Cui, Y.J., and Li, X.L. 2011a. Study on the hydraulic conductivity of Boom clay. Canadian Geotechnical Journal, **48**: 1461–1470. doi:10.1139/t11-048.

Deng, Y.F., Tang, A.M., Cui, Y.J., Nguyen, X.P., Li, X.L., and Wouters, L. 2011b. Laboratory hydro-mechanical characterisation of Boom Clay at Essen and Mol. Physics and Chemistry of the Earth, **36**(17–18): 1878–1890. doi:10.1016/j.pce.2011.10.002.

Dijkstra, T.A., and Dixon, N. 2010. Climate change and slope stability in the UK: challenges and approaches. Quarterly Journal of Engineering Geology and Hydrogeology, **43**(4): 371–385. doi:10.1144/1470-9236/09-036.

Dixon, D.A., Cheung, S.C.H., Gray, M.N., and Davidson, B.C. 1987. The hydraulic conductivity of dense clay soils. *In* Proc. 40th Canadian geotechnical conference. pp. 389–396.

Dixon, D.A., Graham, J., and Gray, M.N. 1999. Hydraulic conductivity of clays in confined tests under low hydraulic gradients. Canadian Geotechnical, **36**(5): 815–825.

Dixon, D.A., Gray, M.N., and Graham, J. 1996. Swelling and hydraulic properties of bentonites from Japan, Canada and USA. *In* Proceedings of the second international congress on environmental geotechnics. pp. 5–8.

Dixon, D.A., Gray, M.N., and Hnatiw, D. 1992. Critical gradients and pressures in dense swelling clays. Canadian Geotechnical,.

Dixon, D.A., Gray, M.N., and Thomas, A.W. 1985. A study of the compaction properties of potential clay—sand buffer mixtures for use in nuclear fuel waste disposal. Engineering Geology, **21**(3): 247–255. Elsevier. doi:10.1016/0013-7952(85)90015-8.

Dixon, N., Dijkstra, T., Forster, A., and Connell, R. 2006. Climate change impact forecasting for slopes (CLIFFS) in the built environment. *In* Engineering Geology for Tomorrow's Cities: Proceedings, 10th International Association of Engineering Geology Congress. Geological Society, London. pp. 1–8.

Doussan, C., and Ruy, S. 2009. Prediction of unsaturated soil hydraulic conductivity with electrical conductivity. Water Resources Research, **45**: 1–12. doi:10.1029/2008WR007309.

Duffie, J., and Beckman, W. 1991. Solar engineering of thermal processes, 2nd edn. John Wiley & Sons, New York. doi:10.1115/1.2930068.

Dugas, W.A., Fritschen, L.J., Gay, L.W., Held, A.A., Matthias, A.D., Reicosky, D.C., Steduto, P., and Steiner, J.L. 1991. Bowen ratio, eddy correlation, and portable chamber measurements of sensible and latent heat flux over irrigated spring wheat. Agricultural and Forest Meteorology, **56**(1): 1–20. Elsevier. doi:10.1016/0168-1923(91)90101-U.

Edlefsen, N.E., and Anderson, A.B.C. 1943. Thermodynamics of soil moisture. Hilgardia.

EEA. 2012. Climate change, impacts and vulnerability in Europe 2012. European Environment Agency, Copenhagen. doi:doi:10.2800/66071.

Evett, S.R., Prueger, J.H., and Tolk, J.A. 2011. Water and energy balances in the soil-plant-atmosphere continuum. *In* Handbook of Soil Sciences: Properties and Processes, 2nd editio. *Edited by* S.M. Huang PM, Li Y. CRC Press, Boca Raton, Florida, USA. pp. 6-1-6–44. doi:10.1201/b11267-8.

Farouki, O.T. 1981. Thermal properties of soils. Series on Rock and Soil Mechanics, **11**: 136. doi:10.1097/00010694-195008000-00030.

Fayer, M., and Walters, T. 1995. Estimated recharge rates at the Hanford Site. PNL-10285, Pacific Northwest Laboratory, Richland, Washington.

Fayer, M.J. 2000. UNSAT-H Version 3.0: Unsaturated soil water and heat flow model. Theory, User Manual , and Examples. *In* model manual.

Fayer, M.J., and Jones, T.L. 1990. UNSAT-H Version 2.0: unsaturated soil water and heat flow model. Publication PNL-6779, Pacific Northwest Laboratory, Richland, Washington.

Ferrari, A., Eichenberger, J., and Laloui, L. 2013. Hydromechanical behaviour of a volcanic ash. Géotechnique, **63**(16): 1433–1446.

Ferrari, A., Laloui, L., and Bonnard, C. 2009. Hydro-mechanical modelling of a natural slope

affected by a multiple slip surface failure mechanism. Computer Modeling in Engineering and Sciences, **52**(3): 217–235.

Fitzgerald, D. 1886. Evaporation. Transactions of the American Society of Civil Engineers, **98**(HY12): 2073–2085.

François, B., Laloui, L., and Laurent, C. 2009. Thermo-hydro-mechanical simulation of ATLAS in situ large scale test in Boom Clay. Computers and Geotechnics, **36**(4): 626–640. Elsevier Ltd. doi:10.1016/j.compgeo.2008.09.004.

Fredlund, D.G., and Dakshanamurthy, V. 1982. Prediction of moisture flow and related swelling or shrinking in unsaturated soils. Geotechnical Engineering, **13**: 15–49.

Fredlund, D.G., and Morgenstern, N.R. 1976. Constitutive relations for volume change in unsaturated soils. Canadian Geotechnical Journal, **13**(3): 261–276. doi:10.1139/t76-029.

Fredlund, D.G., and Rahardjo, H. 1993. Soil mechanics for unsaturated soils. *In* John Wiley & Sons. New York. doi:10.1016/0267-7261(93)90011-F.

Froumentin, M. 2012. TerDOUEST Project ANR-07-PCGU-006-10. Cete Normandie Centre: France.

Gallipoli, D., Gens, A., Sharma, R., and Vaunat, J. 2003. An elasto-plastic model for unsaturated soil incorporating the effects of suction and degree of saturation on mechanical behaviour. Géotechnique, **53**(1): 123–136. doi:10.1063/1.2756072.

Gao, Z.Q. 2005. Determination of soil heat flux in a Tibetan short-grass prairie. Boundary-Layer Meteorology, **114**: 165–178.

Garbrecht, J., Ogden, F.L., DeBarry, P.A., and Maidment, D.R. 2001. GIS and distributed watershed models. I: Data voverages and sources. Journal of hydrologic engineering, **6**(6): 506–514.

Gardner, W. 1958. Some steady-state solutions of the unsaturated moisture flow equation with application to evaporation from a water table. Soil science, **85**(4): 228–232.

Gatmiri, B., and Arson, C. 2008. θ-STOCK, a powerful tool of thermohydromechanical behaviour and damage modelling of unsaturated porous media. Computers and Geotechnics, **35**(6): 890–915. doi:10.1016/j.compgeo.2008.08.008.

Gatmiri, B., and Delage, P. 1997. A formulation of fully coupled thermal-hydraulic-mechanical behaviour of saturated porous media—numerical approach. International Journal for Numerical and Analytical Methods in Geomechanics, **21**(April 1995): 199–225. doi:10.1002/(SICI)1096-9853(199703)21:3<199::AID-NAG865>3.0.CO;2-M.

Gens, A., and Alonso, E.E. 1992. A framework for the behaviour of unsaturated expansive clays. Canadian Geotechnical Journal, **29**: 1013–1032.

Gens, A. 2010. Soil-environment interactions in geotechnical engineering. Géotechnique, **60**(1): 3–74. doi:10.1680/geot.9.P.109.

van Genuchten, M.T.T. 1980. A closed-form equation for predicting the hydraulic conductivity of unsaturated soils. Soil Science Society of America Journal, **44**(5): 892–898. doi:10.2136/sssaj1980.03615995004400050002x.

Gerard, P., Charlier, R., Chambon, R., and Collin, F. 2008. Influence of evaporation and seepage on the convergence of a ventilated cavity. Water Resources Research, **44**(7): W00C02: 1-16. doi:10.1029/2007WR006500.

Gerard, P., Léonard, A., Masekanya, J.P., Charlier, R., and Collin, F. 2010. Study of the soil–atmosphere moisture exchanges through convective drying tests in non-isothermal conditions. International Journal for Numerical and Analytical Methods in Geomechanics, **34**(12): 1297–1320. doi:10.1002/nag.

Gitirana, G. 2005. Weather-related geo-hazard assessment model for railway embankment stability. PhD Thesis, University of Saskatchewan, Saskatoon.

Gitirana, G., Fredlund, M.D., and Fredlund, D.G. 2006. Numerical modelling of soil-atmosphere interaction for unsaturated surfaces. *In* Proc. The 4th international conference on unsaturated soils, Arizona. pp. 658–669.

Glendinning, S., Hughes, P., Helm, P., Chambers, J., Mendes, J., Gunn, D., Wilkinson, P., and Uhlemann, S. 2014. Construction, management and maintenance of embankments used for road and rail infrastructure: implications of weather induced pore water pressures. Acta Geotechnica,: 799–816. doi:10.1007/s11440-014-0324-1.

Gökbulak, F., Şengönül, K., Serengil, Y., Yurtseven, İ., Özhan, S., Cigizoglu, H.K., and Uygur, B. 2015. Comparison of rainfall-runoff relationship modeling using different methods in a forested watershed. Water Resources Management, **29**: 4229–4239. doi:10.1007/s11269-015-1056-1.

Gray, D.M. 1970. Handbook on the principles of hydrology. *In* Canadian National Committee for the International Hydrological Decade. doi:10.1080/10548400802156836.

van de Griend, A.A., and Owe, M. 1994. Bare soil surface resistance to evaporation by vapor diffusion under semiarid conditions. Water Resources Research, **30**(2): 181–188. doi:10.1029/93WR02747.

Grifoll, J., Gastó, J.M., and Cohen, Y. 2005. Non-isothermal soil water transport and evaporation. Advances in Water Resources, **28**(11): 1254–1266. doi:10.1016/j.advwatres.2005.04.008.

Gruber, S. 2005, Mountain permafrost: transient spatial modelling, model verification and the use of remote sensing, PhD Thesis, University of Zurich, Zurich.

Gruber, S., and Haeberli, W. 2007. Permafrost in steep bedrock slopes and its temperature-related destabilization following climate change. Journal of Geophysical Research, **112**(F2): F02S18. doi:10.1029/2006JF000547.

Gruber, S., Hoelzle, M., and Haeberli, W. 2004. Permafrost thaw and destabilization of Alpine rock walls in the hot summer of 2003. Geophysical Research Letters, **31**(13): n/a-n/a. doi:10.1029/2004GL020051.

Hansson, K., Lundin, L.-C., and Šimůnek, J. 2005. Modeling water flow patterns in flexible pavements. Transportation Research Record, **1936**: 131–141. doi:10.3141/1936-16.

Harbeck, G.E., Kohler, M.A., and Koberg, G.E. 1954. Water-loss investigations: Lake Hefner studies, Technical Report. Washington, D.C.

Harbeck, G.E., Kohler, M.A., and Koberg, G.E. 1958. Water-loss investigations: Lake Mead studies, Techncial Report. Washington, D.C.

Harley, C., Hughes, A.R., and Hultgren, K. 2006. The impacts of climate change in coastal marine systems. Ecology,.

Harnos, Z.S., and Csete, L. 2008. Climate change: environment–risk–society. Research Results, Szaktudás Kiadó Ház. Budapest.

Harris, C., Arenson, L.U., Christiansen, H.H., Etzelmüller, B., Frauenfelder, R., Gruber, S., Haeberli, W., Hauck, C., Hölzle, M., Humlum, O., Isaksen, K., Kääb, A., Kern Lütschg, M.A., Lehning, M., Matsuoka, N., Murton, J.B., Nötzli, J., Phillips, M., Ross, N., Seppälä, M., Springman, S.M., and Vonder Mühll, D. 2009. Permafrost and climate in Europe: monitoring and modelling thermal, geomorphological and geotechnical responses. Earth-Science Reviews, **92**(3–4): 117–171. Elsevier B.V. doi:10.1016/j.earscirev.2008.12.002.

Hatfield, J.L., Perrier, A., and Jackson, R.D. 1983. Estimation of evapotranspiration at one time-of-day using remotely sensed surface temperatures. Agricultural Water Management, **7**(1–3): 341–350. doi:10.1016/0378-3774(83)90094-X.

Hecht, F. 1998. BAMG: bidimensional anisotropic mesh generator.

Hecht, F. 2010. FreeFem++, a tool to solve PDE's numerically.

Hecht, F. 2012. New development in FreeFem++. Journal of Numerical Mathematics, **20**(3–4): 251–265. doi:10.1515/jnum-2012-0013.

Hemmati, S. 2009. Etude de l'interaction sol-végétation- atmosphère avec une approche couplée Thermo-Hydro-Mécanique. PhD Thesis, Ecole des Ponts Paristech, Paris.

Hemmati, S., Gatmiri, B., Cui, Y.J., and Vincent, M. 2012. Thermo-hydro-mechanical

modelling of soil settlements induced by soil-vegetation-atmosphere interactions. Engineering Geology, **139**–**140**: 1–16. Elsevier B.V. doi:10.1016/j.enggeo.2012.04.003.

Heusinkveld, B.G., Jacobs, A.F.G., Holtslag, A.A.M., and Berkowicz, S.M. 2004. Surface energy balance closure in an arid region: role of soil heat flux. Agricultural and Forest Meteorology, **122**(1–2): 21–37. doi:10.1016/j.agrformet.2003.09.005.

Hignett, C.T., Gusli, S., Cass, A., and Besz, W. 1995. An automated laboratory rainfall simulation system with controlled rainfall intensity, raindrop energy and soil drainage. Soil Technology, **8**(1): 31–42. doi:10.1016/0933-3630(95)00004-2.

Hillel, D. 2003. Introdution to environmental soil physics. *In* Energy. Academic press.

Horton, R.E. 1919. Rainfall interception. Monthly Weather Review, **47**(9): 603–623. doi:10.1175/1520-0493(1919)47<603:RI>2.0.CO;2.

Howell, T.A., Steiner, J.L., Evett, S.R., Schneider, A.D., Copeland, K.S., Dusek, D.A., and Tunick, A. 1993. Radiation Balance and Soil Water Evaporation of Bare Pullman Clay Loam Soil. ASCE. pp. 922–929.

Hughes, D., Sivakumar, V., Glynn, D., and Clarke, G. 2007. A case study: delayed failure of a deep cutting in lodgement till. Proceedings of the Institution of Civil Engineers - Geotechnical Engineering, **160**(4): 193–202. doi:10.1680/geng.2007.160.4.193.

Hughes, P.N., Glendinning, S., Mendes, J., Parkin, G., Toll, D.G., Gallipoli, D., and Miller, P.E. 2009. Full-scale testing to assess climate effects on embankments. Proceedings of the Institution of Civil Engineers - Engineering Sustainability, **162**(2): 67–79. doi:10.1680/ensu.2009.162.2.67.

Humes, K.S., Kustas, W.P., Moran, M.S., Nichols, W.D., and Weltz, M.A. 1994. Variability of emissivity and surface temperature over a sparsely vegetated surface. Water Resources Research, **30**(5): 1299–1310. doi:10.1029/93WR03065.

Hussain, S. 1997. Validation of coupled heat and moisture flow program in unsaturated porous media. PhD Thesis, University of Toronto, Toronto.

Idso, S.B. 1981. A set of equations for full spectrum and 8 to 14 micron and 10.5 to 12.5 micron thermal radiation from cloudless skies. Water Resources Research, **17**(2): 295–304. doi:10.1029/WR017i002p00295.

Jackson, R.D. 1973. Diurnal changes in soil water content during drying. *In* Field soil water regime. Soil Science Society of America. pp. 37–55.

Jackson, R.D., Reginato, R.J., and Kimball, B.A. 1974. Diurnal soil-water evaporation: Comparison of measured and calculated soil-water fluxes. Soil Science Society of America Proceddings, **38**(6).

Jahangir, M.H., and Sadrnejad, S.A. 2012. A new coupled heat, moisture and air transfer model in unsaturated soil. Journal of Mechanical Science and Technology, **26**(11): 3661–3672. doi:10.1007/s12206-012-0839-z.

Jan, C.D., Yang, S.Y., Su, Y.W., and Haung, W.S. 2016. Investigation about rainfall-induced shallow landslides in CYL and TWR watersheds, Taiwan. Environmental Earth Sciences, **75**(10): 898. doi:10.1007/s12665-015-5215-8.

Jennings, J.E.B., and Burland, J.B. 1962. Limitations to the use of effective stresses in partly saturated soils. Géotechnique, **12**(2): 125–144.

Jensen, M.E., Burman, R.D., and Allen, R.G. 1990. Evapotranspiration and irrigation water requirements. American Society of Agronomy, New York.

Johansen, O. 1975. Thermal conductivity of soils. Trondheim, Norway. doi:10.1063/1.1699752.

Kalliainen, A., and Kolisoja, P. 2011. Modelling of the effect of embankment dimensions on the mechanical behavior of railway track- model scale instrumented test embankments. *In* World congress rainlway research, Lille.

Khire, M. V., Benson, C.H., and Bosscher, P.J. 1997. Water balance modeling of earthen final covers. Journal of Geotechnical and Geoenvironmental Engineering, **123**(8): 744–754.

Knapp, H.V., Durgunoglu, A., and Ortel, T.W. 1991. A review of rainfall-runoff modeling for stormwater management. Illinois District.

Koetse, M., and Rietveld, P. 2009. The impact of climate change and weather on transport: An overview of empirical findings. Transportation Research Part D, **14**: 205–221.

Komatsu, T.S. 2003. Toward a robust phenomenological expression of evaporation efficiency for unsaturated soil surfaces. Journal of Applied Meteorology, **42**(9): 1330–1334. doi:Doi 10.1175/1520-0450(2003)042<1330:Tarpeo>2.0.Co;2.

Kondo, J., Saigusa, N., and Sato, T. 1990. A parameterization of evaporation from bare soil surfaces. Journal of Applied Meteorology, **29**: 385–389.

Kondo, J., Saigusa, N., and Sato, T. 1992. A model and experimental study of evaporation from bare-soil surfaces. Journal of Applied Meteorology, **31**(3): 304–312. doi:10.1175/1520-0450(1992)031<0304:AMAESO>2.0.CO;2.

Konstantinov, A.R. 1968. Evaporation in nature. Leningrad.

Krahn, J., Fredlund, D.G., and Klassen, M.J. 1989. Effect of soil suction on slope stability at Notch Hill. Canadian Geotechnical Journal, **26**(2): 269–278. doi:10.1139/t89-036.

Kustas, W.P., and Daughtry, C.S.. 1990. Estimation of the soil heat flux/net radiation ratio from spectral data. Agricultural and Forest Meteorology, **49**(3): 205–223. doi:10.1016/0168-1923(90)90033-3.

Kuzmin, P.P. 1957. Hydrophysical investigations of land waters. International Association of Hydrological Sciences Publications, **3**: 468–478.

Lal, R., and Shukla, M.K. 2005. Principles of soil physics. The Ohio State University, Columbus, Ohio, U.S.A.

Laloui, L., Ferrari, A., Li, C., and Eichenberger, J. 2016. Hydro-mechanical analysis of volcanic ash slopes during rainfall. Géotechnique, **66**(3): 220–231. doi:10.1680/jgeot.15.LM.001.

Lee, I.M., Lee, H.J., Cheon, J.Y., and Reddi, L.N. 2003. Evaporation theory for deformable soils. Journal of Geotechnical and Geoenvironmental Engineering, **129**(11): 1020–1027. doi:10.1061/(ASCE)1090-0241(2003)129:11(1020).

Lee, J., Cho, W., and Chun, K. 1999. Swelling pressures of a potential buffer material for high-level waste repository. Journal of the Korean Nuclear Society,.

Lee, J., and Khairoutdinov, M. 2012. Validation of a simplified land surface model and its application to the case of shallow cumulus convection development over land. *In* American Geophysical Union, Fall Meeting 2012.

Leung, A., and Ng, C. 2013. Analyses of groundwater flow and plant evapotranspiration in a vegetated soil slope. Canadian Geotechnical Journal, **1218**(October): 1204–1218. doi:10.1139/cgj-2013-0148.

Li, A., Yue, Z., Tham, L., and Lee, C. 2005. Field-monitored variations of soil moisture and matric suction in a saprolite slope. Canadian Geotechnical Journal, **42**: 13–26.

Lim, T.T., Rahardjo, H., Chang, M.F., and Fredlund, D.G. 1996. Effect of rainfall on matric suctions in a residual soil slope. Canadian Geotechnical Journal, **33**(4): 618–628. doi:10.1139/t96-087.

Liu, C., Zhang, X., and Zhang, Y. 2002. Determination of daily evaporation and evapotranspiration of winter wheat and maize by large-scale weighing lysimeter and micro-lysimeter. Agricultural and Forest Meteorology, **111**(2): 109–120. doi:10.1016/S0168-1923(02)00015-1.

Liu, S., Lu, L., Mao, D., and Jia, L. 2007. Evaluating parameterizations of aerodynamic resistance to heat transfer using field measurements. Hydrology and Earth System Sciences, **11**: 769–783. doi:10.5194/hess-11-769-2007.

Lloret, A., and Villar, M. V. 2007. Advances on the knowledge of the thermo-hydro-mechanical behaviour of heavily compacted “FEBEX” bentonite. Physics and Chemistry of the Earth, **32**(8–14): 701–715. doi:10.1016/j.pce.2006.03.002.

López, A., Molina-Aiz, F.D., Valera, D.L., and Peña, A. 2012. Determining the emissivity of the leaves of nine horticultural crops by means of infrared thermography. Scientia Horticulturae, **137**: 49–58. doi:10.1016/j.scienta.2012.01.022.

Luikov, A. V. 1966. Application of irreversible thermodynamics mehtods to investigation of heat and mass transfer. International Journal of Heat and Mass Transfer, **9**: 139–152.

Luikov, A. V. 1965. Application of the methods of thermodynamics of irreversible processes to the investigation of heat and mass transfer. *In* Minsk All-Union Conference on heat and mass transfer. pp. 287–304.

Luikov, A.V. 1964. Heat and mass transfer in capillary-porous bodies. Advances in heat transfer, **1**: 123–184.

Mahfouf, J.F., and Noilhan, J. 1991. Comparative-study of various formulations of evaporation from bare soil using insitu Data. doi:10.1175/1520-0450(1991)030<1354:CSOVFO>2.0.CO;2.

Mahrt, L., and Ek, M. 1984. The influence of atmospheric stability on potential evaporation. Journal of Climate and Applied Meteorology, **23**: 222–234. doi:10.1175/1520-0450(1984)023<0222:TIOASO>2.0.CO;2.

Matyas, E. 1967. Air and water permeability of compacted soils. *In* Testing and Materials. ASTM STP 417 American Society. pp. 160–175. doi:10.1520/STP47264S.

Mbonimpa, M., Montréal, É.P. De, Bédard, C., Aubertin, M., and Bussière, B. 2004. A model to predict the unsaturated hydraulic. *In* 57th Canadian Geotechnical Conference. pp. 16–23.

McCarthy, J. ames J., Canziani, O.F., Leary, N.A., Dokken, D.J., and White, K.S. 2001. Climate Change 2001: Impacts, Adaptation, and Vulnerability (Contribution of Working Group II to the Third Assessment R). The Press Syndicate of the University OF Cambridge.

McKee, C., and Bumb, A. 1984. The importance of unsaturated flow parameters in designing

a hazardous waste site. *In* Hazardous Wastes and Environmental Emergencies (Hazardous Materials Control Research Institute National Conference). Houston, TX. pp. 50–58. doi:10.1023/A:1013109728218.

McKeen, R.G., and Johnson, L.D. 1990. Climate-controlled soil design parameters for mat foundations. Journal of Geotechnical Engineering, **116**(7): 1073–1094.

Meyer, A.F. 1915. Computing runoff from rainfall and other physical data. Transactions of the American Society of Civil Engineers, **78**(2): 1056–1155. ASCE.

Miller, J. 1994. Handbook for agrohydrology. *Edited by*Natural Resources Institute. Chatham, UK.

Milly, P.C.D. 1982. Moisture and heat transport in hysteretic, inhomogeneous prous media: A matric-head based formulation and a numerical model. Water Resources Research, **18**(3): 489–498.

Mohamed, A., Sasaki, T., and Watanabe, K. 2000. Solute transport through unsaturated soil due to evaporation. Journal of Environmental Engineering, **126**(9): 842–848.

Monteith, J.L. 1981. Evaporation and surface temperature. Quarterly Journal of the Royal Meteorological Society, **107**(451): 1–27.

Morton, F.I. 1975. Estimating evaporation and transpiration from climatological observations. doi:10.1175/1520-0450(1975)014<0488:EEATFC>2.0.CO;2.

Mu, W., Yu, F., Li, C., Xie, Y., Tian, J., Liu, J., and Zhao, N. 2015. Effects of rainfall intensity and slope gradient on runoff and soil moisture content on different growing stages of spring maize. Water, **7**(1): 2990–3008. doi:10.3390/w7062990.

Nakano, M., and Miyazaki, T. 1979. The diffusion and nonequilibruim thermodynamic equations of water vapor under temperature gradients. Soil Science, **128**(3): 184–188.

Nelson, F.E., Anisimov, O.A., and Shiklomanov, N.I. 2002. Climate change and hazard zonation in the circum-arctic permafrost regions. Natural Hazards, **26**(3): 203–225.

doi:10.1023/A:1015612918401.

Ng, C.W.W., Zhan, L.T., Bao, C.G., Fredlund, D.G., and Gong, B.W. 2003. Performance of an unsaturated expansive soil slope subjected to artificial rainfall infiltration. Géotechnique, **53**(2): 143–157. doi:10.1680/geot.2003.53.2.143.

Nikulin, G., Kjellström, E., Hansson, U., Strandberg, G., and Ullerstig, A. 2011. Evaluation and future projections of temperature, precipitation and wind extremes over Europe in an ensemble of regional climate simulations. Tellus, Series A: Dynamic Meteorology and Oceanography, **63**(1): 41–55. doi:10.1111/j.1600-0870.2010.00466.x.

O'Connell, P.E. 1991. A historical perspective. *In* Recent Advances in the Modeling of Hydrologic Systems. *Edited by* D.S. Bowles and P.E. O'Connell. Springer Netherlands. pp. 3–30. doi:http://dx.doi.org/10.1016/B978-1-4557-0764-5.00001-0.

Oke, T.R. 1987. Boundary layer climates. *In* Journal of Chemical Information and Modeling, Second edn. Methuen & Co. Ltd. doi:10.1017/CBO9781107415324.004.

Olivella, S., Gens, A., Carrera, J., and E.E., A. 1996. Numerical simulator for a simulator (CODE_BRIGHT) for the coupled analysis of saline media,. Engineering Computations, **13**(7): 87–112.

Passerat de Silans, A. 1986. Transferts de masse et de chaleur dans un soil stratifié soumis a une excitation atmosphérique naturelle. L'institut national polytechique de grenoble.

Penman, H.L.L. 1948. Natural evaporation from open water, bare soil and grass. Proceedings of the Royal Society A: Mathematical, Physical and Engineering Sciences, **193**(1032): 120–145. doi:10.1098/rspa.1948.0037.

Pérez Latorre, F.J., de Castro, L., and Delgado, A. 2010. A comparison of two variable intensity rainfall simulators for runoff studies. Soil and Tillage Research, **107**(1): 11–16. Elsevier B.V. doi:10.1016/j.still.2009.12.009.

Philip, J.R., and De Vries, D.A. 1957. Moisture movement in porous materials under temperature gradients. Eos, Transactions American Geophysical Union, **38**(2): 222–232.

North-Holland Publ. Co.

Pinson, W.T., Yoder, D.C., Buchanan, J.R., Wright, W.C., and Wilkerson, J.B. 2004. Design and evaluation of an improved flow divider for sampling runoff plots. Applied Engineering in Agriculture, **20**(4): 433–438.

Ponce, V.M., and Hawkins, R.H. 1996. Runoff curve number: Has it reached maturity? Journal of Hydrologic Engineering, **1**(1): 11–19.

Potts, D.M., Kovacevic, N., and Vaughan, P.R. 1997. Delayed collapse of cut slopes in stiff clay. Géotechnique, **47**(5): 953–982. doi:10.1680/geot.1997.47.5.953.

Al Qadad, A., Shahrour, I., and Rouainia, M. 2012. Influence of the soil-atmosphere exchange on the hydric profile induced in soil-structure system. Natural Hazards and Earth System Science, **12**(6): 2039–2049. doi:10.5194/nhess-12-2039-2012.

Qiu, G.Y., and Ben-Asher, J. 2010. Experimental determination of soil evaporation stages with soil surface temperature. Soil Science Society of America Journal, **74**(1): 13. doi:10.2136/sssaj2008.0135.

Qiu, G.Y., Yano, T., and Momii, K. 1998. An improved methodology to measure evaporation from bare soil based on comparison of surface temperature with a dry soil surface. Journal of Hydrology, **210**(1–4): 93–105. doi:10.1016/S0022-1694(98)00174-7.

Rahardjo, H., Lee, T.T., Leong, E.C., and Rezaur, R.B. 2004. A flume for assessing flux boundary characteristics in rainfall-induced slope failure studies. Geotechnical Testing Journal, **27**(2): 145–153. doi:10.1520/GTJ11503.

Rahardjo, H., Lee, T.T., Leong, E.C., and Rezaur, R.B. 2005. Response of a residual soil slope to rainfall. Canadian Geotechnical Journal, **42**: 340–351. doi:10.1139/t04-101.

Rahardjo, H., Leong, E.C., and Rezaur, R.B. 2002. Studies of rainfall-induced slope failures. *In* Proceedings of the national seminar, Slope. Bandung, Indonesia. pp. 15–29.

Rahardjo, H., Rezaur, R.B., Leong, E.C., Alonso, E.E., Lloret, A., and Gens, A. 2008.

Monitoring and modeling of slope response to climate changes. *In* Proc. 10th Int. Symp. on Landslides. Xi'an, China. pp. 67–84.

Rahardjo, H., Satyanaga, A., and Leong, E.C. 2013. Effects of flux boundary conditions on pore-water pressure distribution in slope. Engineering Geology, **165**: 133–142. Elsevier B.V. doi:10.1016/j.enggeo.2012.03.017.

Rayhani, M.H., Yanful, E.K., and Fakher, A. 2007. Desiccation-induced cracking and its effect on the hydraulic conductivity of clayey soils from Iran. Canadian Geotechnical Journal, **44**: 276–283. doi:10.1139/t06-125.

Regmi, T.P., and Thompson, A.L. 2000. Rainfall simulator for laboratory studies. Applied Engineering in Agriculture, **16**(6): 641–647.

Rianna, G., Pagano, L., and Urciuoli, G. 2014. Investigation of soil–atmosphere interaction in pyroclastic soils. Journal of Hydrology, **510**: 480–492. Elsevier B.V. doi:10.1016/j.jhydrol.2013.12.042.

Richards, L.A. 1931. Capillary conduction of liquids through porous mediums. Jounal of Applied Physics, **1**(5): 318. AIP Publishing. doi:10.1063/1.1745010.

Robinson, J.D., and Vahedifard, F. 2016. Weakening mechanisms imposed on California's levees under multiyear extreme drought. Climatic Change,: 1–14. doi:10.1007/s10584-016-1649-6.

Rohwer, C. 1931. Evaporation from free water surfaces. *In* Technical Bulletin No 271. Washington, D. C.

Romanenko, V.A. 1961. Computation of the autumn soil moisture using a universal relationship for a large area. *In* Proceedings Ukrainian Hydrometeorological Research Institute (Kiev).

Romero, E., Gens, A., and Lloret, A. 1999. Water permeability, water retention and microstrucutre of unsaturated compacted boom clay. Engineering Geology, **54**: 117–127. doi:10.1016/S0013-7952(99)00067-8.

Romero, E., Vecchia, G.D., and Jommi, C. 2011. An insight into the water retention properties of compacted clayey soils. Géotechnique, **61**(4): 313–328. doi:10.1680/geot.2011.61.4.313.

Romero, E., Villar, M. V., and Lloret, A. 2005. Thermo-hydro-mechanical behaviour of two heavily overconsolidated clays. Engineering Geology, **81**(3): 255–268. doi:10.1016/j.enggeo.2005.06.011.

Rose, C. 1968. Water transport in soil with a daily temperature wave. I. Theory and experiment. Australian Journal of Soil Research, **6**(1): 31–44. doi:10.1071/SR9680031.

Rosenberg, N.J., Blad, B.L., and Verma, S.B. 1983. Microclimate: the biological environment. John Wiley&Sons, New York.

Rouainia, M., Davies, O., O'Brien, T., and Glendinning, S. 2009. Numerical modelling of climate effects on slope stability. Proceedings of the Institution of Civil Engineers - Engineering Sustainability, **162**(2): 81–89. doi:10.1680/ensu.2009.162.2.81.

Rubio, E., Caselles, V., and Badenas, C. 1997. Emissivity measurements of several soils and vegetation types in the 8-4 μm wave band: analysis of two field methods. Remote Sensing of Environment, **59**: 490–521.

Rujikiatkamjorn, C., Indraratna, B., and Bergado, D.T. 2012. 3D numerical modeling of hexagonal wire mesh reinforced embankment on soft bangkok clay. *In* GeoCongress 2012. California: American Society of Civil Engineering. Research. pp. 2263–2272.

Rykaart, M., Fredlund, M., and Stianson, J. 2001. Solving tailings impoundment water balance problems with 3-D seepage software. Geotechnical News, **19**(4): 50–55.

Sadaka, G. 2012. FreeFem++, a tool to solve PDEs numerically. Amiens, France.

Saito, H., Šimůnek, J., and Mohanty, B.P. 2006. Numerical analysis of coupled water, vapor, and heat transport in the vadose zone. Vadose Zone Journal, **5**(2): 784–800. doi:10.2136/vzj2006.0007.

Sajjan, A.K., Gyasi-Agyei, Y., and Sharma, R.H. 2013. Rainfall-runoff modelling of railway embankment steep slopes. Hydrological Sciences Journal-Journal Des Sciences Hydrologiques, **58**(December): 1162–1176. doi:Doi 10.1080/02626667.2013.802323.

Sansoulet, J., Cabidoche, Y.M., Cattan, P., Ruy, S., and Šimůnek, J. 2008. Spatially distributed water fluxes in an andisol under banana plants: experiments and three-dimensional modeling. Vadose Zone Journal, **7**(2): 819. Soil Science Society. doi:10.2136/vzj2007.0073.

Scanlon, B.R., Andraski, B.J., and Bilskie, J. 2002. Miscellaneous methods for measuring matric or water potential. *In* Methods of Soil Analysis. pp. 643–670.

Schelde, K., Thomsen, A., Heidmann, T., and Schjonning, P. 1998. Diurnal fluctuations of water and heat flows in a bare soil. Water Resources Research, **34**(11): 2919–2929.

Schoeneich, P., Dall'Amico, M., Deline, P., and Zischg, A. 2011. Hazards related to permafrost and to permafrost degradation. PermaNET project, state-of-the-art report 6.2.

Seetharam, S.C., Thomas, H.R., and Cleall, P.J. 2007. Coupled thermo/hydro/chemical/mechanical model for unsaturated soils-Numerical algorithm. International Journal for Numerical Methods in Engineering, **70**(12): 1480–1511. doi:10.1002/nme.

Sheng, D., Sloan, S.W., and Gens, A. 2004. A constitutive model for unsaturated soils: thermomechanical and computational aspects. Computational Mechanics, **33**(6): 453–465. doi:10.1007/s00466-003-0545-x.

Šimůnek, J., van Genuchten, M.T., and Šejna, M. 2005. The HYDRUS-1D software package for simulating the one-dimensional movement of water, heat, and multiple solutes in variably-saturated media. Version 3.0. Univ. of California, Riverside, CA.

Šimůnek, J., van Genuchten, M.T., and Šejna, M. 2006. The HYDRUS software package for simulating two- and three- dimensional movement of water, heat, and multiple solutes in variably-saturated media. Version 1.0. Prague, Czech Republic.

Šimůnek, J., van Genuchten, M.T., and Šejna, M. 2008. Development and applications of the HYDRUS and STANMOD software packages and related codes. Vadose Zone Journal, **7**(2): 587. doi:10.2136/vzj2007.0077.

Šimůnek, J., Hendrickx, J.M.H., and Borchers, B. 2001. Modeling transient temperature distributions around landmines in homogeneous bare soils. *In* Proceedings of SPIE, **4394**. pp. 387–397.

Šimůnek, J., Šejna, M., and van Genuchten, M.T. 1999. The HYDRUS-2D software package for simulating the two-dimensional movement of water, heat, and multiple Solutes in variably-saturated media. Version 2.0. Riverside, California.

Singh, V.P., and Xu, C.Y. 1997. Evaluation and generalization of 13 mass-transfer equations for determining free water evaporation. Hydrological Processes, **11**: 311–323. doi:10.1002/(SICI)1099-1085(19970315)11:3<311::AID-HYP446>3.3.CO;2-P.

Smethurst, J., Clarke, D., and Powrie, W. 2012. Factors controlling the seasonal variation in soil water content and pore water pressures within a lightly vegetated clay slope. Géotechnique, **62**(5): 429–446. doi:10.1680/geot.10.P.097.

Smits, K.M., Cihan, A., Sakaki, T., and Illangasekare, T.H. 2011. Evaporation from soils under thermal boundary conditions: Experimental and modeling investigation to compare equilibrium- and nonequilibrium-based approaches. Water Resources Research, **47**(5): 1–14. doi:10.1029/2010WR009533.

Song, W.K. 2014. Experimental investigation of water evaporation from sand and clay using an environmental chamber. PhD Thesis, Université Paris-Est, Paris.

Song, W.K., Cui, Y.J., Tang, A.M., Ding, W.Q., and Tran, T.D. 2013. Development of a large-scale environmental chamber for investigating soil water evaporation. Geotechnical Testing Journal, **36**(6): 20120142. doi:10.1520/GTJ20120142.

Song, W.K., Cui, Y.J., Tang, A.M., Ding, W.Q., and Tran, T.D. 2014. Experimental study on water evaporation from sand using environmental chamber. Canadian Geotechnical

Journal, **51**(2): 115–128. doi:10.1139/cgj-2013-0155.

Stewart, R.D., Liu, Z., Rupp, D.E., Higgins, C.W., and Selker, J.S. 2015. A new instrument to measure plot-scale runoff. Geoscientific Instrumentation, Methods and Data Systems, **4**: 57–64. doi:10.5194/gi-4-57-2015.

Sun, S.F. 1982. Moisture and heat transport in a soil layer forced by atmospheric conditions. PhD Thesis, University of Connecticut, Connecticut.

Suradi, M., Fourie, A.B., and Saynor, M.J. 2016. An experimental and numerical study of a landslide triggered by an extreme rainfall event in northern Australia. Landslides, **13**(5): 1125–1138. doi:10.1007/s10346-015-0606-1.

Sverdrup, H.U. 1946. The humidity gradient over the sea surface. Journal of Meteorology, **3**(1): 1–8. doi:10.1175/1520-0469(1946)003<0001:THGOTS>2.0.CO;2.

Swanson, D.A., Barbour, S.L., Wilson, G.W., and O'Kane, M. 2003. Soil-atmosphere modelling of an engineered soil cover for acid generating mine waste in a humid, alpine climate. Canadian Geotechnical Journal, **40**(2): 276–292. doi:10.1139/t02-116.

Sweeney, D.J. 1982. Some in situ soil suction measurements in Hong Kong residual soil slopes. *In* Proceedings of the 7th Southeast Asian Regional Conference. Hong Kong. pp. 22–26.

Ta, A.N. 2009. Etude de l'interaction sol-atmosphère en chambre environnementale. PhD Thesis, Ecole des Ponts Paristech, Paris.

Tang, A.M., and Cui, Y.J. 2010a. Experimental study on hydro-mechanical coupling behaviours of highly compacted expansive clay. Journal of Rock Mechanics and Geotechnical Engineering, **2**(1): 39–43. doi:10.3724/SP.J.1235.2010.00039.

Tang, A.M., and Cui, Y.J. 2010b. Effects of mineralogy on thermo-hydro-mechanical parameters of MX80 bentonite. Journal of Rock Mechanics and Geotechnical Engineering, **2**(1): 91–96. doi:10.3724/SP.J.1235.2010.00091.

Tang, A.M., Cui, Y.J., and Le, T.T. 2008. A study on the thermal conductivity of compacted bentonites. Applied Clay Science, **41**(3–4): 181–189. doi:10.1016/j.clay.2007.11.001.

Tang, C.S., Cui, Y.J., Shi, B., Tang, A.M., and Liu, C. 2011. Desiccation and cracking behaviour of clay layer from slurry state under wetting-drying cycles. Geoderma, **166**(1): 111–118. doi:10.1016/j.geoderma.2011.07.018.

Tang, C.S., Cui, Y.J., Tang, A.M., and Shi, B. 2010. Experiment evidence on the temperature dependence of desiccation cracking behavior of clayey soils. Engineering Geology, **114**(3–4): 261–266. doi:10.1016/j.enggeo.2010.05.003.

Tang, C.S., Shi, B., Cui, Y.J., Liu, C., and Gu, K. 2012. Desiccation cracking behavior of polypropylene fiber–reinforced clayey soil. Canadian Geotechnical Journal, **49**: 1088–1101. doi:10.1139/t2012-067.

Tedela, N.H. 2009. Rainfall-runoff relationships for small, mountainous, forested watersheds in the eastern united states. PhD Thesis, The University of Georgia, Athens. doi:10.1017/CBO9781107415324.004.

Teng, J.D., Yasufuku, N., Zhang, S., and He, Y. 2016. Modelling water content redistribution during evaporation from sandy soil in the presence of water table. Computers and Geotechnics, **75**: 210–224. doi:10.1016/j.compgeo.2016.02.009.

Teng, T.P., Hung, Y.H., Teng, T.C., Mo, H.E., and Hsu, H.G. 2010. The effect of alumina/water nanofluid particle size on thermal conductivity. Applied Thermal Engineering, **30**(14–15): 2213–2218. Elsevier Ltd. doi:10.1016/j.applthermaleng.2010.05.036.

Thakur, V.K.S., Sreedeep, S., and Singh, D.N. 2006. Laboratory investigations on extremely high suction measurements for fine-grained soils. Geotechnical and Geological Engineering, **24**(3): 565–578. doi:10.1007/s10706-005-1147-5.

Thom, A.S. 1975. Momentum, mass and heat exchange of plant communities. Vegetation and the Atmosphere, **1**: 57–109.

Thomas, H.R. 1985. Modelling two-dimensional heat and moisture transfer in unsaturated soils, including gravity effects. International Journal for Numerical and Analytical Methods in Geomechanics, **9**(6): 573–588.

Thomas, H.R., Cleall, P.J., Li, Y.C., Harris, C., and Kern-Luetschg, M. 2009a. Modelling of cryogenic processes in permafrost and seasonally frozen soils. Géotechnique, **59**(3): 173–184. doi:10.1680/geot.2009.59.3.173.

Thomas, H.R., and He, Y. 1995. Analysis of coupled heat, moisture and air transfer in a deformable unsaturated soil. Géotechnique, **45**(4): 677–689. doi:10.1680/geot.1995.45.4.677.

Thomas, H.R., and He, Y. 1997. A coupled heat-moisture transfer theory for deformable unsaturated soil and its algorithmic implementation. International Journal for Numerical Methods in Engineering, **40**: 3421–3441. doi:10.1002/(SICI)1097-0207(19970930)40:18<3421::AID-NME220>3.0.CO;2-C.

Thomas, H.R., and He, Y. 1998. Modelling the behaviour of unsaturated soil using an elastoplastic constitutive model. Géotechnique, **48**(5): 589–603. doi:10.1680/geot.1998.48.5.589.

Thomas, H.R., He, Y., and Onofrei, C. 1998. An examination of the validation of a model of the hydro/thermo/mechanical behaviour of engineered clay barriers. International Journal for Numerical and Analytical Methods in Geomechanics, **22**(April 1997): 49–71. doi:10.1002/(SICI)1096-9853(199801)22:1<49::AID-NAG908>3.0.CO;2-I.

Thomas, H.R., and King, S.D. 1991. Coupled temperature/capillary potential variations in unsaturated soil. Journal of Engineering Mechanics, **117**(11): 2475–2491. doi:10.1061/(ASCE)0733-9399(1991)117:11(2475).

Thomas, H.R., and King, S.D. 1992. Coupled heat and mass transfer in unsaturated soil—a potential-based solution. International Journal for Numerical and Analytical Methods in Geomechanics, **16**(10): 757–773. doi:10.1002/nag.1610161005.

Thomas, H.R., and King, S.D. 1994. A non-linear, two-dimensional, potential-based analysis of coupled heat and mass transfer in a porous medium. International Journal for Numerical Methods in Engineering, **37**(21): 3707–3722. doi:10.1002/nme.1620372108.

Thomas, H.R., and Rees, S.W. 2009a. Measured and simulated heat transfer to foundation soils. Géotechnique, **59**(4): 365–375. doi:10.1680/geot.2008.59.4.365.

Thomas, H.R., and Sansom, M.R. 1995. Fully coupled analysis of heat, moisture, and air transfer in unsaturated soil. Journal of Engineering Mechanics, **121**(3): 392–405. doi:10.1061/(ASCE)0733-9399(1995)121:3(392).

Thomas, H.R., Vardon, P.J., and Li, Y.C. 2009b. Coupled thermo-hydro-chemo-mechanical modeling for geoenvironmental phenomena. *In* Proc. of Int. Symp. on Geoenvironmental Eng. Hangzhou, China. pp. 320–327.

Thompson, J.F., Soni, B.K., and Weatherill, N.P. 1999. Handbook of grid generation. *In* Handbook of grid generation. *Edited by*S. Wood. doi:10.1201/9781420050349.

Thornthwaite, C.W. 1948. An Approach toward a Rational Classification of Climate. Geographical Review, **38**(1): 55–94.

Thornthwaite, C.W., and Holzman, B. 1939. The determination of evaporation from land and water surfaces. Monthly Weather Review, **67**(1): 4–11. doi:10.1175/1520-0493(1939)67<4:TDOEFL>2.0.CO;2.

Todd, R.W., Evett, S.R., and Howell, T.A. 2000. The Bowen ratio-energy balance method for estimating latent heat flux of irrigated alfalfa evaluated in a semi-arid, advective environment. Agricultural and Forest Meteorology, **103**(4): 335–348. doi:10.1016/S0168-1923(00)00139-8.

Tohari, A., Nishigaki, M., and Komatsu, M. 2007. Laboratory rainfall-induced slope failure with moisture content measurement. Journal of Geotechnical and Geoenvironmental Engineering, **133**(5): 575–587. doi:10.1061/(ASCE)1090-0241(2007)133:5(575).

Toll, D.G. 2001. Briefing: Rainfall-induced landslides in Singapore. *In* Proceedings of the

Institution of Civil Engineers- Geotechnical Engineering. Thomas Telford Ltd. pp. 211–216. doi:10.1680/geng.2001.149.4.211.

Toll, D.G., Lourenco, S.D.N., Mendes, J., Gallipoli, D., Evans, F.D., Augarde, C.E., Cui, Y.J., Tang, A.M., Rojas, J.C., Pagano, L., Mancuso, C., Zingariello, C., and Tarantino, A. 2011. Soil suction monitoring for landslides and slopes. Quarterly Journal of Engineering Geology and Hydrogeology, **44**(1): 23–33. doi:10.1144/1470-9236/09-010.

Toll, D.G., Mendes, J., Gallipoli, D., Glendinning, S., and Hughes, P.N. 2012. Investigating the impacts of climate change on slopes: field measurements. Geological Society, London, Engineering Geology Special Publications, **26**(1): 151–161. doi:10.1144/EGSP26.17.

Toll, D.G., Rahardjo, H., and Leong, E.C. 1999. Landslides in Singapore. *In* Proceedings of the 2nd International Conference on Landslides, Slope Stability and the Safety of Infra-Structures. Singapore. pp. 27–28.

Tubiello, F., Schmidhuber, J., Howden, M., Neofotis, P.G., Park, S., Fernandes, E., and Thapa, D. 2008. Climate change response strategies for agriculture : challenges and opportunities for the 21st century. *In* Agriculture and rural development discussion paper. The World Bank, Washington, DC.

Uchaipichat, A., and Khalili, N. 2009. Experimental investigation of thermo-hydro-mechanical behaviour of an unsaturated silt. Géotechnique, **59**(4): 339–353. doi:10.1680/geot.2009.59.4.339.

USDA-SCS. 2004. Estimation of direct runoff from storm rainfall. *In* National engineering handbook , Part 630 Hydrology. Washington, DC. pp. 1–79.

Várallyay, G. 2002. Climate change and soil processes. Idõjárás,.

Várallyay, G. 2007. Potential impacts of climate change on agro-ecosystems. Agriculturae Conspectus Scientificus, **72**(1): 1–8.

Várallyay, G. 2010. The impact of climate change on soils and on their water management.

Agronomy Research, **8**(2): 385–396.

Várallyay, G., and Farkas, C. 2008. Impact of climate change on soils in Hungary. Climate change: environment-risk-society. Research results.Szaktudás Kiado Haz, Budapest,: 91–129.

Vardon, P.J. 2015. Climatic influence on geotechnical infrastructure: a review. Environmental Geotechnics, **2**(3): 166–174. doi:10.1680/envgeo.13.00055.

Vaunat, J., Romero, E., and Jommi, C. 2000. An elastoplastic hydromechanical model for unsaturated soils. *In* Proceedings of the international workshop on unsaturated soils. *Edited by* A. Tarantino and C. Mancuso. Trento. pp. 121–138.

Verma, S.B., Rosenberg, N.J., Blad, B.L., and Baradas, M.W. 1975. Resistance-energy balance method for predicting evapotranspiration: determination of boundary layer resistance and evaluation of error effects. Agronomy Journal, **68**(5): 776–782. American Society of Agronomy. doi:10.2134/agronj1976.00021962006800050023x.

Viney, R. 1991. An empirical expression for aerodynamic resistance in the unstable boundary layer. Boundary Layer Meteorology, **56**: 381–393.

Voogt, J. a., and Grimmond, C.S.B. 2000. Modeling surface sensible heat flux using surface radiative temperatures in a simple urban area. Journal of Applied Meteorology, **39**: 1679–1699. doi:10.1175/1520-0450(2000)039<1679:MSSHFU>2.0.CO;2.

Voulgari, C. 2015. An experimental model for slopes subject to weathering. *In* International Symposium on Geohazards and Geomechanics (ISGG2015). pp. 1–9. doi:10.1088/1755-1315/26/1/012047.

De Vries, D.A. 1963. Thermal properties of soils. *In* Physics of plant environment (ed. W. R. Van Wijk). *Edited by* W.R. Van Wijk. Amsterdam: North-Holland. pp. 210–235.

De Vries, D.A. 1952. The thermal conductivity of soil. Mededelingen van de Landbouwhogeschool te Wageningen, **52**(1): 173. doi:10.1038/1781074a0.

De Vries, D.A. 1958. Simultaneous transfer of heat and moisture in porous media. Transactions, American Geophysical Union, **39**(5): 909. doi:10.1029/TR039i005p00909.

De Vries, D.A. 1975. Heat transfer in soils. *In* Proceedings of heat and mass transfer in the Biosphere. Part I, Transfer process in plant environment. Scripta Book Co., Washington, D. C. pp. 1–28.

Wakao, N., and Kato, K. 1969. Effective thermal conductivity of packed beds. Journal of Chemical Engineering of Japan, **2**(1): 24–33. doi:10.1252/jcej.2.24.

Wang, H., Xing, X., Li, T., Qin, Z., and Yang, J. 2014. Slope instability phenomenon in the permafrost region along the Qinghai–Tibetan highway, China. *In* Landslides in Cold Regions in the Context of Climate Change. pp. 11–22. doi:10.1007/978-3-319-00867-7.

Wang, J., and Bras, R.L. 1998. A new method for estimation of sensible heat flux from air temperature. Water Resources Research, **34**(9): 2281–2288.

Wang, Q. 2012. Hydro-mechanical behaviour of bentonite-based materials used for high-level radioactive waste disposal. PhD Thesis, Université Paris-Est, Paris.

Wang, W., Kosakowski, G., and Kolditz, O. 2009. A parallel finite element scheme for thermo-hydro-mechanical (THM) coupled problems in porous media. Computers & Geosciences, **35**(8): 1631–1641. doi:10.1016/j.cageo.2008.07.007.

Watanabe, K., and Tsutsui, Y. 1994. A new equipment used for measuring evaporation in a field. Proc. 7th Congr. IAEG,: 309–313.

Weeks, B., and Wilson, G.W. 2006. Prediction of evaporation from soil slopes. Canadian Geotechnical Journal, **43**: 815–829. doi:10.1139/t06-049.

Wei, W., Jia, F., Yang, L., Chen, L., Zhang, H., and Yu, Y. 2014. Effects of surficial condition and rainfall intensity on runoff in a loess hilly area, China. Journal of Hydrology, **513**: 115–126. Elsevier B.V. doi:10.1016/j.jhydrol.2014.03.022.

Westcot, D., and Wierenga, P. 1974. Transfer of heat by conduction and vapor movement in a

closed soil system. Soil Science Society of America,.

Wheeler, S.J., Näätänen, A., Karstunen, M., and Lojander, M. 2003a. An anisotropic elastoplastic model for soft clays. Canadian Geotechnical Journal, **40**(2): 403–418. NRC Research Press Ottawa, Canada. doi:10.1139/t02-119.

Wheeler, S.J., Sharma, R.S., and Buisson, M.S.R. 2003b. Coupling of hydraulic hysteresis and stress-strain behaviour in unsaturated soils. Géotechnique, **53**(1): 41–54. doi:10.1680/geot.2003.53.1.41.

Van Wijk, W.R. 1963. Physics of plant environment. *Edited by*W.R. Van Wijk. Amsterdam: North Holland Publishing Company.

Wilson, G.W. 1990. Soil evaporation fluxes for geotechnical engineering problems. PhD Thesis. University of Saskatchewan, Saskatoon.

Wilson, G.W., Fredlund, D.G., and Barbour, S.L. 1994. Coupled soil-atmosphere modelling for soil evaporation. Canadian Geotechnical Journal, **31**(2): 151–161. doi:10.1139/t94-021.

Wilson, G.W., Fredlund, D.G., and Barbour, S.L. 1995. The prediction of evaporative fluxes from unsaturated soil surfaces. *Edited by* A. and Delage. France. pp. 423–429.

Wilson, G.W., Fredlund, D.G., and Barbour, S.L. 1997. The effect of soil suction on evaporative fluxes from soil surfaces. Canadian Geotechnical Journal, **34**(1): 145–155. doi:10.1139/t98-034.

Wilson, G.W., Machibroda, R.T., Barbour, S.L., and Woyshner, M.R. 1993. Modelling of soil evaporation from waste disposal sites. *In* Proceedings of the joint CSCE-ASCE national conference on environmental engineering. Montreal. pp. 281–288.

Wu, L.Z., and Zhang, L.M. 2009. Analytical solution to 1D coupled water infiltration and deformation in unsaturated soils. International Journal for Numerical and Analytical Methods in Geomechanics, **33**: 773–790. doi:10.1002/nag.

Wu, W., Li, X., Charlier, R., and Collin, F. 2004. A thermo-hydro-mechanical constitutive model and its numerical modelling for unsaturated soils. Computers and Geotechnics, **31**(2): 155–167. doi:10.1016/j.compgeo.2004.02.004.

Xie, X. 1988. An improved energy balance-aerodynamic resistance model used estimation of evapotranspiration on the wheat field. Acta Meteorology Sinica (in Chinese), **46**(1): 102–106.

Xu, Q., and Qiu, C.J. 1997. A variational method for computing surface heat fluxes from arm surface energy and radiation balance systems. Journal of Applied Meteorology, **36**(1): 3–11. doi:10.1175/1520-0450(1997)036<0003:AVMFCS>2.0.CO;2.

Xu, Q., Zhou, B., Burk, S.D., Barker, E.H., Zu, Q., Zhou, B., Burk, S.D., and Barker, E.H. 1999. An air-soil layer coupled scheme for computing surface heat fluxes. Journal of Applied Meteorology, **38**(2): 211–223. doi:10.1175/1520-0450(1999)038<0211:AASLCS>2.0.CO;2.

Yamanaka, T., Inoue, M., and Kaihotsu, I. 2004. Effects of gravel mulch on water vapor transfer above and below the soil surface. Agricultural Water Management, **67**(2): 145–155. doi:10.1016/j.agwat.2004.01.002.

Yamanaka, T., Takeda, A., and Sugita, F. 1997. A modified surface-resistance approach for representing bare-soil evaporation: Wind tunnel experiments under various atmospheric conditions. Water Resources Research, **33**(9): 2117–2128. doi:10.1029/97WR01639.

Yanful, E.K., and Choo, L.P. 1997. Measurement of evaporative fluxes from candidate cover soils. Canadian Geotechnical Journal, **34**(3): 447–459. doi:10.1139/t97-002.

Yanful, E.K., Mousavi, S.M., and Yang, M. 2003. Modeling and measurement of evaporation in moisture-retaining soil covers. Advances in Environmental Research, **7**(4): 783–801. doi:10.1016/S1093-0191(02)00053-9.

Yanful, E.K., Simms, P.H., Rowe, R.K., and Stratford, G. 1999. Monitoring an experimental soil waste near London, Ontario, Canada. Geotechnical and Geological Engineering,

17(2): 65–84. Kluwer Academic Publishers. doi:10.1023/A:1008986103460.

Yang, K., Tamai, N., Koike, T., Yang, K., Tamai, N., and Koike, T. 2001. Analytical solution of surface layer similarity equations. Journal of Applied Meteorology, **40**(9): 1647–1653. doi:10.1175/1520-0450(2001)040<1647:ASOSLS>2.0.CO;2.

Yang, M.D., and Yanful, E.K. 2002. Water balance during evaporation and drainage in cover soils under different water table conditions. Advances in Environmental Research, **6**(4): 505–521. doi:10.1016/S1093-0191(01)00077-6.

Yong, R., Boonsinsuk, P., and Wong, G. 1986. Formulation of backfill materials for a nuclear fuel waste disposal. Canadian Geotechnical Journal, **23**(2): 216–228.

Yue, Z.R. 2008. Thermal regime simulation of embankment and berm in permafrost. Geomechanics and Geoengineering, **3**(2): 97–105. doi:10.1080/17486020801905642.

Yuge, K., Haraguchi, T., Nakano, Y., Kuroda, M., and Anan, M. 2005. Quantification of soil surface evaporation under micro-scale advection in drip-irrigated fields. Paddy and Water Environment, **3**(1): 5–12. doi:10.1007/s10333-004-0058-z.

Yusuf, A.A., and Francisco, H.A. 2009. Climate change vulnerability mapping for southeast asia vulnerability mapping for Southeast Asia. *In* Economy and Environment Program for Southeast Asia (EEPSEA). doi:10.1158/1541-7786.MCR-07-0267.